Optimizing Cartilage Tissue Engineering through Computational Growth Models and Experimental Culture Protocols

Robert John Nims

Submitted in partial fulfillment of the
requirements for the degree of
Doctor of Philosophy
in the Graduate School of Arts and Sciences

COLUMBIA UNIVERSITY

2017

ABSTRACT

Optimizing Cartilage Tissue Engineering through Computational Growth Models and Experimental Culture Protocols

Robert John Nims

Osteoarthritis is a debilitating and irreversible disease afflicting the synovial joints. It is characterized by pain and hindered mobility. Given that osteoarthritis has no cure, current treatments focus on pain management. Ultimately, however, a patient's pain and immobility necessitates joint replacement surgery. An attractive alternative to this treatment paradigm, tissue engineering is a promising strategy for resurfacing the osteoarthritis-afflicted cartilage surface with a biochemically and biomechanically similar tissue to the healthy native cartilage tissue. The most successful cartilage tissue engineered systems to date can repeatably grow constructs ≈4 mm in diameter with native proteoglycan and compressive mechanical properties. Unfortunately, as symptomatic cartilage typically presents only once lesions span large regions of the joint (≈25 mm in diameter), these small construct are of limited use in clinical practice.

Numerous attempts to simply grow a construct large enough to span the size of an osteoarthritic lesion have shown that the growth of large engineered tissues develop heterogeneous properties, emphasizing the need for culture protocols to enhance tissue homogeneity and robustness. In particular, as nutrient limitations drive heterogeneous growth in engineered cartilage, developing strategies to improve nutrition throughout the construct are critical for clinical translation of the technology. To this end, our lab has successfully supplemented nutrient channels within large engineered cartilage constructs to improve the functional properties of developing tissue. However, it is unknown what the optimal nutrient channel spacing is for growing large cartilage constructs of anatomical scale. Additionally, the fundamental factors and mechanisms which drive tissue heterogeneity have not been implicated, making the results of channel-spacing optimizations difficult to translate across different systems.

Computational models of growth, faithful to the physics and biology of engineered tissue growth,

may serve as an insightful and efficient tool for optimally designing culture protocols and construct geometries to ensure homogeneous matrix deposition. Such computational tools, however, are not presently available, owing to the unresolved mechanical and biological growth phenomena within developing engineered cartilage. This dissertation seeks to develop and implement computational models for predicting the biochemical and biomechanical growth of engineered tissues and apply these models to optimizing tissue culture strategies. These models are developed in two stages: 1) based on our recent characterization of the nutrient demands of engineered cartilage, models are developed to simulate the spatial biochemical deposition of matrix within tissue constructs and, subsequently, 2) based on models of biochemical matrix deposition we develop models for simulating the mechanical growth of tissue constructs.

To accomplish these tasks, we first develop models simulating glucose availability within large tissue constructs using system-specific modeling based on our recent characterization of the glucose demands of engineered cartilage. These models led to early insight that we had to enhance the supply of glucose within large tissue constructs to ensure maximal matrix synthesis throughout culture. Experimental validations confirmed that increasing glucose supply enhanced matrix deposition and growth in large tissue constructs.

However, even despite the increased glucose supply, increasing the size of constructs demonstrated that severe matrix heterogeneities were still present. Subsequent nutrient characterization led to the finding that TGF-β transport was significantly hindered within large tissue constructs. Incorporating the influence of glucose and TGF-β into the computational model growth kinetics. Using both nutrients, models recreated the heterogeneous matrix deposition evident in our earlier work and could account for the role of cell seeding density and construct geometry on tissue growth. The insights gathered from this modeling analysis led to important changes in our culture protocols: we could reduce the dose of TGF-β from 10 ng mL^{-1} to 1 ng mL^{-1} for constructs cultured with channels, saving considerable expense while still maintaining a high level of matrix synthesis throughout the construct.

In the presence of sufficient nutrition, we witnessed an unprecedented level of matrix deposition and physical growth of the constructs. In fact, by using developmentally physiologic cell seeding densities (120 million cells mL^{-1}) and providing adequate nutrition, constructs physically grew to 9-times their originally cast size. Despite such encouraging growth, tissue function properties

plateaued at sub-physiologic levels. For insight into the connection between matrix deposition and tissue mechanics, we extended the computational growth models to consider the mechanisms underlying physical growth. Interestingly, we found that a large matrix synthesis mismatch between proteoglycans and collagen gave rise to the excessive tissue swelling. Computational models of this matrix synthesis mismatch predicted the high tissue swelling displayed experimentally only when a damage-able collagen fiber material was implemented. Together, the experimental and modeling evidence suggested a new mechanism of cartilage growth: the high proteoglycan deposition creates a swelling pressure within the nascent tissue which outcompetes the restraining force of newly deposited collagens; this rapid tissue swelling disrupts a functional collagen network from forming. Subsequent analysis suggested that the disruption of the collagen network prevented the formation of collagen crosslinks, stymieing the development of native functional properties.

Based on this insight into the mechanisms of cartilage growth, we developed a culture systems to improve tissue functional properties. Modeling analysis indicated two novel routes for improving tissue mechanics: either through 1) reducing the swelling response (synthesis and deposition) of proteoglycans or 2) enhancing and reinforcing the newly synthesized collagen to prevent disruptions brought on by tissue swelling. We developed a cage culture system for resisting the swelling pressure of deposited proteoglycans and reenforcing the deposition of new collagens. Using this cage system, we grew tissue constructs with enhanced functional properties using two separate scaffold systems – agarose and a cartilage-derived matrix hydrogel – suggesting this mechanism of growth is fundamental to engineered cartilage development.

This work has generated a novel paradigm towards engineering cartilage constructs using biomimetic strategies. Performing simulations with the validated, computational growth models allowed anatomically-sized cartilage constructs to grow into the largest, homogeneous cartilage constructs grown to date. Models presented a new level of insight into the nutrient demands of developing tissues, allowing for the first time the successful development of large tissue constructs grown with developmentally physiologic cell seeding densities. In this way, tissue constructs growth followed a biomimetic approach, based on the high cell densities and cartilage canals and vasculature present during fetal cartilage development. Adequate nutrition led to high levels of tissue growth not previously experienced in vitro, a result of adequately nourishing primary chondrocytes, a cell type which preferentially deposits proteoglycans over collagen. We therefore developed a

cage-based growth system to resist the proteoglycan-induced tissue swelling in a manner similar to the fetal development of cartilage where the resident cells synthesize more collagens than proteoglycans. Together, the use of nutrient growth models, high cell seeding densities, and culture systems to strengthen the collagen-framework of de novo cartilage proved beneficial for engineering anatomically-sized cartilage constructs. The fundamental mechanisms identified here are likely to be universal across a number of engineered cartilage systems and will be adapted to more clinically-relevant cell sources in future our work.

Contents

List of Figures

List of Tables

Acknowledgments

"Get your work in, young fella. Most people will never really get to know the real you. But they'll get to know your work."

-Ray Allen

I have been fortunate to attend Columbia and work on this thesis only due to the kindness and generosity of my funders and I would like to thank the Columbia Presidential Fellowship and the National Institutes of Health.

While at Columbia I have been incredibly lucky to work with my advisor Professor Gerard Ateshian in the Musculoskeletal Biomechanics lab. His enthusiasm for teaching and research has truly been contagious as we've strived forward in search of new scientific understandings of growth and remodeling. Gerard's encouragement and thoughtfulness is a model of what all doctoral advisors should continually pursue. I will forever remember my interview weekend, meeting with Gerard as he regaled us with stories of mixture models of non-intuitive physical phenomena. The opportunity to study and work along side him has been an honor.

I am also grateful for the opportunity to collaborate and receive input and feedback from my top-notch committee members: Professor Clark Hung who has been a wonderful source of new ideas, studies, perspectives, and open doors when it appears they all have closed; Professor Gordana Vunjak-Novakovic, to whom I'm grateful for her support and insightful suggestions on my work; Professor Kristin Myers for always having her door open and providing helpful feedback; and Professor Rob Mauck for his valuable input on this thesis and being a wonderful source of encouragement at conferences.

Since my first day, the lab has always been a source of warmth (emotional warmth...but okay, it's actually physically warm too). I began on the first day with Drs. Mike Albro and Alex Cigan at the ELISA station and I can't think of a better way to have jumped right in; both have provided continuous feedback and support and I have been lucky to have them by my side. Mike has also been a enduring source of mentorship and inspiration over these many years and I've been fortunate for his influence. During my time in the lab I've come to see a whole generation of students leave and begin. What has maintained, though,

is a respect, camaraderie, and passion for the work at hand. For this, I thank both the students who passed this down: Drs. Mike Albro and Sevan Oungoulian; my peers who helped adopt the tradition: Drs. Alex Cigan and Brian Jones; and the generation who has heartily taken up the mission: Krista Durney, Jay Shim, (Big) Jay Hou, and Brandon Zimmerman. Equally so, I've been fortunate to be closely affiliated with the CEL lab team for their generosity, thought-exercises, and scientific results-whodunnits. To this end, I'm particularly appreciative of Dr. Andrea Tan who taught me the craft of tissue engineering, and to Drs. Grace O'Connell, Adam B. Nover, Terri-Ann Kelly, Elena Alegre-Aguaron, Sonal Sampat, and Brendon Roach, Amy Silverstein, Rob Stefani, Eben Estell, and Charlie Cai.

My family and friends have provided me endless support and encouragement. I am eternally indebted. In particular thanks to Tommy, Susie, Barrie, and Binky Ling for your support, hospitality, and for Binky's carrot laden kisses.

The nature of much of this work has been difficult and isolating. Bringing light to these times, I've been most fortunate to have Doris Ling by my side. Her support, compassion, empathy, positivity, and jokes have been the highlight of many of my days and I look forward to many good days to come.

And finally, my parents, John and Kristiina, and sister, Sarah, have provided the love, grounding, perspective, and gardening and woodchuck humor to keep me going. From care packages to homemade spaghetti sauces and salsa, living far removed from home has never felt so close.

For all of this, from all of you, I am thankful.

To my grandparents.

Chapter 1 Introduction

Cartilage tissue engineering (CTE) is a promising cell-based therapy where a biochemically and biomechanically functional cartilage construct is engineered to replace and resurface the degenerative cartilage. CTE research has been ongoing for nearly two-decades and has made enormous strides recently in the repeatability and performance of small engineered constructs which match the mechanical and biochemical properties of native articular cartilage. Despite these advances, however, future success of the field is largely contingent on the ability to translate these promising strategies from the research lab to clinical practice.

Achieving this translation is contingent on addressing two primary limitations in current engineered tissue culture. The first challenge is the ability to grow large, anatomically-sized constructs by scaling up current tissue engineered construct culture. The second challenge is growing tissues which match all of the unique and robust functional mechanical properties typical of native cartilage.

A background on the field of tissue engineering is first introduced. We then introduce the overarching specific aims of this dissertation in the context of the work's significance. Lastly, more detailed specific aims are itemized.

1.1 Background

1.1.1 Cartilage structure and function

Articular cartilage is an avascular and aneural connective tissue lining our diarthrodial joints. The dense extracellular matrix of cartilage imparts the tissue with unique mechanical properties ideally suited for its function as a dynamically loaded tissue (Mow *et al.* , 1984; Park *et al.* , 2004; Kempson, 1980; Ateshian *et al.* , 1997). In addition to being resistant to high dynamic and static loads, cartilage has a very low coefficient of friction (Krishnan *et al.* , 2004; Jones *et al.* , 2015) and good wear properties (Radin *et al.* , 1982; Oungoulian *et al.* , 2015); the biochemical composition and structural organization of cartilage confer the tissue with all of these functional properties. Cartilage is able to withstand the loading environment of activities of daily living often without problems for >80 years. This is essential as the tissue's dense matrix, lack of vasculature, and low cell content limit the natural repair capacity of the tissue, critically-sized defects therefore evolve

into larger defects.

The two predominant structural molecules of native cartilage are proteoglycans, consisting of hyaluronan chains lined with polymeric glycosaminoglycans (GAGs), and collagen (chiefly type II in mature cartilage) (McDevitt, 1973; Kuettner, 1992). The GAGs and collagens play opposing mechanical forces that together provide the robust mechanical properties. Collagen makes up ~80% dw of the extracellular matrix constituents and provides a dense fibrillar network within the tissue to prevent expansive forces (Chahine *et al.* , 2004; Wilson *et al.* , 2004). These fibrils buckle under compressive loading. Conversely, the GAGs within cartilage are negatively charged and impart a high fixed-charge density to the tissue (Maroudas, 1976; Eisenberg & Grodzinsky, 1985; Lai *et al.* , 1991; Setton *et al.* , 1998; Chahine *et al.* , 2005). This fixed-charge density of nearly -300 mEq L^{-1}, among the highest in the body, attracts ions from the interstitial fluid to balance the fixed charges and ensure electoneutrality. The steep ion gradient subsequently attracts the interstitial water into the tissue and the high osmotic pressure that develops causes the tissue to swell and resist compressive deformation. Together, the restraining collagen and expansive GAG mechanical contributions give rise to cartilage's unique non-linear tension-compression properties where the tensile (collagen-dominated) modulus is nearly two orders of magnitude greater than the compressive (GAG- and osmotic-dominated) modulus (Chahine *et al.* , 2004).

Cartilage's high tensile modulus directly effects the frictional and dynamic modulus properties of the tissue, two important measures for cartilage due to its biomechanical role (Krishnan *et al.* , 2003; Krishnan *et al.* , 2004). Under routine compressive loading conditions, cartilage deforms around the loaded tissue. This expansive deformation is resisted by the collagen and high tensile modulus of the tissue (Chahine *et al.* , 2004). Therefore, the external compressive loads are translated into a tensile loading response of the tissue, much like the way a water ballon, when squeezed (compressed), expands in its lateral directions. Furthermore, in the instantaneous loading response, cartilage's interstitial fluid pressurizes (being resisted primarily by the collagen framework), and supports much of the load. This is critical to maintaining cartilage's low friction properties ($\mu \lessapprox 10^{-2}$). Ultimately, an engineered tissue replacement would replicate this dense biochemical composition of native cartilage (both the dense collagen and GAG networks – as both are essential for the unique mechanical properties of native cartilage) .

Apart from the unique biochemical composition of articular cartilage, the tissue's GAG and

collagen networks are arranged heterogeneously from the superficial to deep zones and further influence mechanical properties of the tissue (Chahine *et al.* , 2004; Buckley *et al.* , 2008; Clark, 1990; Shirazi *et al.* , 2008). The highest level of organization is the arcade collagen network, where collagen fibrils are nearly perpendicular to the subchondral bone in the deep zones and then cross over to become parallel to the articular surface in the superficial zone. The "superficial" zone of cartilage is defined as having preferentially parallel collagen fibers relative to the articular surface. The "middle" zone then begins where the collagen fibers begin to cross over and assume a more random orientation. The "deep" zone extends below the middle zone to the subchondral bone and consists mostly of collagen fibers in an aligned direction, perpendicular to the subchondral bone and upper, articulating cartilage surface. This preferential directionality influences mechanical properties significantly, but it is still a debated issue on whether the directed collagen orientation plays a critical role in cartilage's mechanical response once the tissue is dynamically loaded under normal in situ loading states (Jones *et al.* , 2016).

1.1.2 Cartilage development, maintenance, and degeneration

Though mature cartilage has no vasculature and a low cell content, developmental cartilage is highly vascularized and consists of an extremely high cell density as the early precursor mesenchymal cells condense to eventually form bone, the joint space, and the cartilage anlage (Strayer Jr, 1943; Gardner & Gray, 1950; Gardner & O'Rahilly, 1968; Mitrovic, 1977; Doskocil, 1984; Oreja *et al.* , 1995; Bland & Ashhurst, 1996). In the earliest investigated states of the developing cartilage, the tissue consists nearly entirely of cells with little extracellular matrix aside from early, mostly unsulfated hyaluronan deposition (Edwards *et al.* , 1994; Pitsillides *et al.* , 1995). The cells of the early joint, responding to both signaling molecules and mechanical cues, begin to align and define an articular surface on opposing sides of the joint surface. Simultaneously, collagen deposition begins to occur. At this early state collagen types I, II, III, and V are the predominant forms which locate to superficial, deep, and pericellular zones (Bland & Ashhurst, 1996; Craig *et al.* , 1987; Mundlos *et al.* , 1990; Treilleux *et al.* , 1992; Evans *et al.* , 1983). Expansion of the joint at this level (prenatal) is believed to occur mostly from cellular proliferation which continues to develop the long bones, and chondrocytes are highly aligned still in this state. After birth, collagen synthesis and cellular proliferation still occur and

sulfated GAGs are slowly synthesized into the matrix. This is the first significant level of collagen cross linking to occur too, perhaps in response to the tissue becoming increasingly hypoxic (Moriguchi & Fujimoto, 1978; Makris *et al.* , 2014a). Development of cartilage continues to proceed as the subchondral bone below the cartilage begins to ossify. Cartilage canals, a vasculature network stemming from the highly vascularized bone, play a critical role in chondrocyte nutrition until complete ossification and allows the tissue matrix to continue to develop and deposit during the last days of development (Stockwell, 1971b; Wilsman & Van Sickle, 1972; Olstad *et al.* , 2008; Albro *et al.* , 2011).

At the time of skeletal maturation, the subchondral bone becomes fully sealed off from the articular cartilage. The cartilage canals, which to this point have supplied the tissue with vital nutrition fill with matrix. As nutrients are now only accessible from the superficial surface of the tissue, primarily through diffusion, the cell content drop precipitously (Stockwell, 1971a; Stockwell, 1967; Klein *et al.* , 2007). Measurements of developmental cartilage have found the cell content to be 100-300 million cells mL^{-1}. Mature cartilage, on the other hand, has a cell content closer to 5-30 million cells mL^{-1} (Stockwell, 1971a; Temple-Wong *et al.* , 2009). This population of cells that do persist within cartilage have a limited role in the tissue's maintenance. After reaching tissue maturity, studies have found collagen deposition ceases completely in human cartilage (Heinemeier *et al.* , 2016). Similar studies find that proteoglycans, which are not covalently bound within the tissue as the cross-linked collagen network is, slowly diffuse out through the articular surface of the cartilage, suggesting these cells are capable of a continued level of GAG synthesis and deposition within the tissue.

While healthy cartilage can be maintained without damage for many decades, the limited natural repair capacity prevents the joint from rebounding from minor defects or destabilizing effects including aberrant growth factor signaling and mechanical loading. Therefore the small-sized defects that may occur grow into large-sized defects (Ding *et al.* , 2007). Unfortunately, the lack of cartilage innervation means defects go unnoticed until they develop into a size sufficiently large for altered joint kinematics to cause aberrant loading of either the subchondral or surrounding joint capsule soft tissues (Dieppe & Lohmander, 2005). Moreover, these defects lead to bone-on-cartilage and bone-on-bone wear which can further aggravate the delicate equilibrium of the joint. The first radiographic signs of OA are typically focal swelling within the cartilage, but to date the etiology of

OA is unclear. Specifically, while measurements find both focal collagen denaturation and increases GAG deposition near focal damage sites, the initiating event is often unknown.

1.1.3 Cartilage repair in the clinic

Due to the limited regenerative and healing capacity of native cartilage, defects must be repaired or replaced to enable continued mobility and limit pain. Typical current treatments include microfracture surgery, osteochondral allograft, and autologous chondrocyte transplantation (ACI) (McDermott *et al.* , 1985; Steadman *et al.* , 1997; Steadman *et al.* , 2003; Jakob *et al.* , 2002; Knutsen *et al.* , 2004; Peterson *et al.* , 2010). None of these treatments, however, can be used to treat the large-sized defects which arise in osteoarthritis, often leaving this sizable population to wait until a total joint replacement is appropriate.

To this end, cartilage tissue engineering has emerged as a promising regenerative medicine approach to treating small and large sized defects with a tissue construct which is biochemically and biomechanically similar to the native articular cartilage. However, despite several clinical trials of cartilage tissue engineering products, their utility and treatment scope has been limited (primarily by cartilage defect size) (Huang *et al.* , 2016a). Of the eleven (11) cartilage tissue engineering products which have undergone clinical trials, four (4) of these are ongoing, seven (7) have no future development plans, and two (2) have led to products available in Europe only (with no plans for US clinical trials). These limitations of current engineered cartilage products are the subject of continued research.

1.1.4 Cartilage tissue engineering

To generate a cartilage tissue construct, a typical CTE strategy isolates and cultures a chondrogenic cell source within a biocompatible scaffold (Butler *et al.* , 2000). Using modern tissue culture techniques (i.e. a chemically-defined, serum-free media formulations and growth factor supplementation to stimulate matrix production and ensure a chondrogenic phenotype), our lab and a few others have shown that small tissue constructs can routinely be grown to achieve native compressive properties. The growth of engineered constructs is modulated by the culture system used, which is where biomedical engineers can act to develop more functional tissue replacements. There are three important culture factors to consider for system optimization: 1) cell source, 2) scaffold type, and 3)

media formulation and culture configuration with the objective of producing large tissue constructs with functional mechanical properties.

1.1.4.1 Cell source Originally, cell source for cartilage tissue engineering was primary chondrocytes harvested directly from native cartilage and digested out of the matrix (Benya & Shaffer, 1982; Buschmann *et al.* , 1995). Primary chondrocytes are fully differentiated, ensuring matrix synthesis similar to native cartilage. As primary cells are taken directly from the tissue there are limitations on the number of harvestable cells, particularly from a tissue with as low a cellularity as cartilage. Cell passaging is a technique whereby adherent cells can be plated into a two-dimensional environment and allowed to multiply, a method routinely used for enhancing the supply of cells. Two-dimensional (2D) culture, being unnatural for most cells, can lead to "de-differentiation," a phenomenon were a cell phenotype is altered to a non-native state. For chondrocytes, early work suggested that limiting the length of time the cells are cultured in 2D, returning the cells to a three-dimensional (3D) environment to culture, and using growth factors and specific nutrients can help prevent deleterious de-differentiation (Benya & Shaffer, 1982; Bonaventure *et al.* , 1994; Darling & Athanasiou, 2005).

In addition to chondrocytes, adult stem cells are a widely researched cell source of developing engineered cartilage constructs (Tuan *et al.* , 2002; Guilak *et al.* , 2004; Caplan, 2007; He *et al.* , 2009). Adult stem cells have the ability to be transformed into an number of different cells, and are located in adult fat (adipose-derived stem cells), bone marrow (bone marrow stem cells), synovial tissue (synovial derived stem cells), and other connective tissues. Adult stem cells have the advantage of being readily available such that high cell contents can be easily obtained. A challenge to using adult stem cells is first converting them to chondrocytes necessary for synthesizing the matrix molecules required for the structure and mechanical properties of the engineered cartilage construct. Recent advances in adult stem cell techniques, however, have shown great strides in controlling bone marrow derived stem cells into robust engineered cartilage (Mauck *et al.* , 2006; Erickson *et al.* , 2012).

1.1.4.2 Scaffold type Scaffold selection of an engineered tissue is an equally delicate challenge with options including: biologically derived scaffolds, synthetic scaffolds, and scaffoldless strategies. Biologically derived scaffolds include both the agarose and alginate (marine-derived) scaffolds with little biological activity in mammals (Lee & Mooney, 2001;

Benya & Shaffer, 1982; Buschmann *et al.* , 1995; Mauck *et al.* , 2000), and cartilage derived matrix scaffolds (Cheng *et al.* , 2012; Garrigues *et al.* , 2014; Burnsed *et al.* , 2016; Rowland *et al.* , 2016), in which native cartilage is devitalized and cleaned of immunogenic material before breaking the matrix up for use as a scaffold. These scaffolds were originally chosen as a convenient system for homogeneously encapsulating the isolated cell population and maintaining proper cell phenotype. Scaffoldless approaches consist of seeding cells to coalesce and create highly-cellularized constructs which lack the geometrical constraint of a traditional scaffold material (Elder & Athanasiou, 2009; Bhumiratana *et al.* , 2014; Yamashita *et al.* , 2015; DuRaine *et al.* , 2015). Agarose as a scaffold has played a fundamental role in studies of both chondrocyte biology and in early tissue engineering work, as the scaffold retains a high proportion of the synthesized matrix molecules and readily encapsulates chondrocytes and other cells. Both cartilage derived and scaffoldless approaches have gained much attention in recent years and several small clinical trials are ongoing for each system.

1.1.4.3 Culture conditions Culture conditions of engineered cartilage were originally carefully titrated and validated in earlier works to ensure and enhance nutrient (oxygen and glucose) availability (Vunjak-Novakovic *et al.* , 1998; Obradovic *et al.* , 1999; Freed *et al.* , 1993). Most of these culture systems have been replaced with orbital shaking or perfusion platforms (Sittinger *et al.* , 1994), although sufficiency of nutrient availability in most systems is often not interrogated.

Media formulations, originally supplemented with fetal bovine serum (FBS), are now chemically-defined and supplemented with growth factors (Mauck *et al.* , 2003; Van der Kraan *et al.* , 2002). This change has enhanced reproducibility and tissue properties within the field. It is a seldom addressed issue, but one of great importance as engineers design larger sized constructs. Most modern systems utilize a formula consisting of at least glucose, insulin, amino acids, ascorbic acid, glucocorticoids (dexamethasone), and antibiotics/anti-mycotic (to prevent bacterial and mycotic growth) (Cigan *et al.* , 2013). The most notable growth factor administered is TGF-β which has been a fundamental simulator of matrix synthesis and helps maintain the chondrogenic phenotype of not fully differentiated stem cells.

1.1.5 Computational growth models

Interestingly, computational models played a large role in early studies of tissue engineered cartilage. Early models were used to assess the hydrodynamics, media perfusion, and cell seeding efficiency on early scaffolds where cell adherence could not be presumed (Vunjak-Novakovic *et al.* , 1998; Vunjak-Novakovic *et al.* , 1999). Subsequent analysis of the critical nutrient oxygen led to early growth models of the GAG content within the scaffolds based on oxygen availability (Obradovic *et al.* , 2000). This study was followed with an extension which also monitored radial tissue swelling over time (Nikolaev *et al.* , 2010). These seminal studies have illustrated the potential utility of a modeling framework which can examine how culture conditions translate to a tissue's functional properties. Furthermore, the authors illustrated the complex ecosystem in which biological growth phenomena occur. Despite their novelty, these computational models lacked the generalizability required to gain insights on culture conditions as they were fit and validated on the same data sets, had key parameters (such as GAG synthesis behavior, cell proliferation, and infinite supply nutrient concentration boundary conditions) coded directly into the equations, and were developed in a framework which only permitted a two-dimensional, cylindrical analysis. These models also illustrate two distinct classes of computational models which can be applied to engineered tissue growth: those that examine biochemical content only, and those that also predict the evolution of mechanical properties.

1.1.5.1 Biochemical models Biochemical models, the most commonly performed, often focus on using a prototypical nutrient (such as oxygen) to predict the levels of matrix synthesis within a tissue (Sengers *et al.* , 2004; Sengers *et al.* , 2005a; Zhou *et al.* , 2008; Soares & Sacks, 2016). The synthesized soluble matrix products then undergo reversible binding to the engineered scaffold (Wilson *et al.* , 2002; DiMicco & Sah, 2003; Klein & Sah, 2007; van Donkelaar *et al.* , 2011). More generalized models have focused on the dynamic role of cellular proliferation within engineered cartilage, leading to a potentially more faithful model of the evolving tissue system (Galban & Locke, 1999b; Galban & Locke, 1999a). Importantly, and in part due to the original experimental studies, matrix synthesis models are coded with a pre-set level of matrix content, at which matrix synthesis ceases.

1.1.5.2 Mechanical models Mechanical models are typically based on compositional models of native cartilage and have been used to investigate matrix compositional properties and the individual roles of different matrix molecules and collagen fiber orientation (Wilson *et al.* , 2004; Kelly & Prendergast, 2006; Nagel & Kelly, 2012; Khoshgoftar *et al.* , 2011; Khoshgoftar *et al.* , 2013a; Khoshgoftar *et al.* , 2013c). To bridge biochemical and mechanical models, some mechanical modeling approaches have used temporal deposition of material, although the role of growth has yet to be elucidated (Khoshgoftar *et al.* , 2013b).

1.1.5.3 Systems biology models Despite the sophistication of these biochemical and mechanical models, the utility of such model lie in the ability to depict the underlying physics of growth. In modern tissue culture systems, however, growth phenomena are often controlled ultimately by both the cells and growth factor administration schedules. Such advances in tissue culture have left the traditional computational models unable to meet the growth kinetics seen. To this end, recent advances in the field of systems biology have developed faithful models, but these work at the small scale of individual cells. Most notably for this work, TGF-β signaling models develop interesting insight into the modes by which cells respond to it (Zi *et al.* , 2011; Nicolás *et al.* , 2004; Dubrulle *et al.* , 2015). Such models, while only predictive of intracellular signaling cascades, are illuminating in that 1) the stimulation by TGF-β and other growth factors can be titrated and diminished over time and 2) stimulatory doses are influenced over a wide range of concentrations.

1.1.6 Unanswered questions in cartilage tissue engineering

While modern CTE techniques can now routinely engineer small cartilage constructs with native GAG and compressive modulus properties, challenges persist limiting the translation of this technology to clinical treatments. Of these, addressing two key challenges would immediately promote the acceptance of CTE into the clinic: 1) adequate scaling up of culture systems to develop large sized tissue replacements and 2) the development of robust mechanical properties in engineered cartilage constructs to match the native biomechanical environment of the tissue.

Due to the promising advances in CTE systems which approach native mechanical properties in small systems, several recent studies have worked to grow constructs in the shape of entire anatomical articular layers. However, without proper understanding of the nutrient demands within the tissue,

these constructs have exhibited significant matrix heterogeneities. Increased nutrient availability within these large tissues is a critical step for translating these systems to a state of clinical readiness. On this note, our lab's recent efforts to grow large constructs through the assembly of smaller pieces, while a potentially interesting technique for developing constructs of different tissue sizes, were performed irrespective of the high nutrient demands of the tissue. The heterogeneous matrix deposited played a detrimental role as tissue constructs failed at ≈0.2 MPa failure stress from the incomplete matrix deposition within the tissue. Native cartilage has a failure stress of greater than 10 MPa, suggesting that constructs would fail soon after implantation and under normal loading. Overall, the point should be stressed that current tissue engineering protocols are promising enough that overcoming the matrix heterogeneities within large constructs will be a significant advance towards moving constructs to the clinic.

To this end the unique and robust mechanical properties of native cartilage play a significant role in the proper function of the tissue. The high tensile modulus relative to compressive modulus is an essential part of the tissue having such low friction properties. For the engineered tissue constructs to be adequate, long-term replacements, they should best match these native cartilage functional properties. Thus an enduring goal of CTE has been developing native tensile mechanical properties within the tissue and coaxing resident cells into preferentially synthesizing a robust collagen network.

Ultimately, the ability to engineer large, anatomically-sized cartilage constructs with native tensile and compressive mechanical properties will be a major transition point towards moving more promising CTE technologies forward into clinical practice to address the clinical pains and problems which patients face.

1.2 Significance and Specific Aims

Osteoarthritis is degenerative disease of the articular cartilage that manifests itself once defects in the cartilage matrix become large enough to stimulate nerves in both the subchondral bone, ligaments, fat pads, and other soft tissues of the capsule in response to altered mechanical loading of the joint. The unique nature of cartilage, notably featuring a dense network of structural molecules to support the high loading environment, also give rise to a tissue which is avascular, aneural, and has a low resident cell population ultimately limiting the regenerative capacity of the tissue to small defects (Maroudas *et al.* , 1975; Stockwell, 1971a). When this limited repair capability fails, these small defects eventually erode into the large defects typical of symptomatic osteoarthritis (OA). To date, there are no widely-available clinical treatments to repair or resurface these large defects which are the source of much disability. Presently, the gold standard treatment is to manage the pain until the patient can no longer function, followed by a total joint replacement with an artificial joint.

Cartilage tissue engineering (CTE) is a promising cell-based therapy where a biochemically and biomechanically functional cartilage construct is engineered to replace and resurface the degenerative cartilage (Vacanti & Langer, 1999; Butler *et al.* , 2000). Seminal CTE studies nearly two decades ago produced the first promising proof-of-concept results for the engineering and development of a native cartilage analog for replacing defects of symptomatic OA (Benya & Shaffer, 1982; Freed *et al.* , 1993; Buschmann *et al.* , 1995).

Since this early work, an emphasis has been placed on using engineering and computational analyses to develop tissues more similar to native articular cartilage. In the early days of cartilage tissue engineering, the use of serum-based media produced tissues with heterogeneous levels of matrix synthesis and variable success rates. Recent biotechnology advances have improved the success rates and consistency of tissue engineering studies with quantitative and defined culture protocols that repeatedly produce similar results across multiple studies and labs. This level of consistency is encouraging and makes the application of quantitative computational models a suitable solution to addressing a complex, but reproducible, system.

Today's modern CTE techniques successfully engineer small-sized constructs with native GAG content and equilibrium compressive mechanical properties (Byers *et al.* , 2008; Lima *et al.* , 2007). While OA degeneration begins as small-sized defects, OA becomes symptomatic to patients only

once defects exceed ≈5 cm^2(Moisio *et al.* , 2009), limiting the utility and application of such small constructs into clinical practice. To this end, our lab and others have utilized nutrient channels to enhance matrix synthesis within large-sized constructs (Bian *et al.* , 2009a; Buckley *et al.* , 2009; Miller *et al.* , 2012; Sheehy *et al.* , 2014; Sheehy *et al.* , 2011). Our early work demonstrated that channels improve mechanical properties of constructs, although biochemical content was not enhanced with nutrient channels (Bian *et al.* , 2009a). At the same time, other labs were observing that large construct properties were not influenced by the incorporation of nutrient channels (Buckley *et al.* , 2009). Understanding the optimal spacing of channels and the modes by which engineered cartilage growth are influenced by channels therefore became an important milestone as engineers worked to grow large, anatomically-sized cartilage constructs. Too few channels would not allow adequate nutrient availability while too many channels would remove the tissue essential for cells to deposit matrix and develop the structural properties necessary to match native cartilage. Moreover, understanding the influence of enhanced nutrient availability and more homogeneous tissue properties is a critical task for enhancing engineered cartilage mechanical (functional) properties.

The specific aims of this work are focused around the paradigm of developing, informing, and using computational growth models to improve and optimize engineered cartilage culture protocols and using experiments to inform, validate, test, and confirm computational models and predictions. Experiments and models first address the development of computational growth models of the biochemical growth in engineered cartilage constructs. Based on the success of these results and experimental outcomes, models and experimental focus on the mechanical implications of de novo cartilage growth. The specific aims are divided into two distinct, but coordinated, tasks. Specific Aims 1.2, 1.2, and 1.2 (Part I) examine the nutrient conditions within developing engineered cartilage constructs and their influence on the evolving biochemical composition of the tissue. Specific Aims 1.2 and 1.2 (Part II) then utilize the understanding of the biochemical environment from Aims 1.2, 1.2, and 1.2 to develop computational models of evolving mechanical properties within developing tissues, and to enhance culture protocols that improve tissues' functional properties.

Specific Aim 1: Assess critical nutrient availability within engineered cartilage constructs

Specific Aim 1 experimentally characterizes the growth of small engineered tissues and monitors the transport properties of the critical nutrients identified for the [bovine chondrocyte]-[agarose gel] tissue engineering system, being predominately glucose and active TGF-β3. Although these nutrients were identified in previous studies to be critical for growth, using computational models to assess their availability for our own system-specific construct geometries and culture conditions allows us to answer the question of "how best can we ensure adequate nutrient availability." Moreover, as TGF-β plays a transformational role in the nutrient demands of the tissues, further experiments were performed with oxygen and inorganic sulfate to investigate whether TGF-β increases demands of these nutrients as well.

Specific Aim 2: Assess matrix deposition rates and binding characteristics within engineered cartilage constructs

In light of a more fundamental understanding of the critical nutrients of concern in our engineered tissue system, Specific Aim 2 interrogates how matrix synthesis is governed in response to both adequate and inadequate nutrient availability. In small constructs with sufficient nutrition, the critical structural proteins of engineered cartilage are determined and their characteristic deposition behaviors are extracted. This, for the first time, allows us to investigate our prior experimental attempts at growing large-sized anatomical patella constructs.

Specific Aim 3: Develop and validate relations between the key nutrients glucose and active TGF-β3 and the cellular proliferation and matrix synthesis within engineered cartilage. Use models for optimizing the arrangement of nutrient channels within engineered cartilage constructs.

Specific Aim 3 begins constructing the first comprehensive finite element growth models based on the modern, standardized, engineered cartilage culture protocols. This work builds off the nutrient models of Specific Aim 1 and the matrix deposition models of Specific Aim 2. As a first step we grew small constructs with varying TGF-β doses to investigate the various growth

mechanisms behind TGF-β supplementation. Based on the culmination of these previous works, we implemented and developed both matrix synthesis and cellular proliferation models based on the TGF-β availability. While not examined in most models of cartilage growth, the influence of cellular proliferation and initial cell seeding density proved influential in the predictive power of the computational models. This work represents a significant advance in our ability to predictively assess the success of engineered tissue culture based on matrix deposition within constructs of various cell densities and geometries.

Specific Aim 4: Experimentally measure and computationally model mechanisms of the growth underlying engineered cartilage maturation and mechanical growth.

Building off these biochemical growth models, Specific Aim 4 develops physical growth models of engineered cartilage. As cartilage constructs will ultimately be required to undergo implantation in the dynamically loaded joint environment, it is a critical step to determine how culture conditions influence the mechanical properties of the developing tissue in addition to the biochemical content. However, no engineered cartilage growth models had been proposed in the prior literature. The work of this aim therefore presents the first set of experimental and computational models to support a mechanism of matrix synthesis mismatch between GAG synthesis and collagen deposition to explain the large swelling seen in our engineered cartilage. This work further provides the first set of fundamental, generalized modeling for the biological growth of engineered tissues through a mixture of structural constituents. This provides us with a level of modeling sophistication which can now anticipate the developing mechanical properties in engineered cartilage during growth.

Specific Aim 5: Develop and utilize a constraint-based culture system (cage) to improve the functionality of engineered cartilage; test the cage approach in both agarose scaffolds and also cartilage devitalized matrix hydrogel scaffold.

The growth and remodeling insights into engineered cartilage which the computational models of Specific Aim 4 afforded us, presented us with a direct and fundamental target to improve the mechanical properties of engineered cartilage through enhanced support of the developing collagen framework. Specific Aim 5 developed and experimentally cultured constructs within a cage system in the presence of sufficient nutrition to improve the collagen stability of growing tissues. As the

fundamental theories on which a supportive cage was developed are contingent only on the mismatch of GAG and collagen, both agarose and cartilage derived matrix hydrogels were tested within the cage systems. Constructs cultured in cages with both scaffolds had improved mechanical properties and enhanced collagen cross-linking. This suggests the cage system will be a promising advance in the future of cartilage tissue engineering technology.

1.3 Detailed Specific Aims

Specific Aim 1: Assess critical nutrient availability within engineered cartilage constructs

Over a decade ago, a strong translational effort in our lab was made to engineer the first anatomical patella cartilage construct. While an achievement for the time, the study was instructive on the physical limitations of engineering large-sized, engineered cartilage tissues. The purported culprit hindering this initial attempt of engineering an anatomically-sized construct was the inability of critical nutrients to reach within the interior of the constructs. Notably, the patella construct (with an articular layer thickness of up to 7 mm) was significantly larger than any prior cartilage constructs and the tissue displayed severe matrix heterogeneities, with matrix deposition occurring predominantly near the tissue periphery and little deposition occurring within the center of the construct.

In a subsequent effort, coring a single $\varnothing$ 1 mm channel in a $\varnothing$ 4 mm construct or three $\varnothing$ 1 mm channels within a $\varnothing$ 10 mm construct could improve functional tissue properties. Moreover, previous efforts using both serum-based and chemically-defined media formulations had demonstrated increases in functional properties when tissues were cultivated with adequate nutrient supply. Together, these studies suggested that nutrient limitations can be overcome with channels and understanding the precise nutrient deficiencies within large engineered tissues.

To this end, this aim examines the role and availability of such "critical" nutrients and develops computational models based on the consumption of the critical nutrients to determine whether these nutrients are limiting in the culture of large tissue constructs. Based on our experimental work up to this point, we have characterized the role of both glucose and TGF-β for their growth-limiting roles and have characterized the critical internalization (consumption) rates and the growth-limiting concentration of glucose (Cigan *et al.* , 2013; Nims *et al.* , 2015; Albro *et al.* , 2016).

Specific Aim 1.1: Develop and implement computational models based on culture conditions, construct geometries, and consumption kinetics of glucose.

Specific Aim 1.2: Alter culture conditions (glucose supply) to identify a media volume at which glucose will always be at concentrations that promotes growth.

Specific Aim 1.3: Building from Specific Aim 1.2, develop computational models based on the transport and binding of active TGF-β to investigate transport within engineered cartilage.

Specific Aim 1.4: Experimentally measure the dependence of matrix growth on oxygen and sulfate.

Completing these sub-aims will advance our understanding of how the critical nutrients are distributed during engineered cartilage growth and how their availability can be enhanced through culture conditions.

Specific Aim 2: Assess matrix deposition rates and binding characteristics within engineered cartilage constructs

Developing computational growth models further requires models of the matrix synthesis and deposition behaviors within the engineered tissues. For computational efficiency, like the nutrient models previously, modeling only the critical structural molecules for engineered cartilage deposition is essential. In native cartilage the structural molecules are negatively charged proteoglycans (made up of glycosaminoglycans, GAG, chains) and type II collagen. Minor structural proteins however, such as cartilage oligomeric matrix protein (COMP), lubricin, pyridinoline, and hyaluronan, are purported to further play a role in the mechanics of engineered cartilage.

We first struck out to examine the deposition of extracellular matrix proteins and which proteins play a critical role in the developing mechanics of the tissue. The binding and deposition characteristics were then fit according to a computational model description of reversible matrix binding throughout construct culture. Such models can be implemented with the descriptions of glucose availability, a simple relation based on the work of Specific Aim 1.2, to develop computational models of the interactive dependence of glucose availability and matrix deposition.

Specific Aim 2.1: Experimentally characterize the deposition and matrix release profiles of GAG, collagen, and COMP within small engineered cartilage constructs.

Specific Aim 2.2: Computationally fit the matrix deposition and release profiles to a reversible reaction kinetics model of the developing cartilage constructs.

Specific Aim 2.3: Experimentally characterize dependence of correlations of matrix deposition on cell density and hyaluronan content within small engineered constructs.

Specific Aim 2.4: Develop computational models of the interactions between glucose availability (developed and validated in Specific Aim 1) and matrix deposition in an anatomical construct.

Completing these sub-aims will advance our understanding of the critical matrix molecules of engineered cartilage that must be modeled for growth and how simple nutrient availabilities dictate the spatial deposition of matrix growth.

Specific Aim 3: Develop and validate relations between the key nutrients glucose and active TGF-β3 and the cellular proliferation and matrix synthesis within engineered cartilage. Use models for optimizing the arrangement of nutrient channels within engineered cartilage constructs.

Based on the system identification parts in Specific Aims 1.2 and 1.2, we can develop comprehensive computational models for the developing constructs in the presence of glucose and TGF-β via the biochemical deposition and maturation of GAG and collagen within the tissue. While the bulk of the parameters will be built from the models of the first two aims, a relation between the growth of engineered cartilage and the availability of TGF-β remains unknown.

The first investigations into the stimulatory role of TGF-β were crucial in establishing the dose dependence of TGF-β (Byers *et al.* , 2008), but in light of the severe heterogeneity of the tissue, an increased range of TGF-β supplementation levels is required for modeling the differential stimulation of TGF-β. Moreover, based on the experimental channel studies of (Nims *et al.* , 2015)

and (Cigan *et al.* , 2016c), there are contradicting experimental results which may indicate a strong dependence of the channel-spacing optimization on the initial cell seeding densities of the constructs. Models must therefore the able to examine the influence of cell density and proliferation on the growth kinetics of the developing tissue. Once validated, models can be used to assess how different cell culture factors and tissue geometries influence the growth of tissue development.

Specific Aim 3.1: Experimentally investigate the role of a wide range of active TGF-β3 concentrations on cellular proliferation, GAG and collagen deposition, and construct growth.

Specific Aim 3.2: Develop and implement computational models based on the matrix synthesis and binding and nutrient consumption and transport models to link the availability of active TGF-β3 and glucose to cellular proliferation and matrix synthesis. Fit model growth parameters to experiments of Specific Aim 3.1.

Specific Aim 3.3: Using the matrix synthesis and cellular proliferation models of Specific Aim 3.2, validate models against previously published channel studies using channel-specific finite element model geometries and adapting models to reflect: construct geometry, culture conditions (media bath volume, nutrient concentration, and media resupply rate), and initial cell seeding density.

Specific Aim 3.4: Simulate the growth of engineered constructs using a variety of engineered construct geometries and initial cell seeding densities to observe optimal construct geometries to maximize matrix deposition.

Completing these sub-aims will advance our understanding of the complex interactions between the developing biochemical content of engineered tissues with the culture conditions, construct geometry, and cell seeding density of the tissues.

Specific Aim 4: Experimentally measure and computationally model mechanisms of the growth underlying engineered cartilage maturation and mechanical growth.

In both native and engineered cartilage, the biochemical and mechanical properties develop hand and hand with the maturation of the the tissue. To withstand the robust mechanically-loaded environment within the joint, engineered cartilage must match the functional properties of the native tissue. While tissue engineering efforts have been successful in matching the GAG content of native cartilage, it is unclear how the deposition of newly synthesized GAGs and collagens influence the mechanical properties of developing engineered cartilage. Traditional structural models of cartilage, which approximate the mechanical roles of both GAG and collagen, have been validated only for native, mature cartilage in which the tissue has reached a steady-state metabolism with little turnover. Engineered cartilage, however, experiences a rapid level of growth that cannot be adequately explained by these former models.

In Specific Aim 1.2, we will experimentally grow engineered constructs to examine the growth kinetics underlying their mechanical and physical changes. Interestingly, in our prior experiments of Specific Aims 1.2, 1.2, and 1.2, constructs supplied with sufficient nutrition begin to expand and grow when supplied with sufficient nutrition. This swelling is matched by a plateauing in mechanical properties in a phenomenon which the literature deems as "tissue maturation." Despite this "maturation," however, constructs continue to expand and grow under the continued synthesis of matrix proteins. The mechanisms underlying this growth are yet unknown and uncharacterized.

This aim examines the physics of the continued growth using both experimental measures of matrix turnover and changes and computational models to quantitatively describe and validate such changes.

Specific Aim 4.1: Experimentally investigate the role of elevated cell seeding density (120 million cells mL^{-1}) on constructs growth under both untreated and chondroitinase ABC treated constructs.

Specific Aim 4.2: Develop and implement computational damage models based on the experimental matrix synthesis of Specific Aim 4.1 to fit the physical growth (tissue swelling ratio, SR, and unconfined compressive modulus, E_Y). Validate models according to the chondroitinase ABC studies according to SR and E_Y.

Specific Aim 4.3: Synthesize the validated physical growth models with the validated biochemical growth models to develop a comprehensive model informed by culture conditions and construct geometry and predictive of mechanical properties and tissue growth.

Completing these sub-aims will advance our understanding of the mechanism of growth within engineered cartilage constructs.

Specific Aim 5: Develop and utilize a constraint-based culture system (cage) to improve the functionality of engineered cartilage; test the cage approach in both agarose scaffolds and also cartilage devitalized matrix hydrogel scaffold.

The experimental findings of Specific Aim 1.2 illustrate that the high and rapid synthesis of GAG relative to the restraining force of deposited collagen can disrupt the deposition of new collagen within the construct and leads to the plateauing of mechanical properties despite continued matrix synthesis and deposition. To enhance the collagen framework during engineered cartilage development we propose using a mechanical restraint ("cage") system to maintain the mechanical integrity of the nascent collagen framework.

We further suspect that due to the predominance of excess GAG synthesis, relative to collagen synthesis, across the field of tissue engineering, that this method is readily translatable to a number of different engineered cartilage systems. To test this, we apply the cage system to a tissue engineering system using a cartilage derived matrix hydrogel (CDMH) scaffold system. CDMH scaffolds are gaining in popularity as the tissue engineering field looks to match the cellular niche

which chondrocytes typically occupy for improving the properties of developing tissues.

To investigate the use of a cage system to improve functional tissue properties, the following two specific aims are performed.

> **Specific Aim 5.1: Experimentally culture engineered cartilage constructs using an agarose scaffold in a mechanical constraining cage assembly and under free-swelling (control) conditions to assess the mechanical property enhancement when the collagen framework develop is enhanced through cages.**
>
> **Specific Aim 5.2: Experimentally culture engineered cartilage constructs using a cartilage derived matrix hydrogel scaffold in a mechanical constraining cage assembly and under free-swelling (control) conditions to assess the mechanical property enhancement when the collagen framework develop is enhanced through cages.**

Completing these sub-aims will advance our understanding of how experimental methodologies based on the fundamental growth mechanisms of engineered cartilage can produce superior tissues across a range of cartilage tissue engineering systems.

Part I

Biochemical Growth Models and Experiments

Chapter 2 Models of glucose availability in channeled tissue constructs and remediation with increased glucose supply

2.1 Abstract

Cartilage tissue engineering is a promising approach to resurfacing osteoarthritic joints. Existing techniques successfully engineer small-sized constructs with native levels of extracellular matrix (glycosaminoglycans (GAG) or collagen). However, a remaining challenge is the growth of large-sized constructs with properties similar to those of small constructs, due to consumption and transport limitations resulting in inadequate nutrient availability within the interior of large constructs. This study employed system-specific computational models for estimating glucose requirements of large constructs, with or without channels to enhance nutrient availability. Based on glucose requirements for matrix synthesis in cartilage constructs, computational simulations were performed to identify the media volume (MV) and the number of nutrient channels (CH) needed to maintain adequate glucose levels within tissue constructs over the three-day period between media replenishments. In Study 1, the influence of media volume (MV: 5, 10, 15 mL/construct) and number of nutrient channels (CH: 0, 3, 7, 12 per construct) on glucose availability was investigated computationally for ∅10 mm × 2.34 mm cylindrical constructs. Results showed that the conventionally used MV 5 led to deleterious glucose depletion after only 40 h of culture, and that MV 15 was required to maintain sufficient glucose levels for all channel configurations. Study 2 examined experimentally the validity of these predictions, for tissue constructs cultured for 56 days. Matrix elaboration was highest in MV 15/CH 12 constructs (21.6±2.4 %/ww GAG, 5.5±0.7 %/ww collagen, normalized to wet weight (ww) on day 0), leading to the greatest amount of swelling (3.0±0.3 times day-0 volume), in contrast to the significantly lower matrix elaboration of conventional culture, MV 5/CH 0 (11.8±1.6 %/ww GAG and 2.5±0.6 %/ww collagen, 1.6±0.1 times day-0 volume). The computational analyses correctly predicted the need to increase the conventional media levels three-fold to support matrix synthesis in large channeled engineered constructs. Results also suggested that more elaborate computational models are needed for accurate predictive tissue engineering simulations, which account for a broader set of nutrients, cell proliferation, matrix synthesis, and

swelling of the constructs.

2.2 Introduction

Osteoarthritis (OA) is a debilitating, degenerative disease that degrades the articular cartilage of diarthrodial joints, compromising its low-friction, load bearing function (Krishnan *et al.* , 2004; Mow *et al.* , 1984; Stockwell, 1979). OA often becomes symptomatic only after large focal defects (≈5 cm^2) have appeared, eventually progressing to encompass most of the articular surface (Moisio *et al.* , 2009). Cartilage tissue engineering (CTE) is a promising technique for the treatment of OA. In our vision, a tissue replacement would be cultured first in vitro to develop a robust native matrix prior to in vivo implantation into the large focal defects (Hunziker, 2002).

While conventional culture techniques can successfully engineer small constructs (≈0.1 cm^2) approaching native levels of glycosaminoglycans (GAG) and collagen (Lima *et al.* , 2007; Byers *et al.* , 2008), culturing large constructs for resurfacing clinically relevant defect sizes remains a challenge (Hung *et al.* , 2003; Hung *et al.* , 2004). Consumption by cells in the construct's peripheral regions hinders the transport of nutrients critical for matrix synthesis in the inner regions, limiting the size to which functional constructs can be grown. To overcome transport limitations, several strategies have been employed for enhancing nutrient availability. Heywood et al. demonstrated that increasing media volume in cultures of small [primary bovine chondrocyte]-[alginate] constructs enhanced extracellular matrix (ECM) elaboration and homogeneity (Heywood *et al.* , 2006b; Heywood *et al.* , 2006a). More recently, our lab and others have incorporated nutrient channels into large constructs. This reduction in nutrient path length within large constructs produced tissues with higher compressive mechanical properties and improved matrix distribution over channel-free constructs, although differences in total matrix content were insignificant (Bian *et al.* , 2009a; Buckley *et al.* , 2009; Cigan *et al.* , 2016c). Despite these advances, our limited understanding of the specific nutrient requirements for construct synthesis compromises the application of culture strategies to larger constructs. This notion is supported by the variability of media supply rates found in the literature (Table 1) (Heywood *et al.* , 2004; Hu & Athanasiou, 2006; Buschmann *et al.* , 1992; Buckley *et al.* , 2009; Vunjak-Novakovic *et al.* , 1996; Obradovic *et al.* , 1999; Davisson *et al.* , 2002b; Kisiday *et al.* , 2002; Mauck *et al.* , 2002; Nims *et al.* , 2014).

The aim of our study was to formulate and validate system-specific computational models for estimating the nutrient supplies needed to engineer large tissues, with or without nutrient channels. These models may account for system-specific ECM synthesis and nutrient consumption. This study focused specifically on the supply of glucose in the [juvenile bovine chondrocyte]-[agarose gel] CTE system. In our recent experimental study of cellular glucose consumption and matrix synthesis in small constructs (⌀4 mm × 2.34 mm), a glucose concentration of 12.5 mM was identified as the nutrient threshold below which the ECM synthesis ceased (Nims *et al.* , 2014; Cigan *et al.* , 2013). This threshold represented half the initial glucose concentration of 25 mM in standard cell culture media, suggesting that such standard conditions may easily lead to nutrient depletion in tissue engineering studies when the media/cell ratio is inadequate. Indeed, preliminary simulations conducted for this study suggested that our standard culture conditions fail to supply larger (⌀10 mm × 2.34 mm) constructs with adequate glucose levels for ECM elaboration. Consequently, placing nutrient channels into constructs would be ineffective under those conditions, potentially leading to confounding results if nutrient levels were not accounted for.

Motivated by these insights, we investigated whether computational models, informed by this critical glucose threshold and experimentally characterized glucose consumption rates, can identify adequate levels of media volume per construct to ensure optimal matrix synthesis during tissue culture for a variety of channel configurations. To this end, finite element (FE) models were first used to simulate the influences of media volume and nutrient channel density on the glucose concentrations within large constructs (Study 1); in this manner, the theoretical conditions required for sufficient glucose availability were identified. Informed by Study 1, large constructs were experimentally cultured for 8 weeks under these computationally predicted suboptimal and optimal conditions, and their mechanical properties and biochemical composition were assessed (Study 2).

2.3 Methods

2.3.1 Nutrient simulations

Nutrient supply and consumption models were performed in FEBio (www.febio.org) to simulate the glucose concentration in tissue constructs and their surrounding bath throughout a three-day culture period (Ateshian *et al.* , 2014; Maas *et al.* , 2012). These models employ a multiphasic mixture

Study	Cells per construct (millions)	Media volume (mL)	Day	Glucose supply (µmol/million cell/day)
Buschmann, 1992	4.0	2	1	12.4
Vunjak-Novakovic, 1996	7.0	3	1	10.7
Obradovic, 1999	5.0	5	3	8.3
Mauck, 2002	1.7	0.5	3	2.4
Davisson, 2002	20	12.5	3	5.2
Kisiday, 2002	76.8	12	2	1.9
Heywood, 2004	200	20	3	0.7
Hu, 2006	5.5	0.5	1	2.27
Buckley, 2009	3.75	3	3	18.4
Nims, 2014	0.88	0.5	3	4.7
This work	11.0	15	3	11.3

Table 1: Culture conditions were used to calculate the daily media replenishment volume per million cells and the daily moles of glucose replaced per million cells. All media was based on 25 mM glucose except Heywood, 2004.

framework that accounts for chemical reactions, simulating glucose transport from the bath into the construct, glucose diffusion within the construct, and glucose consumption by chondrocytes (Nims *et al.* , 2014). Chondrocytes were not modeled explicitly, but their consumption of glucose was described by a 'sink' rate uniformly distributed across the construct geometry to represent a similarly homogeneous cell-seeding density. In the standard 2-2-3-day media change schedule, the three-day period simulated here represented the longest duration without nutrient replenishment. Based on the system-specific experimental parameters (glucose threshold and glucose consumption rate (Nims *et al.* , 2014; Cigan *et al.* , 2013), simulations were performed to identify the culture conditions that prevent the glucose concentration throughout the construct from dropping below the glucose threshold for ECM synthesis.

Constructs were modeled as being suspended within a well-stirred bath, boundary conditions representative of the experimental configuration (Cigan *et al.* , 2013). The bath was modeled explicitly and well-stirred conditions were simulated using glucose diffusivity one thousand times higher than in the construct (Nims *et al.* , 2014). FE model geometries and meshes (CUBIT, Sandia National Laboratory) matched the geometries of several candidate channel and bath configurations (Figure 2.1): constructs (⌀10 mm × 2.34 mm) suspended within a media bath volume of 5, 10, or 15 mL (MV: 5, 10, and 15) and configured with either 0, 3, 7 or 12 channels (CH: 0, 3, 7, 12), gener-

ating a total of 12 culture conditions. CH groups represent triangular packing arrangements of ∅1 mm channels that may be inscribed symmetrically within a ∅10 mm construct; the MV groups were selected such that the lowest (5 mL/construct) represented a typical media/cell ratio employed in CTE experiments (Table 1), while the highest (15 mL/construct) was predicted to supply adequate glucose according to the nutrient threshold. As these geometries exhibited both axial and radial symmetries, symmetrical representative regions (CH 0, 3, 12: 60°, CH 7: 30°; all: half-thickness) were modeled with symmetry planes (zero-flux boundaries) shown in Figure 2.1 (bottom).

To examine how an infinitely large (or continuous) supply of fresh media would influence construct glucose concentrations, simulations were also run with a fixed 25 mM glucose concentration prescribed at the construct surface (group MV∞).

Glucose was modeled as an uncharged solute with a constant free diffusivity, $D_o = 9.2 \times 10^{-4}$ mm^2 s^{-1}, and mixture diffusivity 8.7×10^{-4} mm^2 s^{-1} (Sengers *et al.* , 2005a); the constructs had solid volume fractions of 2%, typical of freshly cast constructs. Glucose transport and supply were related through mass balance,

$$\frac{\partial c^{glu}}{\partial t} - \text{div}\left(D \text{ grad } c^{glu}\right) = \hat{c}^{glu}$$

where c^{glu} is the glucose concentration and $\hat{c}^{glu}$ is the glucose supply resulting from chemical reactions. A nominal construct cellularity of 60 million cells mL^{-1} was utilized to inform the glucose consumption rates of the construct material. To account for variability in the cell glucose consumption rates, simulations for each culture condition were based on the mean, 1.24×10^{-13} mol h^{-1} cell^{-1}, and 95% confidence interval (CI) limits, 0.69 – 1.81 $\times 10^{-13}$ mol h^{-1} cell^{-1}, of the glucose consumption rate for this culture system (Nims *et al.* , 2014). Cellular glucose consumption was modeled according to Michaelis-Menten kinetics,

$$\hat{c}^{glu} = \frac{V_{max}^{glu} c^{glu}}{K_m + c^{glu}}$$

where V_{max}^{glu} is

the maximal glucose consumption rate of the tissue (with mean value of 2.07 µM s^{-1} and 95% CI limits of 1.15 – 3.03 µM s^{-1}) and K_m is the Michaelis constant, 0.35 mM (Johnson & Goody, 2011;

Windhaber *et al.* , 2003). The initial glucose concentration in both the media and construct materials was 25 mM, based on high-glucose Dulbecco's Modified Eagle Media. Models simulated a 72 h period during which glucose consumption occurred in the construct and glucose transport from the surrounding bath occurred via passive diffusion through the construct. After the culture simulation, the minimum glucose concentration within the construct was determined.

2.3.2 Experimental culture and analysis

Experimental culture is described in both (Cigan *et al.* , 2014) and (Nims *et al.* , 2015). Constructs were cultured as idealized by the models with either 0, 3, or 12 nutrient channels (CH0, 3, 12) and in either 5, 10, or 15 mL media per construct (MV 5, 10, 15).

2.4 Results

2.4.1 Nutrient simulations

Glucose consumption by the cells within constructs caused the projected glucose concentrations to drop throughout the construct and bath substantially below the initial concentration (25 mM), with glucose levels varying spatially throughout the constructs (Figure 2.2). Channels enabled the maintenance of more homogeneous glucose concentrations, whereas channel-free constructs exhibited large concentration gradients between the construct surface and center. The temporal evolution of the minimum glucose concentration (at the construct center) is presented in Figure 2.3, based on average cellular consumption rate. These results show that at low media supply (MV 5), glucose concentrations were below the 12.5 mM threshold for all CH configurations as early as 40 h for CH 0 and 50 h for CH 12 after medium change. Conversely, for MV 15, glucose concentrations exceeded the threshold level throughout the 72 h of culture for all CH groups. The MV 10 group maintained the glucose levels slightly above the threshold for all CH groups at 72 h. However, when examining the effect of cell consumption rate variability (Figure 2.4), results show that the MV 10 groups mostly straddle the critical threshold concentration, especially for CH 0 and CH 3. Only the MV 15 group consistently exceeded the glucose concentration threshold for all channel configurations.

On average, the minimum construct glucose concentration increased by 8.4 mM between the MV 5 and MV 10 groups, and by 2.7 mM between the MV 10 and MV 15 groups (Figure 2.3). For

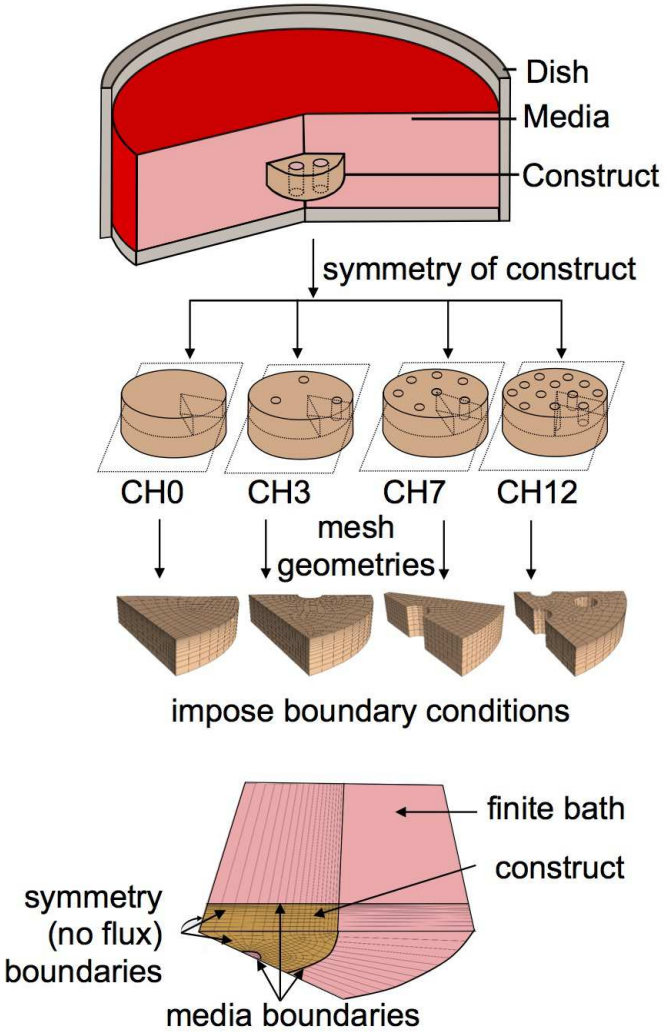

Figure 2.1: Experimental configuration. Theoretical models were developed for channeled constructs suspended in a well-mixed bath. Constructs (with 0, 3, 7, and 12 channels each) were modeled according to the available symmetry (axial and radial). Models featured a finite media bath, either 5, 10, or 15 mL; constructs then had either a media bath boundary conditions (lateral, top, and channel, if present, surfaces) or no flux boundary conditions (sagittal cut edges and bottom transverse plane); as shown is CH 3/MV 5 configuration.

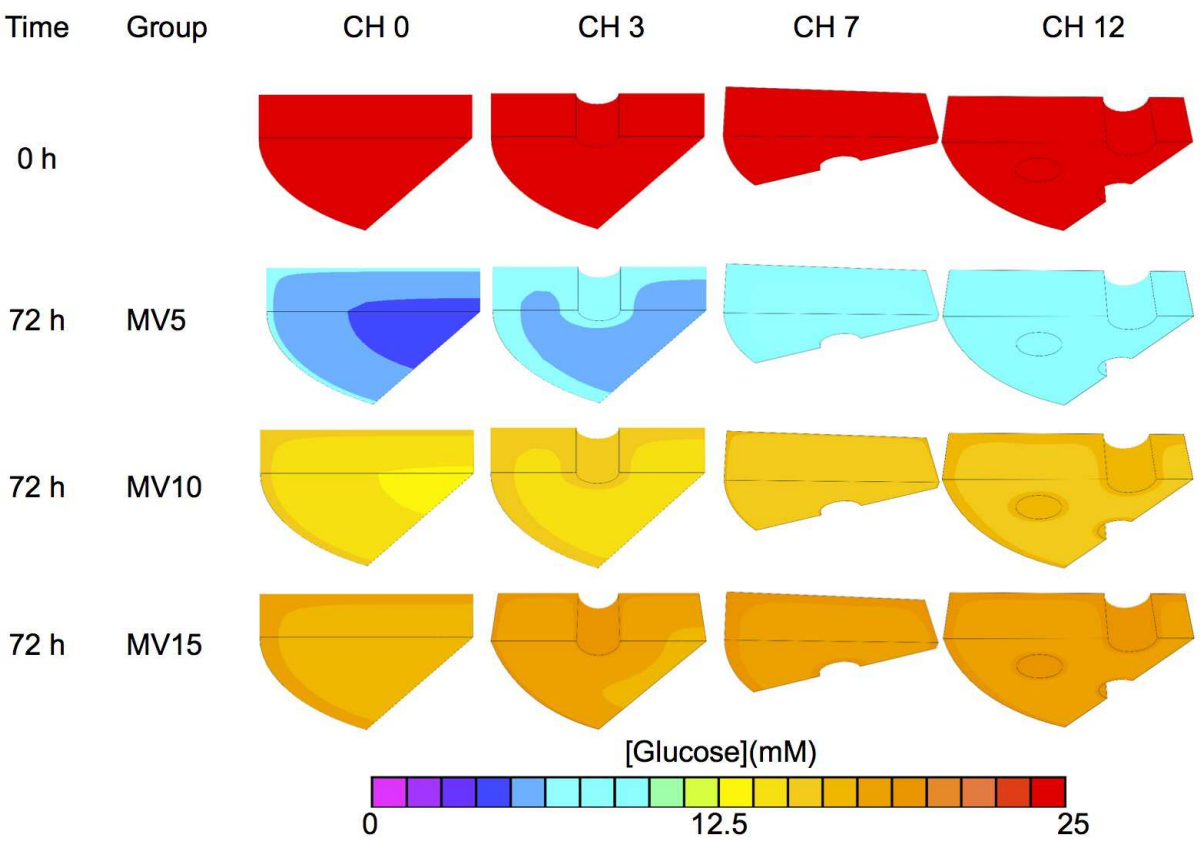

Figure 2.2: Model-predicted influence of channels (0, 3, 7, and 12 channels per construct) and media volume (MV 5, 10, 15 mL per construct) on glucose profiles within constructs after 72 h of culture.

a given MV, the minimum glucose concentration within the construct increased by an average of 0.6 mM between each CH level (i.e. 0 to 3, 3 to 7, or 7 to 12). The MV∞ group further elevated minimum glucose concentrations; minimum construct glucose concentration of the CH 0, 3, 7 and 12 constructs were 23.2, 23.4, 23.8 and 24.4 mM, respectively, at 72 h. From these predictions, it became evident that increasing MV led to diminishing returns in glucose availability; a MV of 15 was sufficient to elevate all CH groups with 95% confidence above the 12.5 mM threshold (Figure 2.4). Therefore, this MV was selected as the highest media volume for experimental culture.

2.4.2 Experimental results

Experimental results are described in depth in both (Cigan *et al.* , 2014) and (Nims *et al.* , 2015) (Figure 2.5). Briefly, construct mechanical properties were similar between all groups, although

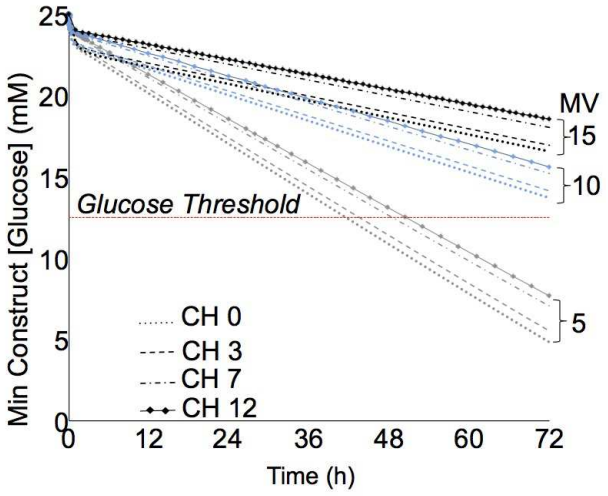

Figure 2.3: Theoretical predictions of the minimum glucose concentration within the construct over the 72 h culture period. Trend lines represent the mean level of glucose consumption for the different channel configurations (dotted line: CH 0; dashed line: CH 3; dot-dashed line: CH 7; line-through dots: CH 12) and media supplementation volumes (light grey: MV 5; dark grey: MV 10; black: MV 15). Horizontal dashed line denotes the critical glucose threshold for matrix synthesis (12.5 mM).

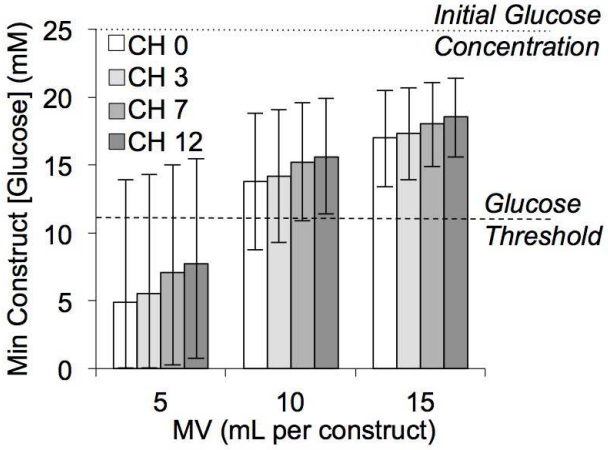

Figure 2.4: Theoretical predictions of the minimum glucose concentration within the construct after the 72 h culture period. Bar value represents mean glucose consumption level; high error bar represents the low 95%-CI consumption level; low error bar represents the high 95%-CI consumption level. Dotted line denotes initial glucose concentration (25 mM); dashed line denotes the critical glucose threshold for matrix synthesis (12.5 mM).

swelling was significantly higher with additional media supply. When normalized to the current day (day 56) wet weight, biochemical contents were similar for all culture groups. Conversely, when normalized to the day-0 (initial) wet weight, constructs grew significantly more with additional channels and media supply.

2.5 Discussion

The objective of this study was to formulate and validate system-specific computational models for estimating nutrient supplies needed to culture large engineered tissues, with or without nutrient channels. Based on our recent investigations, which reported the glucose threshold necessary for matrix synthesis and a representative glucose consumption rate in our CTE system (Nims *et al.* , 2014; Cigan *et al.* , 2013), we focused on the availability of glucose as an essential nutrient. Predictions from the simulations indicated that standard media/cell ratios used in studies of smaller constructs (Table 1) may be inadequate for culturing larger constructs, and that channel incorporation alone would not ameliorate this nutrient depletion. According to the models, higher media volumes would be required for maximal matrix elaboration and greater effectiveness of nutrient channels, as related to glucose.

With this guidance, constructs (CH 0, 3, 12) were experimentally cultured at standard (MV 5 per ∅10 mm × 2.34 mm construct) or elevated (MV 10 and 15) media volumes, to investigate the validity of computational predictions. Prior investigations of this culture system with constructs of this size or smaller have demonstrated that chondrocytes maintain their morphology throughout the construct (Cigan *et al.* , 2013; Benya & Shaffer, 1982; Aydelotte & Kuettner, 1988; Lee & Bader, 1997; Dimicco *et al.* , 2007). When examining total matrix elaboration, as represented by D0ww-normalized compositional measures in Figure 2.5, increasing MV produced significantly greater ECM deposition (GAG and collagen, Figure 2.5D, F). Nutrient channels further increased ECM deposition, with the most dramatic CH-induced enhancements evident in the presence of high MV (Figure 2.5D & F). These experimental results supported the model predictions that standard media/cell levels produced sub-optimal matrix synthesis and that channels at standard media levels do not demonstrate much effectiveness for larger constructs.

While GAG and collagen content normalized by D0ww illustrated differences in ECM synthesis as a function of MV and CH, these differences were not evident when using the more conventional

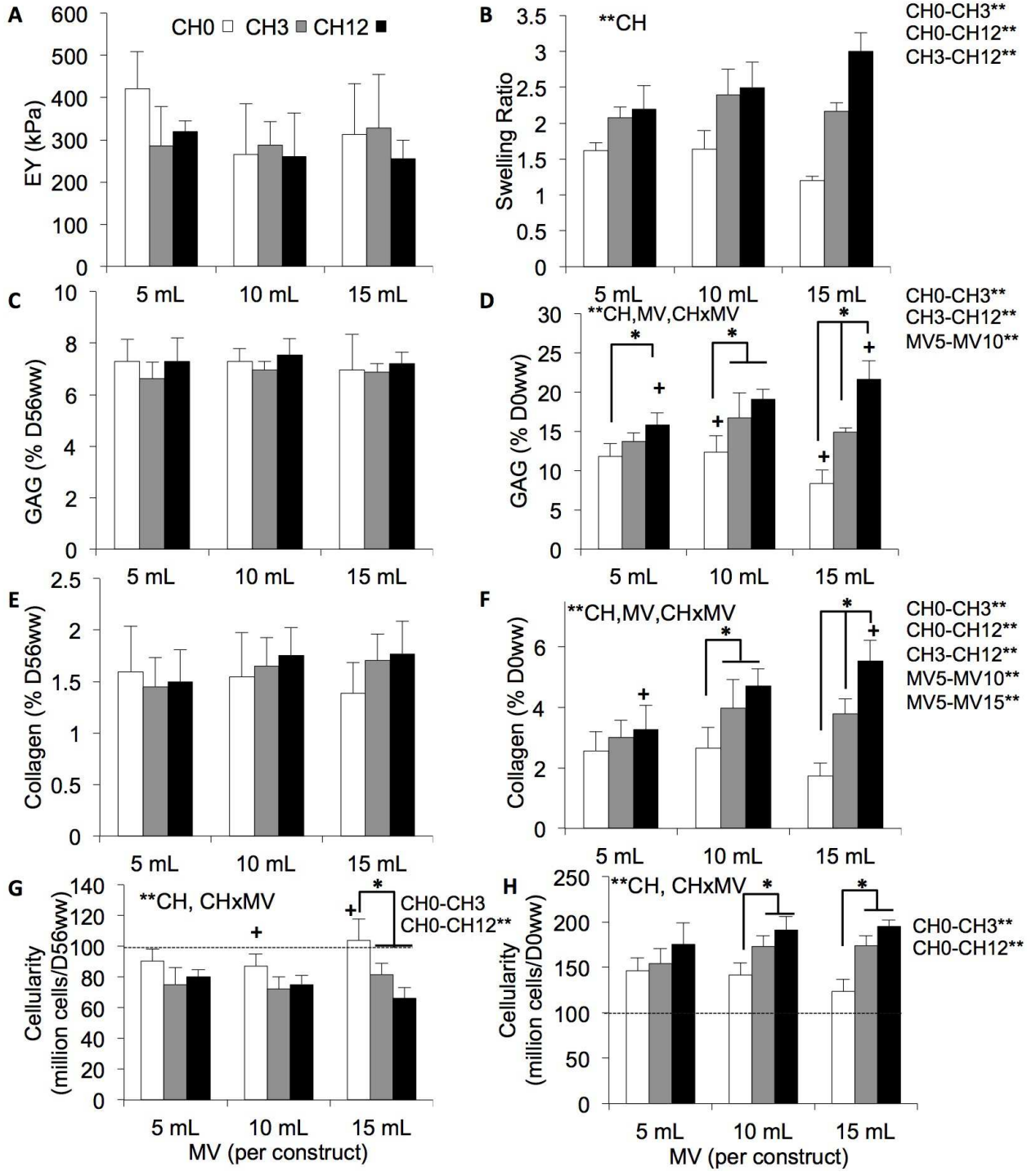

Figure 2.5: Mechanical and biochemical construct properties (day 56), (A) EY (kPa), (B) SR, (C) GAG (%/D56ww), (D) GAG (%/D0ww), (E) collagen (%/D56ww), (F) collagen (%/D0ww), (G) cell density (cell (D56 mL)-1), (H) cell density (cell (D0 mL)-1). *: significance of CH within given MV ($p < 0.05$); +: significance of CH for different MV ($p < 0.05$); **: significance of indicated factors (CH, MV, and/or CH × MV or groups ; $p < 0.05$). Dashed lines (G, H) depict mean day-0 cellularity (99.4 million cells (D0 mL)-1).

normalization to wet weight on the last day of culture (D56ww). Indeed, though greater matrix synthesis was observed with increasing MV and CH, EY showed no significant differences among the groups (Figure 2.5A), presumably because their variable swelling (Figure 2.5B) maintained the fixed-charge density of GAGs at a nearly uniform level (Figure 2.5C).

In prior studies, we have noted that our CTE system is able to produce GAG at native levels (≈6% ww for immature bovine cartilage), but that collagen remains significantly below native values (≈10% ww), as was also observed here (≈7% D56ww GAG in Figure 2.5C and ≈1.5% D56ww collagen in Figure 2.5E). Interestingly, day-0 normalizations suggest that the amount of collagen actually synthesized (almost ≈6% D0ww in Figure 2.5F for the MV 15/CH 12 group) could produce weight ratios closer to native levels, were it not for the substantial swelling (Figure 2.5B) driven by the Donnan osmotic pressure from charged GAG (Eisenberg & Grodzinsky, 1985; Lai *et al.* , 1991; Mow *et al.* , 1998). These results support the value of strategies using exogenous treatments with lysyl oxidase, to strengthen the collagen network by increasing collagen cross-link precursors, to prevent the swelling evident in this study (Athens *et al.* , 2013).

In prior studies of this model system (Bian *et al.* , 2009b), it had been suggested that the higher deposition of GAG might inhibit collagen deposition, possibly due to a steric effect. Histological stains from this study support this hypothesis (Cigan, 2016), especially around channel edges, where a greater proportion of synthesized GAGs may diffuse into the channel due to their natural time constant for binding with the scaffold (Nims *et al.* , 2014), allowing for a more intense ring of deposited collagen. This hypothesis had previously motivated alternative strategies for enhancing collagen deposition by using chondroitinase ABC to enzymatically remove GAG and quell construct swelling (O'Connell *et al.* , 2014).

The amount of glucose available in the culture media was adjusted by changing the media volume per construct instead of modifying the glucose concentration. This choice was motivated by the desire to maintain glucose concentration at the standard 25 mM of high-glucose DMEM, and the concern that large changes in concentration might produce confounding effects due to alterations in osmolality and pH (Heywood *et al.* , 2006a; Zhou *et al.* , 2008). Another potential concern is that large numbers of channels may compromise the construct mechanical integrity, possibly leading to stress concentrations and cracking under loading. No cracking was observed during mechanical testing on day 56, though the possibility that such damage may occur at physiological load

magnitudes should not be discounted. In native cartilage, the network of channels that irrigates the tissue during development and through adolescence eventually disappears. A process whereby channels completely occlude at the time of construct maturation would be similarly beneficial; by day 56 of this study, channels filled by ≈75% (data presented in (Nims *et al.* , 2015)), suggesting that complete filling may occur at a later time point. Depending on the level of elaboration of functional properties in the construct, ensuring free flow of media in the channels for longer culture durations may require periodic material removal. Alternatively, strategies may be needed, such as the injection of cell-seeded agarose, to completely fill channels prior to implantation.

The computational model employed herein builds from earlier efforts to model engineered cartilage nutrient consumption (Lin *et al.* , 2013; Sengers *et al.* , 2005a; Nikolaev *et al.* , 2010; Obradovic *et al.* , 2000; Zhou *et al.* , 2008; Galban & Locke, 1999b) and served as a critical step to develop system-specific models for assessing the culture of the characterized CTE systems. Models may similarly guide future studies by identifying the most promising experimental culture conditions for a given construct geometry and cell density, eliminating less promising ones, and reducing the need for labor- and cost-extensive experimental parametric studies. While the models here did provide insight on the culture of large constructs, subsequent models may be considerably improved in future implementations. Under the current framework, the model predicted that all CH groups within the MV 15 group should produce similar matrix levels. Experimental results, however, demonstrated that for MV 15 groups, CH was a significant factor influencing ECM content, suggesting that additional factors may need to be modeled to account for these observations (Nikolaev *et al.* , 2010; Sengers *et al.* , 2005a). Channels also increased the total construct cell content (Figure 2.5H), implying that channels in constructs may act to both increase nutrient availability and enhance the synthesis capacity of the constructs. Thus, cellular proliferation may need to be incorporated into future growth models when simulating multiple weeks of culture (Lemon & King, 2007; Sengers *et al.* , 2005b). Additionally, early matrix synthesis models implicated oxygen as a limiting nutrient (Nikolaev *et al.* , 2010; Obradovic *et al.* , 1999; Obradovic *et al.* , 2000) and recently our lab has shown that active TGF-β binds extensively to the native ECM suggesting potential transport limitations within engineered constructs (Albro *et al.* , 2013). Therefore, the transport, binding, consumption, and biosynthetic influence of oxygen and TGF-β may need to be included explicitly in future models. Construct

swelling, resulting from ECM synthesis and Donnan osmotic pressure, may also need to be modeled to better reproduce observed phenomena (Figure 2.5B, H). With these improved models, it will become possible to optimize the placement and density of channels for growing full-sized engineered cartilage layers, recognizing the competition between increasing the number of channels to enhance nutrient access and reducing the number of cells available for matrix synthesis.

In summary, computational models are becoming increasingly valuable tools for designing effective culture conditions for engineering large tissue constructs. This study specifically addressed the amount of glucose in our [juvenile bovine chondrocyte]-[agarose gel] CTE system, as a wide range of media and glucose supply rates have been employed in prior studies (Table 1), illustrating the lack of consensus on adequate amounts of this fundamental nutrient. It was found computationally that conventional culture conditions provide inadequate glucose levels for culturing larger constructs, obviating the benefits of nutrient channels. Experimental results demonstrated that significantly enhanced matrix deposition in channeled constructs could be achieved when using higher media volume supplementation (Figure 2.5D, F). This agreement between model prediction and subsequent experimentation encourages further development and validation of predictive models, including models that account for a broader set of nutrients, cell proliferation, matrix synthesis, and swelling of the constructs. These more sophisticated models may be subjected to more stringent quantitative validations of a variety of measures, including matrix composition, mechanical properties and dimensional changes.

2.6 Acknowledgements

Final publication is available from Mary Ann Liebert, Inc., publishers http://dx.doi.org/10.1089/ten.TEC.2014.0451.

Research reported in this publication was supported by the National Institute of Arthritis and Musculoskeletal and Skin Diseases of the National Institutes of Health under Award Numbers R01AR060361, R01AR046568, T32AR059038, 2R01DE016525 and 2P41EB002520. The content is solely the responsibility of the authors and does not necessarily represent the official views of the National Institutes of Health.

Chapter 3 TGF-β transport, binding, and consumption within engineered constructs

3.1 Abstract

Transforming growth factor-β (TGF-β) transport within engineered cartilage is critically hindered, causing steep gradients throughout even small tissue constructs. In addition to diffusion and consumption, TGF-β undergoes reversible binding with the acellular agarose scaffold, encapsulated cells, and developing extracellular matrix, leading to transport limitations in both immature and mature tissue constructs. We have previously reported the transport kinetics of TGF-β based on bulk tissue properties (i.e.. mixtures of cells + scaffold and cells + scaffold + matrix), but characterizing the binding coefficients of the individual constituents (the cells and matrix) has not been examined. The individual binding rates of the agarose, cells, and matrix is essential for building models of long-term culture conditions with evolving matrix compositions and for extending models to different cell seeding densities. To this end, the current study characterizes and validates the individual binding characteristics of the cell constituent within a freshly-seeded construct. We provide the equations for this separation and a simulation comparing the binding of TGF-β with one partner (implicit, partner = scaffold + cells) to two partners (explicit, partner 1 = scaffold, partner 2 = cells). Simulations display similar behavior of both models. These results grant us the ability to change TGF-β binding capacity to a freshly-seeded construct on the basis of a construct's cell seeding density.

3.2 Introduction

Using a mixture framework to model tissue growth will be a significant advance of the current approaches to modeling growth which typically use kinematic and morphometric data to inform the growth of tissues without examining the specific mechanism underlying growth. Conversely, the mixture framework uniquely model the growth of the salient constituents within a tissue and can model growth through chemical kinetic modeling of the constituents. While an attractive framework for a mechanistic understanding of growth, challenges arise in how to accurately model the evolution of the constituents and relate each chemical reaction all available constituents.

Our previous work characterized TGF-β binding as dependent on both agarose, cells, and matrix within immature (cultured for 3 days) and mature (cultured for 28 days) engineered tissue constructs (Albro *et al.* , 2016). These models characterized the binding kinetics against the construct as a whole (henceforth referred to as the "mixture" binding parameters) (Albro *et al.* , 2013; Albro *et al.* , 2016). As our ongoing goal for engineered cartilage growth models is to understand the role of cell seeding density in developing constructs, the goal of the present study was to characterize the individual binding kinetics of TGF-β to cell content.

The mixtures investigated in our earlier work consisted of an acellular agarose scaffold, a freshly seeded construct (acellular agarose scaffold + 60 million cells mL^{-1}), and a mature construct (acellular agarose scaffold + 60 million cells mL^{-1} + 6% GAG). Computational models of the evolving and spatially heterogeneous tissue construct require models of the individual binding kinetics of the construct constituents (agarose, cells, and GAG) with TGF-β.

The present work identifies the specific binding characteristics of agarose and chondrocytes based on the previous measures of binding characteristics determined for the mixtures of acellular, freshly seeded, and mature tissue constructs.

3.3 Methods

We begin with the generalized equation of a reversible reaction

$$A + B^i \rightleftharpoons C^i$$

for $i = \{1, 2\}$ where $i = 1$ denotes the agarose constituent and $i = 2$ denotes the cell constituent, then:

$$\frac{dA}{dt} = \frac{dB^i}{dt} = -\frac{dC^i}{dt} = -k_f^i A B^i + k_r^i C$$

at steady state

$$k_f^i A B^i = k_r^i C^i \Rightarrow \frac{k_f^i}{k_r^i} = \frac{C^i}{A B^i}$$

	N^{eff}	k_f^{eff}	k_r^{eff}	K_{eq}^{eff}
Acellular agarose	60 ng mL^{-1}	1.8 $\times 10^{-6}$ s mL ng^{-1}	2.7 $\times 10^{-5}$ s^{-1}	6.67$\times 10^{-2}$ mL ng^{-1}
Fresh construct	200 ng mL^{-1}	2.7 $\times 10^{-6}$ s mL ng^{-1}	2.5 $\times 10^{-5}$ s^{-1}	1.1$\times 10^{-1}$ mL ng^{-1}
Mature construct	370 ng mL^{-1}	1.6 $\times 10^{-6}$ s mL ng^{-1}	8.3 $\times 10^{-5}$ s^{-1}	1.9$\times 10^{-2}$ mL ng^{-1}

Table 2: Effective binding rates for freshly seeded constructs from (Albro *et al.* , 2016).

using conservation of binding sites (B),

$$N^i = B^i + C^i$$

and conservation of ligand (A),

$$A_{tot} = A + C^1 + C^2.$$

We can rewrite the equation as

$$\frac{dA}{dt} = -k_f^1 A B^1 + k_r^1 C^1 - k_f^2 A B^2 + k_r^2 C^2 = -A\left(k_f^1(N^1 - C^1) + k_f^2(N^2 - C^2)\right) + k_r^1 C^1 + k_r^2 C^2$$

which we want to relate to a single, effective (eff) reaction of the same form:

$$\frac{dA}{dt} = -A k_f^{eff}(N^{eff} - C^{eff}) + k_r^{eff} C^{eff}$$

where we know k_r^{eff},k_f^{eff},N^{eff}. At steady-state

$$A k_f^{eff}(N^{eff} - C^{eff}) = k_r^{eff} C^{eff}$$

$$A_{tot} = A + C^{eff} \Longrightarrow A_{tot} - C^{eff} = A$$

and

$$\left(A_{tot} - C^{eff}\right) K_{eq}^{eff} N^{eff} = (1 + \left(A_{tot} - C^{eff}\right) K_{eq}^{eff}) C^{eff}.$$

$$C^{eff} = \frac{(K_{eq}^{eff} A_{tot} + K_{eq}^{eff} N^{eff} + 1) \pm \sqrt{(K_{eq}^{eff} A_{tot} + K_{eq}^{eff} N^{eff} + 1)^2 - 4K_{eq}^{eff} K_{eq}^{eff} N^{eff} A_{tot}}}{2K_{eq}^{eff}}$$

where we have K_{eq}^{eff}, A_{tot}, N^{eff} from (Albro *et al.* , 2016) as the mixture constants for the agarose + cellular (freshly-seeded construct in Table 2). Taking the physical root for a presumed configuration of a 1 mm × 1 mm × 1 mm cube with an assumed initial concentration of 10 ng mL^{-1}, we find at equilibrium $C^{eff} = \{210, 9.54\}$ ng mL^{-1}, taking the second root due to the physics of the problem.

We can now determine the binding properties of the agarose and cellular constituents individually based on the assumption that the properties of agarose remain constant (all $i = 1$ terms are known). The equations simplify as

$$k_f^{eff}(N^{eff} - C^{eff}) = \left(k_f^1(N^1 - C^1) + k_f^2(N^2 - C^2)\right)$$

$$k_r^1 C^1 + k_r^2 C^2 = k_r^{eff} C^{eff}$$

$$N^{eff} = N^1 + N^2$$

$$A_{tot} = A + C^1 + C^2 = A + C^{eff}$$

from which

$$k_f^{eff}(N^{eff} - C^{eff}) = \left(\frac{k_f^1}{k_r^1}\left(k_r^1 N^1 - k_r^{eff} C^{eff} - k_r^2 C^2\right) + k_f^2(N^{eff} - N^1 - C^2)\right).$$

the assumption that $t = 0$, that $C^{eff}(t = 0) = C^1(t = 0) = C^2(t = 0) = 0$, then

$$k_f^{eff}(N^{eff}) = \left(k_f^1\left(N^1\right) + k_f^2(N^{eff} - N^1)\right) \Longrightarrow \frac{k_f^{eff}(N^{eff}) - k_f^1\left(N^1\right)}{(N^{eff} - N^1)} = k_f^2$$

and we find that $k_f^2 = 3.09 \times 10^{-6}$ s mL ng^{-1}.

At equilibrium

	N_t^i	k_f^i	k_r^i	K_{eq}^{eff}
Agarose	60 ng mL^{-1}	1.8 $\times 10^{-6}$ s mL ng^{-1}	2.7 $\times 10^{-5}$ s^{-1}	6.67$\times 10^{-2}$ mL ng^{-1}
Cells	140 ng mL^{-1}	3.09 $\times 10^{-6}$ s mL ng^{-1}	2.42 $\times 10^{-5}$ s^{-1}	1.27$\times 10^{-1}$ mL ng^{-1}

Table 3: Constituent-specific binding rates for freshly seeded constructs.

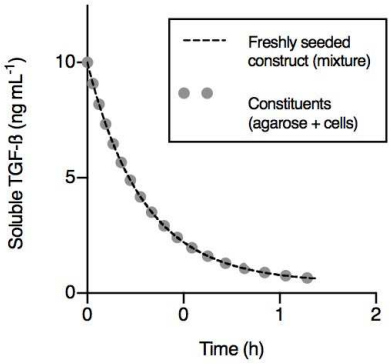

Figure 3.1: Agreement between a mixture and individual constituent TGF-β binding response.

$$\frac{\left(A_{tot}-C^{eff}\right)\left(k_f^1(N^1-C^{eff})+k_f^2(N^2)\right)-k_r^1(C^{eff})}{\left(k_r^2-k_r^1-k_f^1\left(A_{tot}-C^{eff}\right)+k_f^2\right)}=C^2$$

and therefore, $k_r^2 = 2.42 \times 10^{-5}$ s^{-1}.

3.4 Results

Constituent-specific rates are found in Table 3. It should be noted, that because these binding rates are dependent upon the constituents themselves, then agarose parameters are specific for 2% gel and cell parameters are specific for a new cell seeding density of 60 million cells mL^{-1} (based on a 2% agarose gel). The agreement between a freshly seeded construct (parameters based on (Albro *et al.* , 2016)) and the mixture constituents of agarose and cells calculated here is modeled in a simple configuration (assuming a 1 mm $\times$ 1 mm $\times$ 1 mm homogeneous cube with initial TGF-β concentration =10 ng mL^{-1}) Figure 3.1. Initial, transient, and equilibrium responses of the mixture and the two constituents combined are in agreement.

3.5 Discussion

This work identified the binding rates of the individual cell constituents within a freshly seeded engineered construct (Table 3). These values will be part of future comprehensive growth models for generalizing models to various cell seeding densities through both normalized nutrient consumption values (i.e. using nutrient consumption per cell multiplied by the local, present density of cells) and the cellular binding interactions as identified here.

Importantly, both agarose and the cellular phase were identified. While it is unlikely we will change the concentration of agarose, alterations in cell density, both during growth and through changes in initial cell seeding density are common. Calculating the ratio of available TGF-β binding sites per cell, based on this work, comes out to 2.33 ng mL^{-1} TGF-β per million cells mL^{-1}. This ratio can be used for developing models with alterations in cell density from the 60 million cells mL^{-1} of our previous work. The constituent forward and reverse binding rates will be held constant for future work based on the assumption they reflect the actual inherent interactions between TGF-β and the respective constituents (agarose, cells, GAG).

As the aims for the current set of models is to model the agarose + juvenile bovine chondrocyte model, we characterized only the binding coefficients of agarose and cells in this work. In this set-up, little matrix is deposited during the first two weeks of TGF-β administration. Our future efforts to model the growth of mature chondrocytes from canine cartilage will likely require the binding relations between TGF-β and matrix as TGF-β supplementation is delivered continuously throughout culture and once a significant matrix has developed, likely accentuating the transport limitations of TGF-β.

Chapter 4 Synthesis and binding kinetics within developing engineered constructs

4.1 Abstract

Large engineered cartilage constructs typically suffer from inhomogeneous extracellular matrix deposition due to insufficient nutrient availability. Computational models of nutrient consumption and tissue growth can be utilized as an efficient alternative to experimental trials for optimizing the culture of large constructs; such models require system-specific growth and consumption parameters. To inform the modeling of the [bovine chondrocyte]-[agarose gel] system, total synthesis rate (matrix accumulation rate in construct + matrix release rate to media) and matrix retention fractions of glycosaminoglycans (GAG), collagen, and cartilage oligomeric matrix protein (COMP) were measured either in the presence (continuous or transient) or absence of TGF-β3 supplementation. Reversible binding kinetics parameters were then characterized using computational models. These results were combined with our recent nutrient supplementation work to computationally simulate the culture of a human patella-sized tissue construct, reproducing the experimental results from (Hung *et al.* , 2003). Transient TGF-β3 supplementation produced the highest total GAG synthesis rate, highest GAG retention ratio, and highest binding affinity; collagen synthesis was elevated in growth factor supplementation groups over control, with the highest binding affinity observed in the transient supplementation group; both COMP synthesis and retention were lower than those for GAG and collagen. Using these results to inform the modeling of GAG deposition within the large patella construct, computational predictions were consistent with the previous experimental findings without further adjustments to modeling parameters. These results suggest that these nutrient consumption and matrix synthesis models are an attractive alternative for optimizing the culture of large-sized constructs.

4.2 Introduction

Osteoarthritis (OA) is a debilitating disease causing significant pain and immobility as the cartilage of the diarthrodial joints degrades to expose the underlying bone. The low cellularity and avascular nature of adult articular cartilage contribute to the limited capacity of the tissue to heal from minor

injuries and defects, eventually developing into symptomatic OA (Stockwell, 1979). Cartilage tissue engineering (CTE) is a promising strategy targeting the replacement of defective native cartilage with mechanically and biochemically similar engineered cartilage. In CTE, systems usually consist of a cell species (typically chondrocytes, mesenchymal stem cells, or embryonic stem cells) embedded in a biocompatible polymeric scaffold (Kuo *et al.* , 2006). The scaffold maintains the cells in a 3D environment with access to a nutrient rich culture media and retains the extracellular matrix (ECM) products synthesized by the cells. In particular, agarose is a well-characterized, bio-inert scaffold that shows great promise in CTE systems as chondrocytes elaborate a functional ECM when cultured in the three-dimensional agarose environment, reaching native levels of glycosaminoglycans (Benya & Shaffer, 1982; Buschmann *et al.* , 1995; Lima *et al.* , 2007; Byers *et al.* , 2008).

A remaining challenge in CTE is the development of clinically relevant-sized tissue constructs, which are required to repair the large surface defects (>5 cm^2) present in symptomatic OA (Hung *et al.* , 2003; Moisio *et al.* , 2009). Engineered constructs of this size suffer from inhomogeneous ECM deposition as the transport of critical nutrients to the interior of the construct is hindered by consumption of cells along the periphery. Lacking a homogenous and structural ECM, these constructs are unable to support physiologic loads and are therefore unlikely to function successfully upon implantation. In an effort to reduce ECM heterogeneity, strategies for enhancing nutrient transport have been employed such as direct media perfusion, dynamic mechanical loading, and the introduction of nutrient channels into the tissue (Bian *et al.* , 2009a; Lima *et al.* , 2007; Mauck *et al.* , 2000; Buckley *et al.* , 2009; Davisson *et al.* , 2002b; Davisson *et al.* , 2002a). However, quantitative predictive methods for optimizing the culture of large-sized constructs of various sizes remain unexplored.

An overarching aim of our research is to develop and implement continuum growth models to optimize tissue culture protocols for growing large-sized constructs with sufficient nutrient availability and ECM deposition throughout the interior. Such models may prove insightful and efficient in analyzing how nutrient distribution and ECM deposition are affected by culture conditions (Nikolaev *et al.* , 2010; Obradovic *et al.* , 2000; Sengers *et al.* , 2005a; Zhou *et al.* , 2008). Accurate, system-specific, CTE modeling requires knowledge of: 1) the nutrient(s) essential for cell viability and concentrations of the nutrient(s) necessary for tissue growth, 2) consumption rates of the nutrient(s), 3) matrix constituents critical to mechanical integrity, and 4) synthesis rate and

binding kinetics for each essential constituent. Previously, we have identified that tissue growth is diminished at a glucose concentration of 7.5 mM as compared to 25 mM in the [bovine chondrocyte] – [agarose gel] system (Cigan *et al.* , 2013). The present study, therefore, focuses on the remaining tasks: experimentally measuring ECM synthesis and retention to determine the matrix binding kinetics consistent with the measured levels of matrix retention, measuring the rate of glucose consumption for this system, and refining the glucose concentration threshold required for ECM synthesis. To investigate the utility of these parameters, we model the growth of a human patella-sized construct as was performed experimentally by (Hung *et al.* , 2003), by incorporating glucose transport from a periodically refreshed bath, cellular glucose consumption, matrix synthesis as a function of glucose availability, and binding and release of matrix products.

In cartilage, proteoglycans (PGs) and type II collagen are the major ECM structural components. PGs, predominantly consisting of aggregated glycosaminoglycans (GAG), contribute to the compressive stiffness while the fibrillar collagen network contributes to the tensile behavior (Jurvelin *et al.* , 1988; Kempson, 1980). Pyridinoline cross-links between collagen fibrils act to retain and strengthen the PG-collagen network (Eyre & Wu, 2005; Williamson *et al.* , 2003b; Williamson *et al.* , 2003a). In addition, cartilage oligomeric matrix protein (COMP) is a high molecular weight (500 kDa) matrix protein that may play a structural role in cartilage given its high concentration (0.4% ww) in the tissue and binding affinity for both PGs and type II collagen (Chen *et al.* , 2007; Rosenberg *et al.* , 1998; Di Cesare *et al.* , 1996). Here, we experimentally examined the influence of GAG, collagen, COMP and pyridinoline on CTE construct mechanical properties, due to their suggested mechanical roles in native cartilage. An experimentally determined retention fraction was also calculated for GAG, collagen and COMP, and a reversible binding model of each ECM constituent was then used to determine its binding kinetics, similar to prior analyses of native cartilage and CTE constructs (DiMicco & Sah, 2003; Klein & Sah, 2007; Sengers *et al.* , 2004). Due to the earlier success of using transforming growth factor $\beta 3$ (TGF-$\beta 3$) on the culture of the [bovine chondrocyte]-[agarose gel] system, the synthesis rates, retention fractions, and binding constants of GAG, collagen, and COMP were examined in the continuous and temporary (2 week) presence, as well as absence, of TGF-$\beta 3$ (Byers *et al.* , 2008; Lima *et al.* , 2007). To preclude the confounding influence of heterogeneous nutrient availability present in large constructs, the experimental work of this study is performed with small constructs.

4.3 Methods

4.3.1 Cellular isolation and construct culture

Primary chondrocytes were isolated from articular cartilage of bovine calf (2 months old) carpometacarpal joints digested with type IV collagenase (activity = 747 U/g) in high glucose Dulbecco's Modified Eagle's Medium (hgDMEM) (Invitrogen, Carlsbad, CA) supplemented with 5% fetal bovine serum (Invitrogen), amino acids, buffering agents, and 1% antibiotic-antimycotic (Invitrogen) at 37 °C on a shaker for 6 hours (Lima *et al.* , 2007). Cells were encapsulated in 2% agarose (type VII-A) at a density of 30×10^6 cells mL^{-1}. Constructs were cored from the cell-agarose mixture ($\varnothing$4 mm $\times$ 2.3 mm thick) and cultured under static conditions for 45 days in chemically-defined, chondrogenic media (hgDMEM, 100 nM dexamethasone, 100 µg/mL sodium pyruvate, 50 µg/mL L-proline, 1% ITS+ premix (Becton Dickinson, Sparks, MD), 1% antibiotic-antimycotic, and 173 nmol/mL ascorbic acid 2-phosphate) at 37 °C under 5% CO2 tension. Media were supplemented with 10 ng/mL TGF-β3 (R&D Systems, Minneapolis, MN) for either the entire culture period (β3+ group) or for only the first 14 days of culture (β3− group). A control group was cultured without TGF-β3 supplementation. Media were changed three times per week and conditioned media aliquots were taken at each media change. Constructs were removed and characterized after 14, 28, and 45 days (n = 4 per group, time point).

4.3.2 Mechanical characterization

At each time point, constructs were mechanically tested in a custom device using unconfined compression with impermeable metal loading platens. Sample thickness and diameter were measured prior to loading. Samples were equilibrated under a creep load in a bath of phosphate buffered saline for 400 s. A stress relaxation test was then performed by ramping the displacement at a constant rate to 10% of the original thickness over 300 s, then relaxing for 1500 s. The stress relaxation data was curve-fitted to extract mechanical properties similar to previous work (Huang *et al.* , 2012; Cigan *et al.* , 2013). This optimization analysis, performed in FEBio (febio.org), models the CTE constructs as a biphasic material consisting of both an intrinsically incompressible fluid and porous, solid matrix. Here, the solid matrix is modeled as a mixture of a neo-Hookean ground material (e.g., representing the scaffold material and GAGs) and a continuous fiber distribution material

(representing collagen) where fibers sustain tension only, with a linear variation of stress with strain (Ateshian *et al.* , 2009). These fits are able to able to extract the equilibrium compressive modulus E_Y, the hydraulic permeability k, and the fiber modulus ξ. The optimization results fit the experimental data with $R^2 = 0.95 \pm 0.05$ (for all samples), a result consistent with prior results with similar engineered tissue constructs.

Since fiber recruitment in a continuous fiber distribution model depends on the state of strain, the parameter ξ does not represent the actual tensile modulus of the construct. Therefore, the construct tensile modulus, E_T, was determined by modeling the equilibrium response to a homogeneous tensile deformation of a material with the same E_Y and ξ determined from the curve-fitting of the unconfined stress-relaxation response. In a prior study (Huang *et al.* , 2012), it was shown that this method for predicting E_T from unconfined compression stress-relaxation experiments produced a value statistically not different from tensile test measurements.

4.3.3 Biochemical characterization

After mechanical testing, constructs were radially halved and both halves were weighed. The construct masses were used to normalize the biochemical content and to calculate the swelling ratio for each group where

$$swelling\,ratio = \frac{average\ construct\ mass\ at\ time\ point}{average\ construct\ mass\ at\ day\ 0}.$$

One half was digested with proteinase K (MP Biomedical, Santa Ana, CA) and the other half was digested with guanidine. Samples were lyophilized prior to the proteinase K digestion (0.5 mg/ml) as previously described (Hollander *et al.* , 1994). Guanidine digestion was performed with 4 M guanidine HCl at 4 °C for 16 hours. GAG, collagen, and pyridinoline content were measured from the proteinase K digests. GAG content was assayed using the 1,9 dimethylmethylene blue dye-binding (DMMB) assay (Farndale *et al.* , 1986). Collagen and pyridinoline content were assayed after acid hydrolysis of the digests using an ortho-hydroxyproline (OHP) assay (Stegemann & Stalder, 1967) and a pyridinoline specific enzyme linked immunosorbent assay (ELISA; Quidel Corperation, San Diego, CA), respectively. Pyridinoline content was not measured on day 0 due to the low collagen content (≈0). A 1:7.6 OHP:total collagen mass ratio was used to determine collagen content

(Hollander *et al.* , 1994). COMP was measured from the guanidine digests with a COMP specific ELISA (MDBiosciences, St. Paul, MN). GAG and COMP were measured in the conditioned media samples directly, without digestion, using the DMMB assay and COMP ELISA, respectively. Media samples were pooled between two media changes for the COMP assay and the mass of COMP released into the media was averaged over the span of the two sequential media changes. Collagen media concentrations were assayed via the OHP assay of acid-hydrolyzed media samples. Pyridinoline content is presented both as a concentration and a molar fraction to collage: mol pyridinoline/mol collagen triple helix (collagen triple helix MW = 285 kDa) (Grant & Prockop, 1972).

4.3.4 Synthesis rates and retention fractions

For each ECM constituent examined (GAG, collagen, COMP) two distinct rates were measured: (A) the rate at which the constituent accumulated within the scaffold and (B) the rate at which the constituent was released into the media. The scaffold mass accumulation rate, m_c, was the slope of the linear regression of the mass of matrix within each construct (normalized to the construct day 0 reference volume) over the culture period (typical data set and linear regression shown in Figure 4.1A). The media mass release rate, m_m, was the slope of the linear regression of the mass of matrix released into the media (normalized to the construct day 0 volume) over the culture period (typical data set and linear regression shown in Figure 4.1B). The linear regressions for the $\beta 3+$ and control groups were calculated over the entire 45-day culture period (days 0 to 45) and the regressions for the $\beta 3-$ group were calculated after discontinuing TGF-$\beta 3$ supplementation (days 14 to 45). The total synthesis rate was the sum of m_c and m_m. The retention ratio, R_c, of each matrix constituent was calculated by dividing m_c by the total synthesis rate:

$$R_c = \frac{m_c}{m_m + m_c}.$$

The uncertainties of both the total synthesis rates and retention ratios were calculated according to standard uncertainty analysis from the standard deviations associated with the linear regression fits.

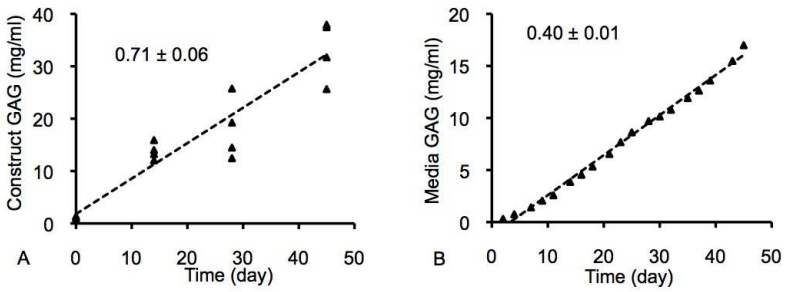

Figure 4.1: Representative synthesis profiles for (A) matrix accumulation in the construct and (B) cumulative matrix release in the media. Synthesis rates were calculated from the slope of the linear regression.

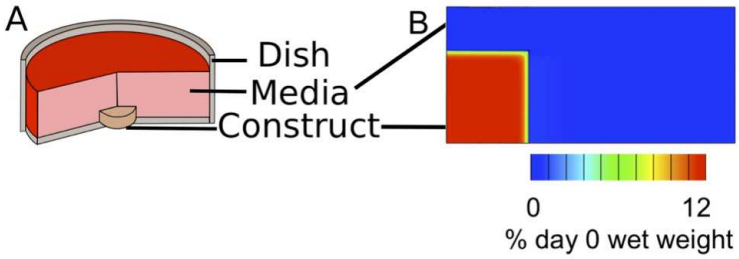

Figure 4.2: (A) Schematic for the experimental set-up idealized in the matrix-binding-diffusion model. (B) A representative result of the bound matrix spatial distributions within the tissue phase of the construct (GAG accumulation in the β3− group).

4.3.5 Binding parameters

The reversible binding kinetics of each matrix constituent were assessed based on the following assumptions: the synthesis rate was based on experimental results; each constituent is synthesized in soluble form and binds reversibly according to the law of mass action; when in soluble form, matrix products undergo Fickian transport with a diffusivity negligibly altered by matrix deposition; soluble matrix products diffuse out of the construct into a well-mixed bath; electric charge effects are neglected; construct swelling as a result of matrix growth is also neglected. All model simulations were performed in the open-source finite element code FEBio (www.febio.org), customized for this application (Ateshian, 2007; Maas *et al.* , 2012). Models consisted of a construct (⌀4 mm × 2.3 mm thick, cell density: 30 million cells mL^{-1}) in a 0.5 mL bath, similar to the day 0 experimental conditions (Figure 4.2). The governing equation for soluble matrix product was the mass balance relation in the presence of chemical reactions,

$$\frac{\partial c}{\partial t} + \operatorname{div} \mathbf{j} = \hat{c}$$

where c is the solute molar concentration and $\mathbf{j} = -Dgradc$ is the molar flux of the solute relative to the construct solid matrix, with D representing the diffusivity. Here, $\hat{c}$ is the net rate of molar supply to the soluble constituent from chemical reactions, combining synthesis and reversible binding according to $\hat{c} = \hat{c}_{syn} + \hat{c}_{rb}$, where $\hat{c}_{syn}$ the synthesis rate is prescribed from experimental measurements and was computed assuming a molar mass of 513 Da for GAG, 500 kDa for collagen, and 524 kDa for COMP. The reversible binding rate is

$$\hat{c}_{rb} = k_f \left[(c + K_d)\, c_b - N_t c \right].$$

Here, k_f is the forward reaction rate, $K_d = \frac{k_r}{k_f}$ is the dissociation constant and k_r is the reverse reaction rate, N_t is the total binding site concentration, and c_b is the concentration of bound matrix product whose temporal evolution is given by $\frac{dc_b}{dt} = \hat{c}_{rb}$, with initial condition $c_b(t = 0) = 0$. Values were taken from the literature for $D^{GAG}$and D^{coll} (for table see (Nims *et al.* , 2014)) for GAG and collagen diffusivities, respectively, (Silver & Trelstad, 1980; DiMicco & Sah, 2003) and for COMP was estimated from 500 kDa dextran (Leddy *et al.* , 2004). The synthesis rate was evaluated from

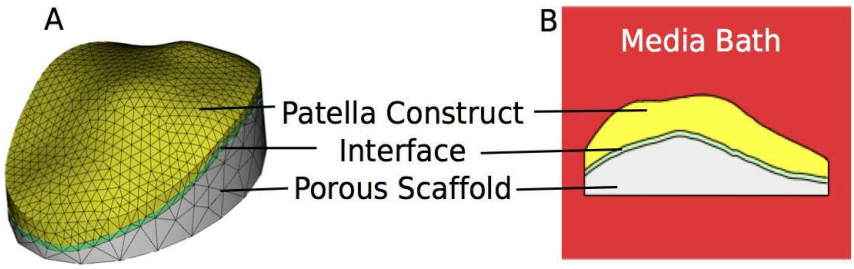

Figure 4.3: (A) Finite element mesh and geometric model of the anatomical patella construct supported on the porous, chondral scaffold, with an intermediary interface layer and (B) a cross sectional image of the construct surrounded within the 75 mL bath.

$\hat{c}_{syn} = (m_c + m_m)/M$ where M is the molar mass. N_t for GAG and collagen were set roughly equal to the average day 45 concentration of the supplementation group with the highest GAG and collagen content, respectively; N_t for COMP was equal to 10 times the day 45 concentration of the group with the highest COMP concentration; at these levels the matrix accumulated in a linear fashion, as observed experimentally. With these parameters taken as constants, k_r and k_f for each constituent were determined by a custom MATLAB optimization wrapper code that matched the experimental matrix release pattern over 45 days to the computationally predicted matrix release.

4.3.6 Human patella-sized construct

As an example of the applicability of the binding and synthesis constants, we attempted to reproduce the results of previous studies of culture of a human patella-sized construct, which analyzed the spatial GAG deposition over 35 days of culture (Hung *et al.* , 2003; Hung *et al.* , 2004). The details of this analysis are included below.

4.3.6.1 Computational anatomical model Three-dimensional finite element models of the patella construct were constructed from the anatomical human patella surfaces obtained using stereophotogrammetry (Ateshian *et al.* , 1991; Ateshian *et al.* , 1992; Hung *et al.* , 2003). The cellular construct was modeled atop an acellular, porous scaffold, similar to the experimental protocol and a 1 mm thick 'interface region' was included (Figure 4.3). The gel construct was seeded at 60 million cells mL^{-1}; this cell density informs both the matrix synthesis and nutrient consumption rates. The model was analyzed with the FEBio finite element software which incorporates transport mechanics and chemical kinetics.

4.3.6.2 Culture conditions The construct was surrounded within a bath containing 75 mL of media (Figure 4.3b). The media was changed three times per week (in a 2-2-3 day manner) over the 35 day culture. Media changes consisted of 'replacing' the conditioned media (glucose concentration < 25 mM and soluble ECM concentration > 0 mM) with fresh media (glucose concentration $= 25$ mM and soluble ECM concentration $= 0$ mM). As this experiment was performed in the absence of TGF-β supplementation, the synthesis and binding parameters for the 'control' case were used.

4.3.6.3 Matrix synthesis and glucose consumption Three chemical reactions were modeled in this finite element analysis. (1) Glucose uptake by cells was based on Michaelis-Menten kinetics; here the maximal cellular glucose consumption rate was experimentally determined (below) and the Michaelis constant, $= 0.35$ mM, was taken from previous experiments on chondrocytes (Windhaber *et al.* , 2003). (2) Soluble GAG synthesis was based on Michaelis-Menten type kinetics where the maximal synthesis rate was taken from our experimental synthesis results (scaled appropriately for the increased cellularity) and the Michaelis constant was the same as the glucose consumption reaction. Additionally, based on our earlier findings that low levels of glucose results in no significant ECM deposition (Cigan *et al.* , 2013), a nutrient threshold level was added into the synthesis equation, such that ECM synthesis was turned off within regions where the glucose concentration was below the threshold level. (3) GAG deposition was modeled using standard reversible binding kinetics of the soluble GAG with the extracellular matrix, based on the parameters curve-fitted to the experimental data of this study. The following additional experiments were performed to identify the remaining necessary parameters (cellular glucose consumption rate and ECM nutrient threshold) for this system.

4.3.6.4 Glucose consumption rate Glucose consumption on various weeks is discussed in (Cigan, 2016). The results of this work demonstrate that the glucose consumption rate through 7 weeks of culture of the system average $1.24 \times 10^{-13} \pm 3.4 \times 10^{-14}$ mol cell^{-1} hr^{-1}, in line with prior work.

4.3.6.5 ECM nutrient threshold ECM nutrient threshold was determined in the previous study (Cigan, 2016). The results of this work demonstrate a critical glucose concentration of 12.5

mM is required to sustain matrix deposition.

4.3.7 Statistics

The biochemical concentrations, equilibrium compressive modulus, E_Y, hydraulic permeability, k, equilibrium tensile modulus, E_T, and swelling ratio of the constructs were compared with a two-way analysis of variance (ANOVA) using Tukey's HSD post hoc test ($\alpha = 0.05$). Synthesis rates were compared with an analysis of covariance of the cumulative mass per construct released to the media and the mass accumulated in the scaffold over the culture time (day 0 to 45 for the control and β3+ groups and day 14 to 45 for the β3− group) (Rohlf & Sokal, 1995). Retention fractions for each matrix constituent were compared using an ANOVA of each group's mean, uncertainty, and n (total number of constructs and media aliquots for each supplementation group) (Cohen, 2002). Data are reported as mean ± standard deviation (for GAG, collagen, mechanical properties, and swelling ratio, n = 4; for COMP and pyridinoline, n = 3). For each group and constituent, the fit between the experimental and binding kinetics model was determined by nonlinear regression for both the construct matrix (sum of bound and soluble matrix within the construct) and cumulative matrix media release.

4.4 Results

4.4.1 Mechanical characterization and biochemical composition

Constructs cultured over the 45-day period developed E_Y values that were highest in the β3− group (Figure 4.4A; $p < 0.001$), consistent with previous studies (Byers *et al.* , 2008; Lima *et al.* , 2007); k was affected by both the course of culture and supplementation (Figure 4.4B; $p < 0.001$), as was E_T (Figure 4.4C; $p < 0.001$); by day 42, the swelling ratio of the constructs was significantly influenced by TGF-β3 (Figure 4.4D; $p < 0.001$) with the most swelling occurring in the β3− group ($p < 0.05$). GAG was highest in the β3− group (Figure 4.5A; $p \leq 0.022$) and collagen levels in the β3− and β3+ groups were higher than the control on days 28 and 45 (Figure 4.5B; $p \leq 0.002$). Collagen concentration was statistically similar between the β3− and β3+ groups ($p = 0.619$). Levels of COMP were similarly affected by TGF-β3 supplementation (Figure 4.5C; $p < 0.001$), with the highest construct COMP concentration observed on day 45 in the β3− group ($p \leq 0.003$), and the

highest overall COMP concentration observed in the β3+ group on day 28 ($p \leq 0.028$). Cessation of TGF-β3 supplementation influenced total pyridinoline concentration (Figure 4.5D; $p < 0.001$) and pyridinoline per collagen was influenced by the presence of TGF-β3 (Figure 4.5E; $p < 0.001$).

4.4.2 Experimental Synthesis Rates and Retention Fractions

GAG, collagen, and COMP levels in constructs and media increased nearly linearly over time (Figure 4.1), as assessed with the coefficient of determination of the linear regression (R^2; for table see (Nims *et al.* , 2014)). Scaffold accumulation rates and media release rates for these constituents were evaluated from the slope of the linear regression. Matrix release into the media generally exhibited a higher R^2 than the scaffold accumulation. The lowest coefficient of determination was the COMP scaffold accumulation for the β3+ group ($R^2 = 0.37$).

Synthesis rates varied with TGF-β3 supplementation (Figure 4.6). GAG scaffold accumulation rate was highest in the β3− group ($p < 0.001$) and GAG media release rates were similar between the three supplementation groups ($p = 0.429$). Collagen scaffold accumulation rate was highest in the β3− and β3+ groups compared with the control ($p < 0.001$) and collagen media release rate was lowest in the β3− group ($p = 0.002$). Overall, COMP synthesis was lower compared to the synthesis of the GAG and collagen (on the order of 102 μg ml^{-1} day^{-1} compared with 1 mg ml^{-1} day^{-1}). The β3+ group had the highest COMP media release rate ($p < 0.001$) and the β3− group had the highest COMP scaffold accumulation rate ($p \leq 0.021$).

For all matrix constituents (Figure 4.7), the β3− group had the highest retention ratio ($p < 0.001$). GAG retention reached a high level ($R_c = 90 \pm 2\%$) in the β3− group. COMP retention was lowest in the β3+ group ($R_c = 7 \pm 2\%$; $p < 0.001$).

4.4.3 Theoretical Model Binding Kinetics

The finite element models of the CTE constructs resulted in matrix accumulation and media release profiles that were similar to the experimental set-up over the 45 day culture of the system (representative profile in [FIG] 6), showing mostly high correlations ($R^2_{construct}$ and R^2_{media} ,for table see (Nims *et al.* , 2014)). The binding constants for a single constituent varied little with supplementation type compared with the variations among the different constituents. The reversible binding parameters in these models produce bound constituent concentrations that are reduced at the pe-

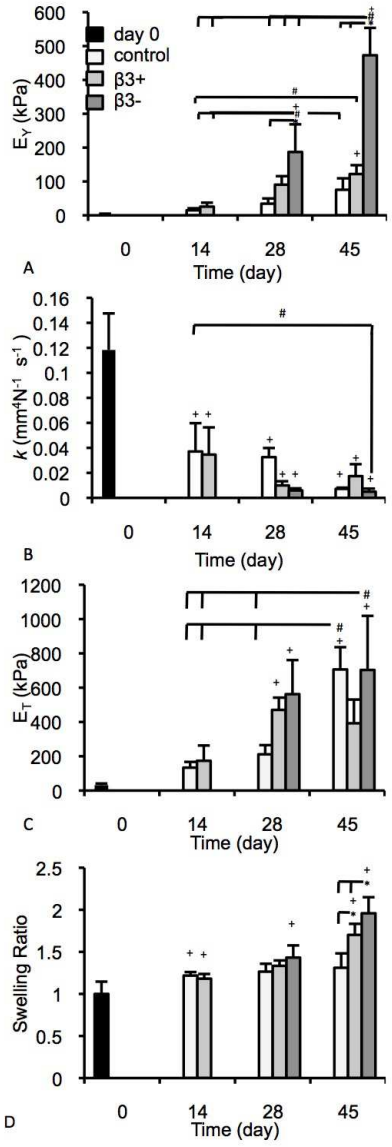

Figure 4.4: Curve-fit mechanical properties (A) E_Y (kPa), (B) k (mm4 N^{-1} s^{-1}), (C) E_T (kPa) and (D) the experimentally determined swelling ratio of constructs over the course of culture. * denotes group significantly differ from indicated group(s) at same time point ($p < 0.05$); + denotes group significantly differ from day 0 properties ($p < 0.05$); # denotes the indicated groups differ significantly ($p < 0.05$).

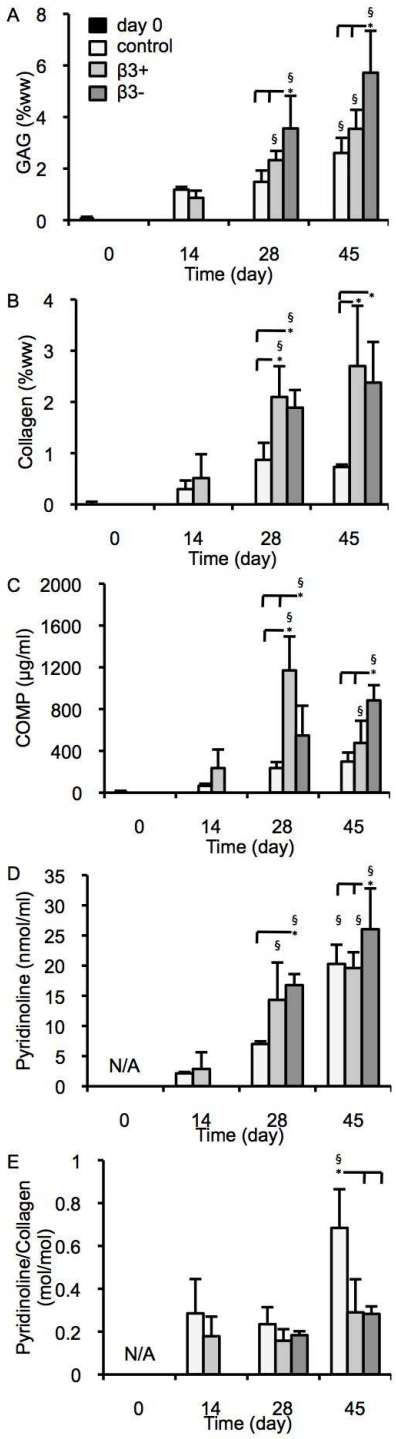

Figure 4.5: Biochemical properties of constructs over the culture period: (A) GAG concentration (%ww), (B) collagen concentration (%ww), (C) COMP concentration (μg/ml), (D) pyridinoline concentration (nmol/ml), and (E) pyridinoline to collagen ratio (mol/mol). * denotes group significantly differ from indicated group(s) at same time point ($p < 0.05$); § denotes group significantly differ from previous time point (day 7 control and β3+ compared to day 0; day 28 β3+ and β3− compared to day 14 β3+).

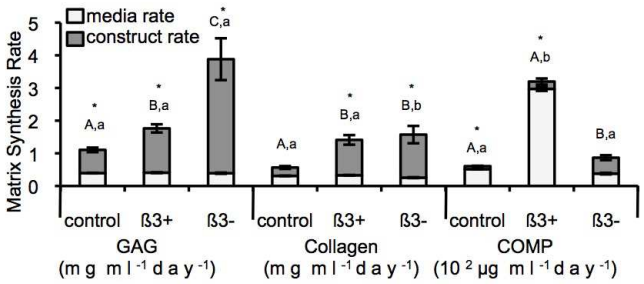

Figure 4.6: Synthesis rates of GAG (mg $ml^{-1}day^{-1}$), collagen (mg $ml^{-1}day^{-1}$), and COMP (102 µg $ml^{-1}day^{-1}$). The total synthesis (total column) is divided between media release rate (light, bottom) and construct accumulation rate (dark, top). * denotes significant differences between media and construct synthesis rates ($p < 0.05$); upper case letters denote groups of significance of construct accumulation for each matrix constituent ($p < 0.05$) and lower case letters denote groups of significance of media release for each matrix constituent ($p < 0.05$); thus for each matrix constituent, groups with the same upper or lower case letters had statistically similar construct matrix accumulation or matrix media release, respectively.

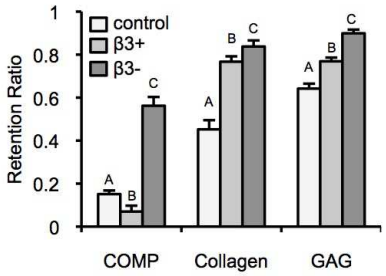

Figure 4.7: Retention ratio of the matrix constituents COMP, collagen, and GAG for each of the TGF-β3 culture treatments: control (light), β3+ (medium), and β3− (dark). Upper case letters denote groups of significance ($p < 0.05$); thus for each matrix constituent: groups with different capital letters were statistically different.

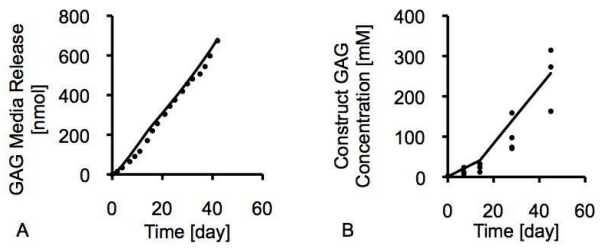

Figure 4.8: Representative (A) cumulative media release and (B) construct accumulation experimental data (circles) and the theoretical model results (line) of the GAG constituent in the β3− group. The inflection at day 14 in (B) reflects changes in synthesis rate and binding kinetics associated with ending TGF-β3 supplementation.

riphery and homogenous within the interior of the tissue (representative result in Figure 4.2B of bound GAG in the $\beta 3-$ group).

4.4.4 Human Patella-Sized Construct

When modeling both nutrient consumption and nutrient-dependent GAG synthesis the models predict glucose concentration profiles with interior glucose concentrations below the 12.5 mM threshold both before (Figure 4.9A, C) and immediately after (Figure 4.9B) a media change. Due to this lack of glucose availability, bound GAG develops solely in the periphery (Figure 4.9D, E, F). These ECM profiles are fundamentally different than the small construct models where ECM accumulation is highest in the interior of the construct. This human patella-sized simulation agrees well with our previous experimental findings (compare Figure 4.9F from this study to Figure 4.9H from (Hung *et al.* , 2004)).

4.4.5 Correlations Between Mechanical Properties and Biochemical Composition

$E_Y$showed a high correlation with GAG concentration (Figure 4.10A; $R^2 = 0.74$). Relatively low correlations were found for E_Y versus collagen or COMP (Figure 4.10B; $R^2 = 0.31$ and Figure 4.10C; $R^2 = 0.32$, respectively). E_Y was moderately correlated to pyridinoline concentration (Figure 4.10D; $R^2 = 0.47$). The swelling ratio displayed a high correlation to GAG concentration (Figure 4.10E; R2 = 0.74), a moderate correlation to collagen concentration (Figure 4.10F; $R^2 = 0.48$), a poor correlation to COMP (Figure 4.10G; $R^2 = 0.27$), and a moderate correlation to pyridinoline (Figure 4.10H; $R^2 = 0.56$). E_T was moderately correlated with GAG and pyridinoline (Figure 4.10I; $R^2 = 0.49$ and

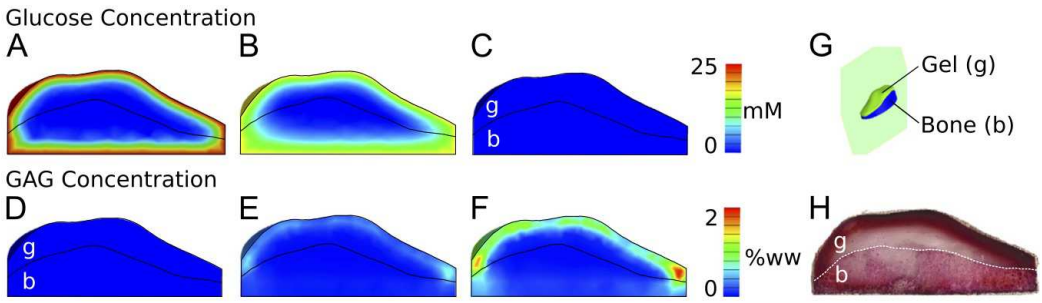

Figure 4.9: Model simulations results (sagittal plane, G) of the glucose concentration distributions (A, B, C) and bound GAG distribution (D, E, F) in patella-sized CTE construct (cellular gel region, "g", gel and acellular bone scaffold interface, "i", and the acellular scaffold, "b") after 35 days of culture. Images were taken either 3 hours (A, D) and immediately before (C, F) a media change and immediately after (B, E) a media change throughout the culture (1 wk: A, D; 3 wk: B, C; 5 wk: C, F). The previous experimental results of GAG accumulation (H) are provided for comparison to the model simulations (F) of this study. Figure 4.9H from (Hung *et al.* , 2004)(figure 7) with kind permission from Springer Science and Business Media.

Figure 4.10L; $R^2 = 0.50$, respectively) and poorly correlated with collagen and COMP (Figure 4.10J; $R^2 = 0.20$ and Figure 4.10K; $R^2 = 0.33$, respectively).

4.5 Discussion

Engineering cartilage constructs large enough to replace defects seen in symptomatic OA requires scaling up the current size of constructs. Presently, thicker and wider constructs experience heterogeneous matrix deposition as steep gradients in nutrient availability develop between the construct's periphery and interior due to cellular consumption and diffusion limitations (Bian *et al.* , 2009a; Hung *et al.* , 2003; Leddy *et al.* , 2004). Computational modeling of the culture conditions may serve as an essential and cost-effective method for determining the efficacy of techniques aimed at enhancing the functional ECM homogeneity. This study measured the synthesis and binding parameters of small [bovine chondrocyte]-[agarose gel] constructs cultured with sufficient media, thereby obviating potentially severe nutrient heterogeneity within the construct. These results were then combined with our prior work that identified glucose as a critical nutrient for this CTE system to model the culture of a human patella-sized construct (Cigan *et al.* , 2013; Hung *et al.* , 2003).

The synthesis rates of all the molecules examined were affected by TGF-β3 supplementation (Figure 4.6). GAG synthesis was elevated by supplementation of TGF-β3 versus control levels, and was further boosted by terminating the supplementation (TGF-β release) after 14 days (β3–

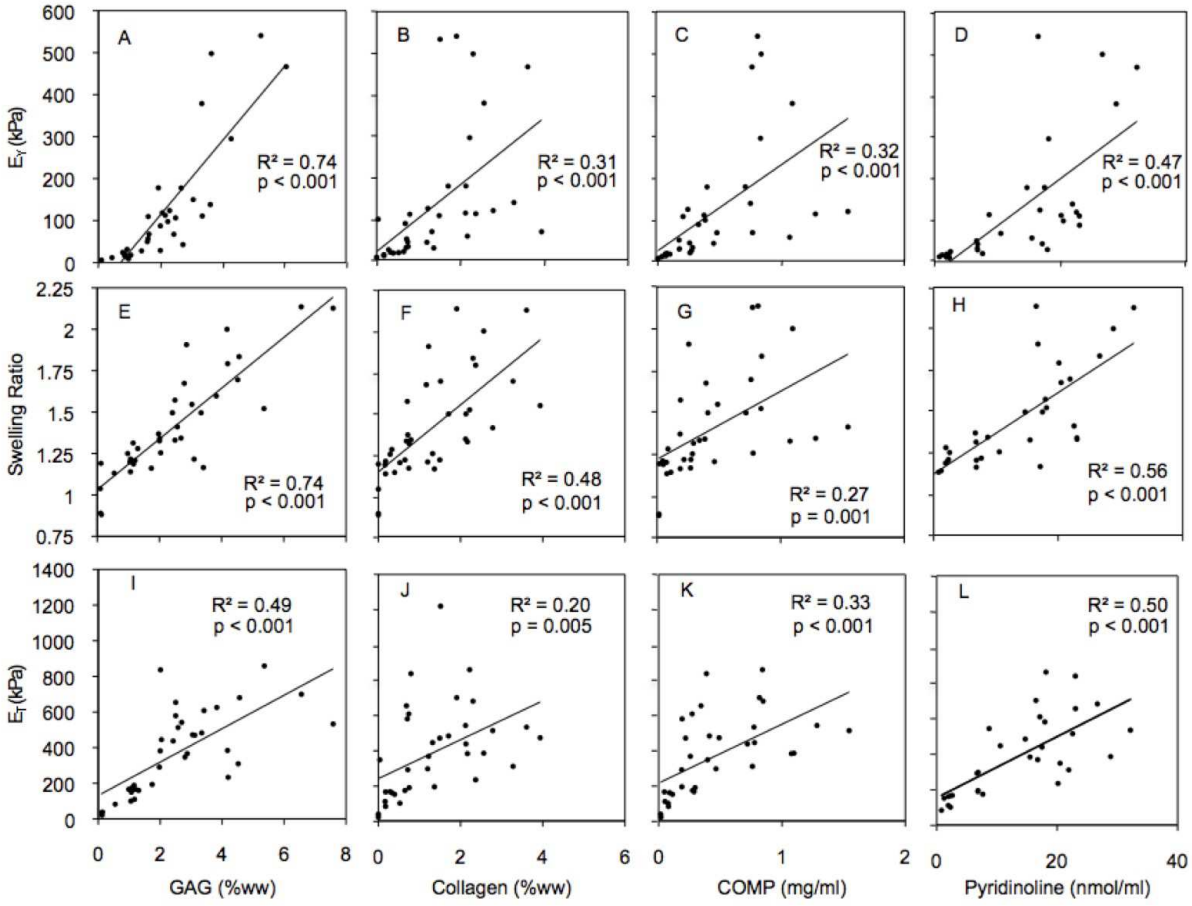

Figure 4.10: Correlations between the mechanical properties E_Y (A-D), swelling ratio (E-H) and E_T (I-L) and the biochemical concentrations of GAG (A, E, I), collagen (B, F, J), COMP (C, G, K) and pyridinoline (D, H, L).

group). This withdrawal not only increased the total synthesis rate of GAG, as shown previously (Byers *et al.* , 2008; Lima *et al.* , 2007), but also increased GAG retention over the continuous treatment group (≈90% retention in the β3− compared with ≈75% retention in the β3+ group). This trend in retention was similar to the trend in the dissociation constants (0.14 µM for the β3− group and 10 µM for the control). A similar experimental (0.22 µM) has been reported for reversible binding between aggrecan and hyaluronate (Watanabe *et al.* , 1997). Previous models of GAG binding kinetics in cartilage have been primarily focused on the binding and degradation of PGs in native cartilage (DiMicco & Sah, 2003). These studies used an experimentally determined binding rate between PGs and hyaluronate (Sandy & Plaas, 1989). The two measures of GAG binding affinity (this study: $2 - 73 \times 10^{-9}$ $\mathrm{mM^{-1}s^{-1}}$; previously: 1.2×10^{-5} $\mathrm{s^{-1}}$;(DiMicco & Sah, 2003) can be reconciled, however, by multiplying the rate constant by the density of binding sites (300 mM). This 'effective forward binding rate' ($6 - 222 \times 10^{-7}$ $\mathrm{s^{-1}}$) is similar between this and the previous work. It should also be noted that this study assumed reversible binding as suggested by prior work on the binding of aggrecan and hyaluronate (Watanabe *et al.* , 1997), while previous models of PG deposition have utilized a model in which bound PG is only re-solubilized by degradation and therefore cannot participate in re-binding (DiMicco & Sah, 2003).

TGF-β3 increased collagen synthesis over control, although termination of supplementation did not subsequently alter the total synthesis rate. This observation suggests that TGF-β primes the chondrocytes for greater collagen synthesis but is not needed continuously, as chondrocytes retain a memory of this exposure; similar behavior has been observed in fibroblasts. Both supplementation groups also have a high retention ratio (84% and 77% for the β3− and β3+ groups, respectively, compared with 44% retention in the control) potentially due the synthesis of small PGs, such as decorin and fibromodulin, which are also upregulated with TGF-β supplementation and which promote collagen fibril formation (Burton-Wurster *et al.* , 2003). Prior studies have analyzed the binding of PGs with collagen (ÖBrink, 1973a; ÖBrink, 1973b; Öbrink *et al.* , 1975); specifically, of the collagen-PG interaction is on the order of 30-1000 nM under low osmotic conditions (Öbrink *et al.* , 1975). This study predicts between 0.2 - 387 nM. As reaching native levels of collagen remains a problem in CTE, these results suggest that increasing construct collagen content will be more greatly impacted by techniques that increase total collagen synthesis (Eleswarapu & Athanasiou, 2013) rather than those which solely increase construct retention.

COMP synthesis was stimulated by TGF-β3. In contrast to GAG and collagen, COMP synthesis does not appear to retain a memory of past exposure to TGF-β3 and was elevated only in the presence of exogenous TGF-β3; these results are similar to studies of superficial chondrocyte monolayers where COMP expression and synthesis are upregulated in response to TGF-β supplementation (Motaung *et al.* , 2011; Recklies *et al.* , 1998). Despite the high COMP synthesis of the β3+ group, retention was much lower than that of GAG and collagen, resulting in much of the COMP (≈93%) to be released into the media. Earlier studies have shown that COMP binds to both aggrecan and chondroitin sulfate under Ca2+ concentrations similar to those present in the culture media used in this study (≈73 nM when binding with heparin, >10 μM when binding to keratan sulfate, and ≈102 nM when binding to chondroitin sulfates (Chen *et al.* , 2007). COMP has also been observed to bind with type II collagen, although the conditions under which binding is favorable (2 mM Zn^{2+}) were not present in this study (= 1.5 nM). In our theoretical model, ranged from 0.23 – 2.4 nM.

COMP levels have rarely been measured quantitatively in engineered cartilage constructs, thus these results offer a novel finding that merits closer analysis. By day 45 the COMP content in the β3− group was 0.09 ± 0.02 %ww, approaching native levels (native healthy/OA: ≈0.4 %ww; rheumatoid arthritis: ≈0.1 %ww) (Di Cesare *et al.* , 1996). Despite this similarity, a strong correlation between COMP levels and compressive mechanical properties was not observed (Figure 4.10C). Additionally, COMP content did not show a strong correlation to construct growth (Figure 4.10G). Based on these findings, COMP synthesis and distribution within engineered constructs may not be as critical as GAG and collagen to the structural integrity and growth of engineered cartilage, suggesting that models of GAG and collagen deposition would be more predictive of construct strength and growth than models of COMP.

Pyridinoline, while not synthesized directly by cells, was also measured (Figure 4.5D, E). Pyridinoline is a mature cross-link connecting multiple collagen triple helices; these bonds spontaneously form between hydroxylysine residues in the collagen triple helix (Eyre & Wu, 2005). Previous studies on engineered cartilage have reported that pyridinoline content typically falls below that seen in native tissue (Yan *et al.* , 2009; Riesle *et al.* , 1998). This study presents the first quantitative assessment of pyridinoline content in the [bovine chondrocyte]-[agarose gel] system. Results demonstrate that the total pyridinoline content was below that typically seen in calf bovine cartilage (98

nmol/g) while the ratio of pyridinoline to collagen within constructs was near native calf bovine cartilage (0.46 mol/mol) (Williamson *et al.* , 2003b). The constructs in this study displayed a moderate correlation between pyridinoline content and EY (Figure 4.10D); similar correlations have been observed in native tissue (Williamson *et al.* , 2003b; Williamson *et al.* , 2003a; Yan *et al.* , 2009). These results suggest that cross-linking occurs at the native levels relative to collagen and that low construct pyridinoline content may suffer from low substrate (collagen) concentrations. Therefore, engineered cartilage mechanical properties may benefit more from techniques used to increase collagen content than by purely increasing cross-linking density.

Establishing computational models for optimizing nutrient distribution in large constructs (Figure 4.9) may prove critical for optimizing the culture condition of anatomically-sized constructs. Two critical requirements are to (a) develop a model of synthesis rates and retention of the matrix and (b) identify which key nutrients control the synthesis of the ECM constituents. This study now provides the matrix synthesis and binding parameters and glucose consumption rates for the [agarose gel]-[bovine chondrocyte] system. As an example of the use of these parameters for computational growth models, we provide the model predictions of GAG distributions throughout a human patella-sized construct, as was performed experimentally (Hung *et al.* , 2003; Hung *et al.* , 2004). The similarities between the model simulations and experimental results suggest that these models would have great predictive power for the optimization of culture conditions for these large constructs. Previously, our lab has demonstrated that the introduction of nutrient channels into large constructs (⌀10 mm) allows for the development of properties similar to small constructs with increased nutrient availability (Bian *et al.* , 2009a). Future modeling work will optimize the culture of such large-sized constructs with nutrient channels.

4.6 Acknowledgments

Final publication is available from Elsevier, http://dx.doi.org/10.1016/j.jbiomech.2013.10.044.

Research reported in this publication was supported by the National Institute of Arthritis and Musculoskeletal and Skin Diseases (Award Numbers R01AR060361 and R01AR046568), the National Institute of General Medical Sciences (Award Number R01GM083925) of the National Institutes of Health, and the Columbia University Presidential Scholarship. The content is solely the responsibility of the authors and does not necessarily represent the official views of the National

Institutes of Health.

Chapter 5 Matrix deposition is influenced by cell content more than hyaluronan content

5.1 Abstract

The mechanism by which the cartilage matrix agglomerates is a complex process involving both enzyme-mediated and spontaneous reactions as well as the slow diffusion of structural macromolecules. Modeling the kinetics of such a problem has been shown to be simplified by reversible bining kinetics of the newly-sythesized soluble matrix and an available binding-site within the construct scaffold and developing tissue. Our previous work has characterized these reversible binding rates, however the relationship and evolution of a developing constructs with its matrix binding-site availability is yet uncharacterized.

The previous work characterized the matrix binding constants (binding site densities and binding kinetics) for engineered cartilage. However, the binding site availability of matrix molecules is expected to increase with tissue growth based on our preliminary experimental work suggesting that matrix deposition continues nearly linearly; conversely, if the binding site density were constant, matrix content would plateau. The aim of the present work is to experimentally relate potential binding site partners with the overall deposition of matrix. We examined whether proteoglycan and collagen deposition were dependent on hyaluronan content and cell content, as two likely matrix binding site partners. Using constructs seeded with different cell densities, we measured and correlated the cell, sulfated proteoglycan, collagen, and hyaluronan contents with small constructs supplemented with sufficient media. Results suggested that cell seeding density correlates best with the overall matrix deposition of both proteoglycans and collagen. The high correlations prompt the use of construct cell density as a proxy for binding site density of both proteoglycans and collagens in biochemical composition models.

5.2 Introduction

Growth modeling in the mixture framework requires information of the binding kinetics for describing matrix deposition. These kinetics require three parameters: 1) a forward reaction rate, 2) a reverse reaction rate, and a 3) density of binding site density for the ligand to bind. We have

previously determined the three parameters in Chapter 4 through quantitative methods to extract both binding constants based on a constant binding site density. This binding site density, however, is likely to change over culture and during growth. An evolution or proxy for the total construct binding site density has not been determined.

In native cartilage, the salient binding partner with proteoglycans in both native and engineered cartilage is hyaluronan, a long carbohydrate which interacts with extracellular receptors and aggrecan via the link protein (Watanabe *et al.* , 1997; Sandy & Plaas, 1989). Both link protein and hyaluronan are associated with proteoglycan stability in native tissue. As a essential requirement of biochemical deposition models is to predict the proteoglycan and collagen deposition, we wondered whether modeling hyaluronan synthesis would be necessary for predicting matrix deposition.

In practice, a modeler will predefine an initial binding site density (we originally used 300 mM as the GAG binding site density and 0.3 mM as the collagen binding site density based on the study of Chapter 4 using small, 30 million cells mL^{-1} constructs). However, in our early attempts to extend models to conditions of elevated cell density (up to 120 million cells mL^{-1}), the available binding site density at these original levels rapidly depleted and the continued matrix synthesis was released into the media, an event not experienced in experimental culture.

Therefore, the current experimental study investigated the role of hyaluronan content on the GAG and collagen content within small engineered constructs. As the insights would be directly applied to our computational models of different cell densities, the influence of initial cell seeding density on the hyaluronan content was examined.

5.3 Methods

5.3.1 Experimental culture

Small constructs ($\varnothing 3 \times 0.8$ mm) were cast as previously described (Nims *et al.* , 2014) with nominally either 30, 60, or 120 million cells mL^{-1} using primary juvenile bovine chondrocytes. Constructs were cultured in excess supply of media and cultured with 10 ng mL^{-1} TGF-β3 for the first 14 days of culture.

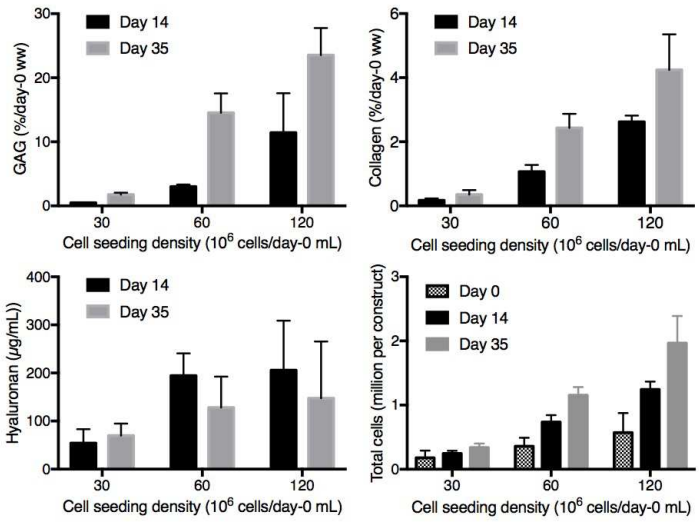

Figure 5.1: Biochemical (GAG, collagen, cells, hyaluronan) properties of small constructs grown with sufficient media.

5.3.2 Biochemical assessment

After 35 days of culture, constructs were removed from culture and digested with proteinase K. Digests were boiled to neutralize the proteinase K enzyme. Digests were then analyzed for cell content, sulfated GAG, collagen, and hyaluronan using an enzyme linked immunosorbent assay (HA ELISA, R&D Systems).

5.4 Results

Constructs grew well with the most growth occurring in the 120 million cells mL^{-1} (Figure 5.1). Hyaluronan deposition was similar between the 60 and 120 million cell mL^{-1} groups. Cell content in all groups increased with culture duration.

Correlation between the matrix constituents and cells were analyzed to gain insight into the best correlates between GAG deposition and matrix constituents (Figure 5.2). Correlations are shown between biochemical content for both current day and day-0 normalizations, as tissue swelling can lead to differences in data interpeteation. Correlations were typically high between factors when both were normalized to day-0 levels. For example, $R^2 = 0.85$ between GAG (%day0-ww) and cells (million cells/day-0 mL) while for the current-day normalizations $R^2 = 0.54$ between GAG (%ww) and cells (million cells/mL). To an even more extreme degree, $R^2 = 0.93$ between collagen

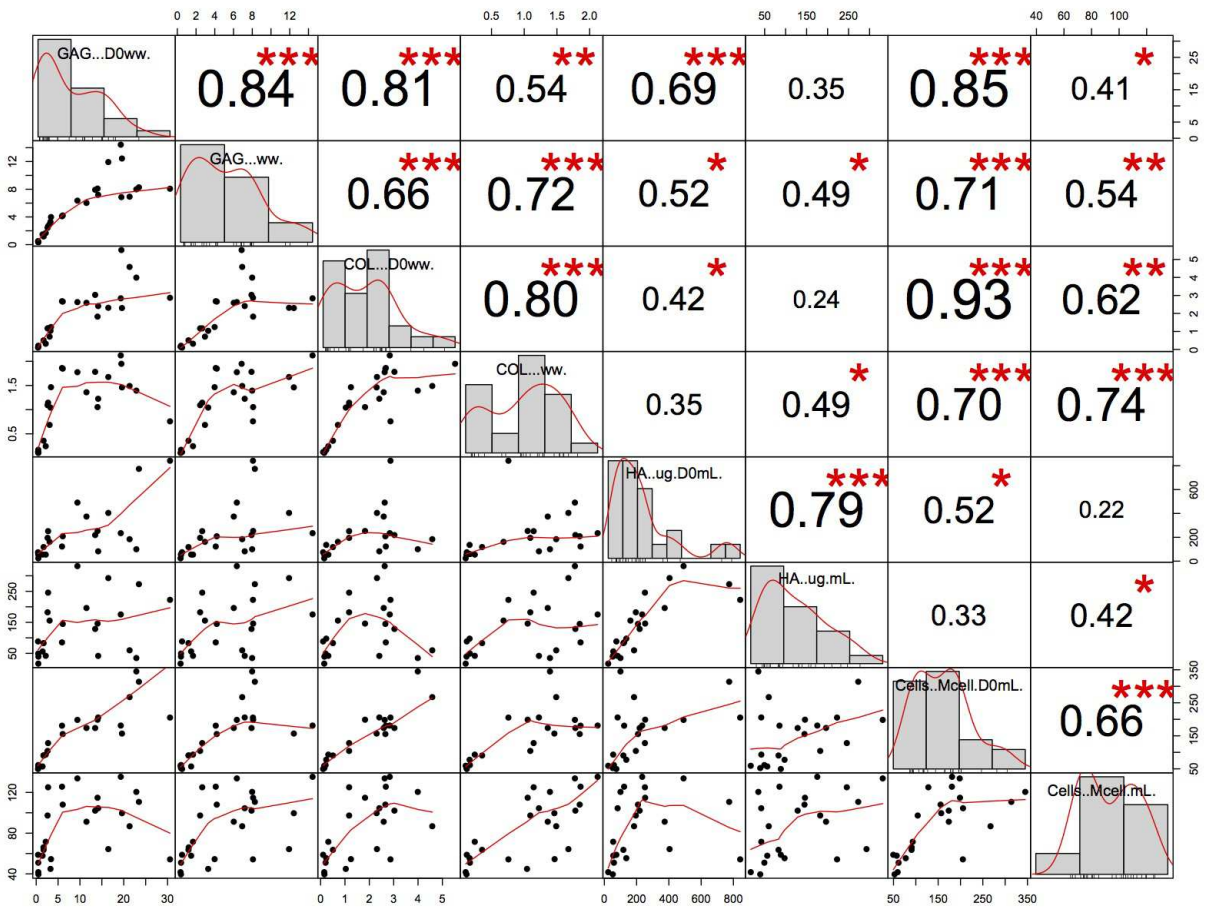

Figure 5.2: Biochemical correlations between total GAG content (normalized to day-0 and current day wet weight), collagen (normalized to day-0 and current day wet weight), hyaluronan (normalized to day-0 and current day wet weight) and cells (normalized to day-0 and current day wet weight). The diagonal displays a histogram of sample distribution of each measure, the upper triangle displays correlation coefficients and p-values (*: $p<0.05$, **: $p<0.01$, ***: $p<0.001$), and the lower triangle displays the data correlations between two measures.

(%day0-ww) and cells (million cells/day-0 mL), while for the current-day normalizations $R^2 = 0.74$ between collagen (%ww) and cells (million cells/mL).

5.5 Discussion

An open question in growth modeling is should the growth kinetics be described to allow the tissue to evolve throughout culture and what constituents should the binding kinetics be related to for modeling such growth. Here, we investigate whether hyaluronan content, a key binding partner of proteoglycans in native cartilage, should be modeled as a proxy for the binding site availability of GAG content. To this end, correlations between GAG and hyaluronan, cellular, and collagen

content were examined in tissue constructs with different cell seeding densities.

GAG and collagen correlations with all constituents were high (Figure 5.2) when both correlated variables are normalized to the referential (day-0) tissue wet weights, suggesting the influence of swelling confounds the data interpretation here. Interestingly, cell content was strongly correlated with both GAG and collagen deposition, with the highest correlation coefficients occurring between the total cell content (normalized to day-0) and the total biochemical content (normalized to day-0). Contrary to our original hypothesis that hyaluronan levels would most strongly correlate with matrix deposition due to the presence of GAG binding sites on hyaluronan, cell density provided the most remarkably robust correlations between all matrix deposition levels.

While this is likely due to a number of complex factors and interactions, including cell surface receptors and increased cellular synthesis with higher cell densities, for modeling purposes we can use this outcome to anticipate the GAG binding site availability through the current cell density within the constructs.

Similarly, the availability of binding sites for collagen deposition is also a complex and evolving process. Collagen fibrils are often spontaneously formed within a developing tissue through telopeptide interactions. This leads to the interesting prospect that collagen deposition begets more availability for collagen deposition. Through this analysis, collagen content was strongly correlated to cell content ($R^2 = 0.93$). For modeling purposes, like the binding sites for GAG, collagen binding sites can be related to the cell density of the local tissue.

The robustness of these correlations also suggests that increasing the cell density of tissues (either through media additives supporting cell proliferations or increasing cell seeding density) will enhance matrix deposition and growth within tissues. This relation, however, is contingent on the adequate availability of media and nutrients. For this work, we used small tissue constructs in a high media volume (3 mL per construct). This media supplementation level exceeds our standard formulation as we attempted to minimize both glucose and TGF-β fluctuations between media changes.

Overall, the work here provides strong evidence for using the cell density as proxy for the binding sites available for both depositing GAG and collagen within our computational growth models and experimental efforts towards increasing the cell seeding density of engineered tissues to enhance matrix deposition.

Chapter 6 TGF-β and glucose availability dictate the growth of large, engineered cartilage constructs

6.1 Abstract

The goal of the present study was to developing matrix deposition models accounting for the complex nutrient, cell, and matrix interactions occurring within growing, engineered cartilage. The previous studies elucidated the nutrient demands (Chapter 2 and (Albro *et al.* , 2016; Cigan *et al.* , 2013)), synthesis and binding kinetics of structural matrix proteins (Chapter 4), and the influence of cell density for both of nutrient availability and matrix binding characterized (Chapters 3 and 5). While the relation between glucose availability and matrix synthesis was established in our earlier works (Cigan *et al.* , 2013), the dependence of TGF-β supplementation on matrix synthesis remains unknown. In this work, we first establish a relationship between matrix synthesis and TGF-β supplementation based on two studies using small [bovine chondrocyte]-[agarose gel] constructs seeding with cell densities. As TGF-β dosing also had a strong influence on chondrocyte proliferation, we further established a relationship between cell proliferation and TGF-β dose. Models featuring both our previous work and the influence of TGF-β on matrix synthesis and cell proliferative were used to simulate the growth of constructs from three of our earlier studies, all with different cell seeding densities and construct geometries. Models reproduced the critical results of each study, and where therefore validated. By capturing the salient results and characteristics of all three studies, the validated models establish the complex and evolving roles of glucose and TGF-β availability, cell density and proliferation, and matrix synthesis and deposition within models of engineered cartilage growth. To extend these models for interrogating the channel density-cell seeding density space, models were run for a range of channel densities and cell seeding densities and suggest a critical cell seeding density necessary for nutrient channels to be beneficial.

6.2 Introduction

Despite significant progress in engineering small cartilage tissue constructs with native biochemical and mechanical properties, the engineering of larger, anatomically-sized constructs has proved difficult. This has hindered the clinical translation of tissue engineered cartilage therapies to re-

pair large, symptomatic osteoarthritis lesions. In particular, the most successful culture protocols are typically performed on small engineered cartilage constructs (volume scales ≈10 µL and length scales ≈1 mm) and often fail when translated to larger, more anatomically-relevant sized cartilage constructs (volume scales ≈100-1000 µL and length scales ≈10-100 mm). Nutrient limitations within these larger tissues cause necrotic cores and severe matrix heterogeneities. The lack of a robust, homogeneous matrix is particularly detrimental for engineered cartilage as it compromises the mechanical integrity of the tissue, producing constructs that would fail upon implantation within the dynamically-loaded joint environment. Clinical adoption of engineered cartilage treatments for osteoarthritis has therefore gained little traction with clinical trials predominantly focusing on treating small focal lesions but with little overall success.

To address this shortcoming, several approaches have emerged in the field to improve the nutrient availability and culture of large engineered constructs (Davisson *et al.* , 2002a; Buckley *et al.* , 2009; Bian *et al.* , 2009a). In particular, our lab and others have supplemented nutrient channels into critically large-sized constructs, enabling our recent engineering of an anatomically-sized cartilage construct with native compressive mechanical properties (Cigan *et al.* , 2016c; Cigan *et al.* , 2016b; Cigan *et al.* , 2014; Bian *et al.* , 2009a). This exciting result suggests that the most promising results achieved in small constructs can be scaled up to anatomically-sized constructs through the judicious placement of nutrient channels. While employing nutrient channels in large constructs is a proven strategy, determining the optimal arrangement and density of nutrient channels for each culture system is a significant task to optimize between the matrix synthesis capacity (increased with fewer channels) and nutrient availability (increased with more channels) of the tissue. Often, these optimizations are left to resource and time intensive trial-and-error experiments. An attractive alternative for optimizing tissue culture conditions would be to use sophisticated computational models of growth, informed by system-specific growth parameters, to provide an efficient strategy for understanding the interplay between matrix deposition and nutrient availability.

Computational models of engineered tissue growth have proven instructive in modeling oxygen and glucose availability and the roles of heterogeneous mechanical properties, but few models have been developed with parameters taken entirely from a single system. System-specific culture optimizations and insights for improving cartilage culture have not been possible (Nikolaev *et al.* , 2010; Obradovic *et al.* , 2000; Sengers *et al.* , 2004; Sengers *et al.* , 2005a;

Sengers *et al.* , 2005b; Zhou *et al.* , 2008). To this end, computational predictions of nutrient availability within large, channeled constructs provided us early insight that increasing matrix synthesis would require increased glucose supply, an outcome experimentally confirmed by increasing the media supply to constructs (Chapter 2 and (Nims *et al.* , 2015)). Importantly, this novel insight was provided from simple models informed with system-specific growth parameters, highlighting the role of computational models for improving culture conditions.

While models correctly instructed us on the beneficial role of enhanced glucose supply, they could not predict the significant role of nutrient channels as was experimentally observed. This suggested a more complex mechanism underlying engineered cartilage growth than glucose alone. Our recent investigation demonstrated active TGF-β exhibits a high degree of non-specific binding in developing tissue constructs and is rapidly internalized by resident cells, leading to significant heterogeneities (Albro *et al.* , 2016). In Chapter 3 we further determined the individual binding characteristics of agarose and cells with active TGF-β. Moreover, TGF-β exhibits differential biosynthetic and proliferative effects on tissue constructs through a wide concentration range (Byers *et al.* , 2008), suggesting that matrix heterogeneities may result from both TGF-β and glucose limitations. We hypothesize that modeling both glucose and TGF-β, important constituents of modern engineered cartilage culture protocols, will be necessary for developing functional growth models for predictive modeling of the influence of nutrient channels in engineered cartilage.

This study aims to establish and validate comprehensive models of the growth of engineered cartilage incorporating biosynthetic models of GAG and collagen based on the local availability of glucose and TGF-β . These models are direct extensions from our prior characterization and modeling studies and will, for the first time, develop matrix synthesis models of the complex nutrient profile within developing tissues. We first develop, parameterize, and validate cell proliferation and matrix synthesis models based on nutrient availability. Importantly, as recent experimental work has demonstrated the importance of increasing the cell density within cartilage constructs to improve tissue properties towards native contents, the models developed here are generalized and validated across a wide range of cell seeding densities. This allows models to examine the complex interactions between nutrient availability, cell density, and construct geometry.

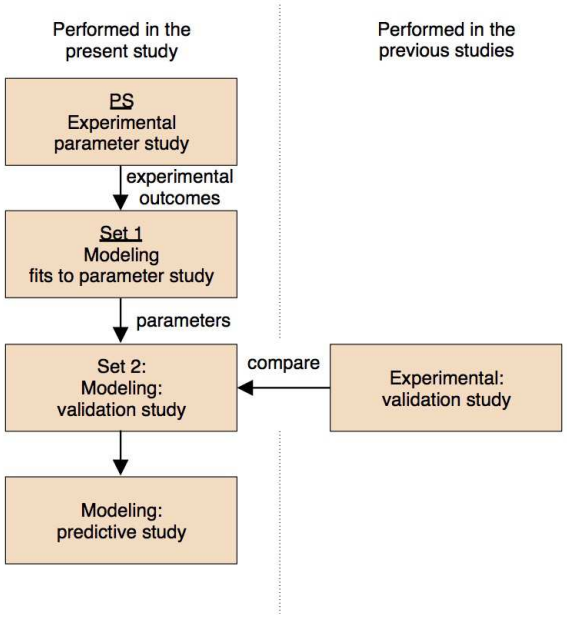

Figure 6.1: Overarching modeling schematic of experiments and modeling interactions.

6.3 Methods

The methods here reflect a union between experimental and computational procedures (Figure 6.1). We first performed experimental parameter studies (PS) to provide data for fitting system-specific growth relations required for the computational models. Models were fit to the experimental PS through a set of growth parameters. These growth parameters were then tested and validated by modeling experimental culture conditions not originally fit with the models. Lastly, models were run through a construct geometry and cell density parameter space to gain insights on our engineered cartilage culture system.

6.3.1 Experimental methods

Experimental protocols followed the well characterized cartilage engineering model of primary juvenile bovine chondrocytes embedded in a 2% agarose gel (type VII-A, Sigma) and cultured in a chemically defined, chondrogenic media based on high glucose (25 mM) Dulbecco's Modified Eagles Media (hgDMEM). Constructs were cultured in a 37 C, 5% CO_2 incubator under orbital rotation. Unless otherwise noted, construct media were supplemented with 10 ng mL^{-1} active TGF-β3 for

the first 14 days of culture. PS were first run on small constructs to estimate the growth parameters necessary for fitting the computational models. Models were validated against many of recently published experimental studies using alternate cell densities, construct geometries, and culture conditions.

6.3.2 Parametric estimation studies on small constructs

Growth parameters were assessed from two parameter studies (PS) using small tissue constructs. Both parameter study 1 (PS1: ∅3 mm × 0.8 mm constructs, initial cell seeding density 20 million cells mL^{-1}, 0.5 mL media per construct, 56 day culture) and parameter study 2 (PS2: ∅3 mm × 2.34 mm constructs, initial cell seeding density 60 million cells mL^{-1}, 1.5 mL media per construct, 28 day culture) focused on the influence of TGF-β dose on cellular proliferation and matrix deposition. TGF-β was supplemented at either 0, 0.01, 0.1, 1, or 10 ng mL^{-1} to constructs over the first 14 days of culture. Cultures were maintained orbitally shaken to ensure adequate nutrient mixing within the media bath. Cultured (PS1: day 56, PS2: day 28) and day 0 constructs were assayed for DNA, GAG, and collagen as previously described (Farndale *et al.* , 1986; Hollander *et al.* , 1994; McGowan *et al.* , 2002).

6.3.3 Lactic acid parametric studies

To determine the influence of lactic acid on growth, a parametric study was run (PS3) using the same culture conditions previously described. Culture system and protocols were similar to those described above with 10 ng mL^{-1} TGF-β supplementation for the first 14 days. A media-to-construct volume ratio of 40 µL/µL was used (based on constructs seeded at 30 million cells mL^{-1}) and orbital culture was performed in an incubator with 5% CO2 at 37 C. Lactic acid (Sigma) was added to fresh culture media at concentrations of 0, 5, 10, 15, 20, 30 and 40 mM. Day 0 and 28 constructs were assayed for DNA and GAG content.

6.3.4 Validation studies taken from the literature

Our previously published studies using the same culture system were used as the validation experiments; culture conditions and results are summarized below. Unless otherwise noted, constructs in these studies were supplemented with 10 ng mL^{-1} active TGF-β3 for the first 14 days of culture.

6.3.4.1 Channel studies: TGF-β The first channel optimization study we performed (Nims *et al.* , 2015) investigated the influence of media volume and construct geometry, testing the growth of constructs parametrically using 5, 10, or 15 mL of media per construct and either 0, 3, or 12 nutrient channels (⌀1 mm) within each ⌀10 mm × 2.34 mm construct. Constructs were seeded with 99 million cells mL^{-1} on day 0 and cultured on racks atop an orbitally shaken plate. This system encouraged media flow within the channels and adequate mixing within the media bath. The results demonstrated that increasing both channel density and media volume increased cell, GAG, and collagen content.

Following this, a subsequent experimental study investigated whether increasing channel density could further enhance growth. Constructs seeded with 45 million cells mL^{-1} and with 0, 12, 19, or 27 nutrient channels were cultured for 56 days with 15 mL media per constructs, based on the maximum growth conditions of the previous study. The results of this study demonstrated that the 12 and 19 channels configurations in a ⌀10 mm × 2.34 mm construct optimized growth (matrix deposition) compared to the 0 and 27 channel constructs.

6.3.4.2 Channel studies: no TGF-β To examine the role of TGF-ß in the growth enhancements of channeled constructs, 0 and 12 channel configurations were cultured in ⌀10 mm × 2.34 mm constructs as described above for 42 days, but without TGF-ß supplementation. Constructs seeded with 60 million cells mL^{-1}. This study did not show any differences in the 0 and 12 channel growth conditions.

6.3.4.3 Quasi-one-dimensional studies To establish the role of active TGF-β in spatial matrix deposition gradients, large constructs (⌀6 mm × 3.2 mm) seeded with 60 million cells mL^{-1} were cultured on the bottom of dish (3 mL per construct), such that the only media-construct interfaces were along the top and lateral faces of the construct. Constructs were cultured for 56 days with 0 or 10 ng mL^{-1} TGF-β supplementation over the first 14 days. After culture, a central ⌀3 mm core of the construct was punched and divided into four equal slices for spatial biochemical analysis (GAG and collagen). Using both experimental and computational methods, we validated that TGF-β within this central core was available nearly entirely through transport from the top surface of the construct, thus making the system "quasi-one-dimensional." Results demonstrated

little matrix deposition and heterogeneity within constructs not supplemented with TGF-β and a high matrix heterogeneity in constructs cultured with TGF-β, with the highest matrix deposition in the top (outer) slice.

6.3.5 Computer models

Models were developed using culture and construct-specific geometries and implemented with growth kinetics and reactions. The framework ensures reactions are spatially dependent and run within each finite element. Each reaction therefore is based on the local (elemental) concentrations of glucose, TGF-β, lactic acid, and cell density.

6.3.6 Finite element geometries of culture conditions and geometries

Finite element models (FEM) were constructed using CUBIT (Sandia Labs) to simulate the culture conditions and tissue geometries used in experimental culture and were modeled in a custom version of FEBio (v. 2.6.0) (Figure 6.2). Models simulated the following culture conditions: a finite-sized, well-stirred media bath surrounding the tissue construct. This bath supplied glucose and TGF-β which were replenished during media changes; media changes also removed lactic acid and soluble matrix which had transported into the bath. Growth reactions (nutrient consumption, matrix synthesis, and matrix and nutrient binding as described below) occurred within the tissue construct. Soluble metabolites (glucose, TGF-β, and lactic acid) and matrix (GAG and collagen) transport (diffusion) occurred between the tissue construct and bath along the media-construct interfaces. Bound nutrients, bound matrix, and cells were only present in the tissue construct. Symmetry was employed where appropriate to reduce computational demand of the FEM.

Two critical FEM were employed here: 1) cylindrical constructs (CYL) and 2) channeled construct units (CHU).

- 1) CYL were modeled as a single cylindrical construct (dimensions reflecting experimental conditions) at the bottom of a media bath (bath volume reflecting experimental conditions), with a media-construct interface along the lateral and top surface of the construct. CYL (Figure 6.2A) models were axisymmetric, so a 3-degree construct slice was modeled.

- 2) CHU (Figure 6.2B, bottom) were modeled as a the symmetry reduced channeled construct

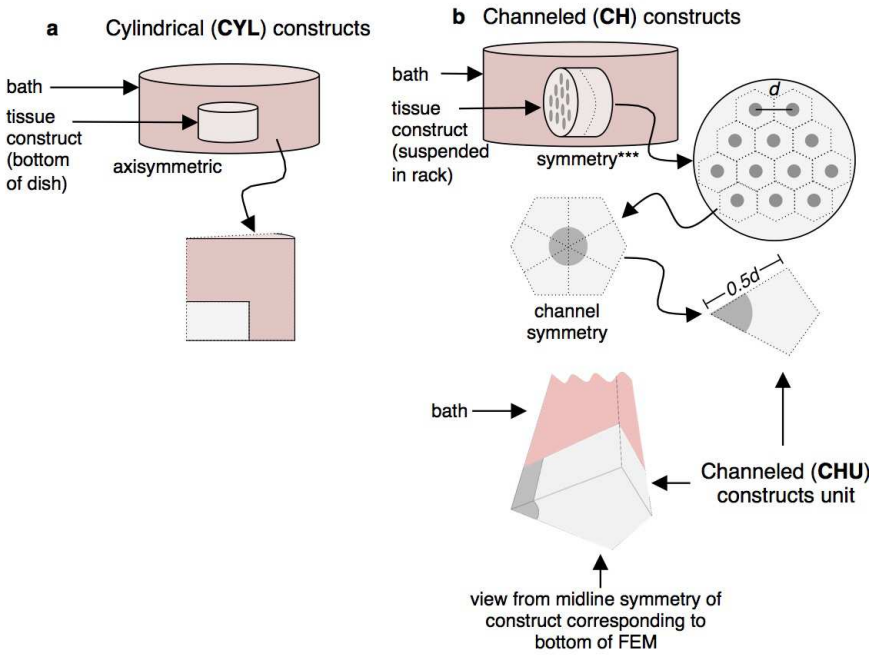

Figure 6.2: Modeling schematic of experiments and modeling interactions.

to model a representative unit of a channeled construct that could be used to model specifically the growth of a large construct based on the inner regions away from the lateral edges. CHU captured a 60 degree slice of the channel surrounding tissue based on axisymmetry of the channel and symmetry of the representative units within the tissue. Axial symmetry was employed to reduce models to one-half the thickness of the construct. The critical dimensions for these CHU were the center-to-center spacing of channels (dependent on channel density), construct thickness (constant to reflect the 2.34 mm thick constructs), and the channel diameter (constant to reflect the ∅1 mm channel). The media-construct interface was along the top and channel surfaces of the construct for CHU.

6.3.7 Modeling nutrient transport, consumption and matrix synthesis, binding

Growth reactions were modeled within the tissue construct material of the FEMs. Growth models were based on our prior studies of glucose and TGF-β consumption and transport and GAG and collagen synthesis and binding. TGF-β binding interactions with the individual tissue constituents agarose and chondrocytes were extracted from the bulk mixture binding characteristics previously reported (Chapter 3). Glucose and TGF-β consumption rates and GAG and collagen synthesis

rates were normalized to a per cell basis such that consumption and synthesis were dependent on the current and spatially-dependent cell density $\hat{c}_{tissue} = \hat{c}_{cell}\left(x,t,c^i\right)\rho\left(x,t,c^i\right)$.

As lactic acid was also used to investigate the role of product inhibition on cellular proliferation and matrix synthesis, lactic acid was modeled as product of glucose metabolism following the chemical reaction

$$\hat{c}^{la} = -2\hat{c}^{glu} = 2\frac{V_{cell}^{glu}\rho^{cell}c^{glu}}{K_m + c^{glu}}$$

where c^{la} and c^{glu} are the concentrations of lactic acid and glucose, respectively, K_m is the Michaelis constant for glucose, V_{cell}^{glu} is the cellular consumption rate of glucose, ρ^{cell} is the local cell density of the tissue, and a hat denotes the constituent's molar supply. Experimentally, the concentration of lactic acid was found to be critical for both matrix synthesis and cell proliferation and was adapted into these models subsequently.

6.3.8 Cell proliferation

Cell proliferation was based on a logarithmic model where the specific growth rate, μ, was used to stimulate proliferation (based on TGF-β, and $c_{thresh}^{TGF\beta} = 1$ pg mL^{-1}) and inhibit proliferation (based on lactic acid):

$$\hat{\rho}^{cell} = \mu\left(c^{la}, c^{TGF\beta}\right)\rho^{cell}$$

$$\mu\left(c^{la}, c^{TGF\beta}\right) = \begin{cases} k_a log\left(c_{max}^{TGF\beta}/c_{thresh}^{TGF\beta}\right) & c_{max}^{TGF\beta} > c_{thresh}^{TGF\beta},\ c^{la} \leq c_{thresh}^{la} \\ k_a log\left(c_{max}^{TGF\beta}/c_{thresh}^{TGF\beta}\right)\left(\frac{K_I}{K_I + c^{la}}\right) & c_{max}^{TGF\beta} > c_{thresh}^{TGF\beta},\ c^{la} > c_{thresh}^{la} \\ 0 & c_{max}^{TGF\beta} \leq c_{thresh}^{TGF\beta} \end{cases}.$$

The parameters for this reaction which must be gathered are K_I and c_{thresh}^{la} from the lactate dosing study (PS3) and k_a and $c_{thresh}^{TGF\beta}$ from a TGF-β dosing study (PS1 and 2).

6.3.9 Matrix synthesis

GAG and collagen synthesis was partitioned into two terms: a basal and TGF-β stimulated terms. Basal synthesis was based on data, both our own and others, demonstrating that chondrocytes, in

the absence of TGF-β stimulation, synthesize most matrix in over the 14 days of culture, before reducing their synthesis rate (modeled here as 50% synthesis reduction in synthesis per cell after day 14). TGF-β stimulated synthesis was modeled as logarithmically dependent on the level of TGF-β consumption. A minimum TGF-β consumption threshold was necessary to elicit matrix stimulation and a maximum TGF-β consumption ceiling was modeled above which no further stimulation was possible. Based on prior models of TGF-β stimulation, consumed TGF-β was normalized to an average per cell level for modeling different cell seeding densities. Lactic acid inhibited matrix synthesis based on empirical data in a similar manner to previously done (Zhou *et al.* , 2008).

Matrix binding site density (N_t), set to a constant in our original work (Chapter 4), was scaled here based on cell density according to the ratio of $N_t^{GAG} = 300$ mM and $N_t^{COL} = 0.3$ mM per 30 million cells mL^{-1} (Chapter 5). This binding site density was modeled to increase with cell proliferation at the same ratio. Binding rates for both GAG and collagen were taken from our earlier work (Chapter 4) as constants that were only dependent on TGF-β administration and release.

Matrix synthesis equations and formulation Like cellular proliferation, matrix synthesis was based on a logarithmic model of consumed TGF-β (a product of the Michaelis-Menten kinetics of soluble TGF-β with cells within the scaffold of the tissue.) The local consumed TGF-β content was normalized with the current local cell density as

$$c_{cell}^{TGF\beta} = \frac{c_{consumed}^{TGF\beta}}{\rho^{cell}}$$

where

$$c_{consumed}^{TGF\beta}(t) = \int_0^t \frac{V_{cell}^{TGF\beta}\rho^{cell}c^{TGF\beta}}{K_m^{TGF\beta} + c^{TGF\beta}} d\tau$$

according to Michaelis-Menten kinetics were $V_{cell}^{TGF\beta}$ is the per cell TGF-β internalization rate and $K_m^{TGF\beta}$ is the Michaelis constant for the reaction (taken from our earlier work to be 1 mM).

Using this measure of TGF-β consumption, matrix synthesis was calculated based on partitioning the matrix synthesis terms into a basal (*basal*) synthesis and TGF-β stimulated (*stim*) synthesis terms

$$\hat{c}_{cell}^{GAG} = \hat{c}_{stim}^{GAG} + \hat{c}_{basal}^{GAG}$$

where

$$\hat{c}_{basal}^{GAG} = \begin{cases} \hat{c}_o^{GAG} f(c^{la}) & t < t_{thresh} \\ 0.5\hat{c}_o^{GAG} f(c^{la}) & t \geq t_{thresh} \end{cases}$$

where $\hat{c}_o^{GAG}$ is taken from our previous work (Chapter 4) and $t_{thresh} = 14$ days.

For the TGF-β stimulation term,

$$\hat{c}_{stim}^{GAG} = \begin{cases} k_a log\left(c_{THRESH}^{TGF\beta}/c_{thresh}^{TGF\beta}\right) f(c^{la}) & c_{cell}^{TGF\beta} \geq c_{THRESH}^{TGF\beta} \\ k_a log\left(c_{cell}^{TGF\beta}/c_{thresh}^{TGF\beta}\right) f(c^{la}) & c_{THRESH}^{TGF\beta} > c_{cell}^{TGF\beta} > c_{thresh}^{TGF\beta} \\ 0 & c_{cell}^{TGF\beta} \leq c_{thresh}^{TGF\beta} \end{cases}$$

where k_a is the matrix synthesis term, $c_{THRESH}^{TGF\beta}$ is the maximal TGF-β consumption and $c_{thresh}^{TGF\beta}$ is the minimal TGF-β for matrix stimulation. As these are synthesis rates based on a cellular basis, local tissue synthesis is equal to

$$\hat{c}_{tissue}^{GAG} = \hat{c}_{cell}^{GAG}\rho^{cell} = \rho^{cell}\left(\hat{c}_{stim}^{GAG} + \hat{c}_{basal}^{GAG}\right).$$

For both the basal and simulated terms, an inhibitory influence of lactic acid is included and governed by

$$f(c^{la}) = \begin{cases} 1 & c^{la} \leq c_{min,thresh}^{la} \\ 1 - \left(\frac{c^{la} - c_{min,thresh}^{la}}{c_{max,thresh}^{la} - c_{min,thresh}^{la}}\right) & c_{max,thresh}^{la} > c^{la} > c_{min,thresh}^{la} \\ 0 & c_{max,thresh}^{la} \leq c^{la} \end{cases}.$$

Illustrative schematic trends of the $\hat{c}_{stim}^{GAG}$ and $f(c^{la})$ are included below.

6.4 Results

6.4.1 Experimental results

6.4.1.1 Parameter studies 1 and 2: TGF-β dosing influence TGF-β played a critical role in the development of biochemical content in engineered cartilage through a large concentration

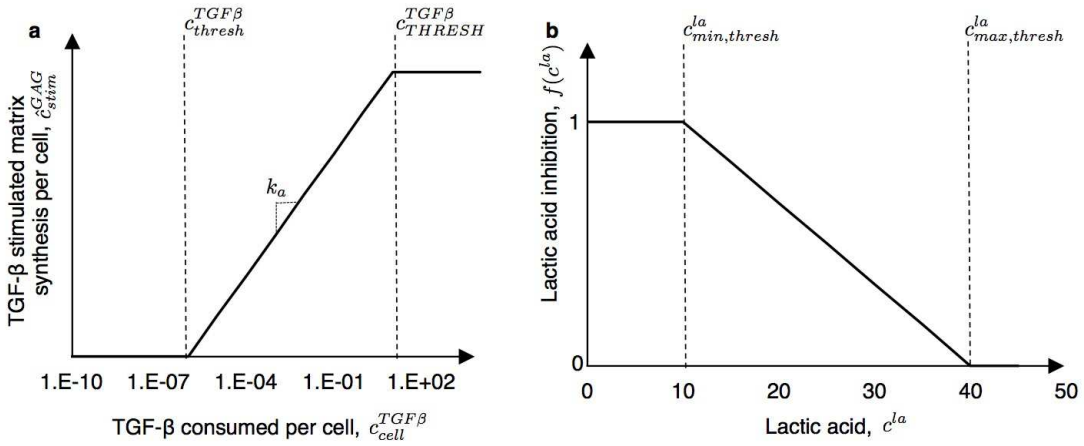

Figure 6.3: Schematics of TGF-β stimulated matrix and lactic acid inhibition models.

range (four-orders of magnitude as measured here). In both PS1 and PS2, increasing TGF-β supplementation levels increased the cell content (Figure 6.4). Cell content generally increased with increasing levels of TGF-β with cellularity trending higher up to a TGF-β dosing of 1 ng mL^{-1}. Groups receiving 1 and 10 ng mL^{-1} had statistically similar cell contents. Similarly, small constructs supplemented with 1 and 10 ng mL^{-1} significantly increased their GAG deposition compared to 0, 0.1, and 1 ng mL^{-1} supplementation groups. A TGF-β dose of 0 ng mL^{-1} produced little matrix deposition. From preliminary studies, most of this GAG deposition occurred prior to day 14. The physical growth of engineered constructs (as measured by the swelling ratio) was elevated in groups with increased TGF-β supplementation, and highest in either the 10 ng mL^{-1} dose group (PS1) or 1 and 10 ng mL^{-1} dose group (PS2).

6.4.1.2 Parameter studies 3: Lactic acid influence Lactic acid treatment produced cellular and biochemical growth differences over the 28 day culture (Figure 6.5). Cell content and tissue swelling (swelling ratio) did not change from day-0 levels when media was supplemented with 40 mM lactic acid. Total cell content was unchanged from the untreated control (0 mM) with lactate supplementation up to 20 mM.

GAG content varied complexly with lactate supplementation. When supplemented with 5 mM lactate, constructs deposited significantly more GAG than all other groups. GAG deposition in the 0, 10, and 20 mM groups were similar. Cell density was significantly higher than day-0 levels for all groups except the 40 mM supplementation group.

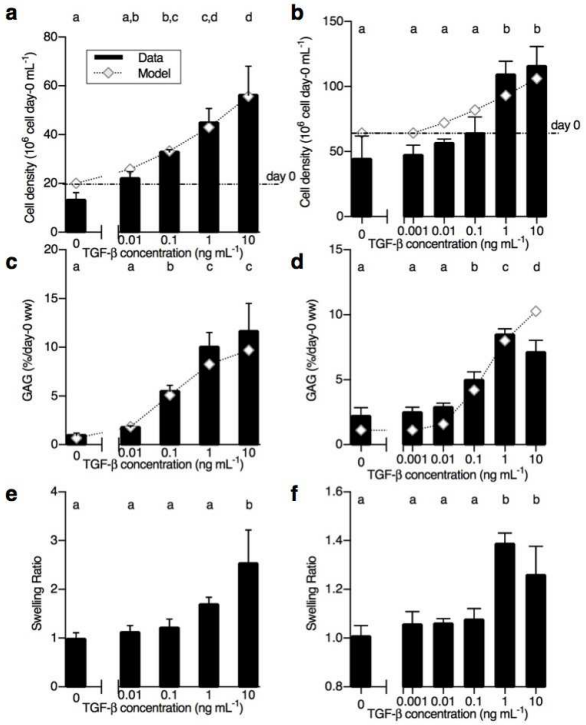

Figure 6.4: Growth parameter study results to the influence of TGF-β dose. Parameter study 1: **a**, **c**, and **e**; parameter study 2: **b**, **d**, and **f**. Data results in columns, model fits are diamonds.

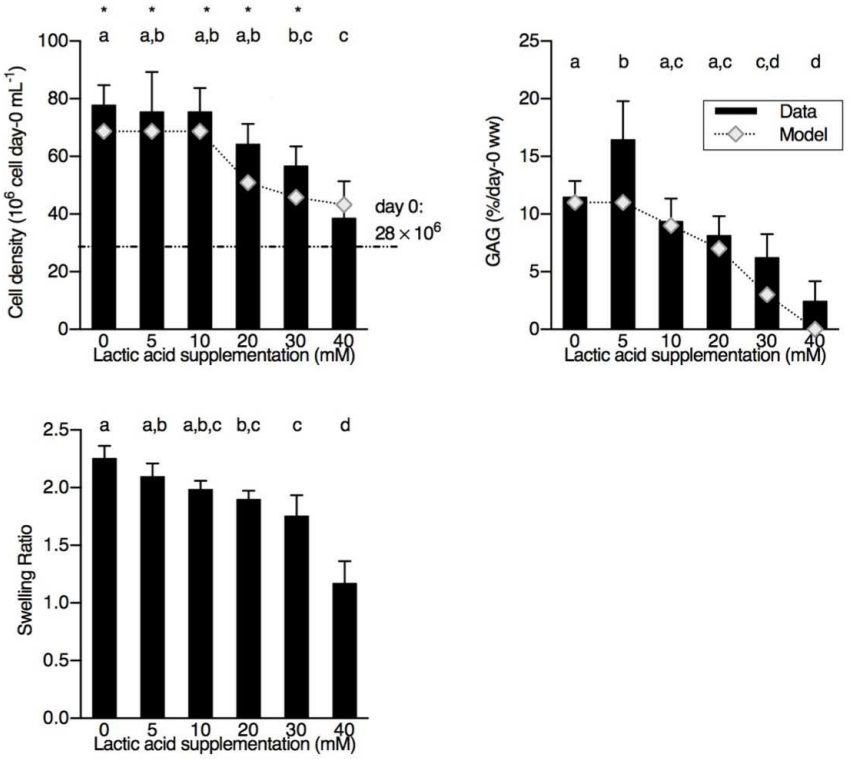

Figure 6.5: Influence of lactic acid on small construct growth. Data results in columns, model fits are diamonds.

Parameter	Value
Cell proliferation	
k_a	5.3×10^{-8} ncell μL^{-1} s^{-1}
$c_{thresh}^{TGF\beta}$	1 pg mL^{-1}
K_l	40 mM
c_{thresh}^{la}	19 mM
Matrix synthesis	
$c_{thresh}^{TGF\beta}$	9×10^{-27} g TGF-β ncell^{-1}
$c_{THRESH}^{TGF\beta}$	$100\times c_{thresh}^{TGF\beta}$
k_a	1.35×10^{-18} nmol GAG μL^{-1} 2^{-1}
Lactic acid inhibition	
$c_{min,thresh}^{la}$	0 mM
$c_{max,thresh}^{la}$	40 mM

Table 4: Growth parameter fits of cell proliferation, matrix synthesis, and lactate inhibition.

6.4.2 Computational results

6.4.2.1 Parameter estimation Model fits to PS1 and PS2 produced close agreement when using the study specific construct geometries, media bath volume, and cell seeding density to inform growth rates (cell proliferation fits: $r_{PS1}^{cell} = 0.99$; $r_{PS2}^{cell} = 0.94$; GAG deposition: $r_{PS1}^{GAG} = 0.99$; $r_{PS2}^{GAG} = 0.99$). Parameters gathered from the studies were both for cellular proliferation and GAG synthesis (Table 4).

6.4.2.2 Validation The computational model growth parameters fit in the previous section were first applied to the growth of the quasi-one-dimensional construct (Figure 6.6). Growth models mimicked the heterogeneous deposition of GAG within TGF-β treated large constructs, where most matrix deposition was evident in the top slice of the construct and little deposition was present in the lower slices ($r_{1D}^{GAG} = 0.92$). Notably, there is a quantitative distinction between the deposition profiles of the top two slices, with the model predicting GAG deposition at ≈12 %Day-0ww while the experimental measurement was ≈5.6 %Day-56ww. The model further matched the matrix deposition profiles of a large construct not treated with TGF-β, exhibiting a slight drop in matrix binding between the bottom and top slices of the construct.

Validations of the channeled constructs were matched in both levels of cellular proliferation and GAG deposition (Figure 6.7A, B). Comparing the models to the first channel study, using 0, 3, or 12

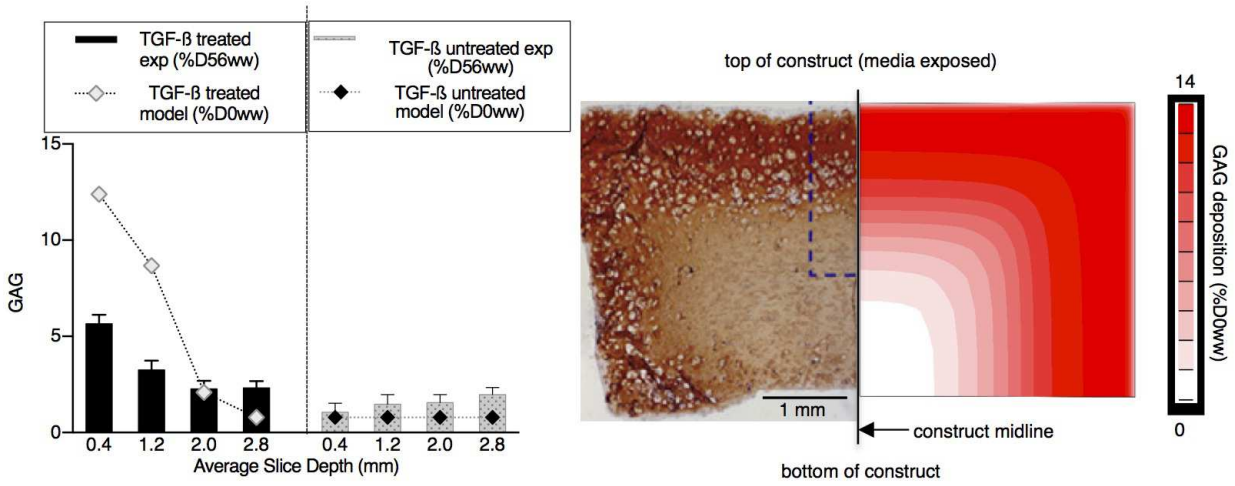

Figure 6.6: Experimental and modeling predictions of the culture of a large, heterogeneous cartilage construct. Quantitative results (left) for both TGF-β supplemented (left pane) and unsupplemented (right pane). Histological and FEM graphical output results also compare well qualitatively.

channels seeded with 99 million cell mL^{-1} and 15 mL of media, computational models displayed an increasing GAG and cell content (normalized to day-0 ww), as did the experimental results. The cell proliferation model had a closer fit to the experimental data than the GAG synthesis. Quantitatively, matrix synthesis models anticipated more GAG deposition than was measured experimentally.

Models of the second channel study changed the construct geometry to increase channel density (0, 12, and 19 channels) while maintaining constant culture conditions (15 mL media per construct) (Figure 6.7C, D). A lower cell seeding density (45 million cells mL^{-1}) was used for this study. Models again matched the trends in both cell proliferation and matrix deposition between the different construct geometries. Experimentally, this channel study displayed an optimal density of channels before which the deposition of matrix declines. In a similar manner, the system-specific growth models matched this plateauing of matrix synthesis potential at elevated channel densities.

6.4.3 Modeling simulations

With the modeling fits and using the CHU FEM geometries, models were run with channel-to-channel spacings from 4.33 mm (corresponding to the same spacing as three ⌀1 mm channels in a ⌀10 mm construct) to 1.1 mm. Using a ⌀1 mm channel geometry, the lowest channel-to-channel spacing approaches 1 mm, although practically achieving this spacing would be experimentally challenging. Cell seeding densities of 30, 45, 60, 75, 100, and 120 million cells mL^{-1} (Figure 6.8)

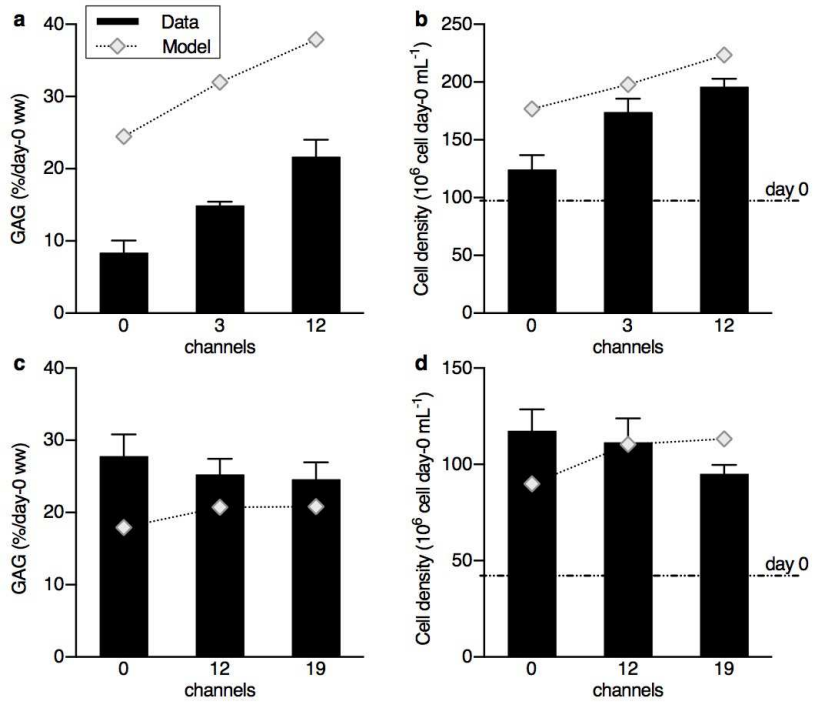

Figure 6.7: Experimental and modeling predictions of the culture of a large-channeled tissue constructs of two previous studies constructs. GAG deposition results (a,c) and cellular proliferation results (b,d) for both the 0-3-12 channel study (a,b) and 0-12-19 channel studies (c,d).

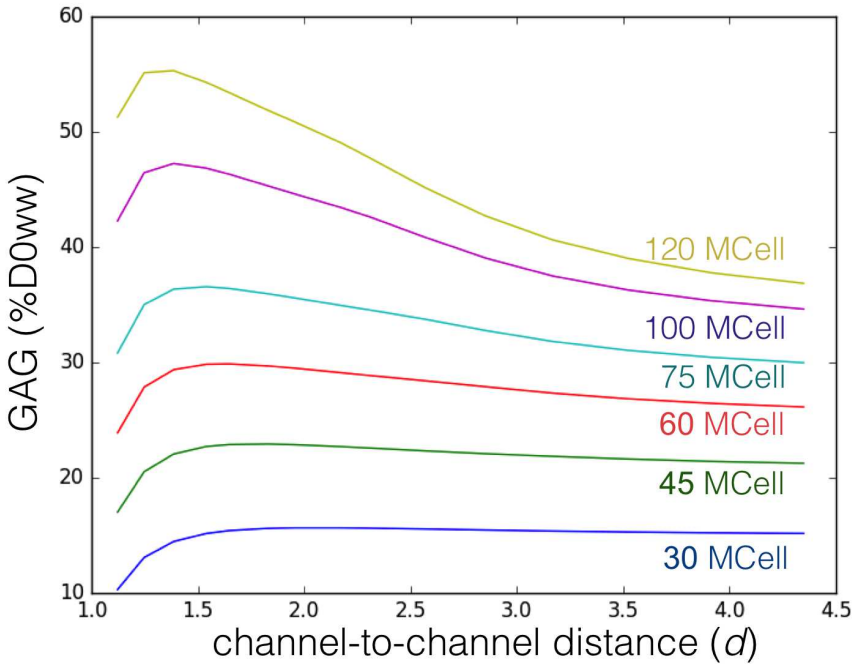

Figure 6.8: Model simulations of GAG deposition constructs with various channel-to-channel spacings and cell densities.

were used. These models displayed a peak in GAG deposition (normalized to day 0 tissue wet weight) only when cell densities exceeded 75 million cells mL^{-1}. Between 120 and 100 million cells mL^{-1}, the optimal channel-to-channel spacing shifted towards a less dense arrangement. At 60 million cells mL^{-1} and below, there was no optimal peak in matrix deposition with a trend towards less GAG deposition as more tissue is removed with the increased channel-to-channel density.

6.5 Discussion

This study presents a comprehensive model of the growth of engineered cartilage using modern tissue engineering technologies. To date, designing tissue engineering studies is largely based on intuition and resource intensive iteration. As promising tissue engineered technologies come of age and achieve success on small engineered tissue constructs using a variety of clinically-relevant cell types, a transition to the clinic by creating large, anatomically-sized constructs for resurfacing entire joint surfaces will begin to take place. For these studies, however, iterative experimental tissue engineering strategies will become a prohibitive limitation to understanding how best to scale culture protocols. Computational models, based on system-specific parameter studies, and validated experimentally such that they exhibit the salient growth phenomena of engineered cartilage, may be an essential tool for designing such large engineered tissues. Despite their necessity and utility, to date, growth models have been limited in their scope and have not yet been used for guiding successful culture protocols. The models we present here take advantage of our recent investigations on the need for and transport of TGF-β, an essential stimulator of matrix synthesis in modern tissue engineering systems.

In particular, parametric models fit the dose-dependence of TGF-β well ($r = 0.99$ for both studies Figure 6.4) and cell proliferation within the engineered cartilage was identified to be TGF-β dependent. Cell proliferation models also exhibited a high goodness of fit ($r \geq 0.94$ Figure 6.4). An important feature of these fitting experiments was the use of constructs with different cell seeding densities and geometries. By developing models faithful to both experiments, we developed a set of modeling relationships which may be applicable to a wide variety of experiments.

Based on the finding that cell density and proliferation was a strong variable dictating the matrix deposition within tissue constructs (Chapters 3 and 5 and Figure 6.4), we were interested as to what factors associated with increased cell density could influence matrix growth. Based on

the literature of engineered cartilage development, we investigated lactic acid (Zhou *et al.* , 2008; Sengers *et al.* , 2005b; Sengers *et al.* , 2005a; Obradovic *et al.* , 1999). The results here (Figure 6.5) demonstrate that both cell proliferation and matrix synthesis are highly determined by lactic acid and at a point, 40 mM as suggested previously (Zhou *et al.* , 2008), there is a complete inhibition of matrix deposition. Lactic acid inhibition was therefore developed within both the cell proliferation and matrix synthesis models based on this finding.

We then constructed models with FE geometries specific to the culture conditions of our studies in the literature (Figure 6.2) for studies using either large, unchanneled construct or channeled construct studies (Albro *et al.* , 2016; Cigan *et al.* , 2016c; Nims *et al.* , 2015). While these studies featured a wide range of cell seeding densities, construct geometries, and culture conditions (presence or absence of TGF-β), model predictions were well matched to the experimental outcomes of both the quasi-1D study (Figure 6.6) and the two channel studies (Figure 6.7). All studies matched the qualitative behavior of matrix expression. The quasi-1D model predicted the most matrix deposition would occur in the top two peripheral slices of constructs supplemented with TGF-β and no significant GAG content variations would be present in constructs not treated with TGF-β. The channel models of constructs with 0, 3, or 12 channels using 99 million cells mL^{-1} predicted an increasing trend in both GAG deposition and cell content with increasing channel density. Lastly, the channel models of constructs with 0, 12, or 19 channels but at a lower cell density (45 million cells mL^{-1}) than the previous study predicted little change in both GAG deposition and cell content with increasing channel density (no statistical differences in the experimental data was detected). Despite these similarities in qualitative behavior, the quasi-1D study and 0-3-12 channel study displayed quantitative discrepancies between experiments and computational predictions. While we are not entirely sure of the nature of the discrepancy, it is important to note that these models did not feature a physical expansion or swelling mechanism. Swelling could increase the path length for diffusion of critical metabolites, reducing growth by either decreasing glucose or increasing lactic acid concentrations. Additionally, as the quasi-1D experimental measurements were not relative to day-0 wet weight, it is possible that allowing the models simulations to swell (which is likely with the 12 %day-0 ww GAG deposition predicted, see Chapter 4). This swelling and matrix dilution of the computational results would make the biochemical agreement of Figure 6.6 closer. However, as all the model predictions captured the salient trends not previously understood or

capable by computational models available to date, we accept these models as validated and propose the quantitative differences result primarily from metabolic heterogeneities of the primary cells.

Validated models were then assessed to examine the complex interactions between tissue geometry and cell seeding density (Figure 6.8). Interestingly, optimal channel densities were predicted to exist for higher cell densities, while lower cell densities (below 75 million cells mL^{-1}) displayed a gradual decline in GAG deposition as the tissue channel density increased. This is particularly striking as the same behavior has been observed in our lab and others. When comparing the experimental results of the 0-3-12 channel study using 99 million cells mL^{-1}, there was a clear benefit to increased channels (Nims *et al.* , 2015). Conversely, when we cultured 0-12-19 channel constructs with 45 million cells mL^{-1}, there was no clear benefit to nutrient channels and even a reduction in properties (Cigan *et al.* , 2016c). Additionally, when other labs have cultured constructs with numerous channels with only 15 million cells mL^{-1}, there was no benefit evidenced by the increased availability of nutrients enhanced with channel supplementation (Buckley *et al.* , 2009; Sheehy *et al.* , 2011). Together, these results make intuitive sense that nutrient channels only benefit tissue growth once nutrition becomes diminished. For the construct sizes tested in vitro, this rarely occurs, even with TGF-β nutrition, until the cell seeding density becomes prohibitively high. These models do suggest a critical role in predicting optimal channel arrangements in large, anatomical constructs, which may have tissue depths up to 7 mm (Hung *et al.* , 2003; Hung *et al.* , 2004).

There are several important advances in the computational models presented here which differ from prior attempts to model engineered cartilage growth. Importantly, using glucose and TGF-β allowed us to model modern tissue culture system where both nutrients are essential for and drive growth. Glucose is often modeled as a proto-nutrient for engineered tissue growth and is essential for cellular metabolism and viability. In our early attempts to engineer an anatomically-sized patella, glucose deficiencies indeed led to heterogeneous matrix deposition.

Since the original culture of the patella over a decade ago, tissue engineering has increasingly used chemically-defined media formulations including TGF-β supplementation to enhance matrix synthesis in constructs. Building off of our recent investigations into the hindered transport of TGF-β, the growth models developed here used TGF-β availability to predict cell proliferation and matrix synthesis. Despite the diverse phenotypic responses TGF-β can elicit, a relatively simple relation between TGF-β levels and cell proliferation and matrix synthesis proved sufficient for the model

here. TGF-β signaling and the subsequent phenotypic responses, however, represent a complex cascade mediated by a number of influences including intracellular signaling molecules (notably the SMAD family), the concentration and duration of TGF-β exposure, and local cell density. Moreover, direct relations between TGF-β signaling cascades and downstream phenotypic events have received little attention in the literature. Phenotypic response studies have predominantly focused on studies within the field of developmental biology (Dubrulle *et al.* , 2015). Models of adult cell responses are still being validated and are based on modeling a gene regulatory network (GRN). GRN may prove useful in modeling the phenotypic changes within cells which still exhibit some stemness and where TGF-β exposure may influence more genotypic changes than cell proliferation and matrix synthesis (Zi *et al.* , 2011; Dubrulle *et al.* , 2015).

As the models here are specific to agarose constructs seeded with primary bovine chondrocytes, developing models for other clinically-relevant tissue culture systems will be required for optimizing more translational systems. While mature cells are typically believed to have a depressed metabolism and may not require the enhancements in nutrient availability provided by nutrient channels, recent studies in fact suggest both mature canine cells and bovine mesenchymal stem cells in large constructs are nutrient-limited (Saxena *et al.* , 2016; Durney *et al.* , 2017; Nims *et al.* , 2017). Specifically for mature canine chondrocytes it is likely that different cellular signaling mechanisms may be at play than in juvenile bovine chondrocytes. Therefore, higher levels of TGF-β may be necessary to elicit similar levels of matrix synthesis, whereas juvenile bovine chondrocytes deposit similar levels of matrix between 1 and 10 ng mL^{-1} TGF-β supplementation. Interestingly, the mechanism by which juvenile bovine chondrocytes are stimulated after only a two-week TGF-β treatment is still unknown. That mature chondrocytes (bovine, canine, and human) require continuous TGF-β supplementation for maximal growth indeed suggests the internal cellular signaling is transient in mature cells compared to the prolonged stimulation after the two-weeks of treatment in juvenile chondrocytes (Cigan *et al.* , 2016a; Chung & Burdick, 2008; Farrell *et al.* , 2014; Ng *et al.* , 2009).

This study presents the first comprehensive computational model for optimizing and evaluating modern tissue engineering culture featuring both glucose and TGF-β dependent growth and a mechanism by which mechanical growth can be modeled spatially based on the simulated deposition of GAG and collagen. This advance will be critical for our future culturing of patella-sized engineered constructs by assessing optimal channel densities in these resource-intensive cultures. Our recent

advances in engineering large, channeled constructs provide the template by which these constructs can be cultured to ensure adequate nutrient mixing and perfusion through the nutrient channels. Our subsequent advances in culturing large constructs within a cage system to retain the tissue and prevent deleterious construct swelling suggests that mechanical properties are further enhanced by enhancing collagen maturity. Together, we are excited by these advances and other improvements in the field towards a promising treatment for resurfacing damaged and denatured osteoarthritic cartilage.

Chapter 7 Varying the concentration of oxygen and inorganic sulfate does not affect [juvenile bovine chondrocyte]-[agarose gel] construct growth when supplied with sufficient glucose and TGF-β

7.1 Abstract

The glucose- and TGF-β-dependent models of Chapter 6 displayed a high fidelity to the experimental results of our earlier studies. Whether additional critical nutrients exist of this system has yet to be determined. Perhaps most notably is the dependence of growth on oxygen as was suggested within the literature and demonstrated with computational models. Additionally, the influence of sulfate on tissue growth has not yet been characterized, but may be essential due to the high deposition and synthesis of sulfated proteoglycans. To this end, the current study examines the influence of oxygen and inorganic sulfate on the growth of small constructs using parametric studies of each nutrient. Using glucose and TGF-β levels that we had previously classified as sufficient for cartilage construct growth, we did not find that depletions of oxygen or inorganic sulfate negatively influenced the growth of engineered cartilage constructs. This work suggest that differences in cell metabolism heterogeneities, cell density, and tissue swelling and mechanics may influence the predictive ability of computational models more than modeling additional nutrients.

7.2 Introduction

The nutritional demands of developing engineered cartilage are important to consider for optimally designing culture protocols that ensure adequate nutrients are supplied to the resident chondrocytes populations within large sized constructs. This is of great interest as the preponderance of engineered cartilage systems produce supraphysiologic levels of GAG and synthesize subphysiolgic levels of collagen. Uncovering simple nutrient alterations which can alter matrix synthesis would present a convenient means by which the mechanics of engineered cartilage could be altered.

To this end, we have analyzed the nutrient demands of engineered cartilage using the [juvenile bovine chondrocyte]-[agarose gel] system supplemented with TGF-β3 for the first 14 days of culture

(Cigan *et al.* , 2013; Albro *et al.* , 2016). The salient findings suggest that glucose can be a limiting dose-dependent nutrient, particularly in large constructs where nutrient gradients can develop from both diffusion and consumption issues, and that TGF-β exhibits a steep dose-dependent alterations in cellular proliferation and matrix synthesis. As TGF-β3 is readily internalized by chondrocytes it has profound influence on tissue heterogeneity.

The chondrogenic media formulation, however, used here consists of 50 additional constituents and inorganic salts which have not been extensively examined for their role in cartilage growth. This section examines two of the previously unexamined nutrients in our culture system: inorganic sulfate and oxygen.

Inorganic sulfate, SO_4^{-2}, plays a critical role in the sulfation of the negatively charged proteoglycans within engineered and native cartilage (Rossi *et al.* , 1998). In cell culture, sulfate is added through magnesium sulfate and is present in a concentration of 810 µM. As a cell culture strategy to reduce sulfation, several studies have tried withholding inorganic sulfate from cell culture media to prevent GAG sulfation and alter the sizes and agglomeration of charged molecules (Sobue *et al.* , 1978; Kato & Gospodarowicz, 1985). It is unclear how such a culture regime will influence cartilage growth de novo.

Oxygen is a widely studied critical nutrient in engineered cartilage growth due to early evidence that withholding gas exchange led to diminished chondrogenic growth in engineered constructs (Obradovic *et al.* , 1999; Obradovic *et al.* , 2000; Heywood *et al.* , 2006b). Moreover, due to the low oxygen content within the mature joint space, oxygen is thought to be a limiting nutrient although chondrocyte viability is unlikely to be diminished by low oxygen tension (Stockwell, 1971a). Atmospherically, oxygen is typically near 21% (normoxic) of the total gas content. Levels within the native joint space are typically limited to 5% (hypoxic) although contents within the deep zone of avascular cartilage can approach 0-1% (anoxic). In cell culture, oxygen content is limited by atmospheric oxygen content and the solubility of oxygen into the cell culture media (Sengers *et al.* , 2005a). Furthermore, once in solution, oxygen must diffuse to the construct, a process enhanced by stirring or shaking the media (Sengers *et al.* , 2005a).

To this end, this study, parametrically varied the availability of sulfate and oxygen to examine the influence of engineered tissue growth. All studies were performed with TGF-β3 supplementation and oxygen further analyzed the influence of TGF-β and TGF-β-free culture conditions.

7.3 Methods

7.3.1 Experimental culture

Small constructs ($\varnothing 3 \times 2.3$ mm) were cast as previously described (Nims *et al.* , 2014) using primary juvenile bovine chondrocytes seeded nominally at 30 million cells mL^{-1}. Constructs were cultured in excess supply of media and cultured with 10 ng mL^{-1} TGF-β3 for the first 14 days of culture unless otherwise noted (Byers *et al.* , 2008). The influence of each nutrient was assessed in independent studies as follows.

7.3.2 Oxygen

Constructs were cultured either in a hypoxic chamber (5% oxygen, 5% CO_2, balance N_2: hypoxic) or under normal conditions (21% oxygen tension, 5% CO_2, balance (atmospheric) N_2: normoxic). Both the normoxic and hypoxic chamber groups were cultured with the same orbitally shaken conditions. Media change was performed under atmospheric conditions. The hypoxic chamber was then flushed for 3 min with sterile 5% CO_2, 95% N_2 gas before sealing until the subsequent media change. Both normoxic and hypoxic groups were further supplemented with either 0, 0.1, 1, or 10 ng mL^{-1} TGF-β3 for the first 14 days of culture. Constructs were cultured for 35 days and received 1.5 mL media per construct per culture change.

7.3.3 Sulfate

Constructs were cultured in a chemically-defined media which lacked $MgSO_4$, the source of exogenous sulfate in culture media (inorganic salt-free high glucose DMEM: US Biologicals; inorganic salts, dexamethasone, ascorbic acid, sodium pyruvate, L-proline: Sigma; ITS+ premix: BDBioscience; antimycotic/antibiotic: Gibco (Lima *et al.* , 2007)). $MgSO_4$ was added to create groups with either 0 µM (0× group, relative to standard media), 81 µM (0.1× group), 405 µM (0.5× group), or 810 µM (1× group) exogenous sulfate. $MgCl_2$ was added to balance the Mg^{2+} concentration between the groups. A control group was also cultured with standard high glucose DMEM (control group; DMEM with inorganic salts: Invitrogen). Constructs were cultured for 6 weeks and media were changed 3 times weekly (1 mL/construct/media change).

7.3.4 Mechanical and Biochemical assessment

At the final time points of each study, constructs were removed from culture and tested mechanically for the unconfined equilibrium compressive modulus (E_Y) before weighing samples for a measure of the growth (via the swelling ratio). Samples were then digested with proteinase K. Digests were then analyzed for cell content, sulfated GAG, and collagen as previously described (McGowan *et al.* , 2002; Farndale *et al.* , 1986; Hollander *et al.* , 1994; Nims *et al.* , 2014; Cigan *et al.* , 2016b).

7.4 Results

7.4.1 Oxygen

Day 0 cell seeding density of constructs was 39 ± 4 million cells mL^{-1}. Tissue swelling ($p<0.001$) and cell density ($p<0.001$) were higher in constructs grown under hypoxic conditions (Figure 7.1). Conversely, hypoxic constructs had a significantly lower E_Y than normoxic constructs ($p < 0.001$). Oxygen conditions resulted in no significant differences in total matrix deposition (GAG, $p=0.32$, and collagen, $p=0.817$, when normalized to day-0 wet weight).

Similar to our previous studies of TGF-β dosing in engineered constructs, tissue swelling, GAG, and collagen were similar between constructs supplemented with 1 and 10 ng mL^{-1} TGF-β, but increased in properties from 0 to 1 ng mL^{-1}.

Additionally, when normalized to day-35 tissue wet weight, oxygen supplementation did not play a significant role in matrix content (data not shown).

7.4.2 Sulfate

Sulfate concentrations did not produce significant changes in E_Y, GAG, collagen, or cell density (Figure 7.2). Tissues grew well even in the complete absence of inorganic sulfate and had equal levels of negatively-charged GAGs as tissues grown with 1× and the standard culture media.

7.5 Discussion

Understanding the entire culture system and the growth limiting nutrients is critical for developing faithful models of the salient growth kinetics at play within engineered cartilage. Our previous work

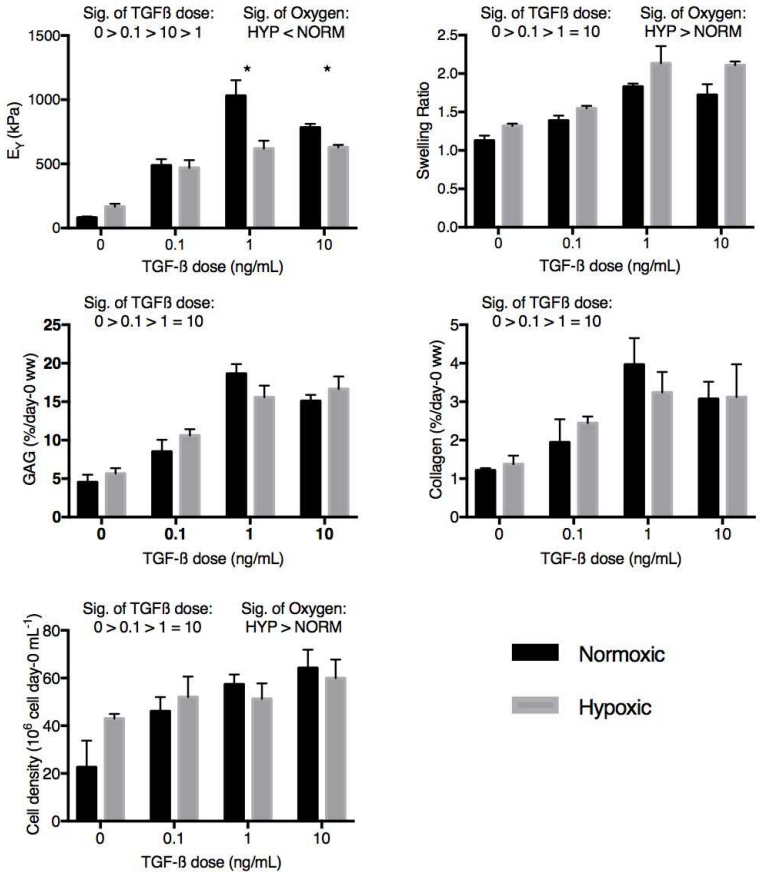

Figure 7.1: Growth of constructs under normoxic and hypoxic conditions with different TGF-β supplementation doses. Significance groupings at top of each chart indicate group-wise differences ($p<0.05$). * denotes significant difference between normoxic and hypoxic groups at given TGF-β dose ($p<0.05$, only for significant interaction ANOVA terms).

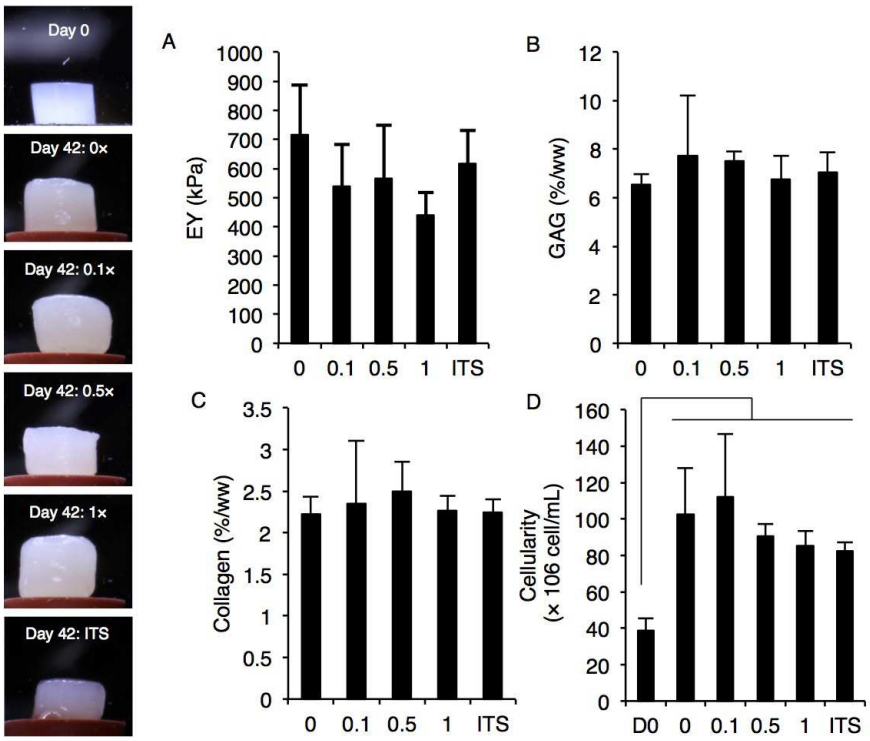

Figure 7.2: Growth of constructs with different levels of inorganic sulfate (supplemented sulfate levels were 0: 0 mM, 0.1: 81 µM, 0.5: 405 µM, 1: 810 µM, ITS: 810 µM using standard media, D0: day 0). Significant differences ($p<0.05$) denoted by line.

to implicate both glucose and TGF-β in the development of engineered cartilage has been successfully incorporated into our computational growth framework (Cigan *et al.* , 2013; Nims *et al.* , 2014; Albro *et al.* , 2016). Questions still remained about the growth kinetics of tissue development particularly: 1) does oxygen, an integral partner in the metabolism of glucose, play a role in matrix synthesis as originally found by Obradovic and colleagues (Obradovic *et al.* , 1999) and 2) can a depletion of inorganic sulfate aid in the development of engineered cartilage through controlling the ratio of sulfated proteoglycan to collagen.

Contrary to these earlier studies, and using a media supply previously found to supply adequate glucose, neither oxygen nor inorganic sulfate played a significant role in matrix deposition.

Oxygen supply did play a complex role with TGF-β supplementation. In particular, despite total matrix synthesis being similar between hypoxic and normoxic groups, cell densities were elevated with hypoxic treatment as was total tissue growth and swelling. This swelling may have negatively influenced mechanical properties as E_Y was lower in the hypoxic treatment.

As a point of interest: there were considerable changes in media coloration between the hypoxic and normoxic treatments. This is likely due to the alteration in metabolism between aerobic and anaerobic processes. Anaerobic respiration (completed without sufficient oxygen) is a more inefficient cellular process, producing 2 adenosine triphosphate (ATP: basic cellular energy carrier) per glucose consumed and producing lactic acid as a byproduct. Conversely aerobic respiration produces 36 ATP molecules per consumed glucose molecule. This suggests that in the absence of oxygen, tissues may quickly run out of sufficient glucose for cellular processes and the production of lactic acid and lowering of pH may be detrimental to tissue growth. However, with our strategy of enhanced glucose supply through increased media volume, there may have been sufficient glucose. Therefore, regardless of metabolic efficiency, energy production may not have been limited by glucose availability and the added media may have helped to limit the lactic acid from decreasing media pH to detrimental levels. Previous studies of the role of oxygen in tissue engineering rarely report whether increased media supply was tested or the production of lactic acid.

Additionally, it is interesting that while there were no statistical differences of the interaction in matrix synthesis or cell density, the cell density in groups without TGF-β suggests that a hypoxic environment may aid in the viability of cells when not supplemented with proliferation-inducing TGF-β. Indeed, the work and models of Chapter 6, cell proliferation of groups not receiving TGF-β

did decrease from day-0 levels. Using modern, TGF-β containing chondrogenic media formulations, however, obviates and masks and potential cell viability loss with enhanced proliferation of cells.

Previous studies have shown that low sulfate concentrations can hinder GAG sulfation by chondrocytes, suggesting that free sulfate may be a critical nutrient required for growth of engineered cartilage (Sobue *et al.* , 1978). This study investigated the influence of exogenous sulfate supplementation on the growth and maturation of tissue engineered constructs in the model [bovine chondrocyte]-[agarose gel] system. The results here illustrate that exogenous sulfate concentration is not a critical nutrient for the present tissue engineering system as neither the mechanical nor the biochemical content was significantly influenced by the level of sulfate supplementation. These results suggest that chondrocytes cultured with insufficient inorganic sulfate can metabolize other sulfur containing molecules to synthesize the sulfate required for GAG sulfation. While this stands in contrast to much of the earlier work on GAG undersulfation in low sulfate conditions, several studies have examined the role of amino acid sulfur in GAG sulfation (Pecora *et al.* , 2006; Rossi *et al.* , 1998). The present study was also conducted for a long duration (42 days) compared with much of the earlier work ($<$ 24 hours), suggesting that chondrocytes may need an extended period before normal sulfated GAG production can be based primarily on amino acid catabolism. The two sulfur-containing amino acids present in tissue culture media are cysteine (nonessential) and methionine (essential), present at 402 µM and 201 µM, respectively. They therefore represent a large source of sulfur in the absence of inorganic sulfate ions. These results highlight that previous measures of sulfate incorporation into sulfated GAG complexes that make up the ECM of native and engineered cartilage may have neglected the role of amino acid metabolism. While this mechanism may play only a minor role in GAG sulfation of chondrocytes with plentiful supply of nutrients (superficial zone chondrocytes), amino acid metabolism may be more common where sulfate concentrations are lower (middle and deep zone chondrocytes).

7.6 Acknowledgements

This study was supported by NIH AR060361, AR046568, and T32AR059038.

Part II

Physical and Mechanical Growth Models and Experiments

Chapter 8 Experiments and models of the mechanism of physical growth of engineered cartilage

8.1 Abstract

Part I established the biochemical growth kinetics of developing engineered cartilage. This insight led to the culture of cartilage constructs in sufficient media. Only once media supply rates became sufficient, tissue constructs began to exhibit a high degree of physical swelling. In fact, the experimental portion of Chapter 3 displayed the greatest disparities in matrix synthesis only when the examining the matrix synthesis relative to day-0 wet weight. As the success of engineered cartilage is only possible with a mechanically robust tissue, the goal of this work was to investigate the mechanisms of tissue swelling and mechanical property development of engineered constructs using both theoretical and experimental methods. To accomplish this, constructs with 120 million cells mL^{-1} were cultured for 105 days; during this culture, constructs grew to nearly 9× their day-0 size. We identified that this high swelling is caused by the rapid proteoglycan synthesis which creates a strong swelling pressure which the nascent collagen network fails to restrain due, in part, to the relatively low synthesis of collagen. We developed computational models to further explain this growth using a damage-based fiber material for collagens and a non-ideal Donnan swelling model for the proteoglycans. Models using the damage-able collagen material explained both the ongoing tissue swelling and the plateau in mechanical properties of the tissue despite continued matrix synthesis, as seen experimentally. We next experimentally investigated whether this "damaged" collagen was measurable. Using the α-chymotrypsin solubilization assay, we measured a high degree (≈60 %) was susceptible to the solubilization assay. Together, models and experiments here suggest a mechanism for understanding the complex physical growth phenomena in developing cartilage constructs.

8.2 Introduction

The adequate nutrition of large constructs has demonstrated a high level of matrix synthesis. The disparities in matrix synthesis became physically evident in the experiments reported in Chapters 2 and 4; the former being due primarily to matrix synthesis mismatches resulting from differences in nutrient supply and the latter due to matrix synthesis mismatches resulting from differences in

TGF-β supplementation. The growth mechanism for these tissues, however, is unknown.

Without understanding the mechanism underlying a developing tissue's mechanical properties, mechanical growth models to date have been based on prior knowledge of the tissue's growth environment (Nikolaev *et al.* , 2010; Khoshgoftar *et al.* , 2014). An incomplete understanding of the growth within engineered cartilage limits the ability of computational models to assess the functional implications of tissue geometries, culture conditions, and cell seeding densities.

Interestingly, despite the significant disparities in construct growth seen in the previous chapters, there were no significant alterations in tissue mechanical properties. This is a surprising finding as we typically assume that more matrix synthesis will directly enhance the mechanical properties of the developing tissues. The experimental results of Chapter 2, however, suggest that both the temporal matrix evolution and physical swelling of constructs will influence and alter their mechanical development. While this is an intriguing prospect, without a more complete understanding of the mechanisms underlying this swelling, it is unknown whether we can translate matrix synthesis into enhanced mechanical properties.

To this end, the physiologic mechanisms governing native cartilage growth are vague. The predominance of native cartilage growth studies have focused more on the biology of growth than the physical growth mechanisms (Bland & Ashhurst, 1996; Clark, 1990; Craig *et al.* , 1987; Doskocil, 1984). Mechanical growth studies, conversely, focus nearly entirely on morphometric analyses with little regard for the underlying structural physics (Carter *et al.* , 2004). Interestingly, from the combination of these studies we can glean that physical growth likely arises due to the differential synthesis of matrix proteins, namely: high collagen and uncharged hyaluronan synthesis levels early in development (prenatal) without significant cross-linking. Synthesized proteoglycans become increasingly negatively charged (via sulfate groups) while collagen synthesis slows from the high prenatal rates to very low levels. During this postnatal development, collagens become increasingly cross-linked (Moriguchi & Fujimoto, 1978) and are relatively susceptible to solubilization via α-chymotrypsin, a marker of collagen turnover and instability (Bank *et al.* , 1997; Bank & te Koppele, 1999; Riley *et al.* , 2002).

To further investigate whether a similar mechanism was at play in the newly developing engineered constructs, we performed a coordinated experimental and modeling study whereby constructs were first grown to produce a high degree of matrix deposition by using a developmentally physi-

ologic cell seeding density. A theoretical damage framework was developed within mixture theory to capture failure and damage during evolving tissue growth. The mechanical contributions of the continuously synthesized collagen and proteoglycan molecules were independently featured to assess whether such a framework and mechanism could explain the continued construct growth and expansion present over the extended culture durations of the samples and the plateauing of construct mechanical properties.

8.3 Methods

8.3.1 Experimental construct growth

In this study, we opted to increase the cell seeding density to 120×10^6 cells/ml, to match native levels in immature tissue ($100 - 300 \times 10^6$ cells/ml (Jadin *et al.* , 2005; Klein *et al.* , 2007)). We also increased media volume per construct to account for the nutrient needs of such elevated cell numbers, consistent with our recent findings (Nims *et al.* , 2015). Finally, we extended the culture duration to 105 days to provide more time for matrix synthesis, and included a CABC treatment group with the digestion occurring from day 14 to 16 using 0.15 U/ml as per our previous protocol (O'Connell *et al.* , 2014). Cylindrical constructs had an initial diameter of 3 mm and height of 2.3 mm. GAG, collagen and DNA content, and equilibrium compressive Young's modulus, were measured using standard protocols described in our previous studies (Nims *et al.* , 2015). Two-way ANOVA ($\alpha = 0.05$) was used to detect statistical differences ($p \leq 0.05$) for the factors of treatment (control and CABC) and time (14/16, 35, 56, 77 and 105 days for control/CABC), with n =4 to 6 samples per group; Turkey-Kramer correction was used for post-hoc testing of the means.

8.3.2 Theoretical model development

The models were constructed using a homogeneous material containing proteoglycan and collagen constituents based on the experimental outcomes. Proteoglycan mechanics were governed by a non-ideal Donnan equilibrium equation and collagen was composed of multi-generation, damageable fibers, corresponding to each day of culture as described below.

8.3.2.1 Bond energy Consider an intact bond species b whose specific bond energy (bond energy per mass) is given by $\psi^b(\mathbf{F})$, where $\mathbf{F}$ is the deformation gradient of all solid constituents. Let

ρ_0^b be the referential mass density (mass per volume in the reference, or undeformed, configuration) of all *intact* bonds of that species. Then, $\Psi_0^b\left(\rho_0^b, \mathbf{F}\right) = \rho_0^b \psi^b\left(\mathbf{F}\right)$ represents the referential strain energy density (strain energy density per volume in the reference configuration) when all bonds are intact. When some of the bonds have failed, the current referential density of remaining intact bonds is ρ_r^b, such that $0 \leq \rho_r^b \leq \rho_0^b$, and the current referential strain energy density is given by

$$\Psi_r^b\left(\rho_r^b, \mathbf{F}\right) = \rho_r^b \psi^b\left(\mathbf{F}\right) = \frac{\rho_r^b}{\rho_0^b} \Psi_0^b\left(\rho_0^b, \mathbf{F}\right) .$$

Thus, the strain energy density of the damaged bond species has been scaled from Ψ_0^b by the fractional ratio of remaining intact bonds to all the original intact bonds, ρ_r^b/ρ_0^b. In this notation the subscript 0 implies that all bonds are intact for that variable, whereas the subscript r implies that only some of the bonds remain intact; for both subscripts, the corresponding variable is normalized by the volume of the material in the reference configuration.

Now consider that bonds in that species have a probability of failure determined by a failure criterion measure $\Xi^b\left(\mathbf{F}\right)$, where the definition of $\Xi^b\left(\mathbf{F}\right)$ follows the classical framework for damage (Simo & Ju, 1987). In this study, it is proposed that the probability that intact bonds of species b will fail at a value of Ξ^b is given by a probability density function (p.d.f.), $f^b\left(\Xi^b\right)$. The choice of p.d.f. is based on a constitutive assumption, with the requirement that the p.d.f. be defined on the appropriate interval for Ξ^b, e.g., the semi-infinite interval $[0, \infty[$ when Ξ^b is a positive semi-definite function of $\mathbf{F}$. The corresponding cumulative distribution function (c.d.f.) of $f^b\left(\Xi^b\right)$ is $F^b\left(\Xi^b\right)$.

Let the failure measure be given by $\Xi_s^b = \Xi^b\left(\mathbf{F}\left(s\right)\right)$ at a particular state of deformation $\mathbf{F}\left(s\right)$, and let the maximum value of Ξ_s^b over the history up until the current time t be given by (Simo & Ju, 1987)

$$\Xi_m^b = \max_{-\infty < s \leq t} \Xi^b\left(\mathbf{F}\left(s\right)\right) .$$

Then, based on the formulation proposed in this study,

$$D^b\left(t\right) = F^b\left(\Xi_m^b\right)$$

represents the fraction of all bonds that have failed up until the current time t, leaving

$$\frac{\rho_r^b}{\rho_0^b} = 1 - D^b$$

as the remaining fraction of intact bonds. Thus, we obtain

$$\Psi_r^b\left(\mathbf{F}\right) = \left(1 - D^b\right)\Psi_0^b\left(\mathbf{F}\right) .$$

8.3.2.2 Thermodynamics To examine the thermodynamics of this process, consider that damage represents a reaction that transforms intact bonds into broken bonds consisting of two or more fragment species c,

$$[\text{intact bond } b] \rightarrow \sum_c [\text{broken bond fragment } c] .$$

The evolving referential density of broken fragments is ρ_r^c, with $\rho_r^c = 0$ prior to any damage, and $\sum_c \rho_r^c = \rho_0^b$ when all bonds b have broken. In this reactive damage framework, it is assumed that the specific strain energy of broken bond fragments is zero, $\psi^c = 0$, therefore the net free energy Ψ_r of the mixture of b and c species is simply

$$\Psi_r\left(\rho_r^a, \mathbf{F}\right) = \sum_{a=b,c} \rho_r^a \psi^a = \Psi_r^b .$$

(This approach precludes the modeling of plasticity, where bonds may break and reform in a loaded state.) The chemical potential μ^a of each species $a = b, c$ may be evaluated from the standard relation (Ateshian & Ricken, 2010),

$$\mu^a\left(\rho_r^a, \mathbf{F}\right) = \frac{\partial \Psi_r}{\partial \rho_r^a} = \psi^a\left(\mathbf{F}\right) ,$$

which shows that the chemical potential is equal to the bond specific free energy, with $\mu^b = \psi^b$ and $\mu^c = 0$. This equivalence between chemical potential and specific free energy occurs because of the simplifying constitutive assumption that ψ^b is not a function of any of the bond densities ρ_r^a. (In physical chemistry of solutions, this same assumption produces *ideal* solutions; we may thus describe our bond mixture model as an ideal mixture.) The rate at which the intact bond density changes

over time is governed by the axiom of mass balance for that constituent (Ateshian & Ricken, 2010),

$$\dot{\rho}_r^b = \hat{\rho}_r^b \,,$$

where $\dot{\rho}_r^b$ is the material time derivative of ρ_r^b and $\hat{\rho}_r^b$ is the referential mass density supply to b from reactions with all other constituents in the mixture, such as the bond-breaking reaction; a constitutive relation must be provided for $\hat{\rho}_r^b$. Similar expressions may be given for the broken fragments c and, according to the axiom of mass balance for the mixture, $\sum_{a=b,c} \hat{\rho}_r^a = 0$. As shown previously in the context of mixture theory (Ateshian & Ricken, 2010), a reaction can proceed spontaneously according to the Clausius-Duhem inequality if and only if

$$\sum_{a=b,c} \hat{\rho}_r^a \mu^a \leq 0 \,.$$

Since $\mu^c = 0$ for all c species, this inequality constraint reduces to $\hat{\rho}_r^b \psi^b \leq 0$, which further implies that $\hat{\rho}_r^b \leq 0$ (thus, $\dot{D}^b \geq 0$) since ψ^b is a positive semi-definite function of the strain. Thus, the thermodynamic constraint simply states that intact bond species may break spontaneously with loading (since their mass supply must be negative) but may not reform spontaneously in this damage framework.

8.3.2.3 Damage Criterion As described in the prior damage mechanics literature (Simo & Ju, 1987), a damage criterion needs to be defined such as

$$\varphi^b \left(\mathbf{F}\left(t\right), \Xi_m^b \right) = \Xi^b \left(\mathbf{F}\left(t\right) \right) - \Xi_m^b \leq 0 \,,$$

where φ^b represents a damage surface whose tensorial normal is

$$\mathbf{N} = \frac{\partial \varphi^b}{\partial \mathbf{F}} = \frac{\partial \Xi^b}{\partial \mathbf{F}} \,.$$

The damage criterion presents the following alternatives: $\varphi^b < 0$ if the current state of deformation is below the current damage threshold, or $\varphi^b = 0$ and the deformation is receding from, or tangent to, the damage ($\mathbf{N} : \dot{\mathbf{F}} \leq 0$), or increasing the damage ($\mathbf{N} : \dot{\mathbf{F}} > 0$). Substituting this into the mass

balance produces the damage evolution constitutive relation,

$$\hat{\rho}_r^b = -\rho_0^b \dot{D}^b = \begin{cases} -\rho_0^b \left. \frac{\partial F^b}{\partial \Xi^b} \dot{\Xi}^b \right|_{\Xi^b = \Xi_m^b} & \varphi^b = 0,\ \mathbf{N} : \dot{\mathbf{F}} > 0 \\ 0 & \text{otherwise} \end{cases},$$

showing that the constitutive relation for $\hat{\rho}_r^b$ is thus predicated on the shape of the c.d.f. $F^b\left(\Xi^b\right)$. Based on this relation, the thermodynamic requirement, $\hat{\rho}_r^b \leq 0$, and the damage progression conditions, $\varphi^b = 0$ and $\mathbf{N} : \dot{\mathbf{F}} > 0$ (implying $\dot{\Xi}^b > 0$ at $\Xi^b = \Xi_m^b$), combine to produce the thermodynamic constraint

$$\frac{\partial F^b}{\partial \Xi^b} \geq 0\,,$$

on the c.d.f.. Therefore, the entropy inequality is satisfied when $F^b\left(\Xi^b\right)$ is a monotonically increasing function over the domain of Ξ^b.

8.3.2.4 Stress For a single bond species b, the state of stress may be evaluated from $\Psi_r = \Psi_r^b$ using the usual relations of hyperelasticity, recalling that ρ_r^b and $\mathbf{F}$ are independent state variables (Ateshian & Ricken, 2010). Thus, for the Cauchy stress,

$$\mathbf{T} = J^{-1} \frac{\partial \Psi_r}{\partial \mathbf{F}} \cdot \mathbf{F}^T = \left(1 - D^b\right) \mathbf{T}_0^b\,,$$

where $\mathbf{T}_0^b$ is evaluated as

$$\mathbf{T}_0^b = J^{-1} \frac{\partial \Psi_0^b}{\partial \mathbf{F}} \cdot \mathbf{F}^T\,.$$

8.3.3 Failure Criterion Measure

The failure criterion measure $\Xi^b\left(\mathbf{F}\right)$ of a particular bond species b may be based on strain invariants, strain energy density, stress invariants, or any other suitable, experimentally validated, measure. Measures that are dependent on the material behavior, such as strain energy density and stress, are based on the behavior of intact bonds, thus Ψ_0^b for the strain energy density, and $\mathbf{T}_0^b$ for the Cauchy stress. Simo (Simo & Ju, 1987) proposed a strain measure,

$$\Xi^b\left(\mathbf{F}\right) = \sqrt{2\Psi_0^b\left(\mathbf{F}\right)}\,,$$

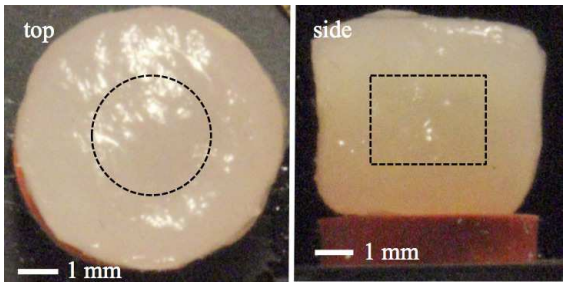

Figure 8.1: Representative engineered cartilage construct from control group at day 105. Dashed lines shows day 0 dimensions.

deemed appropriate for isotropic damage, which was used for this study. It is also possible to select $\Xi^b(\mathbf{F}) = \Psi_0^b(\mathbf{F})$. For applications to biological tissue damage these criteria may be associated with various mechanisms; selection of a specific criterion is dependent on the tissue's constitutive behavior and the applicability of different criteria must be guided by experimental data.

8.4 Results

8.4.1 Experimental construct growth

One of the most striking outcomes of this experimental study was the considerable tissue construct volume growth or expansion from the size of the day-0 construct (Figure 8.1). The control group specimens saw a nearly nine-fold increase in their wet weight (and volume) relative to day 0, while CABC-treated specimens increased more than five-fold (Figure 8.2). Because of this very large swelling ratio J, specifically defined as construct wet weight at a given time point normalized to the day-0 construct ww, GAG and collagen compositional measures are reported using normalization by current day wet weight (final day in culture) to produce conventional fractional measures (%ww, Figure 8.3), and normalization by day 0 wet weight to assess total matrix synthesis (%D0ww, Figure 8.4).

Using conventional measures, GAG content rose significantly above day 14/16 levels to nearly 7%ww by day 56 ($p < 10^{-4}$), then dropped slightly by day 105 (Figure 8.3a); differences were observed between control and CABC treatments only at day 14/16 ($p < 10^{-3}$). Collagen content rose significantly above day 14/16 levels to nearly 2%ww by day 56, then remained unchanged until day 105 (Figure 8.3b); no differences were observed between control and CABC treatments ($p = 0.29$).

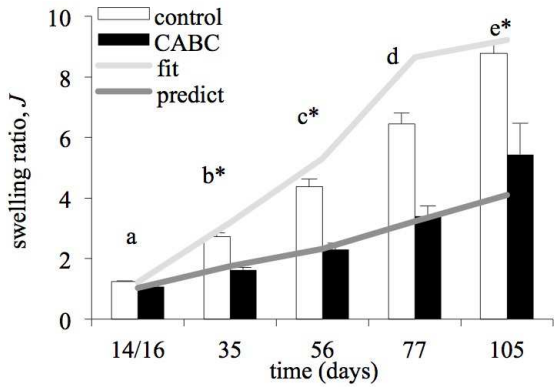

Figure 8.2: Swelling ratio J of engineered cartilage constructs, for control and CABC treatments (bars). Different letters indicate significant differences across time points ($p < 10^{-4}$) and asterisks indicate significant differences between control and CABC at that time point ($p < 10^{-4}$). Solid curves represent the model fitted to control data (fit) and the prediction of CABC data (predict).

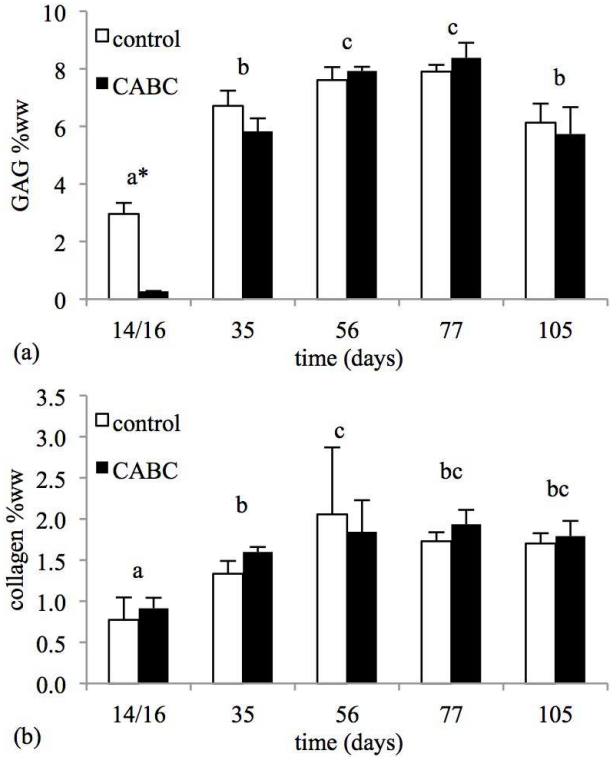

Figure 8.3: GAG and collagen content in engineered constructs, normalized to wet weight on final day of culture (%ww). Different letters indicate significant differences across time points ($p < 10^{-4}$ for GAG and collagen) and asterisks indicate significant differences between control and CABC at that time point ($p < 10^{-3}$ for GAG only).

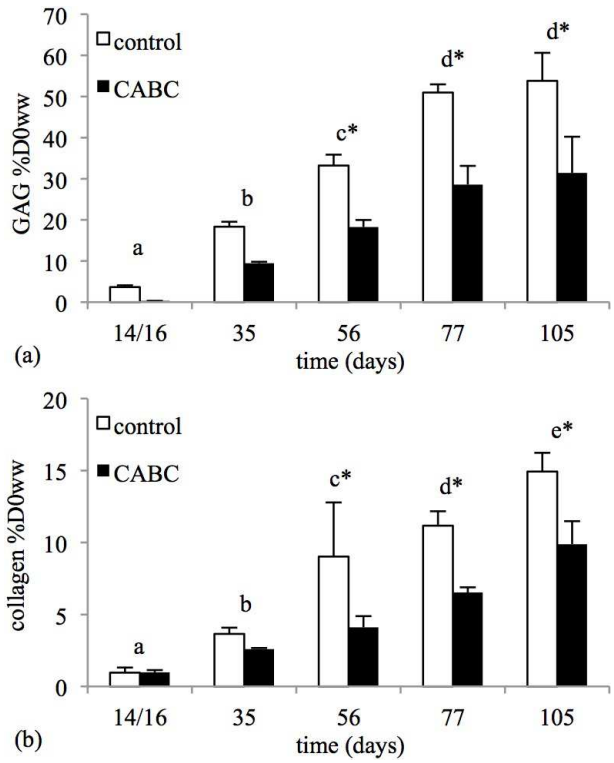

Figure 8.4: GAG and collagen content in engineered constructs, normalized to day 0 wet weight (%D0ww). Different letters indicate significant differences across time points ($p < 10^{-4}$ for GAG and collagen) and asterisks indicate significant differences between control and CABC at that time point ($p < 10^{-4}$ for GAG and $p < 10^{-3}$ for collagen).

Using day 0 normalization, GAG content increased nearly linearly with time ($p < 10^{-4}$), reaching 54 %D0ww in the control group and 31 %D0ww in the CABC group at day 105 (Figure 8.4a). Collagen content similarly rose nearly linearly with time ($p < 10^{-4}$) to 15 %D0ww in the control group and 10 %D0ww in the CABC group at day 105 (Figure 8.4b). From day 56 onward, GAG ($p < 10^{-4}$) and collagen ($p < 10^{-4}$) content in the CABC group were smaller than control.

Total cell content per construct did not exhibit a monotonic trend, though significant differences were found with time in culture ($p < 10^{-4}$); the CABC group exhibited consistently lower cell content than control ($p < 10^{-4}$) (Figure 8.5). Fractional fluid content φ^w in constructs decreased over time until day 35 ($p < 10^{-4}$), then remained nearly constant until day 105 (Figure 8.6); at most time points, CABC constructs had lower fluid content than controls ($p < 10^{-4}$). Finally, the compressive equilibrium Young's modulus rose significantly above day 14/16 levels until day 35, then remained statistically constant until day 105 (Figure 8.7). At two time points, E_Y was higher in the CABC group compared to control ($p < 0.01$).

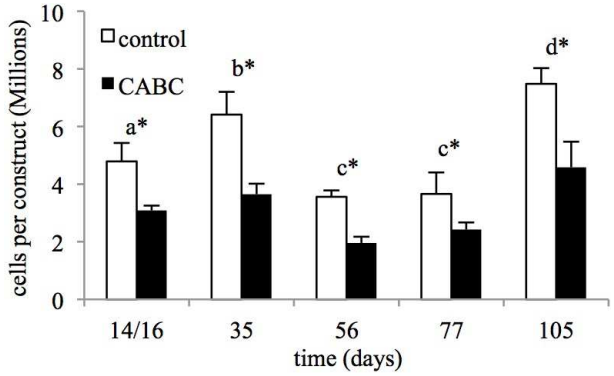

Figure 8.5: Cells per construct as a function of time and treatment. Different letters indicate significant differences across time points ($p < 10^{-4}$) and asterisks indicate significant differences between control and CABC at that time point ($p < 10^{-4}$). On day 0, nominal cell content per construct is 2 million.

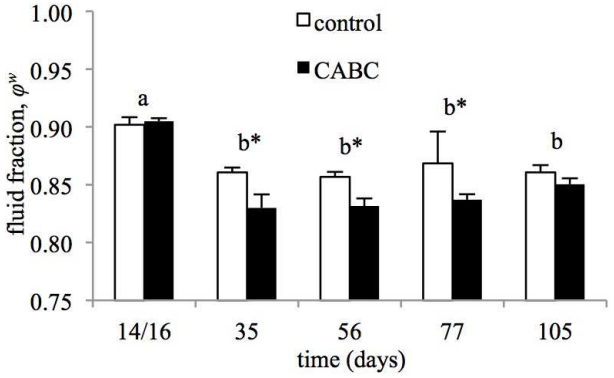

Figure 8.6: Fractional fluid content φ^w in constructs, as a function of time and treatment. Different letters indicate significant differences across time points ($p < 10^{-4}$) and asterisks indicate significant differences between control and CABC at that time point ($p < 10^{-4}$). $\varphi^w = 0.94 \pm 0.02$ on day 0.

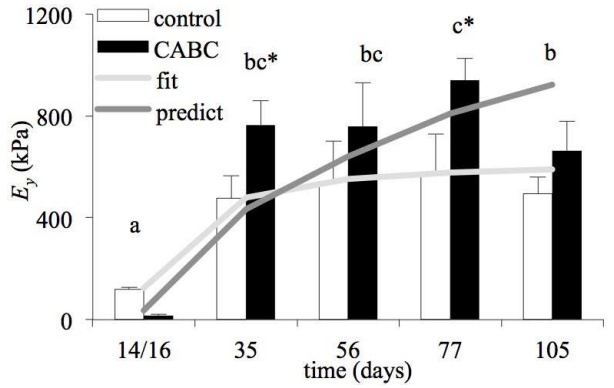

Figure 8.7: Equilibrium compressive Young's modulus E_y in constructs, as a function of time and treatment (bars). Different letters indicate significant differences across time points ($p < 10^{-4}$) and asterisks indicate significant differences between control and CABC at that time point ($p < 10^{-2}$). $E_Y = 12 \pm 5\,\mathrm{kPa}$ on day 0. Solid curves represent the model fitted to control data (fit) and the prediction of CABC data (predict).

8.4.2 Damage in Growing Tissue Constructs

On first pass, results of this experimental study were substantially consistent with our past results (Bian *et al.* , 2009b; Nims *et al.* , 2014), producing comparable GAG and collagen %ww levels and compressive moduli, despite the fact that the cell seeding density was considerably higher. No differences were found in the conventional GAG and collagen measures between control and CABC treatments, though E_Y was significantly higher in the CABC group.

However, once we accounted for the swelling ratio, our interpretation of these results was considerably refined: using a cell seeding density comparable to native juvenile tissue, it was in fact possible to synthesize native levels of collagen in our tissue constructs (15 %D0ww in the control group at day 105), indicating that the primary chondrocytes used in this culture system have not lost their ability to produce sufficient collagen. However, the supra-physiological levels of GAG synthesized over the same time period (54 %D0ww, compared to the native GAG content of 2.8%ww) produced so much swelling, resulting from the excessive GAG deposition-induced swelling-pressure, that the collagen content was diluted (2 %ww). It was experimentally evident that the swelling was caused primarily by the GAGs (consistent with Donnan swelling theory (Overbeek, 1956)), since lower GAG %D0ww levels in the CABC group (Figure 8.4a) produced a lower swelling ratio (Figure 8.2).

The next intriguing outcome was that E_Y was higher in the CABC treatment than control, even though %ww levels of GAG and collagen were not different, and %D0ww were in fact smaller in the CABC group. Since GAG %ww usually correlates strongly with E_Y in tissue constructs (Mauck *et al.* , 2002), this surprising outcome led us to the hypothesis that the large swelling ratios observed in this study could in fact damage the collagen network, whose integrity is critical to prevent uncontrolled swelling (since the agarose hydrogel breaks apart early in the growth process based on visual inspection).

We hypothesized the following specific mechanism: GAG and collagen are synthesized continuously during the growth process, at a nearly constant rate. The charged GAG produces a swelling pressure that expands the tissue construct; this expansion is primarily resisted by the collagen network that was synthesized since the start of culture until the current time. Collagen synthesized at earlier times points is then subjected to more swelling than collagen synthesized most recently,

under the assumption that collagen is incorporated into the network in a stress-free (unswollen) state. Therefore, as time progresses, earlier generations of collagen are subjected to considerable stretching (up to nine-fold swelling for the earliest collagen generation in this study. Figure 8.2), causing them to become damaged. Only the most recent collagen generations remain intact or nearly intact, providing some resistance to swelling while maintaining a regular construct shape (Figure 8.1). At some time point during the culture (e.g., day 35 based on the data), the rate of matrix synthesis and damage equalizes, such that GAG and collagen %ww, and E_Y, all reach a plateau.

Based on our earlier study (Nims *et al.* , 2014), nearly 90% of synthesized GAG and 85% of synthesized collagen is retained in the constructs throughout the culture period, therefore, in our hypothesized mechanism, we expect that damaged collagen mostly remains in the construct, possibly contributing to the structural integrity when newly synthesized generations cross-link with undamaged segments of those collagen fibrils.

Under this hypothesized mechanism, the CABC-treated constructs are subjected to less damage in their earlier generations because of the reduced swelling resulting from the GAG digestion. Therefore the collagen network in the CABC group has a higher tensile stiffness, which effectively translates to greater resistance to compression from a swollen state as shown in our earlier studies on native cartilage (Chahine *et al.* , 2004).

To validate this hypothesized mechanistic interpretation of our experimental observations, we performed a theoretical analysis that captured its salient points. Cartilage constructs were modeled as a mixture of collagen, charged GAGs, and an interstitial fluid containing water and monovalent salt counter-ions (Na^+ and Cl^-). In this case, the mixture stress is

$$\mathbf{T} = -p\mathbf{I} + \mathbf{T}^e$$

where p is the interstitial fluid pressure, $\mathbf{I}$ is the identity tensor, and $\mathbf{T}^e$ is the collagen matrix stress. Under steady state conditions, when interstitial fluid flow and ion diffusion have subsided, the interstitial fluid pressure is given by the Donnan osmotic pressure relative to ambient bath conditions,

$$p = R\theta\Phi\left(\sqrt{(c^F)^2 + (2c^*)^2} - 2c^*\right)$$

where R is the universal gas constant, θ is the absolute temperature, Φ is the osmotic coefficient describing the deviation from ideal Donnan law ($\Phi = 1$ for ideal conditions), c^* is the external NaCl bath concentration, and c^F is the fixed charge density arising from the GAGs. The parameter c^F was calculated directly from the measured GAG %D0ww using

$$c^F = \frac{z^{\mathrm{GAG}}}{M^{\mathrm{GAG}}} \frac{\rho_T}{\varphi^w} \frac{\mathrm{GAG\ \%D0ww}}{100}$$

where z^{GAG} is the charge number and M^{GAG} is the molar mass of GAG ($z^{GAG} = -2$ and $M^{GAG} = 513\,\mathrm{g/mol}$, recognizing that GAG content was measured using a DMMB assay with chondroitin sulfate as the standard); ρ_T is the construct mass density (taken to be $\rho_T = 1\,\mathrm{g/ml}$), and φ^w is the measured fractional fluid content. The only adjustable parameter in this relation is thus Φ.

The collagen matrix stress $\mathbf{T}^e$ was evaluated using the multigenerational growth model formulated in our earlier study (Ateshian & Ricken, 2010): Each generation of collagen was assumed to be deposited in a stress-free reference configuration $\mathbf{X}^\gamma$, coinciding with the current configuration at the start of the generation, $\mathbf{X}^\gamma = \boldsymbol{\chi}(\mathbf{X}, t^\gamma)$, where $\boldsymbol{\chi}$ is the motion, $\mathbf{X}$ is the reference configuration of the first generation (start of day 1 in culture), and t^γ is the time at the start of generation γ. The deformation gradient of each generation is thus $\mathbf{F}^\gamma = \partial\boldsymbol{\chi}/\partial\mathbf{X}^\gamma$ and the collagen in generation γ is subjected to strains calculated from $\mathbf{F}^\gamma$. The construct swelling ratio is given by $J = \det\mathbf{F}$, where $\mathbf{F} \equiv \mathbf{F}^{(1)}$ is the deformation gradient of the first generation. Though collagen synthesis is continuous, a computational scheme employs finite time increments and we chose to have 105 generations, corresponding to the start of each day in culture.

Each collagen generation γ was modeled using a fiber distribution with $N = 210$ fiber bundles corresponding to an isotropic distribution ($R(\mathbf{n}^i) = 1/4\pi$) reflecting the random arrangement of collagen fibers evident in free-swelling tissue constructs. Each bundle was modeled using the constitutive relation of the strain energy density with $\beta_f = 2$ and ξ_f left as a single adjustable parameter (same ξ_f value for all bundles and all generations). The log-normal c.d.f. was used to describe the probability of damage in each bundle of each generation, with adjustable parameters μ_c and σ_c (same values for all bundles). The failure criterion measure was the Simo criterion of the fiber bundle calculated for each collagen generation using $\mathbf{F}^\gamma$ for that generation.

This model was implemented in the FEBio finite element environment to predict construct

swelling and damage, and construct equilibrium compressive modulus under conditions equivalent to the experimental testing protocol (unconfined compression at 10% strain). Using FEBio predictions, the four adjustable material parameters, Φ, ξ_f, μ_c and σ_c, were fitted simultaneously to the mean experimental results for swelling ratio J versus time in culture (Figure 8.2) and compressive modulus E_Y versus time in culture (Figure 8.7), using control group data only ($\Phi = 0.5$, $\xi_f = 31\,\text{kPa}$, $\mu_c = 0.08\,(\text{mJ/mm}^3)^{0.5}$ and $\sigma_c = 1.7$). These fits produced coefficients of determination $R^2_J = 0.81$ and $R^2_{E_y} = 0.93$, respectively. To validate the model, these optimal values were then used to predict J and E_Y for the CABC group, producing coefficients of determination $R^2_J = 0.85$ and $R^2_{E_y} = 0.60$, respectively (Figure 8.2 & 8.7).

The successful curve-fits of control group data, and faithful theoretical predictions of CABC group data, provide a mechanistic validation of our hypothesis that growth is causing collagen damage in our engineered tissue constructs. The fact that the model could predict an initial rise in E_Y followed by a plateau (Figure 8.7), whereas the swelling ratio J rose continuously (Figure 8.2), indicates that the onset of damage with growth can explain the observed responses.

The agreement between theory and experimental data sets (control and CABC groups) is also evident in a scatter plot of J versus GAG %D0ww data, showing a strong correlation with the theoretical model (Figure 8.8a). A scatter plot of E_Y versus GAG %ww from the control and CABC groups here and our prior study of (Nims *et al.* , 2014) produces a moderate correlation (Figure 8.8b).

8.4.3 Observable Damage

Based on the general agreement between experimental results and our hypothesized damage-mechanism model of tissue growth, we investigated methods of measuring the damage directly and quantitatively. In 1997, Bank et al. introduced a simplified measurement of collagen fiber denaturation using $\alpha-$chymotrypsin, which reports the fraction of all collagen in that tissue that has been degraded (i.e., whose triple helix is unwound) (Bank *et al.* , 1997). They demonstrated that this assay could predict higher collagen degradation in cartilage from human osteoarthritic joints ($10.4 \pm 5.6\,\%$) versus normal tissue ($2.1 \pm 1.0\,\%$) suggesting that the technique would serve as a proxy for collagen fiber damage.

We used this assay to assess damage in the control and CABC groups of the current study,

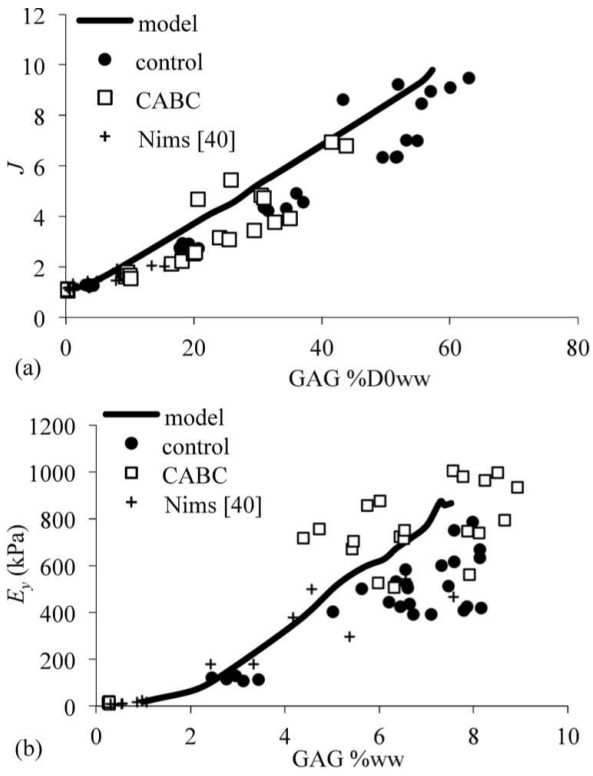

Figure 8.8: Experimental and model responses for (a) swelling ratio J versus GAG %D0ww ($R^2 = 0.79$), and (b) modulus E_y versus GAG %ww ($R^2 = 0.35$).

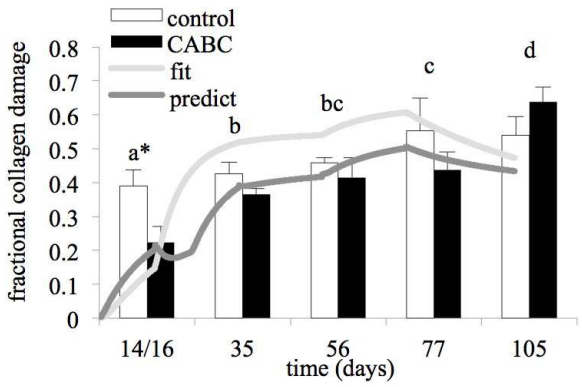

Figure 8.9: Fractional collagen damage measured using $\alpha-$chymotrypsin digestion, as a function of time and treatment (bars). Different letters indicate significant differences across time points ($p < 10^{-4}$) and asterisks indicate significant differences between control and CABC at that time point ($p < 10^{-2}$). Solid curves represent the fractional damage from the model fitted to control data (fit) and the model prediction for CABC data (predict).

as well as damage in native juvenile bovine cartilage from which we harvested chondrocytes for our tissue engineering studies. Native juvenile cartilage ($n = 5$ samples) exhibited $10.1 \pm 0.9\,\%$ denatured collagen, consistent with the $\sim 14\,\%$ value reported previously for young adult bovine cartilage (Temple *et al.* , 2006). Engineered cartilage constructs exhibited damage that increased over time, ranging from $38.9 \pm 4.8\,\%$ at day 14 to $53.9 \pm 5.7\%$ at day 105 for the control group, and from $22.4 \pm 4.6\,\%$ at day 16 to $63.8 \pm 4.4\,\%$ at day 105 for the CABC group (Figure 8.9). A two-way ANOVA for the factors of time in culture and treatment showed significant differences across all factors ($p < 10^{-4}$ for time, indicating a significant increase in damage over time; $p = 0.002$ for treatment, indicating that damage was lower in the CABC group versus control on average; and $p < 10^{-4}$ for day×treatment, indicating that damage was lower in the CABC group only on day 14/16, Figure 8.9). These experimental results confirmed that damage did occur in tissue constructs, well above the baseline level of denatured collagen found in native juvenile cartilage.

For comparison purposes, the fractional damage predicted from the model is also shown in Figure 8.9). This damage was calculated by taking into account the multigenerational growth process: The average of $D\left(\mathbf{n}^i\right)$ over all N fiber bundles of generation γ was denoted by $\bar{D}^\gamma$, which represents the damage in collagen generation γ; since each day produced a new generation, the

fractional damage at the end of day d was evaluated from the cumulative damage until that day,

$$\bar{D} = \frac{1}{d}\sum_{\gamma=1}^{d} \bar{D}^{\gamma}$$

The trend of this theoretical $\bar{D}$ versus time in culture was consistent with the biochemical assay results for both control and CABC groups, though the magnitudes did not match exactly (Figure 8.9). This qualitative agreement was similarly supportive of our hypothesis that growth and swelling cause damage in the collagen matrix of engineered cartilage constructs. The fact that D did not agree exactly with the measured collagen degradation was not surprising, since the model did not propose an explicit constitutive relation between the fraction of collagen that is denatured and the fraction of molecular bonds that are broken.

8.5 Discussion

The objectives of this study were to formulate a damage mechanics framework that employs observable state variables, instead of internal hidden variables as in the prior literature, while recovering the classical formulation for damage in isotropic materials; to show that this new framework was applicable to anisotropic materials without appealing to a tensorial damage measure; to demonstrate its application to fibrous tissues with unidirectional or multi-directional fiber orientations; and to use this framework to test the hypothesis that growth of cartilage constructs can lead to damage of the synthesized collagen matrix.

Most biological tissues exhibit viscoelasticity, which significantly hinders the ability to assess their damage exclusively from mechanical responses (except when the tissue exhibits gross failure). Similarly, damage assays (e.g., biochemistry or Raman spectroscopy) are not always easy to interpret on their own, as they may depend on complex interactions that are not fully understood. Using observable variables to track damage implies that predictions from damage models may be validated experimentally, and experimental damage measures may be interpreted mechanistically by validated models. This combination of theory and experiments can enhance our confidence when testing hypotheses, as demonstrated in the tissue engineering study presented here.

Though we have conducted cartilage tissue engineering studies for nearly two decades, we had not initially suspected that newly synthesized extracellular matrix could rapidly become damaged

during the growth process. In retrospect, the first indication that excessive GAG swelling could cause damage to engineered cartilage was reported in our earlier study, where constructs were found to crack at their center (Bian *et al.* , 2009a), a one-time finding that we attributed to special circumstances. In the current study no cracks were observed in the constructs, but the temporal evolution of construct mechanical properties and swelling led us to hypothesize a more pervasive collagen damage process that we proceeded to investigate more quantitatively.

Had we only performed the biochemical assay (using $\alpha-$chymotrypsin digestion (Bank *et al.* , 1997)), our results would have remained somewhat ambiguous since this assay had not been previously used on engineered tissue constructs. Thus, the elevated levels of denatured collagen found here (Figure 8.9) could have been attributed to the fact that newly synthesized cartilage has relatively high levels of immature collagen that may be responsible for these findings. (Indeed, it was somewhat surprising to us that healthy native juvenile and young adult bovine cartilage exhibit between 10 and 14 % damage (Temple *et al.* , 2006), whereas healthy adult human cartilage only exhibits 2% damage (Bank *et al.* , 1997).) It was the combination of modeling and experiments that increased our confidence in the testing of our hypothesis.

The results of this study have significant implications for our ongoing cartilage tissue engineering efforts: Increasing cell seeding density to levels comparable to neonatal cartilage can produce collagen synthesis that matches native levels; however, we must develop tissue engineering strategies that prevent damage of newly synthesized collagens. This may be achieved by either preventing excessive swelling during the growth process (e.g., suitably constraining the constructs without compromising access to nutrients), or reducing GAG synthesis in the early stages of tissue growth using alternative strategies to CABC (e.g., siRNA to temporarily suppress aggrecan synthesis). These alternative strategies are currently under consideration.

8.6 Acknowledgments

Final publication is available from The Royal Society Publishing http://dx.doi.org/10.1098/rsfs.2015.0063.

Research reported in this publication was supported by the National Institute of Arthritis, Musculoskeletal and Skin Diseases and the National Institute of General Medical Sciences of the National Institutes of Health under award numbers R01AR060361, R01AR043628 and R01GM083925. The

content is solely the responsibility of the author and does not necessarily represent the official views of the National Institutes of Health.

8.7 Data accessibility

Experimental data for engineered cartilage constructs reported in this manuscript are available for download from https://academiccommons.columbia.edu/catalog/ac%3A187860 and the model is available on the FEBio forum at http://mrlforums.sci.utah.edu/forums/.

Chapter 9 Predicting mechanical properties of heterogeneous cartilage constructs

9.1 Abstract

With the fundamental mechanism underlying the growth of engineered constructs (Chapter 8) and material models for the structural proteoglycan and collagen constituents, computational growth models can be used to assess the mechanics of engineered cartilage tissues. Here, we use spatial biochemical data from our previous study to assess the evolution and final spatial and average mechanical properties of the tissue grown in our previous study to intentionally develop TGF-β gradients (the quasi-1D study discussed in Chapter 6 and (Albro *et al.* , 2016)). Proteoglycan and collagen content between days 0 and 56 were simulated to evolve through depositions of the material models described in Chapter 8, such that by the day 56 of the growth simulation, a construct would have the material model equivalents of the day 56 experimental levels of proteoglycans (via the non-ideal Donnan material) and collagen (via the multigenerational damage-able fiber material). Mechanical growth was simulated for the TGF-β treated and untreated constructs, with mechanical properties elevated where TGF-β availability was highest. The average mechanical properties of the experimentally cultured constructs were well matched to the average mechanical properties of the predicted by the models (tested with a simulated unconfined compression test, as performed experimentally). Together, the simulated spatial mechanical properties and close agreement of average mechanical properties to experimentally measured mechanical properties suggest the physical growth phenomena proposed and fit in Chapter 8 is appropriate for predicting mechanical properties of developing cartilage tissue constructs.

9.2 Introduction

With the ability to model the mechanical growth of constructs based on the developing biochemical content, we tested the applicability of these models to the growth of the deliberately heterogeneous growth of large tissue constructs from (Albro *et al.* , 2016). In that study, we cultured constructs such that TGF-β availability within the construct was minimized and could be modeled within the central core of the construct using a one-dimensional analysis. The histology from that study

demonstrated profound matrix heterogeneities were present and that the modulus of the whole construct was lower than that of small constructs cultured with TGF-β ($\approx 400-800$ kPa), although spatial mechanical tests were not performed.

Using the models of tissue mechanics arising from the independent deposition of proteoglycans and collagens we can, for the first time, examine the role heterogeneous matrix deposition has in the development of spatially heterogeneous tissue properties (Chapter 8). To accomplish this, we use the experimentally measured levels of spatial matrix deposition within 4 depth-wise layers of the large tissue construct to providing the biochemical information for the development of the mechanical properties. This informs both the spatial and spatially-averaged mechanical properties, the latter of which we use to compare to the experimentally measured average modulus to validate the fidelity of the model for predicting the growth of large tissue constructs.

9.3 Methods

9.3.1 Experimental culture summary

Large constructs (⌀6 mm × 3.2 mm) seeded with 60 million cells mL^{-1} were cultured on the bottom of a dish (3 mL per construct), such that the only media-construct interfaces were along the top and lateral faces of the construct. Constructs were cultured for 56 days with 0 or 10 ng mL^{-1} TGF-β supplementation over the first 14 days. After culture, a central ⌀3 mm core was punched and divided into four equal slices for depth-dependent biochemical analysis (GAG and collagen). These levels of GAG and collagen deposition would be used to inform the computational mechanical models. TGF-β treated constructs developed a periphery rich in GAG and collagen deposition (see (Albro *et al.* , 2016)) and an interior that presented little matrix. Constructs not supplemented with TGF-β displayed little matrix deposition in all four slices of the construct.

9.3.2 Computational methods

9.3.2.1 Computationally simulating growth The depth-dependent and whole construct mechanical properties (equilibrium compressive Young's modulus, E_Y) were assessed computationally for each of the samples in the active TGF-β and control (unsupplemented) groups (n=8 for each group). Models were run in FEBio (http://www.febio.org, version 2.4.0), based on the models of

Chapter 8, which provides a theoretical and computational framework to model the mechanical growth (tissue swelling and compressive modulus development) of engineered cartilage based on the biochemical content (GAG and collagen content).

Model geometry consisted of the ∅6 × 3.2 mm construct segmented with 24 radial elements and four axial elements. Radial symmetry was enforced to reduce the computational power required for simulations (3-degree slice). The engineered tissue was modeled as a solid mixture of a non-ideal Donnan equilibrium swelling model (describing the behavior of negatively charged proteoglycans, osmotic coefficient = 0.5) and a isotropic fiber distribution (describing the behavior of the collagens). The fiber distributions were multigenerational, replicating successive generations of a deposited collagen network. Additionally, these fiber generations could become damaged due to excessive strain (due to the high deposition of GAGs), which our prior work has shown is necessary to account for the growth patterns and mechanical behaviors of engineered cartilage constructs.

For each sample, the Donnan swelling term and fiber modulus within each slice was determined from the sample- and slice-specific biochemical content. The Donnan model parameter of fixed-charge density was taken directly from the GAG content (assuming 513 g mol^{-1} for chondroitin sulfate). Solid volume fraction (for the FCD estimation) was approximated using a collagen and proteoglycan true density of 1.4 g mL^{-1} and an agarose content of 2% (Khoshgoftar *et al.* , 2013b). The experimental depth-dependent matrix content was normalized to day-56 wet weight, whereas for computational simulations the matrix content was be normalized to day-0 wet weight. To calculate the matrix content normalized to day-0 wet weight, we estimated the tissue swelling of each slice by interpolation of the relation between tissue swelling and GAG normalized to day-0 wet weight (Chapter 8, figure 8.8A). Relating material fiber modulus to collagen content was assumed as directly proportional to the collagen content and fiber modulus of our previous validation study (≈1.5% collagen and 0.028 MPa fiber stiffness, respectively). As presented in that work, the collagen damage was based on Simo damage criterion according to a cumulative log-normal distribution (threshold = 0.08 (mJ mm^{-3})$^{0.5}$ and shape parameter $\sigma_c = 1.5$) (Simo & Ju, 1987).

9.3.2.2 Computationally simulating unconfined mechanical testing After simulating the "growth" period over 56 days by increasing the fixed-charge density (as determined by the experimental GAG content) and adding successive collagen generation deposition (determined by the

experimental collagen content), the samples were "cored" to analyze the one-dimensional mechanical properties by reducing the modulus and swelling of the annuli to leave only the inner ∅ 3 mm section for simulating the mechanical testing.

Samples were first tared (5% displacement) before applying a 10% compression step, consistent with our mechanical testing protocols. The whole-construct Young's modulus was calculated as the difference between pre- and post- compression normalized to the strain of the tissue. Spatial modulus for each construct slice was calculated by normalizing the axial stress to prescribed axial strain (Green-Lagrange strain, referential set to configuration after the "growth" prior to the tare told).

Mechanical growth simulations were performed for each of the 6 constructs experimentally tested, using each sample's own depth-dependent biochemical content. As the predicted average compressive modulus of each sample was also determined, we present the average mechanical properties of the computational predictions as an average ± standard deviations, representing the averaged values over all of the simulated samples within each group (TGF-β treated and untreated).

9.4 Results

The experimental results of (Albro *et al.* , 2016) showed that, due to TGF-β transport limitations, tissues grow heterogeneously. Notably, TGF-β treated constructs developed ≈6 %ww GAG and ≈1.4 %ww collagen within the periphery (TGF-β exposed) of a construct and ≈2 %ww GAG and ≈0.3 %ww collagen within the interior (TGF-β depleted) of the same construct. If not treated with any TGF-β constructs will develop ≈1.5 %ww GAG and ≈0.3 %ww collagen throughout.

Taking these levels of matrix synthesis, we simulated the growth and, similar to the biochemical content, mechanical properties displayed spatial heterogeneity. The periphery of constructs exhibited the most swelling and had an elasticity of ≈540 kPa, whereas the interior region of the same construct, and a construct without TGF-β treatment had an elasticity of ≈20-100 kPa (Figure 9.1).

Model predictions replicated the experimental results of the bulk mechanical tests well (Figure 9.2). In the TGF-β treated constructs, the experimental moduli of 50 ± 10 kPa was not significantly different than the model predictions of 59 ± 16 kPa (p=0.25). In TGF-β unsupplemented constructs, the experimental moduli of 10 ± 6 kPa was significantly lower than the model predictions of 36 ± 20 kPa (p=0.02). TGF-β supplementation increased average tissue mechanical properties when compared

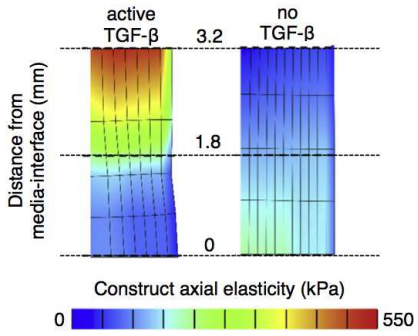

Figure 9.1: Mechanical properties of heterogeneous constructs after the computational growth simulation.

for experiments ($p<0.001$) and growth model predictions ($=0.02$).

9.5 Discussion

The computational models presented in the previous chapter were tested here to assess their capability in simulating heterogeneous spatial mechanical property development and the implications on bulk mechanical properties. Here, both large untreated and large TGF-β treated constructs were tested with the computational growth simulations capturing the complex growth (swelling) phenomena of the developing tissues and development of spatial mechanical properties.

These models rely only on the temporal evolution of mechanical properties as both the developing GAG content, driving the swelling, and the generational deposition of a damage-based collagen material require the rates and timings of both biochemical constituents. Models could therefore simulate the heterogeneous growth of constructs with measured heterogeneous matrix content (Figure 9.1).

Model predictions were similar to experimental measurements of the average construct mechanical properties for tissues treated with TGF-β (Figure 9.2), although model predictions were significantly different than experimental results in constructs not treated with TGF-β. This fact is not unexpected as the material model fits were based on constructs treated with TGF-β (Chapter 8). TGF-β treatment enhances tissue functional properties synergistically when compared to the influence of bulk biochemical content alone. For instance, in Chapter 4 (Figure 4.5A) we found a doubling in GAG content between control (untreated) and TGF-β treated (and withdrawn) tissues by day 45. This is distinct from the mechanical properties of the two groups on the same day (Figure

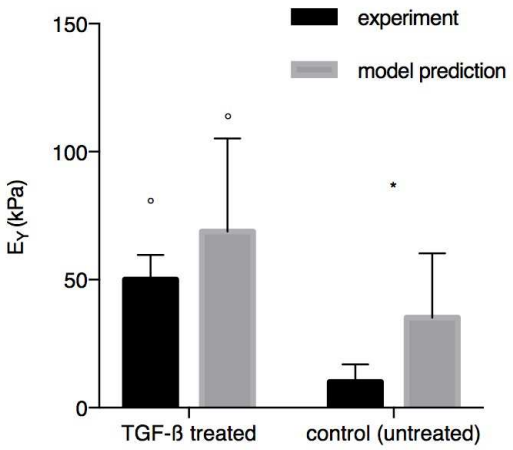

Figure 9.2: Experimental and model predictions of the average mechanical properties constructs. * denotes difference in experiment and model prediction for TGF-β treatment ($p<0.05$). $\circ$ denotes significant increase in TGF-β treatment over control for given measure (experiment or model prediction) ($p<0.05$).

4.4A), where the TGF-β treated and withdrawn constructs have a modulus an order of magnitude higher than control constructs. On this basis, calibrating the material models to constructs not treated with TGF-β would be necessary. However, given that all tissues grown with the intent of attaining native mechanical properties are treated with TGF-β, such models would carry little value.

Importantly, the similarity of the TGF-β treated model predictions to the experimental results and the overall differences between TGF-β treated and untreated samples provides a strong validation of the mechanical models for simulations of the physical growth of engineered cartilage.

Additionally, these models stress the importance of both biochemical constituents in the generation of tissue mechanical properties and suggest a role for strengthening constructs by limiting collagen damage and denaturation or reducing the swelling pressure of deposited GAG to improve tissue mechanics. This is the topic of the following chapter and appendix A.

9.6 Acknowledgements

This work is part of a larger publication, whose final publication is available from Elsevier, publishers, doi: 10.1016/j.biomaterials.2015.10.018.

Research reported in this publication was supported by the National Institute of Arthritis and Musculoskeletal and Skin Diseases and the National Institute of General Medical Sciences of the National Institutes of Health under Award Numbers AR060361, AR043628, and GM083925. The content is solely the responsibility of the authors and does not necessarily represent the official views of the National Institutes of Health.

Chapter 10 Constrained culture enhances functional tissue properties through collagen stability and maturation

10.1 Abstract

When cultured with sufficient nutrient supply, engineered cartilage synthesizes proteoglycans rapidly, producing an osmotic swelling pressure that destabilizes immature collagen and prevents the development of a robust collagen framework, a hallmark of native cartilage. We hypothesized that mechanically constraining the proteoglycan-induced tissue swelling would enhance construct functional properties through the development of a more stable collagen framework. To test this hypothesis, we developed a novel "cage" growth system to mechanically prevent tissue constructs from swelling while ensuring adequate nutrient supply to the growing construct. The effectiveness of constrained culture was examined by testing constructs with both agarose and cartilage-derived matrix hydrogel (CDMH). Constructs were seeded with immature bovine chondrocytes and cultured under free swelling (FS) conditions for 14 days with TGF-β before being placed into a constraining cage for the remainder of culture. Controls were cultured under FS conditions throughout. Agarose constructs cultured in cages did not expand after the day 14 caging while FS constructs expanded to 8$\times$ their day-0 weight after 112 days of culture. In addition to the physical differences in growth, by day 56, caged constructs had higher equilibrium (agarose: 639$\pm$179 kPa and CDMH: 608$\pm$257 kPa) and dynamic compressive moduli (agarose: 3.4$\pm$1.0 MPa and CDMH 2.8$\pm$1.0 MPa) than FS constructs (agarose: 193$\pm$74 kPa and 1.1$\pm$0.5 MPa and CDMH: 317$\pm$93 kPa and 1.8$\pm$1.0 MPa for equilibrium and dynamic properties, respectively). Interestingly, when normalized to final day wet-weight, cage and FS constructs did not exhibit differences in proteoglycan or collagen content. However, caged culture enhanced collagen maturation through the increased formation of pyridinoline crosslinks and improved collagen matrix stability as measured by α-chymotrypsin solubility. These findings demonstrate that physically constrained culture of engineered cartilage constructs improves functional properties through improved collagen network maturity and stability. We anticipate that constrained culture may benefit other reported engineered cartilage systems that exhibit a mismatch in proteoglycan and collagen synthesis.

10.2 Introduction

To date, most engineered cartilage culture techniques produce constructs lacking the comprehensive functional properties of native cartilage, such as equilibrium and dynamic moduli and failure properties in compression and tension, as well as frictional and wear properties. The limitation to growing functional replacement tissues for resurfacing osteoarthritic defects has hindered the clinical translation of cartilage tissue engineering (Moisio *et al.* , 2009; Hung *et al.* , 2003). In particular, native cartilage has a dense type II collagen fibrillar network that provides the tissue with a high tensile modulus, and a negatively-charged glycosaminoglycan (GAG) ground matrix which imparts a high fixed charge density and robust compressive properties to the tissue (Setton *et al.* , 1998; Asanbaeva *et al.* , 2007; Hosseini *et al.* , 2014). The interaction between collagen and GAG gives native cartilage unique compressive and tensile moduli as well as friction and wear properties ideally suited for its physiologic function within the joint (Ateshian *et al.* , 2003; Soltz & Ateshian, 1998). Current engineered cartilage culture protocols successfully develop native GAG content and compressive moduli (Byers *et al.* , 2008); however, achieving native collagen content and tensile properties remains elusive (Huang *et al.* , 2012).

While the sub-physiologic functional properties of cartilage constructs are often attributed to the low cellular metabolism of and biosynthesis by chondrocytes, we have recently shown that chondrocytes seeded at the cell densities present in the developing joint can deposit native levels of collagen, at the expense of producing supraphysiologic levels of GAG (DeGroot *et al.* , 1999; Nims *et al.* , 2016). This rapid and excessive GAG synthesis and deposition results in a high degree of tissue growth and swelling as negatively-charged GAG attracts ions and fluid from the surrounding media bath, increasing the osmotic swelling pressure within the construct. As the nascent collagen framework of engineered tissues provides only modest tensile stiffness (Huang *et al.* , 2012), constructs volumetrically expand under this swelling pressure. This expansion continues throughout culture as adequately nourished chondrocytes will continuously synthesize and deposit GAG. In our earlier work this process resulted in constructs volumetrically growing nearly 800% in wet-weight over 105 days in culture (Nims *et al.* , 2016). This study was also our first promising evidence of constructs synthesizing native collagen contents, which reached 15 %/day-0 wet-weight (%/D0-ww). This deposition, however, was effectively diluted due to the profound tissue swelling.

Moreover, collagen solubility measured as the susceptibility of collagen to α-chymotrypsin digestion, increased during culture. Increases in collagen solubility are associated with collagen destabilization and remodeling phenomena, including collagen denaturation, immaturity, and damage, all of which may weaken the bulk mechanical properties (Bank *et al.* , 1997; Thibault *et al.* , 2002; Temple *et al.* , 2006). Therefore, while both GAG and collagen are necessary for obtaining native cartilage functionality, high GAG deposition outcompetes and destabilizes the collagen network in developing cartilage constructs, hindering their functional properties.

While the mismatch in GAG and collagen synthesis and deposition was originally observed in agarose scaffolds, an open question is whether matrix deposition mismatches may be scaffold-dependent. Differences in scaffold ultrastructure and pore size may lead to different rates of matrix deposition and retention. However, a review of engineered cartilage systems suggests that GAG deposition exceeds collagen deposition in the majority of systems and the matrix deposition ratios do not match mature cartilage in any system (Table 5) (Vunjak-Novakovic *et al.* , 1999; Mauck *et al.* , 2002; Chung *et al.* , 2009; Byers *et al.* , 2008; Ng *et al.* , 2009; Erickson *et al.* , 2012; Makris *et al.* , 2014a; Bhumiratana *et al.* , 2014; Williams & Sah, 2010); thus while the field has been able to successfully promote chondrocyte matrix synthesis, engineered tissues are biochemically distinct from native cartilage. This trend seems to be present across both scaffold and cell types, importantly suggesting translational potential will continue to be limited in response to these matrix synthesis mismatches. The field of cartilage tissue engineering has increasingly turned to extracellular matrix-based scaffolds to mimic the native cartilage environment (Kisiday *et al.* , 2002; Burdick & Prestwich, 2011; Kim *et al.* , 2014; Rowland *et al.* , 2016; Beck *et al.* , 2016; Novak *et al.* , 2016); of these, cartilage-derived and collagen-based scaffolds are widely used in both research and pre-clinical settings (Huang *et al.* , 2016a; Rowland *et al.* , 2016). Although results are promising due to their high initial matrix content, these scaffolds are prone to initial contraction and it is unclear whether they can produce a functional collagen network.

We hypothesize that suppressing GAG-induced construct swelling and growth, while maintaining nutrient access and matrix synthesis, can enhance collagen integrity and thereby lead to enhanced functional properties in both agarose and cartilage-derived matrix hydrogel (CDMH) constructs. To this end, we developed a constraint-based culture system ("cage") that physically confines osmoti-

Study	Scaffold	GAG level	Collagen level	COL:GAG ratio
Vunjak-Novakovic, 1999	3% PGA	4.5 %ww	3.75 %ww	0.83:1
Mauck, 2002	2% agarose	1.5 %ww	1.8 %ww	1.2:1
Chung, 2009	1:1 MeHA	2.5 %ww	0.83 %ww	0.32:1
Byers, 2008	2% agarose	4.6 mg	2.3 mg	0.5:1
Ng, 2010	2% agarose	4.27 %ww	1.06 %ww	0.25:1
Erickson, 2012	1% MeHA	4.8 %/ww	4.8 %/ww	1:1
Makris, 2014	Self-assembled	1.45 %/ww	1.75 %/ww	1.2:1
Bhumiratana, 2014	Self-assembled	75 µg/mg	95 µg/mg	1.26:1
Native cartilage				
Williams, 2011	Native: 1-3 w.o. Bovine	45 mg/g	80 mg/g	1.77:1
Williams, 2011	Native: 1-2 y.o. Bovine	35 mg/g	180 mg/g	5.14:1

Table 5: GAG and collagen (COL) deposition levels and ratios from literature where both biochemical contents are reported. Native biochemical content (bottom two rows) in juvenile and adult bovine tissue are distinct from engineered tissues.

cally induced tissue growth and swelling. Cages were designed to mechanically restrain construct growth within a fixed volume and shape, and provide sufficient nutrient access to the construct. Cages integrated our previously reported tissue culture strategies for optimizing growth, namely the introduction of construct nutrient channels perfused by orbital shaking of the culture system using ample media (Nims *et al.* , 2015; Cigan *et al.* , 2014).

10.3 Methods

10.3.1 Cartilage-derived matrix hydrogel preparation

Hyaline cartilage was harvested from Yorkshire pigs weighing 40-50 kg immediately following euthanasia under a tissue sharing protocol approved by the Columbia University Institutional Animal Care and Use Committee. Hyaline cartilage was dissected free of connective tissue, rinsed in cold sterile normal saline, and stored at -80 °C for at least 24 h.

Cartilage was sectioned to 1 mm thickness and serially washed in an orbital shaker in hypertonic (2×) phosphate-buffered saline (PBS) for 15 min, 0.02 % trypsin for 15 min, and 3 % Tween-20 for 30 min. After each step, cartilage was washed in 2× PBS for 15 min. Cartilage sections were snap-frozen in liquid nitrogen, milled into a fine powder, and lyophilized for 24 hours. Powdered

cartilage was washed in 4 % sodium deoxycholate for 30 min, 2× PBS for 15 min, 0.2 mg mL^{-1} DNase I (Sigma D4527) for 24 hours, 0.1 % peracetic acid for 30 min, and sterile deionized water for 30 min. The cartilage matrix slurry was then snap-frozen in liquid nitrogen, lyophilized for 24 hours, and stored at room temperature.

Dry cartilage matrix powder was digested as previously described (O'Neill *et al.* , 2013). Briefly, 1 g of lyophilized cartilage matrix powder was mixed with 0.1 g pepsin (Sigma P7012) in 0.01 M hydrochloric acid and digested for 18 hours at room temperature (25 °C) under constant stirring. Matrix digests were aliquotted and stored at -80 °C until use. Cells were encapsulated within hydrogels by reconstituting the cartilage matrix digest with 0.1 M sodium hydroxide, 10× PBS, and chondrocytes suspended in culture media to yield a cartilage matrix hydrogel with a final concentration of 6 mg mL^{-1}.

10.3.2 Construct casting and culture

Chondrocytes were isolated from juvenile (4-8 weeks old) bovine carpometacarpal joints and passaged twice in monolayer culture as previously described (Cigan *et al.* , 2016b). Cells were released with 0.05% trypsin and encapsulated in either agarose (Study 1) or CDMH (Study 2).

In Study 1, chondrocytes (120 million cells mL^{-1}) were mixed 1:1 with type VII-A agarose (Sigma) and poured into a glass and Teflon-backed mold with a pattern of pre-arranged pins such that after punching ⌀10 mm × 2.34 mm constructs, each construct possessed 12 × ⌀1 mm nutrient channels (Cigan *et al.* , 2014). In Study 2, chondrocytes (120 million cells mL^{-1}) were mixed with CDMH and gelled at 37 °C and 5% CO_2 before biopsy punching ⌀10 mm × 2.34 mm constructs. Small agarose constructs (⌀3 mm × 2.34 mm) were also cast as scaffold controls for the CDMH constructs. Final nominal cell densities were 60 million cells mL^{-1} for Study 1 and the agarose controls of Study 2, and 33 million cells mL^{-1} in the CDMH constructs of Study 2 prior to scaffold contraction, as described below.

CDMH constructs were cast and initially punched without nutrient channels. Cellular contraction of the CDMH (Awad *et al.* , 2000) reduced the ⌀10 mm × 2.34 mm constructs to approximately ⌀4 mm × 0.8 mm after 14 days of culture. In a preliminary study using CDMH, the scaffold contraction caused such a large increase in cell density that constructs exhibited severe matrix heterogeneities (Figure 10.1). Therefore, to provide adequate nutrient exchange in Study 2, a single

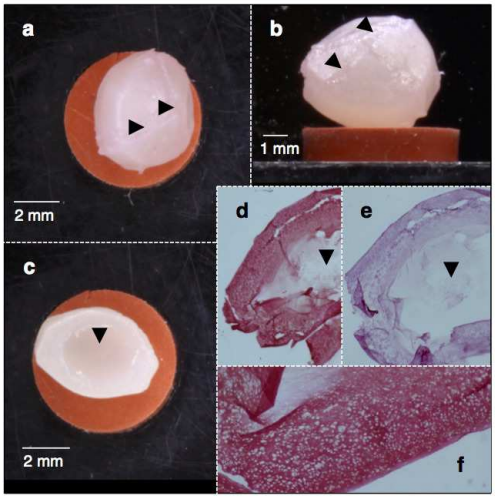

Figure 10.1: Views of a preliminary study using the CDMH where no channels were used. After 60 days, growth and matrix heterogeneities were present, likely due to the high cell density present. {A) top view, crack present (arrow). (B) side view, round growth visible, crack present (arrow). (C) cross sectional view of construct, void interior present (arrow). (D) Safranin-O histology (4×). Note cracking and void interior (arrow). (E) Picrosirius red histology (4×). Note cracking and void interior (arrow). (F) Safranin-O histology (20×). High cell density post scaffold contraction is evident.

⌀1 mm channel was punched in the center of each ⌀4 mm × 0.8 mm CDMH construct on day 14. Constructs in both studies were cultured in standard chemically-defined chondrogenic media under 0.8 Hz orbital shaking, and the large agarose constructs of Study 1 were placed vertically in culture racks to enhance nutrient access (Cigan *et al.* , 2014). Constructs received 10 ng mL^{-1} TGF-β3 supplementation (R&D Systems) for the first 14 days of culture (Cigan *et al.* , 2013). As tissue growth and expansion typically become significant after the 14-day TGF-β priming, constructs were divided into free swelling (FS) and cage groups on day 14 (Byers *et al.* , 2008; Nims *et al.* , 2014). Caged constructs were cultured for the remainder of the study within the cage while FS constructs continued their culture unconstrained. Constructs were assessed in Study 1 on days 0, 14, 56, and 112 and in Study 2 on days 14, 56, and 85 (Figure 10.2A). Prior to cellular contraction CDMH constructs lacked mechanical integrity and were therefore not tested immediately after casting on day 0.

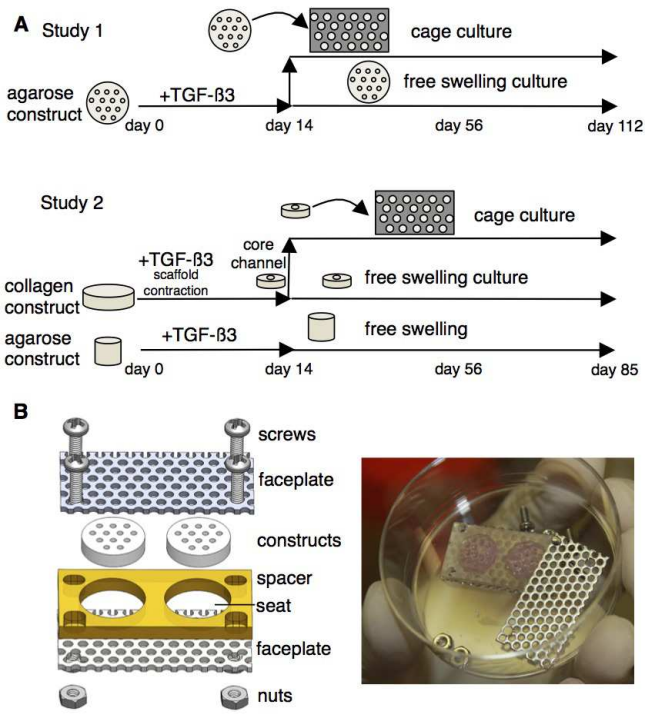

Figure 10.2: (A) Study 1 (agarose) and 2 (collagen) overview including channeling, TGF-β3 supplementation, caging, and construct time points. (B) Cage assembly diagram (left) and with construct (right).

10.3.3 Cage components and manufacturing

Cages consisted of two faceplates abutting a single spacer and the assembly was secured with four pairs of stainless steel screws and nuts (Figure 10.2B). Faceplates consisted of perforated stainless-steel sheets (316, ∅0.625 mm holes, center-to-center spacing 0.094 mm, McMaster-Carr) to allow media flow to the construct while preventing axial swelling. Spacers were made from an impermeable biocompatible material (Study 1: polysulfone, Study 2: polytetrafluoroethylene) and construct seats were sized to fit day 14 construct dimensions (Study 1: ∅10.5 mm × 2.34 mm; Study 2: ∅4 mm × 0.8 mm) and prevent radial swelling. All materials were autoclaved before assembly. Cages were assembled by placing constructs into the seats of the spacer and fastening faceplates to opposing sides of the spacer. To promote nutrient transport, channels were aligned with faceplate perforations and a ∅1 mm biopsy punch was passed through the faceplates and construct to ensure clear media passage. Channels of the cage constructs became progressively occluded in Study 1 and were re-cored once (day 58).

10.3.4 Mechanical testing

Mechanical testing included measurements of compressive unconfined equilibrium modulus at 10% compression (E_Y) and compressive unconfined dynamic modulus (G^*) at 0.01 Hz and 1% strain amplitude, as previously described (Cigan *et al.* , 2014).

10.3.5 Biochemical analyses

Biochemical analyses measured the matrix deposition of negatively-charged GAG using the dimethylmethylene blue dye-binding assay (Farndale *et al.* , 1986) and collagen using the acid hydrolysis-orthohydroxyproline (OHP) assay and a collagen:OHP conversion ratio of 7.6:1 (Hollander *et al.* , 1994; Cigan *et al.* , 2016b). Cell content was measured using the PicoGreen assay (Invitrogen) based on a ratio of 7.7 pg DNA cell^{-1} (McGowan *et al.* , 2002). Cell and matrix concentrations were normalized to the current day wet-weight (%/ww) to provide a measure of the current matrix content, and to the day-0 wet-weight (%/D0-ww) to provide a measure of total matrix deposition (Nims *et al.* , 2015).

Soluble collagen content was measured following the protocol of (Bank *et al.* , 1997): sub-punched ∅3 mm construct cores were desorbed of unbound collagen for 48 h at 4 °C under continuous rotation in a 4 M guanidine HCl buffer solution (0.1 M TrisHCl, 10 µg mL^{-1} pepstatin-A, 1 mM iodoacetamide, 1 mM EDTA, pH 7.3). Constructs were rinsed for 8 h in buffer at 4 °C before adding a 0.5 mg mL^{-1} solution (0.5 mL per sample) of α-chymotrypsin (Sigma) and incubating for 16 h at 37 °C. α-chymotrypsin separates collagens into soluble and intact (bound) fractions corresponding to their stability within the tissue. Aspiration of the incubation buffer isolates the soluble collagen fraction, leaving the intact collagen fraction within the tissue pellet. The aspirant and pellet were assayed with the OHP assay, and collagen solubility was calculated as

$$collagen\ solubility = \frac{soluble\ collagen\ mass}{soluble\ collagen\ mass + intact\ collagen\ mass}.$$

The collagen crosslink pyridinoline (PYD) was measured with a PYD ELISA (Quidel) using the construct acid hydrolysis digests (Nims *et al.* , 2014). PYD content is presented on a per tissue wet-weight basis (nmol mL^{-1}) and a per collagen basis (mol PYD/mol COL) assuming a collagen

molecular weight of 285 kDa (Grant & Prockop, 1972).

10.3.6 Histology

Samples were fixed for 24 h in acid-formalin-ethanol and placed into 70% ethanol prior to sectioning (5 µm slices) (Cigan *et al.* , 2016b). GAG was visualized with 0.01% Safranin-O staining and collagen was visualized with 0.1% Picrosirius Red staining (Kelly *et al.* , 2006).

10.3.7 Statistics

Mechanical and biochemical data were assessed with a two-way ANOVA ($\alpha = 0.05$, computed in R, r-project.org) to determine statistical roles of culture duration (Day), culture group (Group; Study 1: FS versus cage and Study 2: FS versus cage versus agarose), and the interaction (Interaction; duration $\times$ group). Tukey corrected post-hoc comparisons were made between groups exhibiting significant differences ($p \leq 0.05$) according to the ANOVA. Significance differences between the factor groups (Day, Group, Interaction) are noted within the corresponding figure (Figure 10.3, 10.5, 10.6, and 10.7) where significant.

10.4 Results

10.4.1 Study 1: agarose constructs

Free swelling (FS) agarose constructs grew to 8$\times$ their original size after 112 days of culture, while caged constructs swelled significantly less (2$\times$, $p<0.001$), essentially maintaining the size they had achieved prior to being placed in the cage on day 14 (Figure 10.3). FS constructs had dense Safranin-O and Picrosirius Red staining in the periphery, but interior voids were present on days 56 and 112 (Figure 10.3). Caged constructs also exhibited rich Safranin-O and Picrosirius Red staining and maintained tissue integrity on day 56, but by day 112 appeared less organized and interior tears were evident.

Polarized light microscopy images showed no directed tissue ultrastructure in caged constructs, but highly aligned collagen ultrastructure between the interior tissue void and construct periphery of FS tissues, reminiscent of native cartilage (Figure 10.4).

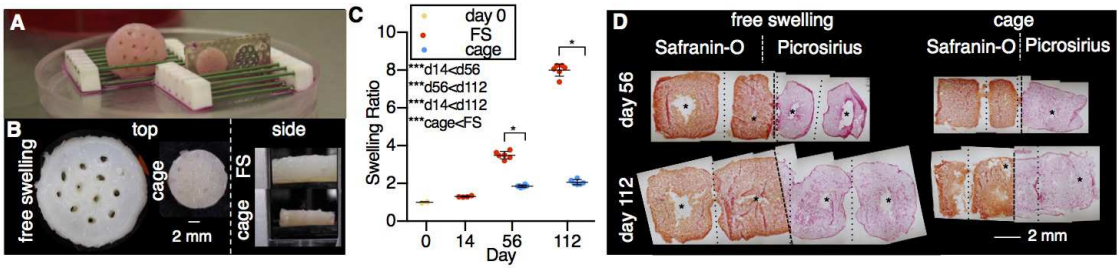

Figure 10.3: Agarose constructs: (A) Image of construct differences from free swelling (left) and cage (right; front faceplate removed for construct viewing) on day 112. (B) Morphologic differences in cage growth from top and side perspectives (FS side view only visualizes middle of construct). (C) Swelling ratio differences between free swelling and caged constructs. Differences between groups are noted where significant: ***$p<0.001$. * denotes differences between groups at same time point ($p<0.05$). Note equal spacing on the x-axis. (D) Histological images (side view) of constructs (Safranin-O displays GAG, Picrosirius displays collagen). Dashed lines are construct midlines and separates Safranin-O and Picrosirius Red images; dotted lines are construct channels or pre-existing channels; * are voids or tears in construct.

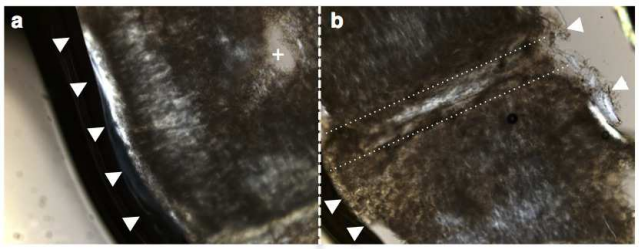

Figure 10.4: Polarized light microscopy images of agarose (A) free swelling and (B) cage construct growth from after 112 days of culture. Collagen alignment was present in the free swelling constructs, likely due to the high tissue swelling. Arrows point along construct periphery, + is interior void, dotted lines surround a channel.

Construct functional properties (Figure 10.5A-B) improved with culture duration before plateauing after day 56 ($p>0.40$ for E_Y and G^* between day 56 and 112), with both E_Y and G^* higher in caged constructs than FS constructs ($p<0.001$). GAG and collagen %/ww contents followed similar temporal trends as mechanical properties and plateaued after day 56 ($p<0.11$ vs day 112, Figure 10.5C-D). GAG content was significantly lower in caged constructs ($p<0.004$); meanwhile collagen content was similar between the groups ($p=0.17$). In contrast, both GAG and collagen matrix deposition (%/D0-ww) increased throughout culture and was significantly higher in FS constructs ($p<0.001$, Figure 10.5E-F). By day 14, constructs had deposited 4.8±0.2 %/D0-ww GAG and 1.7±0.05 %/D0-ww collagen, after which time FS constructs continued to deposit matrix, amounting to 66.6±3.1 %/D0-ww GAG and 14.8±1.7 %/D0-ww collagen by day 112 ($p<0.001$). Caged constructs deposited less matrix once constrained, and matrix deposition did not change after day 56 ($p>0.98$), holding at 14.7±2.6 %/D0-ww GAG and 3.4±0.3 %/D0-ww collagen. Cell densities did not change significantly from day 0 levels (84±14 million cells mL^{-1}) for caged constructs by day 112 (74±8 million cells mL^{-1}, $p=0.56$) but decreased in FS constructs (44±2 million cells mL^{-1}, $p<0.001$) (Figure 10.5G-H). Conversely, total cell content was higher in FS constructs ($p<0.001$) and increased throughout culture by cell proliferation ($p=0.002$). Total cell content in caged constructs did not change with time ($p=0.52$).

PYD content was higher in cage culture than FS for both PYD concentration ($p<0.001$) and PYD normalized to collagen ($p<0.001$) (Figure 10.5I-J). PYD content did not significantly change after day 56 ($p>0.34$) similarly to collagen content. In particular, cage constructs exhibited 70% more PYD when normalized to collagen content and 67% higher PYD concentration than FS constructs on day 112. Collagen solubility increased between days 14 and 56 ($p=0.003$) and was higher in free swelling constructs ($p=0.03$), suggesting collagen was more stable in cage constructs. Fluid volume fractions (Figure 10.5L) changed throughout culture and were higher in cage constructs ($p=0.011$).

10.4.2 Study 2: cartilage-derived matrix hydrogel constructs

CDMH constructs grew significantly over the 85-day culture, (Figure 10.6A), with FS constructs swelling significantly more (3.8×, $p<0.001$) than cage constructs (1.9× swelling) from their day 14 (post-contraction) wet-weight (Figure 10.6B). Adding a channel aided in nutrient availability and the large interior voids seen in our preliminary work (Figure 10.1) were not present in Study

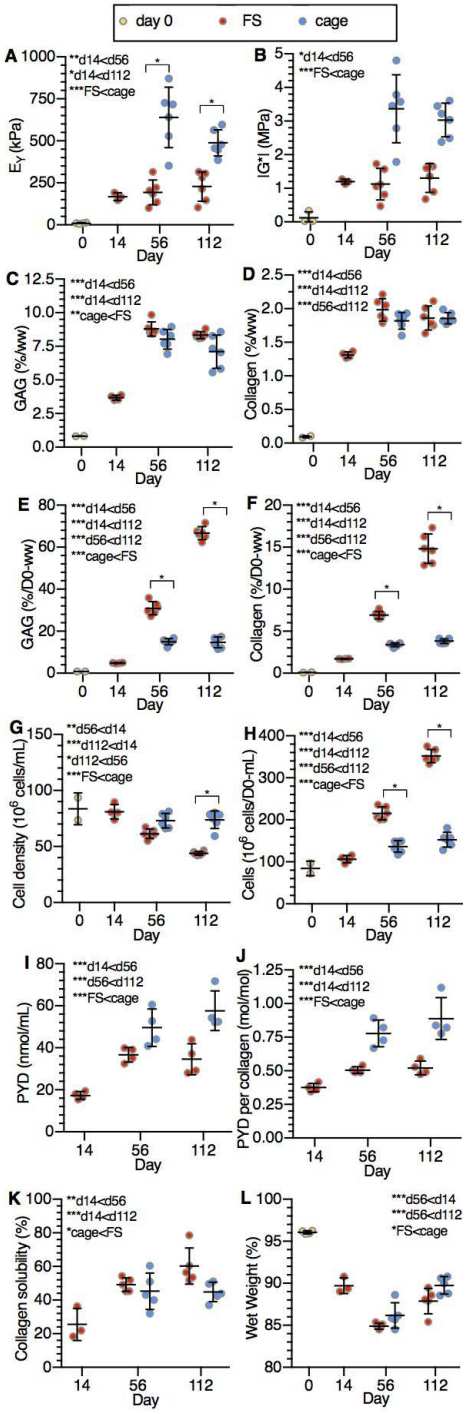

Figure 10.5: Study 1, agarose constructs: mechanical and biochemical measures (A) E_Y, (B) G^*, (C) GAG (%/ww), (D) collagen (%/ww), (E) GAG (%/D0-ww), (F) collagen (%/D0-ww), (G) cell density, (H) total cell content, (I) PYD (nmol/mL), (J) PYD/collagen (mol/mol), (K) collagen solubility, (L) construct water fraction. * denote differences between groups at same time point ($p<0.05$); differences between groups are noted where significant. *: $p<0.05$, ** $p<0.01$, ***$p<0.001$. Note equal spacing on the x-axis.

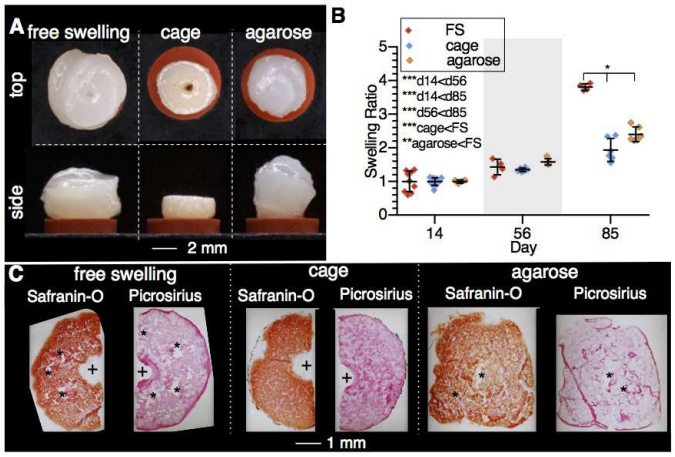

Figure 10.6: CDMH constructs: (A) Morphologic differences (top and side profiles) of free swelling, cage, and agarose constructs on day 85. (B) Swelling ratio differences between free swelling, caged, and agarose constructs. Differences between groups are noted where significant: **p<0.01. ***p<0.001. * denotes differences between groups at same time point (p<0.05). Note equal spacing on the x-axis. (C) Histological (top view) images of constructs (Safranin-O displays GAG, Picrosirius displays collagen) on day 56. + is channel location, * are voids or tears in construct.

2; robust Picrosirius Red and Safranin-O staining was observed throughout the CDMH constructs (Figure 10.6C). In particular, constructs grown in cages exhibited more uniform staining than FS CDMH and agarose gels; CDMH displayed richer Picrosirius Red staining.

Caged growth enhanced E_Y over FS culture (p=0.007) and was similar to agarose control constructs (p=0.99) (Figure 10.7A). G^* was similar between all groups and peaked on day 56 (p=0.001) before returning to day 14 levels by day 85 (p=0.89) (Figure 10.7B). GAG content was also similar between the culture conditions (p=0.52) and increased with culture duration (p=0.005) (Figure 10.7C). Collagen content was higher in constructs with CDMH (p<0.03) and was elevated in caged constructs, although not significantly so (p=0.06) (Figure 10.7D).

GAG and collagen deposition increased throughout culture (p<0.02) (Figure 10.7E-F). GAG deposition was similar between caged CDMH and agarose constructs (p=0.39), which were both lower than FS CDMH constructs (p<0.006), while collagen deposition was similar in the FS and caged CDMH constructs (p=0.10) and increased through day 85 (p<0.014). Due to the initial contraction at 14 days of culture, cell density in the CDMH constructs (350 million cells mL^{-1}) was significantly higher than the cell density in the agarose controls (50 million cells mL^{-1}, p<0.001) (Figure 10.7G). With subsequent construct swelling, cell density within CDMH decreased over culture such that by day 85 the cell density in FS CDMH was similar to agarose constructs (p=0.97), though caged

CDMH constructs still exhibited significantly higher cell density ($p<0.05$). Furthermore, total cell content (cells normalized to day-0 wet-weight) did not change over the culture duration in CDMH ($p=0.15$), indicating no active cell proliferation in this scaffold type (Figure 10.7H).

10.5 Discussion

Constrained cage growth of engineered cartilage reduced swelling (Figure 10.3C & Figure 10.6B) and improved construct functional properties in both the agarose and cartilage-derived matrix hydrogel (CDMH) constructs (Figure 10.5A-B & Figure 10.7A-B), supporting our hypothesis that rapid GAG deposition can hinder the properties of developing engineered cartilage constructs. We developed this strategy based on our prior observation that while cartilage constructs can synthesize GAG and collagen to match native levels, chondrocytes synthesize GAG more rapidly than collagen (Nims *et al.* , 2016).

Here, the mismatch in matrix deposition in FS constructs resulted in extreme tissue swelling and growth (8× in agarose constructs, Figure 10.3C, and 3.8× in CDMH, Figure 10.6C) and disrupted maturation of an intact collagen network (Figure 10.5I-K for agarose), thereby weakening the tissue (Williamson *et al.* , 2003b) (Figure 10.5A-B for agarose; Figure 10.7A-B for CDMH). Cage culture constrained swelling and excessive deposition of GAG and improved engineered cartilage functional properties in constructs with both agarose (Figure 10.5A-B) and CDMH (Figure 10.7A-B).

Therefore, mechanical constraints against swelling can enhance functional properties by preventing excessive proteoglycan deposition (agarose: Figure 10.5E; CDMH: Figure 10.7E), a widespread issue across engineered cartilage tissues (Table 5). However, cages also constrained total collagen deposition (agarose: Figure 10.5F; CDMH: Figure 10.7F), so that concentrations of GAG and collagen were similar in FS and caged constructs when accounting for the tissue swelling disparities (agarose: Figure 10.5C-D; CDMH: Figure 10.7C-D).

The best mechanical properties achieved in this study were observed in caged agarose (Figure 10.5A-B) and CDMH (Figure 10.7A-B) constructs on day 56. The equilibrium Young's modulus in unconfined compression was E_Y=639±179 kPa for agarose constructs and E_Y=608±257 kPa for CDMH constructs and the dynamic unconfined compression modulus at 0.01 Hz was G^*=3.4±1.0 MPa for agarose constructs and G^*=2.8±1.0 MPa for CDMH constructs. For comparison purposes, we have previously measured E_Y=660±230 kPa and G^*=6.5±2.1 MPa in immature bovine carti-

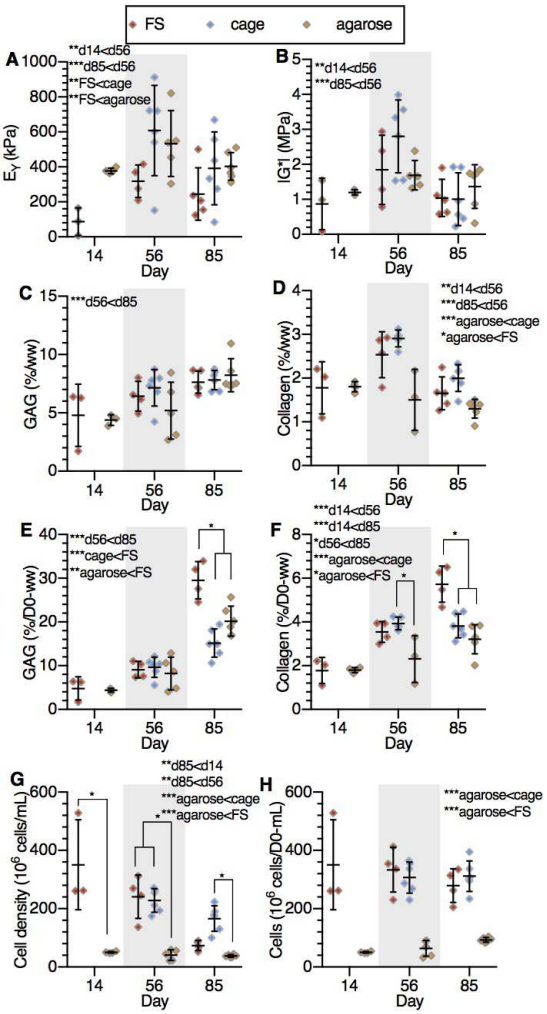

Figure 10.7: CDMH: mechanical and biochemical measures of Study 2 constructs (A) E_Y, (B) G^*, (C) GAG (%/ww), (D) collagen (%/ww), (E) GAG (%/D0-ww), (F) collagen (%/D0-ww), (G) cell density, (H) total cell content. * denote differences between groups at same time point ($p<0.05$); differences between groups are noted where significant. *: $p<0.05$, ** $p<0.01$, ***$p<0.001$. Note equal spacing on the x-axis.

lage (Park & Ateshian, 2006). Therefore, E_Y in the best constructs matches the native level while G^* is half the native value. These findings are consistent with the observation that GAG levels in this group of constructs (agarose: 8.0±0.7 %/ww; CDMH: 7.7±0.8 %/ww) are higher than native cartilage levels (3.3±0.8 %/ww) while collagen content (agarose: 1.8±0.1 %/ww; CDMH: 2.9±0.2 %/ww) is lower than native levels (9.5±2.1 %/ww) (Basalo *et al.* , 2005). Proteoglycans are known to enhance the compressive properties (Chen *et al.* , 2001; Guterl *et al.* , 2010), as manifested in E_Y, whereas collagen enhances the tensile properties (Kempson *et al.* , 1973) and thus the dynamic unconfined compression modulus G^* (Park & Ateshian, 2006). Despite the increase in GAG content from day 56 to 85, CDMH functional properties declined between these time points as did collagen content (Figure 10.7A-D); unlike the agarose cage constructs, CDMH swelling ratio increased for all groups between day 56 and 85, suggesting swelling was still possible in the CDMH constructs due to heterogeneous construct sizing after cellular contraction (Figure 10.3B).

While matrix deposition was nearly constant in FS constructs throughout culture (nearly linear rise in %/D0-ww for FS agarose constructs in Figure 10.5E-F starting on day 14 and CDMH constructs in Figure 10.7E-F), net deposition ceased in caged constructs after day 56. However, despite this dramatic difference in net matrix deposition, both FS and caged constructs had similar matrix concentrations (agarose: ≈8.0 %/ww GAG and ≈1.9 %/ww collagen; CDMH ≈7.3 %/ww GAG and ≈2.4 %/ww collagen). These two observations suggest a signaling role of the extracellular matrix to control chondrocyte matrix synthesis. In FS constructs negative feedback cues may be continually diluted by the swelling effect, promoting continuous matrix synthesis. Conversely, when construct swelling is prevented, these signals concentrate and inhibit matrix synthesis. While the nature of this signaling mechanism was not identified here, recent studies have implicated TRPV-4 channels in the transduction of extracellular environment signals to matrix synthesis modulation (O'Conor *et al.* , 2014). TRPV-4 is responsive to the osmotic environment which is regulated by the GAG %/ww concentration; thus, the observed plateau in GAG %/ww for both groups (Figure 10.5C) would be consistent with this type of signaling mechanism.

Despite cessation of net matrix deposition, caged constructs developed higher PYD content and better functional properties. In effect, the 54 % increase in PYD between FS and caged agarose constructs (Figure 10.5I-J) correlated with a threefold increase in E_Y and G^* on day 56 (Figure 10.5A-B) and a 10 % decrease in solubility (Figure 10.5K). This finding sug-

gests that enhancing collagen maturity is critical to developing functional engineered cartilage (Riesle *et al.* , 1998; Asanbaeva *et al.* , 2007). PYD and other intermolecular collagen crosslinks form spontaneously between enzymatically (lysyl oxidase, LOX) formed residues on adjacent collagen molecules (Siegel, 1974; Eyre *et al.* , 1984). The observation that collagen maturation is promoted by constrained growth is strong evidence that the physical expansion of a growing engineered tissue hinders the formation of PYD and prevents collagen maturation due to collagen content dilution. Makris et al. demonstrated that mechanical properties can be increased with increased PYD content by treating self-assembled cartilage constructs with exogenous LOX (Makris *et al.* , 2014b). However, even the highest LOX dose did not develop tissue matching the functionality of native cartilage. In comparison to their study, the constrained culture approach of the current study increased PYD content more than exogenous LOX supplementation alone. These results demonstrate that collagen-collagen proximity needs to be maintained to enhance PYD kinetics in engineered cartilage. Furthermore, the considerable enhancement in E_Y and G^* between FS and caged groups may not have resulted entirely from the increased PYD levels, since other types of crosslinks may also exist in cartilage (Eyre *et al.* , 2010) that were not characterized here.

The constraint strategy employed here increased collagen stability and maintained cell viability but did not improve collagen content, even though PYD of caged constructs matched native levels in adult bovine cartilage (0.74-0.97 mol PYD/mol COL) (Williamson *et al.* , 2003a) when normalized to collagen content. This deficiency in collagen content likely explains why tissue construct G^* remains below that of native cartilage. In previous work our lab and others digested existing GAG using the enzyme chondroitinase ABC to temporarily increase collagen content relative to GAG. Though initially promising, these treatments proved deleterious to cellular health and viability, stymieing further matrix synthesis (Bian *et al.* , 2009b; Natoli *et al.* , 2009; O'Connell *et al.* , 2014). Therefore, while the constrained culture presented here will likely prove critical in enhancing tissue functionality and collagen stability, the field of cartilage tissue engineering still requires strategies to enhance collagen content while maintaining cell viability.

The non-intuitive strategy of constrained growth only became evident after our extensive work to enhance and optimize growth conditions utilizing native cell densities in young cartilage with sufficient nutrient availability (Cigan *et al.* , 2016b; Nims *et al.* , 2016). Based on our recent studies suggesting that cell densities approaching native levels of developmental cartilage produce superior

quality cartilage, elevated cell densities were seeded in both agarose (89 million cells mL^{-1}) and collagen (250 million cells mL^{-1}) scaffolds (Stockwell, 1979). Physiologic cell densities, while proven effective for both juvenile bovine and adult human chondrocytes, require adequate nutrition to the developing tissue. Tissue constructs of either high cell density or of anatomical dimensions, or both, are particularly prone to nutrient scarcities and subsequent heterogeneous matrix deposition and growth (Huang *et al.* , 2016b; Saxena *et al.* , 2016; Moutos *et al.* , 2016; Hung *et al.* , 2003). We have previously directly demonstrated that both ample media and judiciously placed nutrient channels can meet the high metabolic requirements of developing cartilage (Cigan *et al.* , 2016c; Cigan *et al.* , 2016b; Cigan *et al.* , 2016a; Nims *et al.* , 2015). While the need for channels was previously demonstrated in an agarose scaffold system, this study suggests that channels can also improve contracted collagen-based scaffold culture where the cell density reached remarkably high levels. This suggests that channels may prove beneficial across other systems even with exceedingly high cell densities. In particular, scaffoldless systems, which exhibit high cell densities, often display heterogeneous matrix deposition and growth, despite their small size and may benefit from nutrient channel placement, similar to the collagen scaffolds constructs here (Huang *et al.* , 2016b; Bhumiratana *et al.* , 2014; Hadidi *et al.* , 2015).

Cages were specifically designed to allow media transport through the nutrient channels. The steel faceplates used here were adequate for the current study, but the selection of cage materials will be dependent on the tissue culture system. In this study we placed the constructs in cages only after 14 days of free swelling culture, coinciding with the termination of TGF-β supplementation. We have previously shown that steel has a high binding affinity for active TGF-β, suggesting that culture systems requiring continuous TGF-β supplementation will require different materials (Albro *et al.* , 2016; Albro *et al.* , 2013).

This study demonstrated that cages may be used effectively for constraining the swelling of engineered constructs resulting from high levels of matrix deposition. The primary benefits of this cage system were to enhance mature crosslink formation and to better maintain the desired construct dimensions, leading to better functional properties than free swelling controls. This approach was shown to be effective using agarose as well as cartilage-derived collagen scaffolds. Therefore this novel constrained culture approach holds promise for improving functional properties of large anatomically sized constructs in a variety of tissue engineering systems (Cigan *et al.* , 2016b).

10.6 Acknowledgement

This manuscript is currently in revision for submission to Tissue Engineering Part A.

We thank Dr. Sevan R. Oungoulian and Mr. Mohamed Haroun for their assistance in developing and constructing culture cages. Research reported in this publication was supported by the National Institutes of Health under Award Numbers R01AR060361, R01AR046568, T32AR059038, R01DE016525 and P41EB002520. The content is solely the responsibility of the authors and does not necessarily represent the official views of the National Institutes of Health.

Part III

Conclusions and Future Directions

Chapter 11 Conclusions and Future Directions

The work of this dissertation was to address the dearth of computational models of tissue growth, specifically through developing both biochemical and mechanical models by which tissue engineering protocols can be improved by both optimizing nutrient availability and enhancing the functional properties during culture. The insights gained here by elucidating the critical nutrients of developing cartilage constructs, the dependence of cartilage growth on the nutrients, and the physical mechanisms by which engineered cartilage grows has enhanced our fundamental understanding of biological growth phenomena and has been fruitful in developing strategies by which tissue properties can be enhanced through engineering solutions. Moreover, the computational models developed and validated have been instructive in the optimization of culture protocols and the interactions between nutrient availability, construct geometry, and cell density of developing tissues.

11.1 Conclusions

11.1.1 Glucose and TGF-β supply are critical for engineered cartilage development

Chapters 2, 3, 6, and 7 establish the basis for understanding the complex role and interactions of multiple nutrients within large, engineered cartilage constructs. In particular, glucose abundance is critical for the growth of engineered cartilage and can be readily enhanced in culture through additional media volume. Conversely, TGF-β is a transport limited nutrient which differentially regulates the growth of constructs over a wide concentration range. Culture protocols, such as the addition of different concentrations of TGF-β or the addition of more media for added glucose, can be adapted depending on tissue geometry and cell seeding density, two critical factors we establish for leading to heterogeneous TGF-β gradients and changes in media glucose depletion. The computational models here were developed such that when coupled with finite element models specific to the culture geometry and several system-specific growth parameters, many culture systems can quickly be analyzed and optimized for culturing large-sized constructs. Perhaps most critical for this optimization is establishing the relation between TGF-β dose and tissue growth due to the near certainty that through either transport limitations (in large constructs) or cellular internalization (in highly cellularized constructs) TGF-β availability will be critically limited within the interior of

constructs.

Interestingly, based on the studies here that demonstrated juvenile bovine chondrocytes respond to 1 and 10 ng mL^{-1} TGF-β similarly, channel supplementation can lead to reduced loads of TGF-β being necessary for culture. This result was later confirmed in subsequent channel studies using $\varnothing$10 mm constructs. This likely stems from the responsiveness of the juvenile cells to TGF-β and therefore such insights will require a more complete understanding of each tissue system before applying across systems. Regardless, taking care to ensure adequate glucose and TGF-β availabilities is a proven strategy for enhancing large sized tissue constructs.

11.1.2 Elevated cellularities for improved tissue development

With the benefit of the insight of nutrient availability from the computational growth models, Chapters 5 and 8 provided strong evidence for the improvements of tissue culture possible through increased cell seeding densities when care is taken to ensure adequate nutrient supply. Prior evidence in the literature that increased cell seeding densities improve tissue properties has been met with studies which provide counter evidence, suggesting lower cellularities provide better results. In this work we were able to achieve native collagen contents when constructs were seeded with cellularities approaching those reached in native developing tissue constructs. This suggests that engineering cartilage through biomimetic approaches of nutrient channels (to enable sufficient nutrient availability) and high cell seeding density (to improve matrix synthesis capacity) may benefit the development of scaffolded engineered cartilage systems like the high cell seeding density of self-assembled systems has aided the development of those systems. Furthermore, the analysis of chapter 5 suggests that increased cell densities in the presence of adequate nutrition may aid engineered cartilage growth regardless of the scaffold system. Specifically, the presence of a high density of cells may aid in the retention of matrix products and tissue development more than strategies and systems targeting the retention of matrix products.

11.1.3 GAG and collagen synthesis mismatches drive tissue mechanics and swelling

While the functional properties of native cartilage have long been known to be imparted by the mechanical composition of the tissue, in chapter 4, 8, and 9 we examined the growth mechanisms of developing cartilage constructs. The impact of a high GAG synthesis and low collagen synthesis,

once thought promising due to the abundance of matrix being deposited, was shown to be a significant limitation to our culturing of functional tissue constructs. Specifically, the inability for our tissue constructs to develop a functional collagen network as robust as the native collagen network may be a widespread issue influencing the growth of engineered cartilage tissues. This is particularly important as we hope to eventually engineered constructs which can be implanted to span the entire joint surface, making achievement of native mechanical properties an essential task. Fortunately, we identified that elevated GAG synthesis and depressed collagen synthesis is at the heart of this tissue leads us to develop strategies specifically targeting this growth mismatch phenomena.

11.1.4 Quelling tissue swelling improves tissue functionality

Ultimately, strategies to enhance tissue functionality during growth will require strengthening or reinforcing the nascent collagen framework. Chapter 10 presented a successful strategy for preventing the deleterious swelling of the tissue constructs which results from the rapid deposition of GAG by culturing constructs within a cage system to restrain the physical growth and swelling. The cage system improved mechanical functional properties in both constructs using agarose and a cartilage-derived matrix hydrogel scaffold systems. Cages achieved this functional improvement by enhancing collagen stability and increasing the level of collagen pyridinoline crosslinking. Together, this implies the mechanism of native growth may arise from delayed GAG synthesis early in development which allows for sufficient collagen cross linking before the proteoglycan induced tissue swelling. For improving the functionality of engineered constructs, cages proved useful and will help additional systems which have achieved physiologic or supra physiologic levels of matrix synthesis.

11.1.5 Critical modeling approaches, relations, and takeaways

The ultimate goal of the models developed and validated here has been to truly test the predictive outcomes of a comprehensive model, capturing the salient aspects of tissue growth. To achieve the consistency required for quantitative agreement, we utilized the repeatable model system of juvenile bovine chondrocyte encapsulated within an agarose gel, a system our lab has been characterizing for over a decade. Importantly, our cell source has remained stable over these years and there has been considerable overlap and training from researcher to researcher, thereby maintaining a consistency in tissue harvest and culture protocols and limiting most heterogeneities to animal-to-

animal differences of the primary cells. For the nature of the quantitative modeling work here, this has allowed modeling fits, results, and predictions to be extended throughout all of our published literature on the system.

To this point, and in an concerted effort to develop the most comprehensive engineered cartilage models to date, we exclusively used our previously published data sets, covering a wide range of culture conditions (media volumes and TGF-β supplementation levels), construct geometries, and cell seeding densities, to validate the models developed here. The final product has not just been a series of computational models but an insight of the different factors which can be altered and their influence on the modeling relations put forth here. For example, changing the cell type within a construct will change a number of the specific growth relations, but what will ultimately dictate a construct's success or failure is whether the cells will be able to receive adequate nutrition (glucose and TGF-β) and synthesize adequate matrix (proteoglycans and collagens). To achieve either of these goals, for instance, the density of channels may need to be altered with guidance from computational models, which will subsequently required fitting experiments as purposed here.

Therefore, for any new system to be characterized for modeling, the critical relations of the nutrient demands for the system are: the nutrient demands (i.e. glucose and, more influentially, TGF-β) of the tissue, the transport of TGF-β within the cell-seeded scaffold, and the dependence of matrix synthesis and deposition on TGF-β availability. To characterize the synthesis and binding kinetics of matrix for a given cell type and within a given scaffold: measure overall matrix synthesis and matrix release to the media, determine the relation and kinetics of matrix binding sites within a tissue, and monitor overtime to determine if synthesis plateaus or remains constant in the presence of adequate nutrition. To establish models based on the number of cells within a construct: establish the relations between nutrient requirements and consumption and matrix synthesis and deposition rates for different cell densities. Lastly, to model growth of a system based on matrix content, monitor the growth profiles (tissue swelling, mechanical modulus) over time and examine whether increases in functional properties and swelling are correlated with matrix swelling; does construct growth continue indefinitely or cease (when cultured with sufficient nutrition)? Can these be correlated with additional matrix factors (pyridinoline, soluble collagen, hyaluronan)?

11.2 Future Directions

11.2.1 Translation to clinically-relevant cell models

The work of this dissertation has drawn on our experience with juvenile bovine chondrocytes, cells which are metabolically active and robust, even at low cell densities. Given the need for clinical translation, a first step towards engineering large-sized constructs with adult and mature cell sources would be developing an understanding of the unique nutritional requirements of mature cells which are less metabolically active. Both glucose and TGF-β are still likely necessary to consider for mature cells and our preliminary data on mature canine chondrocytes suggests increasing TGF-β doses up to 50 ng mL^{-1} may be necessary for achieving homogeneous tissue properties even in small engineered constructs (forthcoming: Nims et al. Transactions of ORS, 2017, see Appendix). TGF-β doses of this magnitude in juvenile bovine cells have previously been shown to initiate more catabolic activity than anabolic, therefore requiring more quantitative TGF-β dosing studies to understand the role of matrix developing and synthesis in adult constructs.

Furthermore, it is interesting that despite achieving similar biochemical contents as juvenile constructs, mature constructs often have much lower mechanical properties. Quantitative analysis of the developing matrix content (cross links, hyaluronan) in adult constructs may provide structural insights into how the mechanical models presented here can be extended and incorporate the physics and phenomena important for more sensitive mature cells.

11.2.2 Patella constructs: application to canine and human

The direct application of these mature constructs is to treat large-sized defects within adult canine (model system) and humans (clinical translation). With our ongoing work to characterize the nutrient demands of mature engineered cartilage constructs, we can develop channels arrays within anatomical shapes (Figure 11.1). As Chapter 10 highlights the novel use of a cartilage derived matrix hydrogel, then the use of this strategy, proven effective for growing constructs when supplemented with nutrient channels, for creating an anatomical construct will be an ongoing pursuit.

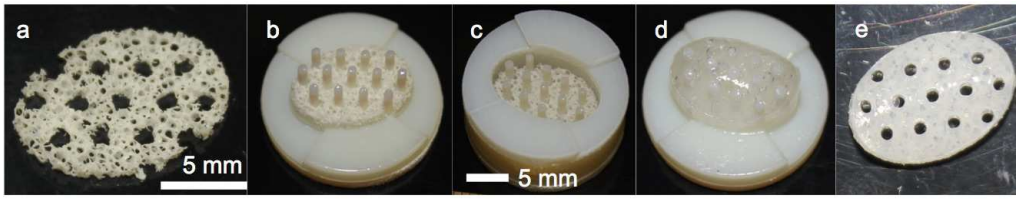

Figure 11.1: A schematic for creating large, anatomical constructs supplemented with nutrient channels.

References and Appendices

References

Albro, Michael B, Banerjee, Rajan E, Li, Roland, Oungoulian, Sevan R, Chen, Bo, Del Palomar, Amaya P, Hung, Clark T, & Ateshian, Gerard A. 2011. Dynamic loading of immature epiphyseal cartilage pumps nutrients out of vascular canals. *Journal of biomechanics*, **44**(9), 1654–1659.

Albro, Michael B, Nims, Robert J, Cigan, Alexander D, Yeroushalmi, Kevin J, Alliston, Tamara, Hung, Clark T, & Ateshian, Gerard A. 2013. Accumulation of exogenous activated TGF-β in the superficial zone of articular cartilage. *Biophysical journal*, **104**(8), 1794–1804.

Albro, Michael B, Nims, Robert J, Durney, Krista M, Cigan, Alexander D, Shim, Jay J, Vunjak-Novakovic, Gordana, Hung, Clark T, & Ateshian, Gerard A. 2016. Heterogeneous engineered cartilage growth results from gradients of media-supplemented active TGF-β and is ameliorated by the alternative supplementation of latent TGF-β. *Biomaterials*, **77**, 173–185.

Asanbaeva, Anna, Masuda, Koichi, Thonar, Eugene J, Klisch, Stephen M, & Sah, Robert L. 2007. Mechanisms of cartilage growth: modulation of balance between proteoglycan and collagen in vitro using chondroitinase ABC. *Arthritis & Rheumatism*, **56**(1), 188–198.

Ateshian, GA, Soslowsky, LJ, & Mow, VC. 1991. Quantitation of articular surface topography and cartilage thickness in knee joints using stereophotogrammetry. *Journal of biomechanics*, **24**(8), 761–776.

Ateshian, GA, Rosenwasser, MP, & Mow, VC. 1992. Curvature characteristics and congruence of the thumb carpometacarpal joint: differences between female and male joints. *Journal of biomechanics*, **25**(6), 591–607.

Ateshian, GA, Warden, WH, Kim, JJ, Grelsamer, RP, & Mow, VC. 1997. Finite deformation biphasic material properties of bovine articular cartilage from confined compression experiments. *Journal of biomechanics*, **30**(11), 1157–1164.

Ateshian, Gerard A. 2007. On the theory of reactive mixtures for modeling biological growth. *Biomechanics and modeling in mechanobiology*, **6**(6), 423–445.

Ateshian, Gerard A, & Ricken, Tim. 2010. Multigenerational interstitial growth of biological tissues. *Biomechanics and modeling in mechanobiology*, **9**(6), 689–702.

Ateshian, Gerard A, Soltz, Michael A, Mauck, Robert L, Basalo, Ines M, Hung, Clark T, & Lai, W Michael. 2003. The role of osmotic pressure and tension-compression nonlinearity in the frictional response of articular cartilage. *Transport in porous media*, **50**(1-2), 5–33.

Ateshian, Gerard A, Rajan, Vikram, Chahine, Nadeen O, Canal, Clare E, & Hung, Clark T. 2009. Modeling the matrix of articular cartilage using a continuous fiber angular distribution predicts many observed phenomena. *Journal of biomechanical engineering*, **131**(6), 061003.

Ateshian, Gerard A, Nims, Robert J, Maas, Steve, & Weiss, Jeffrey A. 2014. Computational modeling of chemical reactions and interstitial growth and remodeling involving charged solutes and solid-bound molecules. *Biomechanics and modeling in mechanobiology*, **13**(5), 1105–1120.

Athens, Aristos A, Makris, Eleftherios A, & Hu, Jerry C. 2013. Induced collagen cross-links enhance cartilage integration. *PloS one*, **8**(4), e60719.

Awad, Hani A, Butler, David L, Harris, Matthew T, Ibrahim, Rania E, Wu, Ying, Young, Randell G, Kadiyala, Sudha, & Boivin, Gregory P. 2000. In vitro characterization of mesenchymal stem cell-seeded collagen scaffolds for tendon repair: Effects of initial seeding density on contraction kinetics. *Journal of biomedical materials research*, **51**(2), 233–240.

Aydelotte, Margaret B, & Kuettner, Klaus E. 1988. Differences between sub-populations of cultured bovine articular chondrocytes. I. Morphology and cartilage matrix production. *Connective tissue research*, **18**(3), 205–222.

Bank, RA, & te Koppele, JM. 1999. Proteolytic degradation of the collagen network results in cartilage with inferior biomechanical properties.

Bank, Ruud A, Krikken, Marianne, Beekman, Bob, Stoop, Reinout, Maroudas, Alice, Lafebers, Floris PJG, & Te Koppele, Johan M. 1997. A simplified measurement of degraded collagen in tissues: application in healthy, fibrillated and osteoarthritic cartilage. *Matrix Biology*, **16**(5), 233–243.

Basalo, Ines M, Raj, David, Krishnan, Ramaswamy, Chen, Faye H, Hung, Clark T, & Ateshian, Gerard A. 2005. Effects of enzymatic degradation on the frictional response of articular cartilage in stress relaxation. *Journal of biomechanics*, **38**(6), 1343–1349.

Beck, Emily C, Barragan, Marilyn, Libeer, Tony B, Kieweg, Sarah L, Converse, Gabriel L, Hopkins, Richard A, Berkland, Cory J, & Detamore, Michael S. 2016. Chondroinduction from Naturally Derived Cartilage Matrix: A Comparison Between Devitalized and Decellularized Cartilage Encapsulated in Hydrogel Pastes. *Tissue Engineering Part A*, **22**(7-8), 665–679.

Benya, Paul D, & Shaffer, Joy D. 1982. Dedifferentiated chondrocytes reexpress the differentiated collagen phenotype when cultured in agarose gels. *Cell*, **30**(1), 215–224.

Bhumiratana, Sarindr, Eton, Ryan E, Oungoulian, Sevan R, Wan, Leo Q, Ateshian, Gerard A, & Vunjak-Novakovic, Gordana. 2014. Large, stratified, and mechanically functional human cartilage grown in vitro by mesenchymal condensation. *Proceedings of the National Academy of Sciences*, **111**(19), 6940–6945.

Bian, L, Angione, SL, Ng, KW, Lima, EG, Williams, DY, Mao, DQ, Ateshian, GA, & Hung, CT. 2009a. Influence of decreasing nutrient path length on the development of engineered cartilage. *Osteoarthritis and Cartilage*, **17**(5), 677–685.

Bian, Liming, Crivello, Keith M, Ng, Kenneth W, Xu, Duo, Williams, David Y, Ateshian, Gerard A, & Hung, Clark T. 2009b. Influence of temporary chondroitinase ABC-induced glycosaminoglycan suppression on maturation of tissue-engineered cartilage. *Tissue Engineering Part A*, **15**(8), 2065–2072.

Bland, Yvette S, & Ashhurst, Doreen E. 1996. Development and ageing of the articular cartilage of the rabbit knee joint: distribution of the fibrillar collagens. *Anatomy and embryology*, **194**(6), 607–619.

Bonaventure, J, Kadhom, N, Cohen-Solal, L, Ng, KH, Bourguignon, J, Lasselin, C, & Freisinger, P. 1994. Reexpression of cartilage-specific genes by dedifferentiated human articular chondrocytes cultured in alginate beads. *Experimental cell research*, **212**(1), 97–104.

Buckley, Conor T, Thorpe, Stephen D, & Kelly, Daniel J. 2009. Engineering of large cartilaginous tissues through the use of microchanneled hydrogels and rotational culture. *Tissue Engineering Part A*, **15**(11), 3213–3220.

Buckley, Mark R, Gleghorn, Jason P, Bonassar, Lawrence J, & Cohen, Itai. 2008. Mapping the depth dependence of shear properties in articular cartilage. *Journal of biomechanics*, **41**(11), 2430–2437.

Burdick, Jason A, & Prestwich, Glenn D. 2011. Hyaluronic acid hydrogels for biomedical applications. *Advanced materials*, **23**(12).

Burnsed, Olivia A, Schwartz, Zvi, Marchand, Katherine O, Hyzy, Sharon L, Olivares-Navarrete, René, & Boyan, Barbara D. 2016. Hydrogels derived from cartilage matrices promote induction of human mesenchymal stem cell chondrogenic differentiation. *Acta Biomaterialia*, **43**, 139–149.

Burton-Wurster, N, Liu, W, Matthews, GL, Lust, G, Roughley, PJ, Glant, TT, & Cs-Szabo, G. 2003. TGF beta 1 and biglycan, decorin, and fibromodulin metabolism in canine cartilage. *Osteoarthritis and cartilage*, **11**(3), 167–176.

Buschmann, Michael D, Gluzband, Yehezkiel A, Grodzinsky, Alan J, Kimura, James H, & Hunziker, Ernst B. 1992. Chondrocytes in agarose culture synthesize a mechanically functional extracellular matrix. *Journal of Orthopaedic Research*, **10**(6), 745–758.

Buschmann, Michael D, Gluzband, Yehezkiel A, Grodzinsky, Alan J, & Hunziker, Ernst B. 1995. Mechanical compression modulates matrix biosynthesis in chondrocyte/agarose culture. *Journal of cell science*, **108**(4), 1497–1508.

Butler, David L, Goldstein, Steven A, & Guilak, Farshid. 2000. Functional tissue engineering: the role of biomechanics. *Journal of biomechanical engineering*, **122**(6), 570–575.

Byers, Benjamin A, Mauck, Robert L, Chiang, Ian E, & Tuan, Rocky S. 2008. Transient exposure to transforming growth factor beta 3 under serum-free conditions enhances the biomechanical and biochemical maturation of tissue-engineered cartilage. *Tissue Engineering Part A*, **14**(11), 1821–1834.

Caplan, Arnold I. 2007. Adult mesenchymal stem cells for tissue engineering versus regenerative medicine. *Journal of cellular physiology*, **213**(2), 341–347.

Carter, Dennis R, Beaupré, Gary S, Wong, Marcy, Smith, R Lane, Andriacchi, Tom P, & Schurman, David J. 2004. The mechanobiology of articular cartilage development and degeneration. *Clinical orthopaedics and related research*, **427**, S69–S77.

Chahine, Nadeen O, Wang, Christopher CB, Hung, Clark T, & Ateshian, Gerard A. 2004. Anisotropic strain-dependent material properties of bovine articular cartilage in the transitional range from tension to compression. *Journal of biomechanics*, **37**(8), 1251–1261.

Chahine, Nadeen O, Chen, Faye H, Hung, Clark T, & Ateshian, Gerard A. 2005. Direct measurement of osmotic pressure of glycosaminoglycan solutions by membrane osmometry at room temperature. *Biophysical journal*, **89**(3), 1543–1550.

Chen, Faye Hui, Herndon, Mary E, Patel, Nichlesh, Hecht, Jacqueline T, Tuan, Rocky S, & Lawler, Jack. 2007. Interaction of cartilage oligomeric matrix protein/thrombospondin 5 with aggrecan. *Journal of Biological Chemistry*, **282**(34), 24591–24598.

Chen, SS, Falcovitz, YH, Schneiderman, R, Maroudas, A, & Sah, RL. 2001. Depth-dependent compressive properties of normal aged human femoral head articular cartilage: relationship to fixed charge density. *Osteoarthritis and Cartilage*, **9**(6), 561–569.

Cheng, Nai-Chen, Estes, Bradley T, Young, Tai-Horng, & Guilak, Farshid. 2012. Genipin-crosslinked cartilage-derived matrix as a scaffold for human adipose-derived stem cell chondrogenesis. *Tissue engineering Part A*, **19**(3-4), 484–496.

Chung, Cindy, & Burdick, Jason A. 2008. Influence of three-dimensional hyaluronic acid microenvironments on mesenchymal stem cell chondrogenesis. *Tissue Engineering Part A*, **15**(2), 243–254.

Chung, Cindy, Beecham, Michael, Mauck, Robert L, & Burdick, Jason A. 2009. The influence of degradation characteristics of hyaluronic acid hydrogels on in vitro neocartilage formation by mesenchymal stem cells. *Biomaterials*, **30**(26), 4287–4296.

Cigan, Alexander D, Nims, Robert J, Albro, Michael B, Esau, John D, Dreyer, Marissa P, Vunjak-Novakovic, Gordana, Hung, Clark T, & Ateshian, Gerard A. 2013. Insulin, ascorbate, and glucose have a much greater influence than transferrin and selenous acid on the in vitro growth of engineered cartilage in chondrogenic media. *Tissue Engineering Part A*, **19**(17-18), 1941–1948.

Cigan, Alexander D, Nims, Robert J, Albro, Michael B, Vunjak-Novakovic, Gordana, Hung, Clark T, & Ateshian, Gerard A. 2014. Nutrient channels and stirring enhanced the composition and stiffness of large cartilage constructs. *Journal of biomechanics*, **47**(16), 3847–3854.

Cigan, Alexander D, Roach, Brendan L, Nims, Robert J, Tan, Andrea R, Albro, Michael B, Stoker, Aaron M, Cook, James L, Vunjak-Novakovic, Gordana, Hung, Clark T, & Ateshian, Gerard A. 2016a. High seeding density of human chondrocytes in agarose produces tissue-engineered cartilage approaching native mechanical and biochemical properties. *Journal of biomechanics*, **49**(9), 1909–1917.

Cigan, Alexander D, Durney, Krista M, Nims, Robert J, Vunjak-Novakovic, Gordana, Hung, Clark T, & Ateshian, Gerard A. 2016b. Nutrient Channels Aid the Growth of Articular Surface-Sized Engineered Cartilage Constructs. *Tissue Engineering Part A*, **22**(17-18), 1063–1074.

Cigan, Alexander D, Nims, Robert J, Vunjak-Novakovic, Gordana, Hung, Clark T, & Ateshian, Gerard A. 2016c. Optimizing nutrient channel spacing and revisiting TGF-beta in large engineered cartilage constructs. *Journal of biomechanics*.

Cigan, Alexander Drake. 2016. *Nutrient channels to aid the growth of articular surface-sized engineered cartilage constructs*. Ph.D. thesis, Columbia University.

Clark, John M. 1990. The organisation of collagen fibrils in the superficial zones of articular cartilage. *Journal of anatomy*, **171**, 117.

Cohen, Barry H. 2002. Calculating a factorial ANOVA from means and standard deviations. *Understanding Statistics: Statistical Issues in Psychology, Education, and the Social Sciences*, **1**(3), 191–203.

Cote, Allison J, McLeod, Claire M, Farrell, Megan J, McClanahan, Patrick D, Dunagin, Margaret C, Raj, Arjun, & Mauck, Robert L. 2016. Single-cell differences in matrix gene expression do not predict matrix deposition. *Nature communications*, **7**.

Craig, FIONA M, Bentley, GEORGE, & Archer, CHARLES W. 1987. The spatial and temporal pattern of collagens I and II and keratan sulphate in the developing chick metatarsophalangeal joint. *Development*, **99**(3), 383–391.

Darling, Eric M, & Athanasiou, Kyriacos A. 2005. Rapid phenotypic changes in passaged articular chondrocyte subpopulations. *Journal of Orthopaedic Research*, **23**(2), 425–432.

Davisson, Twana, Sah, Robert L, & Ratcliffe, Anthony. 2002a. Perfusion increases cell content and matrix synthesis in chondrocyte three-dimensional cultures. *Tissue Engineering*, **8**(5), 807–816.

Davisson, Twana, Kunig, Sabine, Chen, Albert, Sah, Robert, & Ratcliffe, Anthony. 2002b. Static and dynamic compression modulate matrix metabolism in tissue engineered cartilage. *Journal of Orthopaedic Research*, **20**(4), 842–848.

DeGroot, Jeroen, Verzijl, Nicole, Bank, Ruud A, Lafeber, FPJG, Bijlsma, Johannes WJ, & TeKoppele, Johan M. 1999. Age-related decrease in proteoglycan synthesis of human articular chondrocytes. *Arth & Rheum*, **42**, 1003–9.

Di Cesare, Paul E, Carlson, Cathy S, Stolerman, Elliot S, Hauser, Nik, Tulli, Hermina, & Paulsson, Mats. 1996. Increased degradation and alteered tissue distribution of cartilage oligomeric matrix protein in human rheumatoid and osteoarthritic cartilage. *Journal of orthopaedic research*, **14**(6), 946–955.

Dieppe, Paul A, & Lohmander, L Stefan. 2005. Pathogenesis and management of pain in osteoarthritis. *The Lancet*, **365**(9463), 965–973.

Dimicco, MA, Kisiday, JD, Gong, H, & Grodzinsky, AJ. 2007. Structure of pericellular matrix around agarose-embedded chondrocytes. *Osteoarthritis and cartilage*, **15**(10), 1207–1216.

DiMicco, Michael A, & Sah, Robert L. 2003. Dependence of cartilage matrix composition on biosynthesis, diffusion, and reaction. *Transport in porous media*, **50**(1-2), 57–73.

Ding, Cicuttini, Cicuttini, Flavia, & Jones, Graeme. 2007. Tibial subchondral bone size and knee cartilage defects: relevance to knee osteoarthritis. *Osteoarthritis and cartilage*, **15**(5), 479–486.

Doskocil, M. 1984. Formation of the femoropatellar part of the human knee joint. *Folia morphologica*, **33**(1), 38–47.

Dubrulle, Julien, Jordan, Benjamin M, Akhmetova, Laila, Farrell, Jeffrey A, Kim, Seok-Hyung, Solnica-Krezel, Lilianna, & Schier, Alexander F. 2015. Response to Nodal morphogen gradient is determined by the kinetics of target gene induction. *Elife*, **4**, e05042.

DuRaine, Grayson D, Brown, Wendy E, Hu, Jerry C, & Athanasiou, Kyriacos A. 2015. Emergence of scaffold-free approaches for tissue engineering musculoskeletal cartilages. *Annals of biomedical engineering*, **43**(3), 543–554.

Durney, Krista M, Nims, Robert J, Law, Wing-Sum A, Cook, James L, Hung, Clark T, & Ateshian, Gerard A. 2017. Mature canine cells in full-scale engineered cartilage recapitulate mechanical and biochemical properties with nutrient channels. Transactions of the ORS.

Edwards, JC, Wilkinson, LS, Jones, HM, Soothill, P, Henderson, KJ, Worrall, JG, & Pitsillides, AA. 1994. The formation of human synovial joint cavities: a possible role for hyaluronan and CD44 in altered interzone cohesion. *Journal of anatomy*, **185**(Pt 2), 355.

Eisenberg, Solomon R, & Grodzinsky, Alan J. 1985. Swelling of articular cartilage and other connective tissues: electromechanochemical forces. *Journal of Orthopaedic Research*, **3**(2), 148–159.

Elder, Benjamin D, & Athanasiou, Kyriacos A. 2009. Hydrostatic pressure in articular cartilage tissue engineering: from chondrocytes to tissue regeneration. *Tissue Engineering Part B: Reviews*, **15**(1), 43–53.

Eleswarapu, Sriram V, & Athanasiou, Kyriacos A. 2013. TRPV4 channel activation improves the tensile properties of self-assembled articular cartilage constructs. *Acta biomaterialia*, **9**(3), 5554–5561.

Erickson, Isaac E, Kestle, Sydney R, Zellars, Kilief H, Farrell, Megan J, Kim, Minwook, Burdick, Jason A, & Mauck, Robert L. 2012. High mesenchymal stem cell seeding densities in hyaluronic acid hydrogels produce engineered cartilage with native tissue properties. *Acta biomaterialia*, **8**(8), 3027–3034.

Evans, HELEN B, Ayad, SHIRLEY, Abedin, MZ, Hopkins, S, Morgan, K, Walton, KW, Weiss, JACQUELINE B, & Holt, PJ. 1983. Localisation of collagen types and fibronectin in cartilage by immunofluorescence. *Annals of the rheumatic diseases*, **42**(5), 575–581.

Eyre, David R, & Wu, Jiann-Jiu. 2005. Collagen cross-links. *Pages 207–229 of: Collagen*. Springer.

Eyre, David R, Koob, Thomas J, & Van Ness, Kirk P. 1984. Quantitation of hydroxypyridinium crosslinks in collagen by high-performance liquid chromatography. *Analytical biochemistry*, **137**(2), 380–388.

Eyre, David R, Weis, Mary Ann, & Wu, Jiann-Jiu. 2010. Maturation of collagen ketoimine cross-links by an alternative mechanism to pyridinoline formation in cartilage. *Journal of Biological Chemistry*, **285**(22), 16675–16682.

Farndale, Richard W, Buttle, David J, & Barrett, Alan J. 1986. Improved quantitation and discrimination of sulphated glycosaminoglycans by use of dimethylmethylene blue. *Biochimica et Biophysica Acta (BBA)-General Subjects*, **883**(2), 173–177.

Farrell, Megan J, Fisher, Matthew B, Huang, Alice H, Shin, John I, Farrell, Kimberly M, & Mauck, Robert L. 2014. Functional properties of bone marrow-derived MSC-based engineered cartilage are unstable with very long-term in vitro culture. *Journal of biomechanics*, **47**(9), 2173–2182.

Freed, LE, Vunjak-Novakovic, G, & Langer, R. 1993. Cultivation of cell-polymer cartilage implants in bioreactors. *Journal of cellular biochemistry*, **51**(3), 257–264.

Galban, Craig J, & Locke, Bruce R. 1999a. Analysis of cell growth kinetics and substrate diffusion in a polymer scaffold. *Biotechnology and Bioengineering*, **65**(2), 121–132.

Galban, Craig J, & Locke, Bruce R. 1999b. Effects of spatial variation of cells and nutrient and product concentrations coupled with product inhibition on cell growth in a polymer scaffold. *Biotechnology and bioengineering*, **64**(6), 633–643.

Gardner, Ernest, & Gray, DJ. 1950. Prenatal development of the human hip joint. *American Journal of Anatomy*, **87**(2), 163–211.

Gardner, ERNEST, & O'Rahilly, RONAN. 1968. The early development of the knee joint in staged human embryos. *Journal of anatomy*, **102**(Pt 2), 289.

Garrigues, N William, Little, Dianne, Sanchez-Adams, Johannah, Ruch, David S, & Guilak, Farshid. 2014. Electrospun cartilage-derived matrix scaffolds for cartilage tissue engineering. *Journal of biomedical materials research Part A*, **102**(11), 3998–4008.

Grant, Michael E, & Prockop, Darwin J. 1972. The biosynthesis of collagen. *New England Journal of Medicine*, **286**(5), 242–249.

Guilak, Farshid, Awad, Hani A, Fermor, Beverley, Leddy, Holly A, & Gimble, Jeffrey M. 2004. Adipose-derived adult stem cells for cartilage tissue engineering. *Biorheology*, **41**(3-4), 389–399.

Guterl, Clare Canal, Hung, Clark T, & Ateshian, Gerard A. 2010. Electrostatic and non-electrostatic contributions of proteoglycans to the compressive equilibrium modulus of bovine articular cartilage. *Journal of biomechanics*, **43**(7), 1343–1350.

Hadidi, Pasha, Yeh, Timothy C, Hu, Jerry C, & Athanasiou, Kyriacos A. 2015. Critical seeding density improves the properties and translatability of self-assembling anatomically shaped knee menisci. *Acta biomaterialia*, **11**, 173–182.

He, Fan, Chen, Xiaodong, & Pei, Ming. 2009. Reconstruction of an in vitro tissue-specific microenvironment to rejuvenate synovium-derived stem cells for cartilage tissue engineering. *Tissue Engineering Part A*, **15**(12), 3809–3821.

Heinemeier, Katja M, Schjerling, Peter, Heinemeier, Jan, Møller, Mathias B, Krogsgaard, Michael R, Grum-Schwensen, Tomas, Petersen, Michael M, & Kjaer, Michael. 2016. Radiocarbon dating reveals minimal collagen turnover in both healthy and osteoarthritic human cartilage. *Science Translational Medicine*, **8**(346), 346ra90–346ra90.

Heywood, Hannah K, Sembi, Preetkamal K, Lee, David A, & Bader, Dan L. 2004. Cellular utilization determines viability and matrix distribution profiles in chondrocyte-seeded alginate constructs. *Tissue engineering*, **10**(9-10), 1467–1479.

Heywood, Hannah K, Bader, Dan L, & Lee, David A. 2006a. Glucose concentration and medium volume influence cell viability and glycosaminoglycan synthesis in chondrocyte-seeded alginate constructs. *Tissue engineering*, **12**(12), 3487–3496.

Heywood, Hannah K, Bader, Dan L, & Lee, David A. 2006b. Rate of oxygen consumption by isolated articular chondrocytes is sensitive to medium glucose concentration. *Journal of cellular physiology*, **206**(2), 402–410.

Hollander, Anthony P, Heathfield, Terrence F, Webber, Carolyn, Iwata, Yukiko, Bourne, Robert, Rorabeck, Cecil, & Poole, A Robin. 1994. Increased damage to type II collagen in osteoarthritic articular cartilage detected by a new immunoassay. *Journal of Clinical Investigation*, **93**(4), 1722.

Hosseini, Sayyed Mohsen, Wu, Yabin, Ito, Keita, & van Donkelaar, Corrinus C. 2014. The importance of superficial collagen fibrils for the function of articular cartilage. *Biomechanics and modeling in mechanobiology*, **13**(1), 41–51.

Hu, Jerry C, & Athanasiou, Kyriacos A. 2006. A self-assembling process in articular cartilage tissue engineering. *Tissue engineering*, **12**(4), 969–979.

Huang, Alice H, Baker, Brendon M, Ateshian, Gerard A, & Mauck, Robert L. 2012. Sliding contact loading enhances the tensile properties of mesenchymal stem cell-seeded hydrogels. *Eur Cell Mater*, **24**, 29–45.

Huang, Brian J, Hu, Jerry C, & Athanasiou, Kyriacos A. 2016a. Cell-based tissue engineering strategies used in the clinical repair of articular cartilage. *Biomaterials*, **98**, 1–22.

Huang, Brian J, Huey, Daniel J, Hu, Jerry C, & Athanasiou, Kyriacos A. 2016b. Engineering biomechanically functional neocartilage derived from expanded articular chondrocytes through the manipulation of cell-seeding density and dexamethasone concentration. *Journal of tissue engineering and regenerative medicine*.

Hung, Clark T, Lima, Eric G, Mauck, Robert L, Taki, Erica, LeRoux, Michelle A, Lu, Helen H, Stark, Robert G, Guo, X Edward, & Ateshian, Gerard A. 2003. Anatomically shaped osteochondral constructs for articular cartilage repair. *Journal of biomechanics*, **36**(12), 1853–1864.

Hung, Clark T, Mauck, Robert L, Wang, Christopher C-B, Lima, Eric G, & Ateshian, Gerard A. 2004. A paradigm for functional tissue engineering of articular cartilage via applied physiologic deformational loading. *Annals of biomedical engineering*, **32**(1), 35–49.

Hunziker, ERNST B. 2002. Articular cartilage repair: basic science and clinical progress. A review of the current status and prospects. *Osteoarthritis and cartilage*, **10**(6), 432–463.

Jadin, Kyle D, Wong, Benjamin L, Bae, Won C, Li, Kelvin W, Williamson, Amanda K, Schumacher, Barbara L, Price, Jeffrey H, & Sah, Robert L. 2005. Depth-varying density and organization of chondrocytes in immature and mature bovine articular cartilage assessed by 3D imaging and analysis. *Journal of Histochemistry & Cytochemistry*, **53**(9), 1109–1119.

Jakob, Roland P, Franz, Torsten, Gautier, Emmanuel, & Mainil-Varlet, Pierre. 2002. Autologous osteochondral grafting in the knee: indication, results, and reflections. *Clinical orthopaedics and related research*, **401**, 170–184.

Johnson, Kenneth A, & Goody, Roger S. 2011. The original Michaelis constant: translation of the 1913 Michaelis–Menten paper. *Biochemistry*, **50**(39), 8264–8269.

Jones, Brian, Hung, Clark T, & Ateshian, Gerard. 2016. Biphasic analysis of cartilage stresses in the patellofemoral joint. *Journal of Knee Surgery*, **29**(02), 092–098.

Jones, Brian K, Durney, Krista M, Hung, Clark T, & Ateshian, Gerard A. 2015. The friction coefficient of shoulder joints remains remarkably low over 24h of loading. *Journal of biomechanics*, **48**(14), 3945–3949.

Jurvelin, J, Säämänen, AM, Arokoski, J, Helminen, HJ, Kiviranta, I, & Tammi, M. 1988. Biomechanical properties of the canine knee articular cartilage as related to matrix proteoglycans and collagen. *Engineering in medicine*, **17**(4), 157–162.

Kato, Yukio, & Gospodarowicz, Denis. 1985. Sulfated proteoglycan synthesis by confluent cultures of rabbit costal chondrocytes grown in the presence of fibroblast growth factor. *The Journal of cell biology*, **100**(2), 477–485.

Kelly, Daniel J, & Prendergast, Patrick J. 2006. Prediction of the optimal mechanical properties for a scaffold used in osteochondral defect repair. *Tissue engineering*, **12**(9), 2509–2519.

Kelly, Terri-Ann N, Ng, Kenneth W, Wang, Christopher C-B, Ateshian, Gerard A, & Hung, Clark T. 2006. Spatial and temporal development of chondrocyte-seeded agarose constructs in free-swelling and dynamically loaded cultures. *Journal of biomechanics*, **39**(8), 1489–1497.

Kempson, GE, Muir, Helen, Pollard, C, & Tuke, M. 1973. The tensile properties of the cartilage of human femoral condyles related to the content of collagen and glycosaminoglycans. *Biochimica et Biophysica Acta (BBA)-General Subjects*, **297**(2), 456–472.

Kempson, Geoffrey E. 1980. The mechanical properties of articular cartilage. *The joints and synovial fluid*, **2**, 177–238.

Khoshgoftar, Mehdi, van Donkelaar, Corrinus C, & Ito, Keita. 2011. Mechanical stimulation to stimulate formation of a physiological collagen architecture in tissue-engineered cartilage: a numerical study. *Computer methods in biomechanics and biomedical engineering*, **14**(02), 135–144.

Khoshgoftar, Mehdi, Wilson, Wouter, Ito, Keita, & van Donkelaar, Corrinus C. 2013a. The effect of tissue-engineered cartilage biomechanical and biochemical properties on its post-implantation mechanical behavior. *Biomechanics and modeling in mechanobiology*, **12**(1), 43–54.

Khoshgoftar, Mehdi, Wilson, Wouter, Ito, Keita, & van Donkelaar, Corrinus C. 2013b. The effects of matrix inhomogeneities on the cellular mechanical environment in tissue-engineered cartilage: an in silico investigation. *Tissue Engineering Part C: Methods*, **20**(2), 104–115.

Khoshgoftar, Mehdi, Wilson, Wouter, Ito, Keita, & van Donkelaar, Corrinus C. 2013c. Influence of tissue-and cell-scale extracellular matrix distribution on the mechanical properties of tissue-engineered cartilage. *Biomechanics and modeling in mechanobiology*, **12**(5), 901–913.

Khoshgoftar, Mehdi, Wilson, Wouter, Ito, Keita, & van Donkelaar, Corrinus C. 2014. Influence of the temporal deposition of extracellular matrix on the mechanical properties of tissue-engineered cartilage. *Tissue Engineering Part A*, **20**(9-10), 1476–1485.

Kim, Hwan D, Heo, Jiseung, Hwang, Yongsung, Kwak, Seon-Yeong, Park, Ok Kyu, Kim, Hyunbum, Varghese, Shyni, & Hwang, Nathaniel S. 2014. Extracellular-Matrix-Based and Arg-Gly-Asp–Modified Photopolymerizing Hydrogels for Cartilage Tissue Engineering. *Tissue Engineering Part A*, **21**(3-4), 757–766.

Kisiday, J, Jin, M, Kurz, B, Hung, H, Semino, C, Zhang, S, & Grodzinsky, AJ. 2002. Self-assembling peptide hydrogel fosters chondrocyte extracellular matrix production and cell division: implications for cartilage tissue repair. *Proceedings of the National Academy of Sciences*, **99**(15), 9996–10001.

Klein, TJ, & Sah, RL. 2007. Modulation of depth-dependent properties in tissue-engineered cartilage with a semi-permeable membrane and perfusion: a continuum model of matrix metabolism and transport. *Biomechanics and modeling in mechanobiology*, **6**(1-2), 21–32.

Klein, Travis J, Chaudhry, Manu, Bae, Won C, & Sah, Robert L. 2007. Depth-dependent biomechanical and biochemical properties of fetal, newborn, and tissue-engineered articular cartilage. *Journal of biomechanics*, **40**(1), 182–190.

Knutsen, Gunnar, Engebretsen, Lars, Ludvigsen, Tom C, Drogset, Jon Olav, Grøntvedt, Torbjørn, Solheim, Eirik, Strand, Torbjørn, Roberts, Sally, Isaksen, Vidar, & Johansen, Oddmund. 2004. Autologous chondrocyte implantation compared with microfracture in the knee. *J Bone Joint Surg Am*, **86**(3), 455–464.

Krishnan, Ramaswamy, Park, Seonghun, Eckstein, Felix, & Ateshian, Gerard A. 2003. Inhomogeneous cartilage properties enhance superficial interstitial fluid support and frictional properties, but do not provide a homogeneous state of stress. *Journal of biomechanical engineering*, **125**(5), 569–577.

Krishnan, Ramaswamy, Kopacz, Monika, & Ateshian, Gerard A. 2004. Experimental verification of the role of interstitial fluid pressurization in cartilage lubrication. *Journal of Orthopaedic Research*, **22**(3), 565–570.

Kuettner, Klaus E. 1992. Biochemistry of articular cartilage in health and disease. *Clinical biochemistry*, **25**(3), 155–163.

Kuo, Catherine K, Li, Wan-Ju, Mauck, Robert L, & Tuan, Rocky S. 2006. Cartilage tissue engineering: its potential and uses. *Current opinion in rheumatology*, **18**(1), 64–73.

Lai, W Michael, Hou, JS, & Mow, Van C. 1991. A triphasic theory for the swelling and deformation behaviors of articular cartilage. *Journal of biomechanical engineering*, **113**(3), 245–258.

Leddy, Holly A, Awad, Hani A, & Guilak, Farshid. 2004. Molecular diffusion in tissue-engineered cartilage constructs: Effects of scaffold material, time, and culture conditions. *Journal of Biomedical Materials Research Part B: Applied Biomaterials*, **70**(2), 397–406.

Lee, David A, & Bader, Dan L. 1997. Compressive strains at physiological frequencies influence the metabolism of chondrocytes seeded in agarose. *Journal of Orthopaedic Research*, **15**(2), 181–188.

Lee, Kuen Yong, & Mooney, David J. 2001. Hydrogels for tissue engineering. *Chemical reviews*, **101**(7), 1869–1880.

Lemon, G, & King, JR. 2007. Multiphase modelling of cell behaviour on artificial scaffolds: effects of nutrient depletion and spatially nonuniform porosity. *Mathematical Medicine and Biology*, **24**(1), 57–83.

Lima, Eric G, Bian, Liming, Ng, Kenneth W, Mauck, Robert L, Byers, Benjamin A, Tuan, Rocky S, Ateshian, Gerard A, & Hung, Clark T. 2007. The beneficial effect of delayed compressive loading on tissue-engineered cartilage constructs cultured with TGF-β3. *Osteoarthritis and Cartilage*, **15**(9), 1025–1033.

Lin, Tze-Hung, Jhang, Han-Yun, Chu, Feng-Cheng, & Chung, CA. 2013. Computational modeling of nutrient utilization in engineered cartilage. *Biotechnology progress*, **29**(2), 452–462.

Maas, Steve A, Ellis, Benjamin J, Ateshian, Gerard A, & Weiss, Jeffrey A. 2012. FEBio: finite elements for biomechanics. *Journal of biomechanical engineering*, **134**(1), 011005.

Makris, Eleftherios A, Responte, Donald J, Paschos, Nikolaos K, Hu, Jerry C, & Athanasiou, Kyriacos A. 2014a. Developing functional musculoskeletal tissues through hypoxia and lysyl oxidase-induced collagen cross-linking. *Proceedings of the National Academy of Sciences*, **111**(45), E4832–E4841.

Makris, Eleftherios A, Responte, Donald J, Paschos, Nikolaos K, Hu, Jerry C, & Athanasiou, Kyriacos A. 2014b. Developing functional musculoskeletal tissues through hypoxia and lysyl oxidase-induced collagen cross-linking. *Proceedings of the National Academy of Sciences*, **111**(45), E4832–E4841.

Maroudas, A. 1976. Balance between swelling pressure and collagen tension in normal and degenerate cartilage. *Nature*, **260**(5554), 808–809.

Maroudas, Alice, Leaback, DH, & Stockwell, RA. 1975. Glycosaminoglycan turn-over in articular cartilage [and discussion]. *Philosophical Transactions of the Royal Society of London B: Biological Sciences*, **271**(912), 293–313.

Mauck, RL, Yuan, X, & Tuan, RS. 2006. Chondrogenic differentiation and functional maturation of bovine mesenchymal stem cells in long-term agarose culture. *Osteoarthritis and cartilage*, **14**(2), 179–189.

Mauck, Robert L, Soltz, Michael A, Wang, Christopher CB, Wong, Dennis D, Chao, Pen-Hsiu Grace, Valhmu, Wilmot B, Hung, Clark T, & Ateshian, Gerard A. 2000. Functional tissue engineering of articular cartilage through dynamic loading of chondrocyte-seeded agarose gels. *Journal of biomechanical engineering*, **122**(3), 252–260.

Mauck, Robert L, Seyhan, Sara L, Ateshian, Gerard A, & Hung, Clark T. 2002. Influence of seeding density and dynamic deformational loading on the developing structure/function relationships of chondrocyte-seeded agarose hydrogels. *Annals of biomedical engineering*, **30**(8), 1046–1056.

Mauck, Robert L, Nicoll, Steven B, Seyhan, Sara L, Ateshian, Gerard A, & Hung, Clark T. 2003. Synergistic action of growth factors and dynamic loading for articular cartilage tissue engineering. *Tissue engineering*, **9**(4), 597–611.

McDermott, AGP, Langer, F, Pritzker, KPH, & Gross, AE. 1985. Fresh Small-Fragment Osteochondral Allografts: Long-term Follow-up Study on First 100 Cases. *Clinical orthopaedics and related research*, **197**, 96–102.

McDevitt, CA. 1973. Biochemistry of articular cartilage. Nature of proteoglycans and collagen of articular cartilage and their role in ageing and in osteoarthrosis. *Annals of the rheumatic diseases*, **32**(4), 364.

McGowan, KB, Kurtis, MS, Lottman, LM, Watson, D, & Sah, RL. 2002. Biochemical quantification of DNA in human articular and septal cartilage using PicoGreen® and Hoechst 33258. *Osteoarthritis and Cartilage*, **10**(7), 580–587.

Miller, Jordan S, Stevens, Kelly R, Yang, Michael T, Baker, Brendon M, Nguyen, Duc-Huy T, Cohen, Daniel M, Toro, Esteban, Chen, Alice A, Galie, Peter A, Yu, Xiang, *et al.* . 2012. Rapid casting of patterned vascular networks for perfusable engineered three-dimensional tissues. *Nature materials*, **11**(9), 768–774.

Mitrovic, Dragoslav R. 1977. Development of the metatarsophalangeal joint of the chick embryo: morphological, ultrastructural and histochemical studies. *American Journal of Anatomy*, **150**(2), 333–347.

Moisio, Kirsten, Eckstein, Felix, Chmiel, Joan S, Guermazi, Ali, Prasad, Pottumarthi, Almagor, Orit, Song, Jing, Dunlop, Dorothy, Hudelmaier, Martin, Kothari, Ami, *et al.* . 2009. Denuded subchondral bone and knee pain in persons with knee osteoarthritis. *Arthritis & Rheumatism*, **60**(12), 3703–3710.

Moriguchi, Takahiko, & Fujimoto, Daisaburo. 1978. Age-related changes in the content of the collagen crosslink, pyridinoline. *Journal of biochemistry*, **84**(4), 933–935.

Motaung, Shirley CKM, Di Cesare, Paul E, & Hari Reddi, A. 2011. Differential response of cartilage oligomeric matrix protein (COMP) to morphogens of bone morphogenetic protein/transforming growth factor-β family in the surface, middle and deep zones of articular cartilage. *Journal of tissue engineering and regenerative medicine*, **5**(6), e87–e96.

Moutos, Franklin T, Glass, Katherine A, Compton, Sarah A, Ross, Alison K, Gersbach, Charles A, Guilak, Farshid, & Estes, Bradley T. 2016. Anatomically shaped tissue-engineered cartilage with tunable and inducible anticytokine delivery for biological joint resurfacing. *Proceedings of the National Academy of Sciences*, **113**(31), E4513–E4522.

Mow, Van C, Holmes, Mark H, & Lai, W Michael. 1984. Fluid transport and mechanical properties of articular cartilage: a review. *Journal of biomechanics*, **17**(5), 377–394.

Mow, VC, Ateshian, GA, Lai, WM, & Gu, WY. 1998. Effects of fixed charges on the stress–relaxation behavior of hydrated soft tissues in a confined compression problem. *International Journal of Solids and Structures*, **35**(34), 4945–4962.

Mundlos, S, Engel, H, Michel-Behnke, I, & Zabel, B. 1990. Distribution of type I and type II collagen gene expression during the development of human long bones. *Bone*, **11**(4), 275–279.

Nagel, Thomas, & Kelly, Daniel J. 2012. The composition of engineered cartilage at the time of implantation determines the likelihood of regenerating tissue with a normal collagen architecture. *Tissue Engineering Part A*, **19**(7-8), 824–833.

Natoli, Roman M, Revell, Christopher M, & Athanasiou, Kyriacos A. 2009. Chondroitinase ABC treatment results in greater tensile properties of self-assembled tissue-engineered articular cartilage. *Tissue Engineering Part A*, **15**(10), 3119–3128.

Ng, Kenneth W, Lima, Eric G, Bian, Liming, O'Conor, Christopher J, Jayabalan, Prakash S, Stoker, Aaron M, Kuroki, Keiichi, Cook, Cristi R, Ateshian, Gerard A, Cook, James L, *et al.* . 2009. Passaged adult chondrocytes can form engineered cartilage with functional mechanical properties: a canine model. *Tissue Engineering Part A*, **16**(3), 1041–1051.

Nicolás, Francisco J, De Bosscher, Karolien, Schmierer, Bernhard, & Hill, Caroline S. 2004. Analysis of Smad nucleocytoplasmic shuttling in living cells. *Journal of cell science*, **117**(18), 4113–4125.

Nikolaev, NI, Obradovic, B, Versteeg, Henk K, Lemon, G, & Williams, David J. 2010. A validated model of GAG deposition, cell distribution, and growth of tissue engineered cartilage cultured in a rotating bioreactor. *Biotechnology and bioengineering*, **105**(4), 842–853.

Nims, Robert J, Cigan, Alexander D, Albro, Michael B, Hung, Clark T, & Ateshian, Gerard A. 2014. Synthesis rates and binding kinetics of matrix products in engineered cartilage constructs using chondrocyte-seeded agarose gels. *Journal of biomechanics*, **47**(9), 2165–2172.

Nims, Robert J, Cigan, Alexander D, Albro, Michael B, Vunjak-Novakovic, Gordana, Hung, Clark T, & Ateshian, Gerard A. 2015. Matrix production in large engineered cartilage constructs is enhanced by nutrient channels and excess media supply. *Tissue Engineering Part C: Methods*, **21**(7), 747–757.

Nims, Robert J, Durney, Krista M, Cigan, Alexander D, Dusséaux, Antoine, Hung, Clark T, & Ateshian, Gerard A. 2016. Continuum theory of fibrous tissue damage mechanics using bond kinetics: application to cartilage tissue engineering. *Interface focus*, **6**(1), 20150063.

Nims, Robert J, Durney, Krista M, Law, Wing-Sum A, Tan, Andrea R, Roach, Brendan L, Cook, James L, Hung, Clark T, & Ateshian, Gerard A. 2017. Heterogeneity of engineered cartilage constructs using adult canine chondrocytes is reduced with higher TGF-β concentrations. Transactions of the ORS.

Novak, Tyler, Seelbinder, Benjamin, Twitchell, Celina M, van Donkelaar, Corrinus C, Voytik-Harbin, Sherry L, & Neu, Corey P. 2016. Mechanisms and Microenvironment Investigation of Cellularized High Density Gradient Collagen Matrices via Densification. *Advanced Functional Materials*.

Obradovic, Bojana, Carrier, Rebecca L, Vunjak-Novakovic, Gordana, Freed, Lisa E, *et al.* . 1999. Gas exchange is essential for bioreactor cultivation of tissue engineered cartilage. *Biotechnology and bioengineering*, **63**(2), 197–205.

Obradovic, Bojana, Meldon, Jerry H, Freed, Lisa E, & Vunjak-Novakovic, Gordana. 2000. Glycosaminoglycan deposition in engineered cartilage: experiments and mathematical model. *AIChE Journal*, **46**(9), 1860–1871.

ÖBrink, Björn. 1973a. The influence of glycosaminoglycans on the formation of fibers from monomeric tropocollagen in vitro. *European Journal of Biochemistry*, **34**(1), 129–137.

ÖBrink, Björn. 1973b. A study of the interactions between monomeric tropocollagen and glycosaminoglycans. *European Journal of Biochemistry*, **33**(2), 387–400.

Öbrink, Björn, Laurent, Torvard C, & Carlsson, Birgit. 1975. The binding of chondroitin sulphate to collagen. *FEBS letters*, **56**(1), 166–169.

O'Connell, GD, Nims, RJ, Green, J, Cigan, AD, Ateshian, GA, & Hung, CT. 2014. Time and dose-dependent effects of chondroitinase ABC on growth of engineered cartilage. *European cells & materials*, **27**, 312.

O'Conor, Christopher J, Leddy, Holly A, Benefield, Halei C, Liedtke, Wolfgang B, & Guilak, Farshid. 2014. TRPV4-mediated mechanotransduction regulates the metabolic response of chondrocytes to dynamic loading. *Proceedings of the National Academy of Sciences*, **111**(4), 1316–1321.

Olstad, K, Ytrehus, B, Ekman, S, Carlson, CS, & Dolvik, NI. 2008. Epiphyseal cartilage canal blood supply to the distal femur of foals. *Equine veterinary journal*, **40**(5), 433–439.

O'Neill, John D, Freytes, Donald O, Anandappa, Annabelle J, Oliver, Juan A, & Vunjak-Novakovic, Gordana V. 2013. The regulation of growth and metabolism of kidney stem cells with regional specificity using extracellular matrix derived from kidney. *Biomaterials*, **34**(38), 9830–9841.

Oreja, Maria Teresa Castaño, Rodriguez, Maximino Quintáns, Abelleira, Antonio Crespo, García, Manuel Avelino Giráldez, García, Miguel Angel Saavedra, & Barreiro, Francisco Javier Jorge. 1995. Variation in articular cartilage in rabbits between weeks six and eight. *The Anatomical Record*, **241**(1), 34–38.

Oungoulian, Sevan R, Durney, Krista M, Jones, Brian K, Ahmad, Christopher S, Hung, Clark T, & Ateshian, Gerard A. 2015. Wear and damage of articular cartilage with friction against orthopedic implant materials. *Journal of biomechanics*, **48**(10), 1957–1964.

Overbeek, J Th. 1956. The Donnan equilibrium. *Progress in biophysics and biophysical chemistry*, **6**, 57.

Park, S, Hung, CT, & Ateshian, GA. 2004. Mechanical response of bovine articular cartilage under dynamic unconfined compression loading at physiological stress levels. *Osteoarthritis and cartilage*, **12**(1), 65–73.

Park, Seonghun, & Ateshian, Gerard A. 2006. Dynamic response of immature bovine articular cartilage in tension and compression, and nonlinear viscoelastic modeling of the tensile response. *Journal of biomechanical engineering*, **128**(4), 623–630.

Pecora, Fabio, Gualeni, Benedetta, Forlino, Antonella, Superti-Furga, Andrea, Tenni, Ruggero, Cetta, Giuseppe, & Rossi, Antonio. 2006. In vivo contribution of amino acid sulfur to cartilage proteoglycan sulfation. *Biochemical Journal*, **398**(3), 509–514.

Peterson, Lars, Vasiliadis, Haris S, Brittberg, Mats, & Lindahl, Anders. 2010. Autologous chondrocyte implantation a long-term follow-up. *The American journal of sports medicine*, **38**(6), 1117–1124.

Pitsillides, Andrew A, Archer, Charles W, Prehm, Peter, Bayliss, Michael T, & Edwards, JC. 1995. Alterations in hyaluronan synthesis during developing joint cavitation. *Journal of Histochemistry & Cytochemistry*, **43**(3), 263–273.

Radin, Eric L, Swann, David A, Paul, Igor L, & Mcgrath, Paul J. 1982. Factors influencing articular cartilage wear in vitro. *Arthritis & Rheumatism*, **25**(8), 974–980.

Recklies, Anneliese D, Baillargeon, Linon, & White, Chantal. 1998. Regulation of cartilage oligomeric matrix protein synthesis in human synovial cells and articular chondrocytes. *Arthritis & Rheumatism*, **41**(6), 997–1006.

Riesle, J, Hollander, AP, Langer, R, Freed, LE, & Vunjak-Novakovic, G. 1998. Collagen in tissue-engineered cartilage: Types, structure, and crosslinks. *Journal of cellular biochemistry*, **71**(3), 313–327.

Riley, Graham P, Curry, Valerie, DeGroot, Jeroen, van El, Benno, Verzijl, Nicole, Hazleman, Brian L, & Bank, Ruud A. 2002. Matrix metalloproteinase activities and their relationship with collagen remodelling in tendon pathology. *Matrix Biology*, **21**(2), 185–195.

Rohlf, F James, & Sokal, Robert R. 1995. *Statistical tables*. Macmillan.

Rosenberg, Krisztina, Olsson, Henric, Mörgelin, Matthias, & Heinegård, Dick. 1998. Cartilage oligomeric matrix protein shows high affinity zinc-dependent interaction with triple helical collagen. *Journal of Biological Chemistry*, **273**(32), 20397–20403.

Rossi, Antonio, Kaitila, Ilkka, Wilcox, William R, Rimoin, David L, Steinmann, Beat, Cetta, Giuseppe, & Superti-Furga, Andrea. 1998. Proteoglycan sulfation in cartilage and cell cultures from patients with sulfate transporter chondrodysplasias: relationship to clinical severity and indications on the role of intracellular sulfate production. *Matrix biology*, **17**(5), 361–369.

Rowland, Christopher R, Colucci, Lina A, & Guilak, Farshid. 2016. Fabrication of anatomically-shaped cartilage constructs using decellularized cartilage-derived matrix scaffolds. *Biomaterials*, **91**, 57–72.

Sandy, John D, & Plaas, Anna HK. 1989. Studies on the hyaluronate binding properties of newly synthesized proteoglycans purified from articular chondrocyte cultures. *Archives of biochemistry and biophysics*, **271**(1), 300–314.

Saxena, Vishal, Kim, Minwook, Keah, Niobra M, Neuwirth, Alexander L, Stoeckl, Brendan D, Bickard, Kevin, Restle, David J, Salowe, Rebecca, Wang, Margaret Ye, Steinberg, David R, *et al.* . 2016. Anatomic mesenchymal stem cell-based engineered cartilage constructs for biologic total joint replacement. *Tissue Engineering Part A*, **22**(3-4), 386–395.

Sengers, BG, Van Donkelaar, CC, Oomens, CWJ, & Baaijens, FPT. 2005a. Computational study of culture conditions and nutrient supply in cartilage tissue engineering. *Biotechnology Progress*, **21**(4), 1252–1261.

Sengers, Bram G, Oomens, Cees WJ, & Baaijens, Frank PT. 2004. An integrated finite-element approach to mechanics, transport and biosynthesis in tissue engineering. *Journal of biomechanical engineering*, **126**(1), 82–91.

Sengers, Bram G, Heywood, Hannah K, Lee, David A, Oomens, Cees W, & Bader, Dan L. 2005b. Nutrient utilization by bovine articular chondrocytes: a combined experimental and theoretical approach. *Journal of biomechanical engineering*, **127**(5), 758–766.

Setton, LA, Tohyama, H, & Mow, VC. 1998. Swelling and curling behaviors of articular cartilage. *Journal of biomechanical engineering*, **120**(3), 355–361.

Sheehy, Eamon J, Buckley, Conor T, & Kelly, Daniel J. 2011. Chondrocytes and bone marrow-derived mesenchymal stem cells undergoing chondrogenesis in agarose hydrogels of solid and channelled architectures respond differentially to dynamic culture conditions. *Journal of tissue engineering and regenerative medicine*, **5**(9), 747–758.

Sheehy, Eamon J, Vinardell, Tatiana, Toner, Mary E, Buckley, Conor T, & Kelly, Daniel J. 2014. Altering the architecture of tissue engineered hypertrophic cartilaginous grafts facilitates vascularisation and accelerates mineralisation. *PloS one*, **9**(3), e90716.

Shirazi, R, Shirazi-Adl, A, & Hurtig, M. 2008. Role of cartilage collagen fibrils networks in knee joint biomechanics under compression. *Journal of biomechanics*, **41**(16), 3340–3348.

Siegel, Robert C. 1974. Biosynthesis of collagen crosslinks: increased activity of purified lysyl oxidase with reconstituted collagen fibrils. *Proceedings of the National Academy of Sciences*, **71**(12), 4826–4830.

Silver, FH, & Trelstad, RL. 1980. Type I collagen in solution. Structure and properties of fibril fragments. *Journal of Biological Chemistry*, **255**(19), 9427–9433.

Simo, JC, & Ju, JW. 1987. Strain-and stress-based continuum damage models. *International journal of solids and structures*, **23**(7), 821–840.

Sittinger, M, Bujia, J, Minuth, WW, Hammer, C, & Burmester, GR. 1994. Engineering of cartilage tissue using bioresorbable polymer carriers in perfusion culture. *Biomaterials*, **15**(6), 451–456.

Soares, Joao S, & Sacks, Michael S. 2016. A triphasic constrained mixture model of engineered tissue formation under in vitro dynamic mechanical conditioning. *Biomechanics and modeling in mechanobiology*, **15**(2), 293–316.

Sobue, Mitsuko, Takeuchi, Jun, Ito, Kenichiro, Kimata, Koji, & Suzuki, Sakaru. 1978. Effect of environmental sulfate concentration on the synthesis of low and high sulfated chondroitin sulfates by chick embryo cartilage. *Journal of Biological Chemistry*, **253**(17), 6190–6196.

Soltz, Michael A, & Ateshian, Gerard A. 1998. Experimental verification and theoretical prediction of cartilage interstitial fluid pressurization at an impermeable contact interface in confined compression. *Journal of biomechanics*, **31**(10), 927–934.

Steadman, J Richard, Rodkey, William G, Singleton, Steven B, & Briggs, Karen K. 1997. Microfracture technique forfull-thickness chondral defects: Technique and clinical results. *Operative techniques in orthopaedics*, **7**(4), 300–304.

Steadman, J Richard, Briggs, Karen K, Rodrigo, Juan J, Kocher, Mininder S, Gill, Thomas J, & Rodkey, William G. 2003. Outcomes of microfracture for traumatic chondral defects of the knee: average 11-year follow-up. *Arthroscopy: The Journal of Arthroscopic & Related Surgery*, **19**(5), 477–484.

Stegemann, Hermann, & Stalder, Karlheinz. 1967. Determination of hydroxyproline. *Clinica Chimica Acta*, **18**(2), 267–273.

Stockwell, RA. 1967. The cell density of human articular and costal cartilage. *Journal of anatomy*, **101**(Pt 4), 753.

Stockwell, RA. 1971a. The interrelationship of cell density and cartilage thickness in mammalian articular cartilage. *Journal of anatomy*, **109**(Pt 3), 411.

Stockwell, RA. 1971b. The ultrastructure of cartilage canals and the surrounding cartilage in the sheep fetus. *Journal of anatomy*, **109**(Pt 3), 397.

Stockwell, Robert Amos. 1979. *Biology of cartilage cells*. Vol. 7. CUP Archive.

Strayer Jr, Luther M. 1943. The embryology of the human hip joint. *The Yale journal of biology and medicine*, **16**(1), 13.

Temple, Michele M, Xue, Yang, Chen, Michael Q, & Sah, Robert L. 2006. Interleukin-1α induction of tensile weakening associated with collagen degradation in bovine articular cartilage. *Arthritis & Rheumatism*, **54**(10), 3267–3276.

Temple-Wong, Michele M, Bae, Won C, Chen, Michael Q, Bugbee, William D, Amiel, David, Coutts, Richard D, Lotz, Martin, & Sah, Robert L. 2009. Biomechanical, structural, and biochemical indices of degenerative and osteoarthritic deterioration of adult human articular cartilage of the femoral condyle. *Osteoarthritis and Cartilage*, **17**(11), 1469–1476.

Thibault, Marc, Robin Poole, A, & Buschmann, Michael D. 2002. Cyclic compression of cartilage/bone explants in vitro leads to physical weakening, mechanical breakdown of collagen and release of matrix fragments. *Journal of orthopaedic research*, **20**(6), 1265–1273.

Treilleux, Isabelle, Mallein-Gerin, Frederic, Le Guellec, Dominique, & Herbage, Daniel. 1992. Localization of the expression of type I, II, III collagen, and aggrecan core protein genes in developing human articular cartilage. *Matrix*, **12**(3), 221–232.

Tuan, Rocky S, Boland, Genevieve, & Tuli, Richard. 2002. Adult mesenchymal stem cells and cell-based tissue engineering. *Arthritis Res Ther*, **5**(1), 1.

Vacanti, Joseph P, & Langer, Robert. 1999. Tissue engineering: the design and fabrication of living replacement devices for surgical reconstruction and transplantation. *The Lancet*, **354**, S32–S34.

Van der Kraan, PM, Buma, P, Van Kuppevelt, T, & Van den Berg, WB. 2002. Interaction of chondrocytes, extracellular matrix and growth factors: relevance for articular cartilage tissue engineering. *Osteoarthritis and Cartilage*, **10**(8), 631–637.

van Donkelaar, CC, Chao, G, Bader, DL, & Oomens, CWJ. 2011. A reaction–diffusion model to predict the influence of neo-matrix on the subsequent development of tissue-engineered cartilage. *Computer methods in biomechanics and biomedical engineering*, **14**(05), 425–432.

Vunjak-Novakovic, G, Martin, I, Obradovic, B, Treppo, S, Grodzinsky, AJ, Langer, R, & Freed, LE. 1999. Bioreactor cultivation conditions modulate the composition and mechanical properties of tissue-engineered cartilage. *Journal of Orthopaedic Research*, **17**(1), 130–138.

Vunjak-Novakovic, Gordana, Freed, Lisa E, Biron, Robert J, & Langer, Robert. 1996. Effects of mixing on the composition and morphology of tissue-engineered cartilage. *AIChE Journal*, **42**(3), 850–860.

Vunjak-Novakovic, Gordana, Obradovic, Bojana, Martin, Ivan, Bursac, Predrag M, Langer, Robert, & Freed, Lisa E. 1998. Dynamic cell seeding of polymer scaffolds for cartilage tissue engineering. *Biotechnology progress*, **14**(2), 193–202.

Watanabe, Hideto, Cheung, Sau C, Itano, Naoki, Kimata, Koji, & Yamada, Yoshihiko. 1997. Identification of hyaluronan-binding domains of aggrecan. *Journal of Biological Chemistry*, **272**(44), 28057–28065.

Williams, Gregory M, & Sah, Robert L. 2010. In vitro modulation of cartilage shape plasticity by biochemical regulation of matrix remodeling. *Tissue Engineering Part A*, **17**(1-2), 17–23.

Williamson, Amanda K, Masuda, Koichi, Thonar, Eugene J-MA, & Sah, Robert L. 2003a. Growth of immature articular cartilage in vitro: correlated variation in tensile biomechanical and collagen network properties. *Tissue engineering*, **9**(4), 625–634.

Williamson, Amanda K, Chen, Albert C, Masuda, Koichi, Thonar, Eugene J, & Sah, Robert L. 2003b. Tensile mechanical properties of bovine articular cartilage: variations with growth and relationships to collagen network components. *Journal of Orthopaedic Research*, **21**(5), 872–880.

Wilsman, Norman J, & Van Sickle, David C. 1972. Cartilage canals, their morphology and distribution. *The Anatomical Record*, **173**(1), 79–93.

Wilson, Christopher G, Bonassar, Lawrence J, & Kohles, Sean S. 2002. Modeling the dynamic composition of engineered cartilage. *Archives of biochemistry and biophysics*, **408**(2), 246–254.

Wilson, W, Van Donkelaar, CC, Van Rietbergen, B, Ito, K, & Huiskes, R. 2004. Stresses in the local collagen network of articular cartilage: a poroviscoelastic fibril-reinforced finite element study. *Journal of biomechanics*, **37**(3), 357–366.

Windhaber, Robin AJ, Wilkins, Robert J, & Meredith, David. 2003. Functional characterisation of glucose transport in bovine articular chondrocytes. *Pflügers Archiv*, **446**(5), 572–577.

Yamashita, Akihiro, Morioka, Miho, Yahara, Yasuhito, Okada, Minoru, Kobayashi, Tomohito, Kuriyama, Shinichi, Matsuda, Shuichi, & Tsumaki, Noriyuki. 2015. Generation of scaffoldless hyaline cartilaginous tissue from human iPSCs. *Stem cell reports*, **4**(3), 404–418.

Yan, Dan, Zhou, Guangdong, Zhou, Xu, Liu, Wei, Zhang, Wen Jie, Luo, Xusong, Zhang, Lu, Jiang, Ting, Cui, Lei, & Cao, Yilin. 2009. The impact of low levels of collagen IX and pyridinoline on the mechanical properties of in vitro engineered cartilage. *Biomaterials*, **30**(5), 814–821.

Zhou, Shengda, Cui, Zhanfeng, & Urban, Jill PG. 2008. Nutrient gradients in engineered cartilage: metabolic kinetics measurement and mass transfer modeling. *Biotechnology and bioengineering*, **101**(2), 408–421.

Zi, Zhike, Feng, Zipei, Chapnick, Douglas A, Dahl, Markus, Deng, Difan, Klipp, Edda, Moustakas, Aristidis, & Liu, Xuedong. 2011. Quantitative analysis of transient and sustained transforming growth factor-β signaling dynamics. *Molecular systems biology*, **7**(1), 492.

Appendix A Silencing ribonucleic acids for altering chondrocytes gene expression

A.1 Introduction

One of the major findings of this dissertation was that non-native matrix synthesis and deposition rates can negatively influence the mechanical functionality of engineered cartilage. Therefore, in the present aim we try to use gene silencing techniques to knockdown protein expression of molecules and protein which contribute to the formation of fixed charges within the extracellular matrix, the driver of the high osmotic swelling pressure which develops. While siRNAs were able to knockdown mRNA expression, protein expression was not different than control constructs.

A.2 Introduction

One of the ongoing challenges in tissue engineering is developing strategies to control matrix composition for engineering tissues with biochemical and biomechanics properties to match the native tissue. As previously discussed, cartilage tissue engineering technologies suffer from excess proteoglycan (GAG) synthesis and little collagen and synthesis. Strategies that enhance the collagen to GAG synthesis ratio are likely to enhance the mechanical competency of the tissue.

One potential strategy for decreasing GAG synthesis is silencing RNA (siRNA), a technique for specifically targeting the destruction of gene sequences and inhibiting the protein translation of deleterious proteins. siRNAs stimulate in intracellular complex which specifically targets complementary mRNAs and degrades them, preventing future peptide translation and eventual synthesis of the target protein. As siRNAs work solely within a cell targeting specific, complementary mRNA, they're believed to be safe for clinical applications and their activity eventually diminishes as cellular proliferation reduces their concentration to below effective levels. To this end, siRNA technologies have been used in several clinical trials to exhibit the synthesis of disease modifying proteins

In chondrocytes, GAG synthesis and sulfation is a well coordinated biochemical pathway, thereby presenting numerous targets by which we may be able to alter GAG synthesis or decrease GAG sulfation. In particular, two possible sites for this action would be 1) decreasing the overall synthesis the aggrecan core protein (the predominant proteoglycan in cartilage) and 2) decreasing the enzymes

gene target	sense sequence (5'→3')	antisense sequence (5'→3')
aggrecan (var 1)	CCUUUGACGUGAGCGUAGAtt	UCUACGCUCACGUCAAAGGca
aggrecan (var 2)	CCUUUGACGUGAGCGUAGAtt	UCUACGCUCACGUCAAAGGca
xylotransferase 1	GCAUAAAACUGUACAGAAAtt	UUUCUGUACAGUUUUAUGCat
xylotransferase 2	CCAGGUUCAUCAAGAAACAtt	UGUUUCUUGAUGAACCUGGag

Table 6: siRNA sequences for *Bos taurus*.

involved in the sulfation of proteoglycans (xlyotransferases).

In this study we investigated the growth of engineer constructs under the treatment of specifically targeted siRNAs for inhibiting both the synthesis of aggrecan and the sulfation of GAG. Ultimately we're interested in decreasing the synthesis of proteoglycan proteins, but as siRNA efficiency is measured by mRNA down regulation, we use both RT-qPCR and standard biochemical assays to associate how effective siRNA treatments were.

A.3 Methods

A.3.1 Experimental methods

For these studies, chondrocytes were plated in two-dimensions until reaching 90% confluence as previously described (Cigan *et al.* , 2016b). At this level, fetal bovine serum supplemented media was removed and cells were washed with sterile PBS. Transfection agent (siRNA + Lipofectamine 3000, described below) in Optimem-reduced serum media was applied to chondrocytes for 6 hours in static incubator culture. Cells were then washed for transfection agent and lifted (0.05% trypsin) before casting into constructs as previous described (Nims *et al.* , 2014). Small constructs were cast for all studies.

A.3.2 Gene knockdown

Transfection was performed by mixing the target siRNA (Invitrogen) with Lipofectamine as advised by the manufacturer in OptiMem media. This transfection media was applied to plated cells for 6 hours before immediate cell lifting and construct casting or PCR analysis.

siRNAs for aggrecan (two variants: siACAN1 and siACAN2) and xylotranferase 1 and 2 (siXYL1 and siXYL2, respectively) were transfected to chondrocytes. Details of siRNA sequences is found in Table 6.

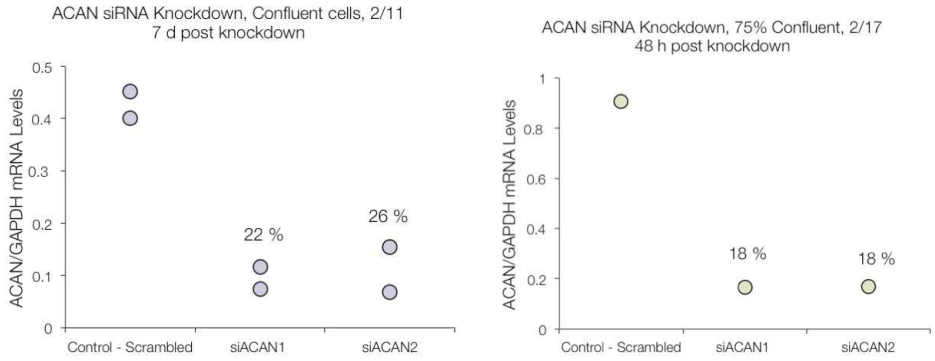

Figure A.1: Gene knockdown of siACANs.

A.3.3 PCR

Gene expression of ACAN knockdowns was assessed via qRTPCR following the procedure listed on our lab's protocol server. Briefly, cells were lysed and RNA was isolated using trireagent. Nano drop testing confirmed high purity RNA which was maintained at -80 degrees to prevent degradation in between steps. RNA underwent RT-PCR in a thermocycler before assessing gene activity (normalized to the housekeeper GAPDH) with qPCR (Jacob's lab).

A.3.4 Biochemical assessment

At both early and late time points, constructs were assessed for mechanical and biochemical properties as previously described (Cigan *et al.* , 2016c; Hollander *et al.* , 1994; Farndale *et al.* , 1986; McGowan *et al.* , 2002).

A.4 Results

Gene assays indicated that siACAN1 and siACAN2 displayed a high level of (>80%) gene knockdown (Figure A.1). Interestingly this gene knockdown did not significantly influence biochemical content of constructs after 35 days of culture (Figure A.2).

Conversely, the application of si-xylosidetransferase had a large impact on the mechanical development of constructs (Figure A.3). However, when normalized to cell content, biochemical properties of the constructs were unaffected only influenced by siXYL2, but this treatment also negatively impacted the collagen content of the constructs.

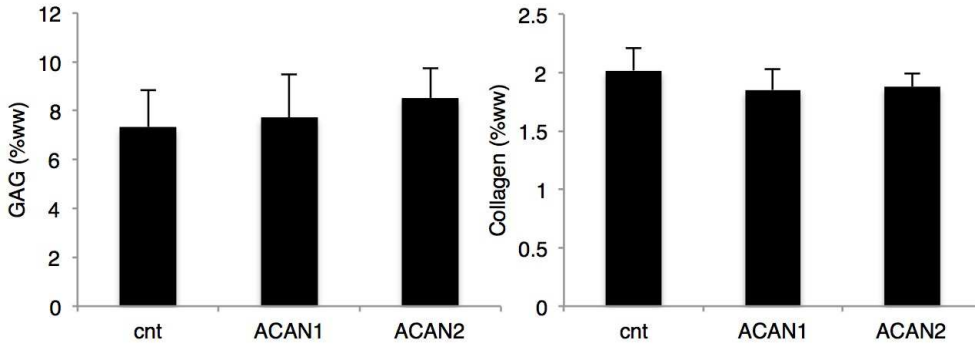

Figure A.2: Protein expression of siACANs.

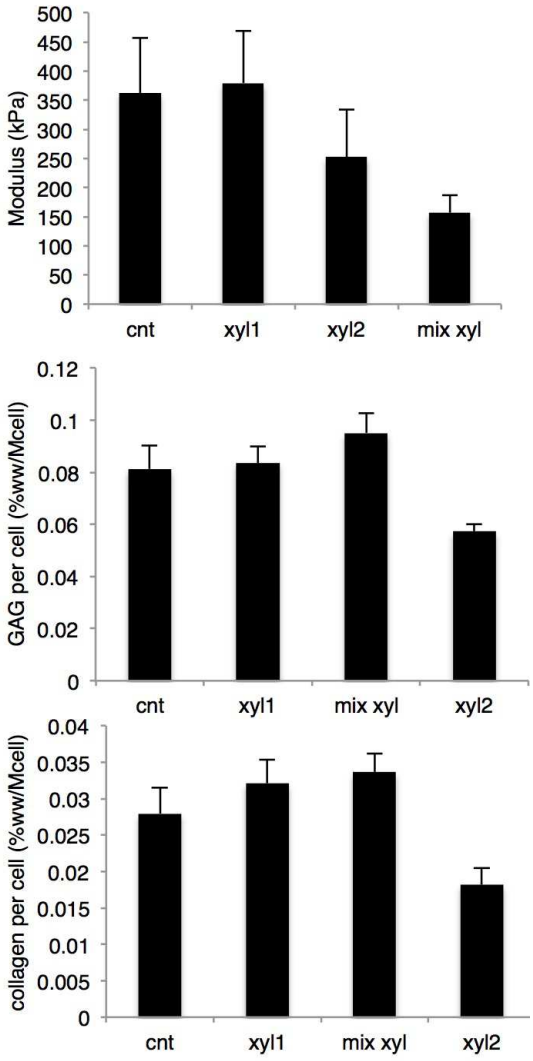

Figure A.3: Protein expression of siXYLs.

A.5 Discussion

Gene silencing is an attractive and reversible methodology to alter gene expression of engineered tissues. However, despite the promise, our results here suggest that altering the phenotype is a complicated process by which juvenile bovine chondrocytes. Interestingly, the xylotransferase activity diminished both tissue mechanics and biochemical output. So, while the siACAN response was not strong enough to elicit a phenotypic response, the siXYL response negatively impacted overall cell activity. This is not desirable and is similar to our recent investigations into the role of chondroitinase ABC (O'Connell *et al.* , 2014).

Recent studies have further demonstrate the disconnect between mRNA expression and a cell's phenotypic response (Cote *et al.* , 2016), suggesting that more investigation on this subject. Such advances would benefit the control of engineered cartilage and other tissues mechanics during growth.

Appendix B Heterogeneity of engineered cartilage constructs using adult canine chondrocytes is reduced with higher TGF-β concentrations

B.1 Abstract

Based on the bulk of this dissertation, it is understood the importance of TGF-β for juvenile bovine chondrocyte constructs. In application for future work, this study examines the role of TGF-β in a adult canine chondrocyte system. Adult chondrocytes are one of the most common cell sources for engineered cartilage constructs. Without understanding the TGF-β requirements of these cells, engineering anatomic functional cartilage constructs will likely suffer from heterogeneous and incomplete matrix synthesis. This work investigates the interactions of cell density and TGF-β supplementation on engineered cartilage functional properties and identifies parameter sets for optimizing nutrient channel placement in large constructs seeded with adult canine constructs for our preclinical studies.

B.2 Introduction

Prior cartilage tissue engineering studies using immature bovine chondrocytes have shown that TGF-β supplementation is a key nutrient for controlling matrix synthesis and deposition, as it exerts both mitogenic and biosynthetic influences when administered at a wide range of concentrations (Van der Kraan *et al.* , 2002). Recently, we have shown that active TGF-β concentrations are highly heterogeneous within large cartilage constructs, due to cellular internalization and extracellular binding interactions, leading to similarly heterogeneous matrix synthesis (Albro *et al.* , 2016). Optimally spaced nutrient channels within large constructs significantly mitigated this heterogeneity, allowing us to engineer more consistent constructs up to 40 mm in diameter, using TGF-β3 at 1 ng mL^{-1} (Cigan *et al.* , 2016b).

Though juvenile chondrocytes are a convenient cell source for developing tissue culture strategies, adult chondrocytes are more clinically applicable for engineered cartilage constructs. Yet, relatively little is known about the metabolic requirements needed to optimize culture conditions when using adult chondrocytes. This incomplete understanding limits the engineering of functional

anatomic cartilage constructs due to heterogeneities in matrix deposition. To address this limitation, this study evaluated the mitogenic and functional influence of TGF-ß3 on adult canine chondrocyte-seeded constructs. While our long-term goal is to produce anatomic constructs for implantation, the present work determined the responses of smaller tissue constructs to 1, 10 and 50 ng mL^{-1} TGF-β3 to test the hypothesis that matrix heterogeneities exist in mature canine chondrocyte seeded cartilage constructs and is ameliorated with additional TGF-β supplementation. Furthermore, since prior work with both juvenile bovine chondrocytes and adult human chondrocytes has shown a strong influence of growth with increasing cell seeding density (Nims *et al.* , 2016; Cigan *et al.* , 2016a), in this study we seeded constructs with 30, 60, or 90 million cells mL^{-1}. Upon culturing for 28 days, matrix heterogeneity became visually evident, so construct heterogeneity was assessed with spatial mechanical properties testing.

B.3 Methods

Engineered cartilage constructs were cast and punched ($\varnothing$ 3 mm × 2.34 mm) using third-passage adult canine chondrocytes (3 dogs, tibial plateau and glenoid) in a 2% agarose gel with an initial cell seeding density of 30, 60, or 90 million cells mL^{-1}. Chemically defined media were supplemented with TGF-β3 throughout culture (Kelly *et al.* , 2006). Constructs with 30 and 90 million cells mL^{-1} were supplemented with 1 and 10 ng mL^{-1} TGF-β3 and constructs with 60 million cells mL^{-1} were supplemented with 1, 10, and 50 ng mL^{-1}. Constructs were cultured for 28 days. Equilibrium compressive modulus (E_Y), dynamic modulus (G* at 0.01 Hz), and spatial mechanical properties, were measured as previously described (Cigan *et al.* , 2014).

For spatial mechanical characterization, constructs were diametrically halved, treated with calcein AM and imaged on a confocal microscope (2× objective) under axial loading. VIC2D (Correlated solutions) was used to analyze the images and extract strain fields. A MATLAB script averaged the axial strains in 9-platen-to-platen bins after cropping the outer 20% of the construct diameter, to produce a quasi-one dimensional analysis through the construct thickness. Spatial tissue modulus was computed by normalizing the tissue stress at 15% nominal bulk tissue strain to the spatial strain maps.

Histological samples were sectioning (5 µm) and staining for collagen (Picrosirius red) and live/dead images were taken after an additional 28 days of culture (day 56) for long-term viability

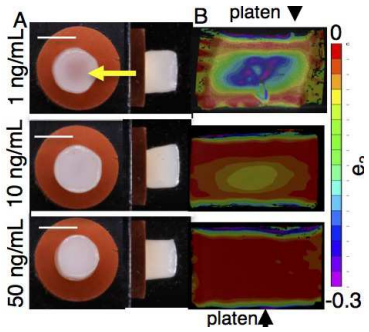

Figure B.1: Gross images (A, arrow is translucent center, scale = 3 mm) and strain maps (B, arrow is platen loading) of 60 million cell/mL and 1, 10, and 50 ng mL^{-1} TGF-β.

assessment. Two-way ANOVA examined the influence of cell density, TGF-β concentration, and their interaction and were run in R (v. 3.3.0). ANOVA examined E_Y in the center depth-wise bin.

B.4 Results

B.4.1 Morphology

After 28 days of culture, growth of the canine constructs was dependent on both cell density and TGF-β3 concentration. Constructs supplemented with 1 ng mL^{-1} TGF-β3 were visually more translucent within the construct center versus constructs treated with 10 ng mL^{-1} and 50 ng mL^{-1} (Figure B.1).

B.4.2 Mechanical properties

For all cell seeding densities, the 1 ng mL^{-1} TGF-β dose produced the lowest bulk E_Y (average of all 1 ng mL^{-1} samples 189±31 kPa, p<0.001, Figure B.2A) and G* (0.68±0.14 MPa, p<0.001, not shown). Cell density alone did not play a significant role in either E_Y or G*; 50 ng mL^{-1} produced similar E_Y (p=0.69) to the 10 ng mL^{-1} group but had a higher G* (2.1±0.1 MPa versus 1.8±0.2 MPa, p=0.005). In contrast to the bulk mechanical properties, spatial mechanical properties exhibited significant differences with TGF-β dose and cell density. For the 1 ng mL^{-1} dose, the center minimal E_Y averaged 44±14 kPa for all cell densities, although there was less spatial heterogeneity with increased cell density (Figure B.2C). For the 10 ng mL^{-1} dose, the center bin had the highest spatial E_Y for the 30 million cell mL^{-1} group (733±395 kPa) and was significantly higher than the center bin E_Y for the 90 million cell mL^{-1} group (107±25 kPa, p=0.005) (Figure B.2D). Within

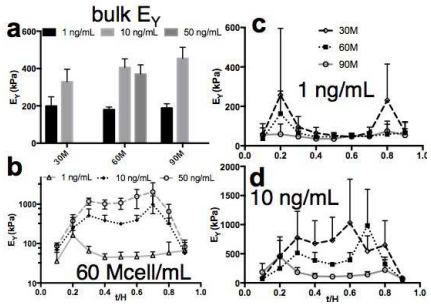

Figure B.2: A. Bulk construct E_Y. B. Spatial E_Y of 60 million cell mL^{-1} group with 1, 10, and 50 ng mL^{-1} TGF-β. C. 1 ng mL^{-1} TGF-β on 30, 60, 90 million cell mL^{-1} constructs spatial E_Y. D. 10 ng mL^{-1} TGF-β on 30, 60, 90 million cell mL^{-1} E_Y.

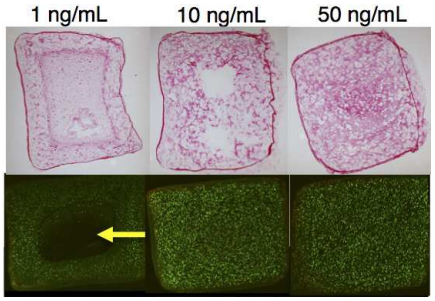

Figure B.3: Picrosirius red (top) and live/dead viability staining (bottom) images from 60 million cells mL^{-1} cultured with 1, 10, or 50 ng mL^{-1} TGF-β. Arrow is cell sparse region.

the 60 million cell mL^{-1} constructs, increasing TGF-β concentration significantly increased the core E_Y from 46±14 kPa for 1 ng mL^{-1} dosing, to 317±17 kPa for 10 ng mL^{-1} dosing, to 1078±342 kPa for 50 ng mL^{-1} dosing (Figure B.2B).

B.4.3 Histology

Histological images for both GAG and collagen showed preferential matrix deposition in the periphery of the construct for the 1 ng mL^{-1} and 10 ng mL^{-1} constructs and homogeneous deposition within constructs treated with 50 ng mL^{-1} TGF-β (Figure B.3, top). Cell viability was maintained throughout constructs supplemented with 10 and 50 ng mL^{-1} TGF-β (Figure B.3C).

B.5 Discussion

This study investigated the interactions between cell seeding density and TGF-β concentration when using adult canine chondrocyte-seeded engineered constructs, critical factors in the culture of engineered cartilage but yet untested in such a combinatorial manner. In contrast to many

studies utilizing juvenile bovine chondrocytes, adult canine chondrocytes produced heterogeneously deposited matrix despite the small size of the tissue constructs used here. Bulk mechanical tests of tissue constructs produced near native E_Y and G* functional properties for adult canine cartilage (E_Y~250 kPA and G*~2.6 MPa (Ng *et al.* , 2009)) with 10 ng/mL TGF-β across all cell densities. More sensitive spatial testing and histology revealed TGF-β transport limitations produced low functional properties in the center of the construct when cell density was elevated, or with insufficient TGF-β supplementation. Histological images confirmed that matrix content was largely confined to the construct periphery even for TGF-β doses up to 10 ng mL^{-1}, suggesting that severe matrix heterogeneities would be present as construct size increases in efforts to resurface larger-sized tissue defects. This finding contradicts the standard notion that adult cells are typically less metabolically active in vitro and may require fewer nutrients than juvenile cells. TGF-β availability and heterogeneities should be considered must be taken into consideration even when culturing adult chondrocytes, as the TGF-β threshold required for synthesizing matrix may be higher than it is for juvenile cells.

B.6 Acknowledgements

NIH R01 AR060361, T32 AR059038.

Appendix C Thesis Publications

C.1 Full length manuscripts

- **Nims, R. J.**, Cigan, A. D., Durney, K. M., Albro, M. B., Hung, C. T., Ateshian, G. A. Optimizing engineered cartilage growth with computational models of nutrient utilization, matrix deposition, and cellular proliferation. In preparation.
- **Nims, R. J.**, Ateshian, G. A. Reactive constrained mixtures for modeling biological tissues. In revision: *Journal of Elasticity*.
- **Nims, R. J.**, Cigan, A. D., Durney, K. M., Jones, B. K., O'Neill, J. D., Law, W. A., Vunjak-Novakovic, G., Hung, C. T., Ateshian, G. A. Constrained cage culture improves engineered cartilage functional properties by enhancing collagen network stability. In revision: *Tissue Engineering: Part A*.
- Cigan, A. D., Durney, K. M., **Nims, R. J.**, Vunjak-Novakovic, G., Hung, C. T., Ateshian, G. A. (2016). Nutrient channels aid the growth of articular surface-sized engineered cartilage constructs. *Tissue Engineering: Part A*, **22 (17-18)**, 1063-1074.
- Cigan, A. D., **Nims, R. J.**, Vunjak-Novakovic, G., Hung, C. T., Ateshian, G. A. (2016). Optimizing nutrient channel spacing and revisiting TGF-β in large engineered cartilage constructs. *Journal of Biomechanics*, **49 (10)**, 2089-2094.
- Cigan, A. D., Roach, B. L., **Nims, R. J.**, Tan, A. R., Albro, M. B., Stoker, A. M., Cook, J. L., Vunjak-Novakovic, G., Hung, C. T., Ateshian, G. A. (2016). High seeding density of human chondrocytes in agarose produces tissue-engineered cartilage approaching native mechanical and biochemical properties. *Journal of Biomechanics*, **49 (9)**, 1909-1917.
- **Nims, R. J.**, Durney, K. M., Cigan A. D., Dusseaux, A., Hung, C. T., Ateshian, G. A. (2016). Continuum theory of fibrous tissue damage mechanics using bond kinetics: application to cartilage tissue engineering. *Interface Focus* **6**, 20150063.
- Albro, M. B.*, **Nims, R. J.***, Durney, K. M., Cigan A. D., Shim, J. J, Vunjak-Novakovic, G, Hung, C. T., Ateshian, G. A. (2016). Heterogeneous engineered cartilage growth results from gradients of media-supplemented active TGF-β and is ameliorated by the alternative supplementation of latent TGF-β. *Biomaterials*, **77**, 173-185. * shared authorship.
- **Nims, R. J.**, Cigan A. D., Albro, M. B., Vunjak-Novakovic, G, Hung, C. T., Ateshian, G. A. (2015). Matrix production in large engineered cartilage constructs is enhanced by nutrient channels and excess media supply. *Tissue Engineering: Part C*, **21 (7),** 747-757.
- Cigan A. D., **Nims, R. J.**, Albro, M. B., Vunjak-Novakovic, G, Hung, C. T., Ateshian, G. A. (2014). Nutrient Channels and Stirring Enhanced the Composition and Stiffness of Large Cartilage Constructs. *Journal of Biomechanics*, **47 (16),** 3847-3854.
- O'Connell G. D., **Nims, R. J.**, Green J., Cigan A. D., Ateshian, G. A., Hung, C. T. (2014). Time and dose-dependent effects of chondroitinase ABC on growth of engineered cartilage. *European Cells and Materials*, **27**, 312–320.
- Ateshian, G. A., **Nims, R. J.**, Maas, S., Weiss, J. A. (2014). Computational modeling of chemical reactions and interstitial growth and remodeling involving charged solutes and solid-bound molecules. *Biomechanics and Modeling in Mechanobiology*, **13 (5)**, 1105–20.

- **Nims, R. J.**, Cigan A. D., Albro, M. B., Hung, C. T., Ateshian, G. A. (2014). Synthesis rates and binding kinetics of matrix products in engineered cartilage constructs using chondrocyte-seeded agarose gels. *Jounal of Biomechanics*, **47 (9)**, 2165–2172.

- Albro, M. B., **Nims, R. J.**, Cigan A. D., Yeroushalmi, K. J., Alliston, T., Hung, C. T., Ateshian, G. A. (2013). Accumulation of exogeneous activated TGF-β in the superficial zone of articular cartilage. *Biophysics Journal*, **104 (8)**, 1794–1804.

- Cigan A. D., **Nims, R. J.**, Albro, M. B., Esau, J. D., Dreyer, M. P., Vunjak-Novakovic, G., Hung, C. T., Ateshian, G. A. (2013). Insulin, ascorbate, and glucose have a much greater influence than transferrin and selenous acid on the in vitro growth of engineered cartilage in chondrogenic media. *Tissue Engineering: Part A*, **19 (17-18)**, 1941–1948.

- Albro, M. B., **Nims, R. J.**, Cigan A. D., Yeroushalmi, K. J., Shim, J. J., Hung, C. T., Ateshian, G. A. (2013). Dynamic mechanical compression of devitalized articular cartilage does not activate latent TGF-β. *Journal of Biomechanics*, **46 (8)**, 1433–1439.

- Albro, M. B., Cigan A. D., **Nims, R. J.**, Yeroushalmi, K. J., Oungoulian, S. R., Hung, C. T., Ateshian, G. A. (2012). Shearing of synovial fluid activates latent TGF-β. *Osteoarthritis Cartilage*, **20 (11)**, 1374–1382.

C.2 Conference Abstracts and Podium Presentations

- Stefani, R. M., Roach, B. L., Silverstein, A. M., **Nims, R. J.**, Lee, J. H., Ateshian, G. A., Bulinski, J. C., Hung, C. T. (2017). Electric Field Modulation of Synovial Fibroblast Migration for Cartilage Repair. In: *63st Annual Meeting of the Orthopaedic Research Society.* San Diego, CA, USA.

- Law, W. A., Durney, K. M., **Nims, R. J.**, Vunjak-Novakovic, G, Hung, C. T., Ateshian, G. A. (2017). Chondrocytes produce native-like ECM organization using MatriTek as a scaffold for cartilage tissue engineering when nutrient channels and CAGE strategies are employed. In: *63st Annual Meeting of the Orthopaedic Research Society.* San Diego, CA, USA.

- Durney, K. M., **Nims, R. J.**, Law, W. A., Cook, J. L., Hung, C. T., Ateshian, G. A. (2017). Mature canine cells in full-scale engineered cartilage recapitulate native mechanical and biochemical properties with nutrient channels. In: *63st Annual Meeting of the Orthopaedic Research Society.* San Diego, CA, USA.

- **Nims, R. J.**, Durney, K. M., Law, W. A., Tan, A. R., Roach, B. L., Cook, J. L., Hung, C. T., Ateshian, G. A. (2017). Heterogeneity of engineered cartilage constructs using adult canine chondrocytes is reduced with higher TGF-β concentrations. In: *63st Annual Meeting of the Orthopaedic Research Society.* San Diego, CA, USA.

- **Nims, R. J.**, Cigan, A. D., Durney, K. M., Jones, B. K., Law, W. A., Hung, C. T., Ateshian, G. A. (2017). Constrained tissue culture reduces collagen solubility and promotes collagen maturation to improve engineered cartilage functional properties. In: *63st Annual Meeting of the Orthopaedic Research Society.* San Diego, CA, USA.

- Hung, C. T., Tan, A. R., Roach, B. L., Nover, A. B., Cigan, A. D., **Nims, R. J.**, Marra, K. G., Cook, J. L., Ateshian, G. A. (2016). Strategies for Functional Tissue Engineering of Articular Cartilage. In: *Biomedical Engineering Society Meeting.* Minneapolis, MN, USA.

- Durney, K. M., **Nims, R. J.**, Boorman-Padgett, J. F., Suh, J., Koo, H. J., Smirnova, P. V., Salamone, G. T., Jones, B. K., Oungoulian, S. R., Hung, C. T., Ateshian, G. A. (2016). Principle component analysis of friction force hysteresis curves for detecting fatigue and failure and generating S-N curves for articular cartilage. In: *Summer Biomechanics, Bioengineering and Biotransport Conference.* National Harbor, MD, USA.

- Zimmerman, B., **Nims, R. J.**, Ateshian, G. A. (2016). Experimental measurements of osmotic pressure and concentration-dependent behavior in articular cartilage. In: *Summer Biomechanics, Bioengineering and Biotransport Conference.* National Harbor, MD, USA.

- Cigan, A. D., **Nims, R. J.**, Vunjak-Novakovic, G., Hung, C. T., Ateshian, G. A. (2016). Joint surface-sized engineered cartilage with nutrient channels reaches native mechanical and biochemical properties . In: *62st Annual Meeting of the Orthopaedic Research Society.* Orland, FL, USA.

- **Nims, R. J.**, Cigan, A. D., Jones, B. K., Durney, K. M., Hung, C. T., Ateshian, G. A. (2015). A multigen-erational collagen damage model explains engineered cartilage growth and remodeling phenomena.In: *Summer Biomechanics, Bioengineering and Biotransport Conference.* Snowbird Resort, UT, USA.

- Albro, M. B., **Nims, R. J.**, Durney, K. M., Cigan, A. D., Shim, J. J., Vunjak-Novakovic, G., Hung, C. T., Ateshian, G. A. (2015). Heterogeneous growth of engineered cartilage results from gradients of media supplemented active TGF-β and is ameliorated through the alternative supplementation of latent TGF-β. In: *61st Annual Meeting of the Orthopaedic Research Society.* Las Vegas, NV, USA.

- Durney, K.M., **Nims, R. J.**, Albro, M. B., Hung, C. T., Ateshian, G. A. (2015). Raman spectrographic characterization of cartilage matrix swelling via lysyl oxidase inhibition in immature explants and tissue constructs. In: *61st Annual Meeting of the Orthopaedic Research Society.* Las Vegas, NV, USA.

- **Nims, R. J.**, Cigan, A. D., Albro, M. B., Hung, C. T., Ateshian, G. A. (2015). Glucose- and TGF-β-dependent matrix synthesis models explain heterogeneous matrix deposition in large engineered tissues. In: *61st Annual Meeting of the Orthopaedic Research Society.* Las Vegas, NV, USA.

- Cigan, A. D., **Nims, R. J.**, Albro, M. B., Hung, C. T., Ateshian, G. A. (2015). Characterization of a human chondrocyte-agarose system for engineering cartilage: the importance of cell seeding density. In: *61st Annual Meeting of the Orthopaedic Research Society.* Las Vegas, NV, USA.

- **Nims, R. J.**, Cigan, A. D., Albro, M. B., Hung, C. T., Ateshian, G. A. (2014). Inorganic sulfate supplementation is not required for extracellular matrix sulfation in engineered cartilage. In: *60th Annual Meeting of the Orthopaedic Research Society.* New Orleans, LA, USA.

- Albro, M. B., Durney, K. M., Shim, J. J., Cigan, A. D., **Nims, R. J.**, Jones, B. K., Hung, C. T., Ateshian, G. A. (2014). Synovial fluid and physiologic levels of cortisol, insulin, and glucose in media maintain the homeostasis of immature bovine cartilage explants over long-term culture. In: *60th Annual Meeting of the Orthopaedic Research Society.* New Orleans, LA, USA.

- Albro, M. B., Durney, K. M., Shim, J. J., **Nims, R. J.**, Cigan, A. D., Hung, C. T., Ateshian, G. A. (2014). Endogenous stores of latent TGF-β function to maintain the mechanical integrity of articular cartilage independent of physiologic mechanical loading: Assessment through the novel validation of the specificity of a small molecule TGF-β inhibitor. In: *60th Annual Meeting of the Orthopaedic Research Society.* New Orleans, LA, USA.

- Cigan, A. D., **Nims, R. J.**, Albro, M. B., Quien, M. M., Atkatsh, K. M., Hung, C. T., Ateshian, G. A. (2014). Elevated matrix production in large engineered cartilage constructs is facilitated by nutrient channels and sufficient media. In: *60th Annual Meeting of the Orthopaedic Research Society.* New Orleans, LA, USA.

- Cigan, A. D., **Nims, R. J.**, Albro, M. B., Vunjak-Novakovic, G, Hung, C. T., Ateshian, G. A. (2013). Effects of media stirring and presence of nutrient channel on functional properties of large engineered cartilage constructs. In: *ASME Summer Bioengineering Conference.* Sunriver, OR, USA.

- **Nims, R. J.**, Cigan, A. D., Albro, M. B., Vunjak-Novakovic, G, Hung, C. T., Ateshian, G. A. (2013). Binding and release kinetics of glycosaminoglycans and collagen in engineered cartilage under TGF-β supplementation. In: *ASME Summer Bioengineering Conference.* Sunriver, OR, USA.

- **Nims, R. J.**, Cigan, A. D., Albro, M. B., Park, D. B., Vunjak-Novakovic, G, Hung, C. T., Ateshian, G. A. (2013). Engineered cartilage supplemented with channels increases nutrient availability throughout large constructs: a finite element study. In: *11th International Symposium of Computer Methods in Biomechanics and Biomedical Engineering.* Salt Lake City, UT, USA.

- Cigan, A. D., **Nims, R. J.**, Albro, M. B., Quien, M. M., Vunjak-Novakovic, G, Hung, C. T., Ateshian, G. A. (2013). Identification of a glucose concentration threshold critical for tissue growth in engineered cartilage. In: *59th Annual Meeting of the Orthopaedic Research Society.* San Antonio, TX, USA.

- **Nims, R. J.**, Cigan, A. D., Albro, M. B., O'Connell, G. D., Park, D. B., Hung, C. T., Ateshian, G. A. (2013). Frequent chondroitinase treatment in engineered cartilage with native levels of cell seeding density does not enhance collagen deposition and is detrimental to chondrocytes. In: *59th Annual Meeting of the Orthopaedic Research Society.* San Antonio, TX, USA.

- Albro, M. B., **Nims, R. J.**, Cigan, A. D., Chen, Y. B. C., Hung, C. T., Ateshian, G. A. (2013). Dynamic mechanical compression of articular cartilage does not activate latent TGF-β. In: *59th Annual Meeting of the Orthopaedic Research Society.* San Antonio, TX, USA.

- Ateshian, G. A., **Nims, R. J.**, Cigan, A. D., Albro, M. B., Hung, C. T. (2012). Finite element modeling of matrix synthesis and binding kinetics in a biphasic-solute material. In: *ASME Summer Bioengineering Conference.* Fajardo, PR, USA.

- Cigan, A. D., **Nims, R. J.**, Albro, M. B., Breves, S. L., Hung, C. T., Ateshian, G. A. (2012). Insulin and ascorbate have a much greater influence than transferrin and selenous acid on the growth of engineered cartilage in chondrogenic media. In: *ASME Summer Bioengineering Conference.* Fajardo, PR, USA.

- **Nims, R. J.**, Cigan, A. D., Albro, M. B., Wood, K. C., Hung, C. T., Ateshian, G. A. (2012). Engineered cartilage constructs retain a much greater fraction of synthesized GAG and collagen than COMP. In: *58th Annual Meeting of the Orthopaedic Research Society.* San Francisco, CA, USA.

- Albro, M. B., Cigan, A. D., **Nims, R. J.**, Chen, Y. B. C., Hung, C. T., Ateshian, G. A. (2012). Synthesis and incorporation of latent TGF-β in the superficial zone of immature bovine articular cartilage. In: *58th Annual Meeting of the Orthopaedic Research Society.* San Francisco, CA, USA.

- Albro, M. B., **Nims, R. J.**, Cigan, A. D., Chen, Y. B. C., Hung, C. T., Ateshian, G. A. (2012). Accumulation of exogenous active TGF-beta in the superficial zone of immature bovine articular cartilage. In: *58th Annual Meeting of the Orthopaedic Research Society.* San Francisco, CA, USA.